Fundamental Study on High Strength Bolted Tensile Joints(Dissertation_全文)

AUTHOR(S):

Yamaguchi, Takashi

FUNDAMENTAL STUDY
ON
HIGH STRENGTH BOLTED TENSILE JOINTS

TAKASHI YAMAGUCHI

MARCH 1996

Fundamental Study
on
High Strength Bolted Tensile Joints

A Dissertation
Submitted to
the Faculty of Engineering of Kyoto University

In Partial Fulfillment
of the Requirements for the Degree of
Doctor of Engineering

by

Takashi Yamaguchi

1996

Abstract

This dissertation presents a fundamental study on high strength bolted tensile joints with special attention to the mechanical behavior such as contact/separation behavior and the joint stiffness by experimental and analytical approach.

Firstly, the mechanical behavior of high strength bolts under static and cyclic loading is studied considering the bolt pre-stress force. Especially, load-deformation characteristics of different cross section such as bolt shank and bolt thread and the local stress state is investigated. In addition, the effect of the bolt pre-stress force on fatigue life is also discussed.

Secondly, the high strength bolt and its adjacent structural element are studied with special attention to the stiffness of such basic joint system. The contact/separation behavior of flange plates is investigated experimentally and analytically. Furthermore, parametric study using 2-dimensional axisymmetric finite element analysis is carried out and the evaluation formula for the stiffness of such joints is proposed based on the multiple regression analysis.

Thirdly, the mechanical behavior on the split tee flange joints under static loading is discussed by experimental and analytical approach. This split tee flange joint is the simplest high strength bolted tensile joints. Here, the contact/separation behavior is investigated in detail by 3-dimensional finite element analysis. Furthermore, the cyclic behavior and fatigue strength which may be crucial to split tee flange joints when applied to bridge structures, is also investigated experimentally and the fatigue strength estimation method is proposed. In addition, 2-dimensional finite element model using the effective width coefficients is proposed as the simple analytical method useful for the practical design.

Finally, as an application of the high strength bolted tensile joints, high strength bolted tube flange joints subjected to combined bending and tension is studied experimentally in detail. Experimental results are assessed based on results obtained from basic studies on such as high strength bolts, high strength bolt and its adjacent flange plate and split tee flange joints. Then, based on these results the rational simple design procedure for the tube flange joints considering the effective cross sectional area is proposed.

Acknowledgments

This dissertation is synthesis of the author's research work at the Department of Civil Engineering of Kyoto University. First of all, the author wishes to express sincere gratitude to Professor Eiichi Watanabe of Kyoto University, for his excellent guidance and continuous encouragement throughout course of this study. If this dissertation makes a contribution to academic research, most of the credit should be directed to him.

The author also wishes to express grateful appreciation to Associate Professor Kunitomo Sugiura of Kyoto University, for his suitable advice during the course of this study and making this manuscript better. Acknowledgment also goes to Dr. Tomoaki Utsunomiya, Instructor of Kyoto University, for his useful help.

In the study, a series of experiments was carried out on the specimens carefully fabricated by KOBELCO Co., Ltd..under guidance of Mr. Shun-ichiro Kasai of Kobe Steel, Ltd. A lot of technical advice and his invaluable assistance and advice is sincerely acknowledged.

The author is also thankful to excellent students of the Structural Mechanics Laboratory, Kenji Fujitani, Tetsuya Matsumuro Kazutoshi Nagata, Takehiro Takasuka, et al. for their assistance in writing the manuscript. Especially, the author is thankful to Kenji Fujitani and Tetsutya Matumuro for the collaboration in experiments.

Finally, the author expresses his deep appreciation to his parents, Mr. Katsumi Yamaguchi and Mrs. Akiko Yamaguchi, for their infinite affection and complete devotion for the completion of this dissertation. This dissertation is dedicated to them.

Table of Contents

List of Tables

List of Figures

List of Photos

Chapter 1

Introduction

1.1 General Remarks on High Strength Bolted Tensile Joints

Generally speaking, a structural system is assembled from individual parts or members by fastening them together by some means. Welding is one of such means and the other is to use fasteners such as pins or rivets and bolts. Although the former has been often utilized at present time due to its recent remarkable developments, the quality control is still very difficult to be accomplished. On the other hand, the fastener method is a traditional connection method and can be thought to be much simpler compared with the welding because of its relatively easy quality control. Accordingly, the fasteners have been the versatile connection method in the past and these are still playing an important role in the current construction environments.

The connection using fasteners may be classified into 2 types; that is, use of pins/rivets and bolts. For many years rivets were the means of connecting members adopted by many engineers because of easiness of design using simple elementary mechanics in which load transferring mechanism shown in Fig. 1.1(a) is assumed. However, it has become virtually obsolete because the highly skilled crews are required and the danger of fire exists and the high level noise is caused in driving rivets. Therefore, from the view point of the labor cost and rational design of the joints, bolts superior to pins and rivets have taken them over.

The bolted connection can be further classified into 3 types such as the bearing type, the friction type and the tension type. The load transfer mechanism of the bearing type is similar to that of pins and rivets fasteners. The difference may be the existence of the friction between plates which is not considered in the design because of insignificant friction resistance. If the bolt pre-stress force is introduced, the friction resistance is found to increase, so that the friction type is proposed. The load transferring mechanism of friction type is shown in Fig. 1.1(b). The friction type is expected to transfer the load by the friction force resulting between two plates as shown in Fig. 1.1(b). Because of this load transferring mechanism, the friction type is better than the bearing type from the view point of fatigue behavior and the stiffness. However, the reduction of stress concentration and the increase of friction resistance depends on the magnitude of the compressive force between two plates; that is, the high pre-stress force have to be introduced to the bolts. This made the engineers develop the high strength bolt allowing the higher bolt pre-stress force in order to improve better friction resistance. Therefore, the friction type has become the most popular connection method of primary members in bridge and building structures in the recent days.

On the other hand, the tension type is also utilizing the contact compressive force between two plates given by the bolts; it is considered to be a joint more efficiently to use high strength bolts than the friction type. The friction force in the friction type acts perpendicular to the contact compressive force and its given by multiplying the friction coefficient between plates to the contact compressive force; whereas; for the tension type the contact compressive force will directly tend to cancel out with the applied external load. The schematic view of the load transferring mechanism for the tension type is shown in Fig. 1.1(c).

In case that the flange plate is thick enough, the tensile load applied to joints may not cause an additional increase in the bolt force, if the applied external tensile load is smaller than the bolt pre-stress force, the bolt force is kept constant due to the cancellation of the applied external loads by release of the compressive force between two plates. Because of difference in the load transferring mechanism, the load carrying capacity per a bolt of the tension type is higher than that of other types; therefore, the tension type so called the high strength bolted tensile joints is considered to be the most superior and desired to be used in practice.

Recently, the constructor/fabricator is being threatened by the social trend that the experienced workers in the fabrication factory and the experts in erection are predicted to decrease. Furthermore, construction of structures are expected to be undertaken at the locations where the erection is more difficult, such as mountainous district, deep underground, offshore environment because of shortage of the land in Japan. Therefore, the easiness of erection is the most important factor for the future construction. At the present time, the best and simples procedure may be such that structural members and complex joint details are pre-fabricated by welding in the automated factory and then assembled by bolts at the construction site. The bolted connection may be preferred at the construction site to the welding.

Furthermore, ductile structures are desirable to have higher energy absorption capacity form the view point of the earthquake resistance. Because of the redundancy of bolted connections, the flexibility and the energy absorption capacity can be made very high and in particular those of the tension type can be controlled very easily by varying the thickness of the flange plate or the bolt pre-stress force. Therefore, the bolted connection, particularly the tension type can be implemented in the structures as energy absorption devices in the future. In addition, the tension type is desired from an aesthetic design point of view. In case of friction type or bearing type of connection, numerous number of heads and nuts of the high strength bolts appears on the outer surface of the members at the connection; whereas, in case of tensile joints, the bolts can be hidden inside the section of members, so that the surface of the connected section is smoothen and good appearance can be achieved.

Although the tension type has many advantages over the other types of bolted connections and welding connections, it has not been used as the joints of primary members of bridge structures in civil engineering field. It has been mainly used at the connection of structures constructed in the mountain area such as the steel erosion control dam, the transmission tower, the joints of the temporary facilities for construction ,the joints of the pipe lines and auxiliary fuel tank for rockets. As for building structures,

construction procedure is based on assembly on site, therefore, such joints have been frequently used at the connection of beams and columns. The main reason why it has not been used as the connection of primary members of civil engineering structures is that the design procedure is not specified in Japanese specifications for highway bridges(JSHB)[1]. Therefore, considering the circumstances mentioned above, the reliable and rational design procedure for the tension type should be established as urgently as possible and further study to understand the mechanical behavior of the tension type must be carried out.

1.2 Classification of High Strength Bolted Tensile Joints

In general, tensile joints are classified into two types according to the length of bolts. One type is called as short connection type with short bolts as shown in Fig. 1.2(a). Two plates are connected by short bolts, so that these plates are usually stiffened by triangular rib plates. The other type is called as long connection type with long bolts and additional ring plates, namely, double flanges stiffened by rectangular rib plates. Typical example of this type of joints is shown in Fig. 1.2(b).

As shown in Fig. 1.2(a), the applied load is transferred through flange plates with bolts, where the premature failure of flange plates are prevented by longitudinal stiffeners. Main technical problems of these joints are summarized as follows: Firstly, the most remarkable demerit is the occurrence of the prying force. The mechanism of the prying force is shown in Fig. 1.3. "R" in this figure designates the prying force. It is mainly caused by the deformation of the flange plate. This prying force occurs as an increase of contact compressive force at the outside of the bolt. The occurrence of the prying force is considered to be critical for the high strength bolted tensile joints because little increase in bolt force can be allowed due to the high pre-stress force initially given e.g. up to 80% of yield force of bolts. However, in case that the flange plate is thick enough, the deformation of the flange plate is negligible, so that the prying force can be limited at very low level. In order to prevent the occurrence of such a prying force, the bending stiffness of the flange plates; thus, the thickness of the flange plates is the key. Therefore, the flange plates are usually stiffened by longitudinal rib plates in practice. As mentioned here, previous studies on this type of joints have focused on only this prying force. Secondary, it is recognized that not only the structural details are very simple but also its erection procedure is very easy; therefore, it is possible that structural members are fabricated from steel plates and pipes by cutting and welding in automated factory and their assembly will be carried out on site. Two typical examples of the short connection type are shown in Fig. 1.4. One type is split tee type connection and another type is end plate connection. Split tee type connection is the simplest among short connection types and it consists of T-shape members and high strength bolts. High strength bolts are located at both sides of the tee web plate. On the other hand, end plate type connection consists of endplates welded at the end of the beam and high strength bolts. The former is often utilized in the United States, the latter is often used in Germany.

On the other hand, the long connection type is proposed because the prying force is very hard to occur due to the structural detail as shown in Fig. 1.2(b). However, the structural complexity has forced designers not to use this type of connection. Recently it is found that the deformation capacity of the joint as well as its energy absorption capacity is considered to be high, so that this type of joints is considered to be suitable for structures subjected to the loading with large intense. Very little study on this type of connection has been made in the past. However, due to aforementioned better characteristics, a lot of research activities are on going recently. Particularly, this long connection type is used at the connection of the suspension bridge tower, namely, Kurushima Strait Bridge under construction, and further utilization of long connection type is expected in the future.

1.3 State of the Arts on Study of High Strength Bolted Tensile Joints

The past studies are classified into 4 groups such as the study on short connection type, both split tee flange joints and end plate connections, the study on long connection type and the study on tube flange joints. Almost all the past studies are for short type connection and those are basically based on the experimental results. These are carried out for the application to building structures. However very little study for other connections can be found.

The studies on split tee flange joints have been carried out extensively in 1960-1970's. The main objectives of these studies were to estimate the prying force which is necessary for estimation of the maximum strength of the joints. In Japan, B. Kato and A. Tanaka who have proposed the design formula considering the prying force in 1968 are the first investigators on tensile joints[2]-[4]. The prying force is estimated by the cantilever model in which the deflection of the beam and the elongation of the bolt are taken into consideration. The amount of the prying force is varied as the thickness of the flange plate. Moreover, in 1972, T. Hashimoto and M. Fujimoto have also proposed the formula to estimate the prying force based on the analytical results for the bolt and plates adjacent to the bolt[5]-[8]. Consequently, in 1975, H. Tanaka and T. Tanaka have proposed the design formula which is used in the current design code for buildings in Japan[9][10]. In this formula, the estimation of the prying force is carried out by plastic analysis on cantilever model. On the other hand, in the United States, R. T. Douty and W. McGire proposed design formula using the cantilever model for estimation of the prying force[11]. In this formula, the prying force is assumed to be applied at the edge of the flange plate. Basically, these were the experimental studies in order to investigate the prying force vs. structural parameters such as the thickness of the flange plate, the position of the bolt, the bolt pre-stress force applied to the bolt. Although the many modified methods to estimate prying force have been proposed and various design formulas have been established, there exists many ambiguity in the applicable range for structural parameters. Furthermore, the various design formulas have been implemented with rigorous safety margin. Therefore, the general

and rational estimation method for general tensile joints should be established.

Almost all the studies on end plate connections are also based on the experimental results. Many bending tests for the beams which have end plate connections were carried out and mechanical behavior and the estimation of the maximum strength for this type of connections were investigated[12]-[15]. For example, A.N. Sherbourne carried out the bending test for bolted beam to column connections and proposed the design method based on fully plastic bending moment, considering the behavior of high strength bolt and that of end-plate in 1961. In 1973, M. Fujimoto and T. Hashimoto also carried out bending tests for end-plate connections and investigated applicability of the design formula for split tee connections to end plate connection experimentally.

As for the tube flange joint, the studies were based on the experimental approach as well as analytical approach. In 1966, K. Washio and K. Wakiyama et al. carried out the tensile loading test and investigated the mechanical behavior considering the thickness of the flange plate and the number of the bolt[16]. In 1972, K. Wakiyama and S. Kikukawa also carried out the tensile loading test in which focused are the prying action, that is, the effect of the prying force on tensile strength of tube joints was investigated[17]. In 1979, B. Kato and R. Hirose carried out the tensile loading test and investigated load carrying capacity under tension and proposed was the estimation method of load carrying capacity using yielding line theory[18]. In addition, there is a research work on limit state design method on tube flange joints with rib plate and without rib plates by S. Igarashi, K. Wakiyama and I. Inoue et al. [19][20]. Moreover, in 1992, E. Watanabe and co-workers carried out the monotonic bending test for the tube flange joints with rib plates and without rib plates and simple design method for general loading condition was proposed[21].

On the other hand, as for long connection type, the key studies have not been done yet as compared with lots of progress for short type connection. But fundamental studies have been carried out in 1960's in the architectural engineering field[13]. Recently, the research activity is becoming more active in civil engineering field since 1984. T. Nishiwaki and N. Masuda et al. have conducted a series of the tensile loading test for long connection type and investigated its mechanical behavior in which focused are the bolt pre-stress force, thickness of the base plate and change of bolt force[22]-[31]. As a result, the applicability of long type connection was found to be very high. In addition, T. Nishiwaki and Kuroda et al. investigated the effect of the contact surface on the mechanical behavior by the loading test as well as 2-dimensional finite element analyses, where the dimensions of the joints such as the position of the bolt, the number of the bolt, the length of the bolt were investigated in detail. Particularly, in 1995, the big movement occurred in Japan; that is, the connection of the tower for suspension bridge, namely, Kurushima Bridge was designed and being construction by tensile joints. Before this application, finite element analysis was carried out in order to assess the applicability of the joints and to investigate the mechanical behavior[32]. This construction is the first application to use tensile flange joints as the connection of primary members of bridge structures in Japan.

1.4 Technical Problems to be Solved for Future Application

According to the literature survey, the following problems are still considered to be solved in order to develop the rational design procedure of high strength bolted tensile flange joints.

(1) The rational estimation of the maximum load carrying capacity of tensile joints considering the prying action:
The applicable ranges of structural dimensions of the connection, such as the thickness of the flange plate, the width of the flange plate, the distance between the loading edge and the center of the bolt are made not clear in the estimation of the maximum strength in current design specification. Because the estimation is based on the experimental results and limited only for joints with thick flange plates. Therefore, the effect of each parameter on strength estimation is investigated in detail and estimation method applicable to wide range of parameters should be developed.

(2) The estimation of rigidity of the connection:
In the past studies, only an attention is paid to the load carrying capacity, not to the deformation or rigidity of the joints. However, from the view point of limit state design or energy absorption, the rigidity and deformation are important factors. For example, for accurate stability analysis on frame structures, to know the joint rigidity is very important. In addition, flexible structures which can absorb more energy at joints are desired for earthquake resistant design.

(3) Failure mode and its related strength:
It is desirable to choose the favorable failure mode by varying the geometrical configuration of the connection. For example, if the joint has thick flange plate, it will fail at the bolt whose strength and stiffness are high. On the other hand, if it has very thinner flange plate, it will be fail at the flange plate which is considered to be ductile. It is very important to control the failure mode from the view point of the demand required to joints. If the high earthquake resistance is required, the bending failure in the flange plate is desired to occur because energy absorption of this mode is high. On the other hand, if the high load carrying capacity is required, the bolt failure should be chosen. Therefore, it is necessary to understand the relation of structural dimensions and each failure mode.

(4) Investigation of mechanical behavior under cyclic loading:
In the application of tensile joints for civil engineering structures, the fatigue strength is very important factor, different form building structures. That is, the live load applied to the civil engineering structures is relatively large and dynamically applied as comparison with those to building structures. However, there is little information available about tensile joint behavior under cyclic and dynamic loading and there is only a report by Hirokawa et al.[34] in civil engineering. Therefore, the mechanical behavior under cyclic loading of this type of joints and the fatigue strength should be investigated.

1.5 Objectives and Scopes

This study focuses on the most popular tensile joints, that is, the short connection type. The objectives of this study are an investigation of the mechanical behavior of tensile joints under both static and cyclic loading in detail as well as feasibility study of its application to civil engineering structures. First of all, the mechanical behavior of the high strength bolt, which is the basic component of the joints, is investigated considering the effective cross sectional area, in other words, the stiffness and bolt pre-stress force. Secondly, the mechanical behavior of the split tee flange joint, which is the typical type of short connection type, is investigated where attention is paid to the contact/separate behavior, the stiffness of the joint. In addition, mechanical behavior of short connection type under cyclic loading is also an objective in this study. Lastly, the mechanical behavior and the simple design method for the tube flange joints are investigated as the application of the high strength bolted tensile flange joints.

Following Chapter 1 which describes the current status of the joint design and the applicability of the joints, in Chapter 2, the mechanical behavior of the high strength bolt is discussed. The high strength bolts are the most important component for bolted joints. Especially, the mechanical behavior under both monotonic and cyclic loading is investigated. The loading test and finite element analysis are carried out for static behavior, then the effective cross sectional area and the stiffness of the bolt is assessed by taking into consideration the bolt thread. In addition, the fatigue test for the bolt and stress concentration analysis by finite element analysis are carried out for understanding of the cyclic behavior, then the fatigue strength is assessed considering the bolt pre-stress force.

In Chapter 3, the mechanical behavior of the high strength bolt and adjacent joint elements is discussed. The tensile loading test as well as finite element analysis for such structural models are carried out. Paying attention to load transferring mechanism at joints, a contribution of bolts and adjacent plate elements is assessed. Finally, the stiffness and its effective cross sectional area are discussed.

In Chapter 4, the mechanical behavior of the split tee flange joint is discussed in detail as one of the basic assembly. Both static behavior and cyclic behavior of it is investigated. The tensile loading test and 3-dimensional finite element analysis are carried out for static behavior, namely, the mechanical behavior focusing on the contact surface, its stiffness and effective cross sectional area. In addition, as for the cyclic behavior, the cyclic loading test is carried out by paying attention to not only the overall deformation behavior of the split tee flange joints but also the local deformation behavior of the bolts and the flange plates. Furthermore, stress concentration analysis for the split tee flange joint is also carried out,

then the fatigue strength is assessed considering the failure mode and local stresses in the joints.

It is not suitable to carry out three dimensional analysis for designing the joints of structures all the time. Proper parameter limitation in the design specification or simple analysis method should be provided for saving time in the tedious design procedure for joints. Therefore, the simple analysis of the split tee flange joint, that is, 2-dimensional finite element analysis using the effective width coefficient is proposed and its applicability is investigated in Chapter 5.

In Chapter 6, the application of the high strength bolted tensile flange joint is discussed. For the tube flange joint used for steel erosion control dams, the loading test is carried out subjected to bending and tension. The mechanical behavior of such joints is discussed and compared to those of basic unit of tensile joints such as split tee joints. In addition, the simple design method for it is proposed based on these results.

In Chapter 7, the conclusions obtained from this study are summarized and the future research needs are also discussed.

References

1) Japan Road Association : Specifications of Highway Bridges(JSHB), Maruzen, 1991(in Japanese).
2) B.Kato, A.Tanaka : High Strength Bolted Tensile Joints -Influence of Bolt Pre-stress Force-, Journal of Structural and Construction Engineering, No. 146, Apr. 1968, pp. 21-27, Architectural Institute of Japan(in Japanese).
3) B.Kato, A.Tanaka : Experimental Study on High Strength Bolted Tensile Joints -Mechanical Behavior under monotonic tensile loading-, Journal of Structural and Construction Engineering, No. 147, May 1968, pp. 33-41, Architectural Institute of Japan(in Japanese).
4) B.Kato, A.Tanaka : Experimental Study on High Strength Bolted Tensile Joints -Connection Behavior of beam-column-, Journal of Structural and Construction Engineering, No. 151, Sep. 1968, pp. 31-38, Architectural Institute of Japan(in Japanese).
5) M.Fujimoto, T.hashimoto : High Strength Bolted Tensile Joints -Part 1 Axisymmetric elastic analysis for identification of initial stiffness of the plate(1)-, Journal of Structural and Construction Engineering, No. 164, Oct. 1969, pp. 27-33, Architectural Institute of Japan(in Japanese).
6) M.Fujimoto, T.Hashimoto : High Strength Bolted Tensile Joints -Part 1 Axisymmetric elastic analysis for identification of initial stiffness of the plate(2)-, Journal of Structural and Construction Engineering, No. 165, Nov. 1969, pp. 67-76, Architectural Institute of Japan(in Japanese).
7) M.Fujimoto, T.Hashimoto : High Strength Bolted Tensile Joints -Part 2 Analysis on Split Tee Joints(1)-, Journal of Structural and Construction Engineering, No. 190, Dec. 1971, pp. 59-67, Architectural Institute of Japan(in Japanese).
8) M.Fujimoto, T.Hashimoto : High Strength Bolted Tensile Joints -Part 2 Analysis on Split Tee Joints(2)-, Journal of Structural and Construction Engineering, No. 191, Jan. 1972, pp. 7-18, Architectural Institute of Japan(in Japanese).
9) T.Tanaka, A.Tanaka : Design Formulas for the Strength of T-stub Connection, JSSC Vol. 11 No. 120, Dec. 1975, pp. 5-10(in Japanese).
10) Architectural Institute of Japan : Recommendation for the Design Fabrication of High Strength Bolted Joints, Maruzen, Mar. 1993(in Japanese).
11) R.T.Douty, W.McGire : High Strength Bolted Moment Connections, Journal of the Structural Division, Proceedings of ASCE, Vol. 91, No. ST2, Apr. 1965, pp. 101-128.
12) A.N.Sherbourne : Bolted Beam to Column Connections, The Structural Engineer, June 1961, pp. 203-210.
13) T.Naka, B.Kato, S.Yoshimoto : High Strength Bolted Connections -Beam-Column Connections by High Strength Bolts-, Journal of Structural and Construction Engineering, No. 60, Oct. 1958, pp. 541-544, Architectural Institute of Japan(in Japanese).
14) K.Tanaka, Mukushiro, Analysis on High Strength Bolted Tensile Joints using End-Plate Connection, Summaries of Technical Papers of Annual Meeting(Tohoku Branch), AIJ, Oct. 1973, pp. 1177-1178(in Japanese).
15) T.Hashimoto : Study on End-Plate Connections -Part 2 Mechanical Behavior of End-Plate Connections, Summaries of Technical Papers of Annual Meeting(Tohoku Branch), AIJ, Oct. 1973, pp. 1179-1180(in Japanese).
16) K.Washio, K.Wakiyama, T. Iawanari : Study on Tube Flange Joints, Summaries of Technical Papers of Annual Meeting(Kinki Branch), AIJ, May 1966, Structure Material Construction, pp. 185-188(in Japanese).
17) K.Wakiyama, S.Kikukawa, Experimental Study on Mechanical Behavior of High Strength Bolted Tube Flange Joints, Summaries of Technical Papers of Annual Meeting(Kinki Branch), AIJ, June 1972, Structure II, pp. 157-160(in Japanese).
18) B.Kato, R.Hiorose : Bolted Tension Flange Joints of Circular Hollow Section Tubes, Journal of Structural and Construction Engineering, No. 339, May 1984, pp. 73-83, Architectural Institute of Japan(in Japanese).
19) S.Igarashi, K.Wakiyama, K.Inoue, T.Matsumoto, Y.Murase : Limit design of high strength bolted tube flange joints Part 1. Joint without rib-plates and ring-stiffeners, Journal of Structural and Construction Engineering, No. 354, Aug. 1985, pp. 52-66, Architectural Institute of Japan(in Japanese).
20) S.Igarashi, K.Wakiyama, K.Inoue, T.Matsumoto, Y.Murase : Limit design of high strength bolted tube flange joints Part 2. Joint with rib-plates and ring-stiffeners, Journal of Structural and Construction Engineering, No. 358, Dec. 1985, pp. 71-82, Architectural Institute of Japan(in Japanese).

21)E.Watanabe, K.Sugiura, T.Yamaguchi, S.Kasai : Design Method of High Strength Bolted Tube Flange Joints, Journal of Structural Engineering, JSCE, Vol. 38A, Mar. 1992, pp. 1-12(in Japanese).

22)K.Horie, T.Nishiwaki, N.Masuda, et al. : High Strength Bolted Tensile Joint -Long Connection Type- Part 1, Proc. of the 39th Annual Conference of JSCE, 1, JSCE, Oct. 1984, pp. 309-310(in Japanese).

23)K.Horie, T.Nishiwaki, N.Masuda, et al. : High Strength Bolted Tensile Joint -Long Connection Type- Part 2 Proc. of the 40th Annual Conference of JSCE, 1, JSCE, Oct. 1985, pp. 929-930(in Japanese).

24)T.Nishiwaki, N.Masuda, M.Minagawa et al. : High Strength Bolted Tensile Joint -Long Connection Type- Part 3 Proc. of the 41th Annual Conference of JSCE, 1, JSCE, Nov. 1986, pp. 563-564(in Japanese).

25)T.Nishiwaki N.Masuda, M.Minagawa : High Strength Bolted Tensile Joint -Long Connection Type- Part 4 Proc. of the 42th Annual Conference of JSCE, 1, JSCE, Sep. 1987, pp. 514-515(in Japanese).

26)M. Kuroda, T.Nishiwaki, N.Masuda et al. : Stress Behavior on High Strength Bolted Tensile Joint - Long Connection Type- Proc. of the 43th Annual Conference of JSCE, 1, JSCE, Oct. 1988, pp. 560-561(in Japanese).

27)T.Nishiwaki, N.Masuda, M.Minagawa et al. : Bolt Axial Force of Tension-Type Connection by Long Bolts, Journal of Structural Engineering, JSCE, Vol. 35A, Mar. 1989, pp. 991-999(in Japanese).

28)T.Nishiwaki, N.Masuda, M.Minagawa et al. : Bolt Axial Force of Long Bolt Tension Type Connections using Spring Model, Proc. of JSCE, No. 416/I-13, Apr. 1990, pp. 403-410(in Japanese).

29)T.Nishiwaki, M.Kuroda, N.Masuda, Y.Suzuki : Load Transferring Mechanism of Long Bolt Tension Type Connections considering Contact Surface, Proc. of JSCE, No. 428/I-15, Apr. 1991, pp. 87-96(in Japanese).

30)T.Nishiwaki, M.Kuroda, N.Masuda : Bolt Length and Hole Alignment in Long Bolt Tension Type Connections, Proc. of JSCE, No. 437/I-17, Oct. 1991, pp. 115-123(in Japanese).

31)M. Kuroda, T.Nishiwaki, N.Masuda et al. : Experimental Study on Tension Type Connections by Long Bolts Located at the One Side only, Proc. of the 45th Annual Conference of JSCE, 1, JSCE, Sep. 1990, pp. 298-299(in Japanese).

32)H.Ohashi, Y.Yanaka, Y.Mizukawa, A.Umeda : Mechanical Behavior of Long Tension Type Bolted Connections for Towers of a Suspension Bridge, Journal of Structural Engineering, JSCE, Vol. 41A, Mar. 1995, pp. 991-1001.

33)K.Ohi, H.Kondo, K.Takanashi et al. : Earthquake Response Tests on Steel Frames with Semi-Rigid Connections, Journal of Structural Engineering, AIJ, Vol. 39B, Mar. 1993, pp. 155-164(in Japanese).

34)H.Yamanari, K.Ogawa, Kurobane : Inelastic Behavior of Semi-Rigid Corner Connections with RHS Columns and Wide Flange Beams, Journal of Structural Engineering, AIJ, Vol. 40B, Mar. 1993, pp. 703-710(in Japanese).

35)Y.Miki, K.Horikawa : Fatigue Behavior on Split Tee Flange Joints, Proc. of the 46th Annual Conference of JSCE, 1, JSCE, Sep. 1991, pp. 606-607(in Japanese).

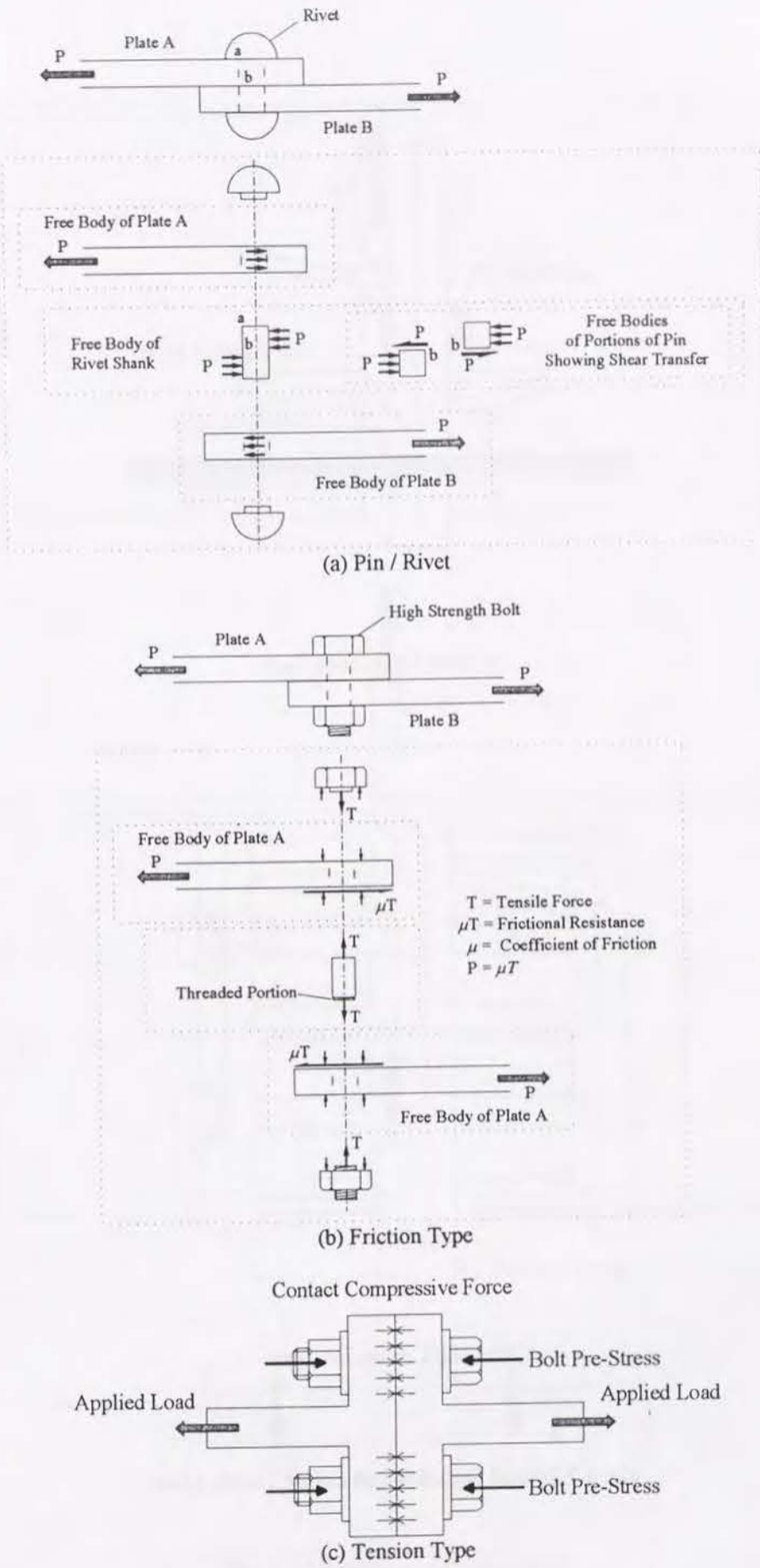

Fig. 1.1 Load Transferring Mechanism of the Connection using Fastener

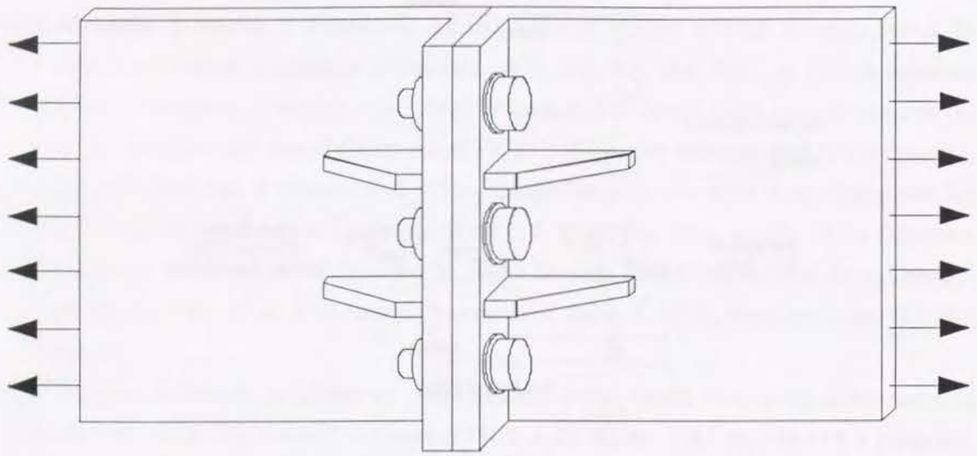

(a) Short Connection Type

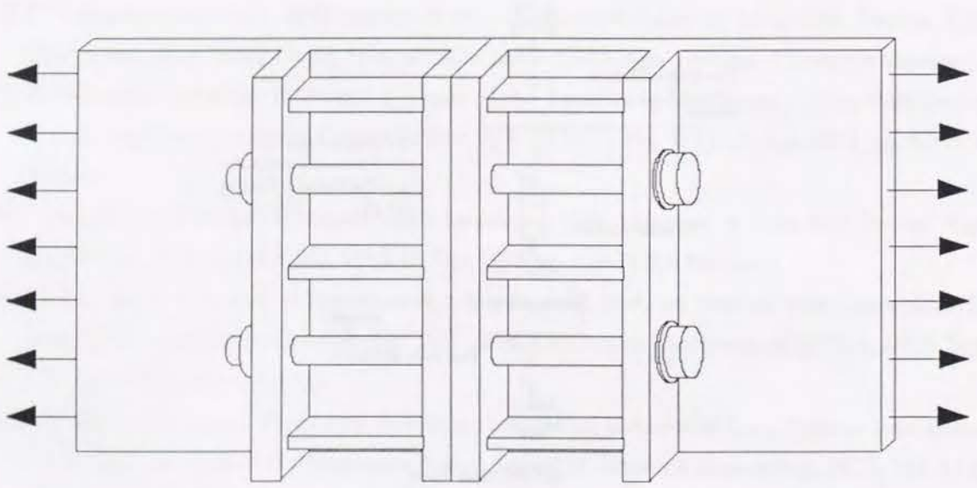

(b) Long Connection Type

Fig. 1.2 Typical High Strength Bolted Tensile Joints

(a)

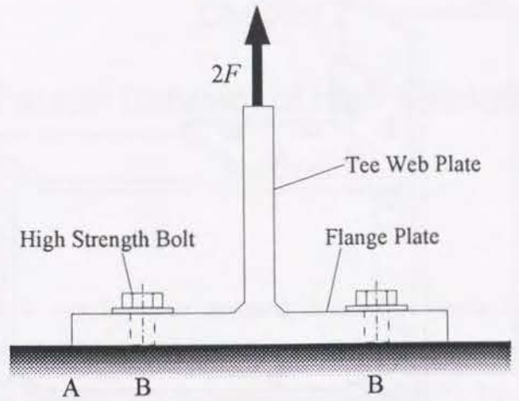

(b)

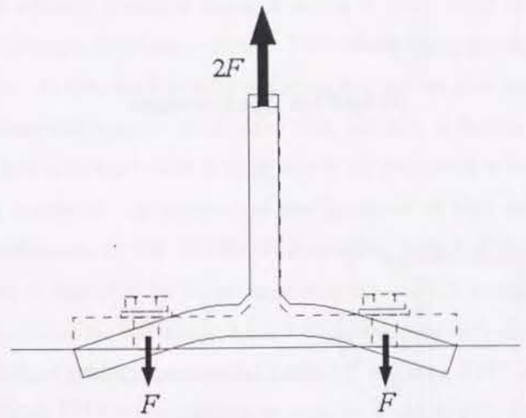

(c)

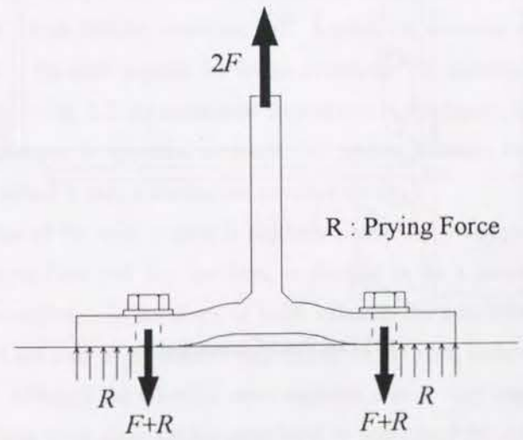

Fig. 1.3 Mechanism of Prying Force

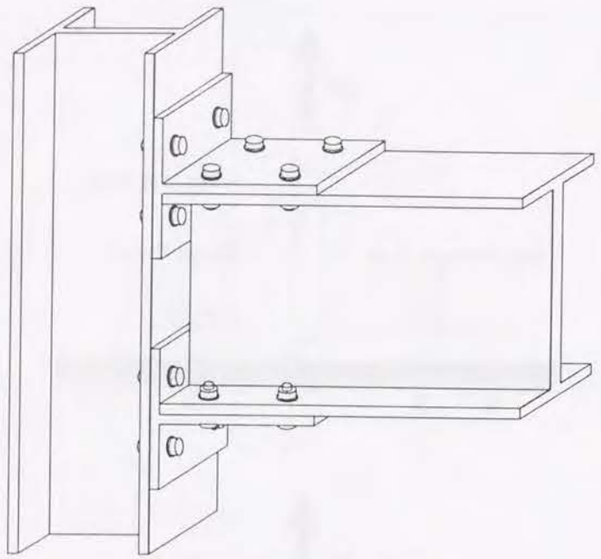

(a) Split Tee Type Connection

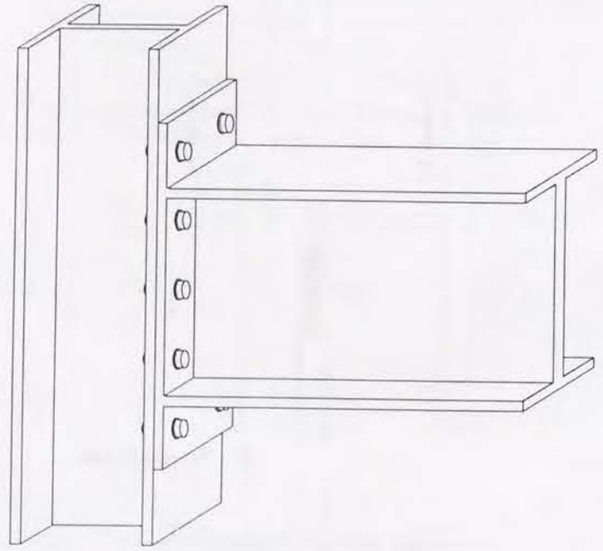

(b) End Plate Connection

Fig. 1.4 Typical Examples of Short Connection Type

Chapter 2

Mechanical Behavior of High Strength Bolts

2.1 Introduction

The high strength bolt is very important structural element for tensile flange joints. Therefore, to understand the mechanical behavior is very important not only for tensile joints but also for general bolted joints. The high strength bolt consists of the hexagonal head, bolt shank, bolt thread, nut, and washer as shown in Fig. 2.1. Since it is made of high strength steel, the strength of bolt is higher up to 100 (kgf/mm^2) compared to ordinary structural steels. It is one of the features that high strength bolts are manufactured keeping the torque coefficient constant. The manufacturing process of the high strength bolt is summarized as follows: At first, the bolt is formed using low carbon alloy steel or special steel such as chromium steel, chromium-molybdenum steel. After that, the bolt is heated up to about 800 °C for hardening and then the bolt is further heated at about 400 °C for tempering at last.

The material properties and geometrical configurations of high strength bolts and nuts are prescribed by the specification of JIS B1186-*1979*(Japanese Industrial Specification)[1]. The high strength bolt and nut set is classified by the material property and the nominal diameter. The nominal diameter is equivalent to that of the bolt shank. It has 3 strength grades such as F8T, F10T and F11T. The material property for all three grades is tabulated in Table 2.1. In Japan, F10T is generally used for bridge structures and strength grade F11T is prohibited to be used due to the delayed fracture frequently occurred in 1970's[2]. On the other hand, it has 7 nominal diameters, such as M12, M16, M20, M22, M24, M27 and M30. The number which follows character "M" denotes the diameter of the bolt in millimeters. Among these M22 bolt is the most popular for bridge structures. The geometrical configuration of bolts specified in JIS is shown in Fig. 2.2. As understood from shown in this figure, the shape of the bolt is very complicated and the geometry is specified in detail. The portion between bolt shank and bolt threads named incomplete bolt thread is only a section not specified clearly.

Since the shape of the cross section is suddenly changed at incomplete bolt thread section, the stress concentration occur here and this has been is thought to be a cause of delayed fracture. As mentioned above, the complexity in geometry of bolts indicates the possibility of failure at other high stress concentrated part not only at incomplete bolt thread. In the past, numerous studies on bolts have been carried out[3][4]. Although the effective cross sectional area is very important to understand joint behavior, its physical basis is not clear. On the other hand, to understand the deformation and the stiffness of bolts is very important to understand load transferring mechanism at joints and to design joints considering the deformation capacity or joint flexibility from the view point of earthquake resistance of

structures. Therefore, in this chapter; the mechanical behavior of bolts is investigated in detail by means of the experimental and analytical approaches.

2.2 Mechanical Behavior under Monotonic Loading

2.2.1 Experimental approach

(a) Outline of tensile loading test

The high strength bolt consists of different cross sectional area along bolt axis, so that the evaluation for overall bolt stiffness is very difficult. In this study, in order to estimate the overall stiffness of the high strength bolt accurately, the stiffness of the bolt shank and the bolt thread are evaluated separately by a tensile loading test. Therefore, the objective of this experiment is to evaluate total stiffness of the bolt taking into account the bolt thread; that is, effective cross sectional area based on the ratio of bolt thread to total bolt length between head and nut. The information obtained through this experiment is considered to be utilized for the design of bolted joints such as tensile joints, friction type joints.

In this section, monotonic loading test for two types of the bolt which has different nominal diameter, namely, M12 and M20 are described. The dimensions of all the specimens are summarized in Table 2.2. Five specimens for each nominal diameter are prepared in this experiment. Since the bolt shank and bolt thread should be prepared long enough to measure the average displacement(elongation) with a certain gage length, the bolt specimens are specially manufactured with enough length for both the bolt shank and the bolt thread.

The tensile loading is carried out by the testing machine by SHIMADZU as shown in Fig. 2.3, whose loading capacity is +/- 30 (tonf) under static loading (+/- 20 (tonf) under dynamic loading) and the displacement stroke is +/- 50 (mm). This is a electrically controlled closed loop hydraulic actuator. The schematic view of the setup used in this experiment is shown in Fig. 2.4. As shown in this figure, hinge connections are used in order to avoid the eccentric loading. As for the measuring system used in the experiment, the average elongation along the bolt shank, the average elongation within the bolt thread and the total elongation between bolt head and nut are measured separately as shown in Fig. 2.5. The strain gage type displacement transducer with resolution of 500 (μ/mm) such as shown in this figure is used for the measurement of the total displacement, and extensometer with gage length of 30 (mm) is used for the measurement of the elongation at the bolt thread and the elongation of the bolt shank is measured by another extensometer with gage length of 12.5 (mm). The loading is operated by the micro computer and control command from the computer is send to analog-controller of actuator through GP-IB. In addition on line measuring are made by the same computer.

(b) Experimental results and discussions

All the test specimens are failed at the bolt thread within about 10 (mm) away from the edge of the nut as

shown in Fig. 2.6. It is observed that the fracture surface of each specimen is fine enough to conclude that the failure is brittle. The load-average strain curves obtained from the experiment are also shown in Fig. 2.7. As the elongation depends on the stiffness of bolts, the elongation is normalized by a certain gage length; namely, the average strain is used for estimation of the load-displacement behavior of each cross section. In this figure, the horizontal axis shows the average strain and the vertical axis shows the tensile load. It is understood that the strain at the bolt thread is larger than that of the bolt shank, and that the total strain of the bolt is larger than that of the bolt shank and smaller than that of the bolt thread. Therefore, load-displacement curve of bolts is considered to depend on relative length of the bolt thread.

The initial tangential slopes of each load-average strain curve in Fig. 2.7 are calculated by the least square method and elastic properties of bolt materials are summarized in Table 2.3. In addition, the maximum loads of each specimen are tabulated in Table 2.4. It is found that maximum load is higher than the nominal value given in the specification of JIS, so that the quality of bolt specified in JIS is satisfied. As shown in Fig. 2.7, after the tensile load reached to the peak load, the load began to decrease although the overall elongation increase. Therefore, it is understood that the elastic unloading occurs at the bolt shank; and that the severe plastic deformation takes place only in bolt thread.

2.2.2 Analytical approach

(a)Outline of analytical method

The finite element analysis is carried out in order to investigate the mechanical behavior, especially, local load-deformation relationship at different cross section such as bolt shank and bolt thread. The effect of various parameters on the mechanical behavior could not be made clear by only experiments due to time and cost limitation. Furthermore, it is also difficult to investigate the local average stress/strain states by only experiments due to structural complexity and size of bolts.

In this section, 2 dimensional finite element analysis is carried out in order to understand the local stress/strain state for three types of bolts, M12, M20 and M22. Although the material is same, it is considered that the difference in nominal diameter may cause different relation in inelastic state. Here, the bolt is modeled as the axisymmetric problem. Dimensions of the analytical models are referred to those of specimens used in the experiment. Namely, geometrical configurations of analytical models are reproduced to be same with test specimens as much as possible. The shape of the bolt thread and the transition area between bolt shank and bolt thread, in other words, incomplete bolt thread are also referred to the specific value of JIS. Boundary condition is also assumed as shown in Fig. 2.8. Tensile load is applied at the end of the bolt as an uniform load. Furthermore, the displacement in the axial direction is fixed at the bolt head. Finite element discretization by triangle elements with constant strain for each bolt are shown in Fig. 2.9. Particularly, the location considered to have a high stress concentration such as the bolt thread and the bolt shank near the bolt head, is discretized by fine mesh. The number of elements and nodal points for each analytical model is listed in Table 2.5. Material

properties used in this analysis is also given in Table 2.6. These values are referred to the nominal values of high strength steel specified by JIS. Moreover, the stress-strain relationship of the material is assumed to be elastic perfectly-plastic.

(b) Analytical results

Load-average strain curves obtained by the finite element analysis are shown in Fig. 2.10. The comparison of the initial slope of load-average strain curves obtained by the finite element analysis to that obtained by the experiment is shown in Table 2.7. The slope based on the effective cross sectional area specified in JIS is also shown by a solid line for reference. It can be seen that analytical results are in good agreement with the experimental results; so that it is considered that the modeling such as discretization, boundary condition are applicable. Next, the load-stiffness curves are shown in Fig. 2.11. Stiffness in these figures means the slope of the load-average strain curve and it is calculated by dividing the increment of load by corresponding increment of average strain. It is found from these figures that the stiffness of the bolt shank is almost same as that given by the cross sectional area of the bolt shank for all the cases and that the stiffness of the bolt thread is lower than that obtained based on the effective cross section specified by JIS. However, it is found that the overall stiffness of the bolt is little higher than that based on the effective cross sectional area specified in JIS, and the stiffness estimation by JIS is considered to be a little conservative. But the estimation of the effective cross sectional area by JIS may happen to be smaller if the bolt has much longer bolt thread within clamped length, namely, distance between the bolt head and the nut,. Furthermore, it is found that the stiffness of the bolt is kept high even the tensile load reached to the bolt pre-stress force.

It is concluded that the effective cross sectional area of the high strength bolt including the bolt shank and the bolt thread significantly depends on the length of the bolt thread, and that effective cross sectional area specified in JIS may be a little conservative if the bolt and the nut set is properly used.

2.2.3 Assessment of the effective cross sectional area of the high strength bolt

As the high strength bolt has different cross section along the longitudinal axis of bolts such as bolt shank, bolt thread, not like PC tendons with the uniform cross section, it is difficult to estimate the effective cross sectional area which represents the overall stiffness of the bolt. This effective cross sectional area of bolts is very important for design of the joints from the view point of joint-deformability and working stress check. The accurate estimation of the stiffness of the bolt is needed for rational design of the joints. In JIS, effective cross sectional area has been determined based on only the strength. However, in case that the various limit states are considered, the estimation of the effective cross sectional area should be made based on strength and the deformation of joint element.

The model that bolt shank and bolt thread are connected in series as shown in Fig. 2.12 is utilized for this assessment. The stiffness of each section is determined by results of the tensile loading test, whose values are already listed in Table 2.7. The total stiffness of the model can be obtained from

the following equation.

$$\frac{1}{k_0}=\frac{1}{k_1}+\frac{1}{k_2} \tag{2.1}$$

in which k_0, k_1, and k_2 are total stiffness, stiffness of the bolt shank and stiffness of the bolt thread respectively. Total stiffness obtained using above equation is shown in Table 2.8. It is understood that the stiffness obtained by the proposed model and that obtained from experiments are in good agreement; therefore, it is concluded that the proposed model is accurate enough to estimate the stiffness of the bolts with various length. Comparison of the effective cross sectional area specified in JIS to the effective cross sectional area obtained by the proposed model are shown in Fig. 2.13. The effective cross sectional area of the bolt, A_0 is defined by the following equation.

$$A_0=\frac{x+s}{\left\{\frac{x}{(EA)_1}+\frac{s}{(EA)_2}\right\}E} \tag{2.2}$$

in which E, $(EA)_1$, $(EA)_2$ are Young's modulus of bolt material, slope of the load-strain curve at the bolt shank, the slope of the load-strain curve at the bolt thread respectively. And x, s are the length of the bolt shank and the length of bolt thread respectively

The horizontal axis shows the length of the bolt threads or the bolt shank, the vertical axis shows the effective cross sectional area which relates to the stiffness. It is found from these figures that if the length of bolt threads is short compared with the length of the bolt shank, the effective cross sectional area is larger than that specification in JIS. On the other hand, it is understood that if the length of the bolt threads becomes much larger, the effective cross sectional area by JIS is smaller than the actual cross sectional area. Therefore, it is concluded that if the bolt threads length is less than the 0.4 times of bolt shank length, the effective cross sectional area by JIS becomes conservative. In case of M12 and M20, the length of bolt thread suggested by JIS is less than 25 (mm) and 30 (mm) respectively, so that the length of bolt shank should be more than 62.5 (mm) and 70 (mm) respectively.

2.2.4 Simple analysis of high strength bolt

In general, the analytical approach is considered to be very powerful for the parametric study on engineering problems including many structural parameters, particularly for 3-dimensional structures. 3-dimensional analysis may be required in order to investigate the structural behavior of bolted connections in detail. But geometry of the high strength bolts is very complex such as the incomplete bolt thread and the bolt thread, so that the bolts have to be discretized with fine mesh. Therefore simple model of high strength bolts is needed in terms of load-deformation relation where the shape of the bolt thread must be taken into consideration. In this section, based on load-strain relationship obtained from the

aforementioned tensile loading test, the simple modeling of the bolt is proposed.

In this study, two simple modeling are proposed and those are schematically shown in Fig. 2.14. These modeling are described in detail as follows:

Model A : Assume the cross sectional area of the bolt thread is same as that of the bolt shank,

Model B : Assume the Young's modulus of the bolt thread is same as that of the bolt shank.

The cross section of Model A is constant along the bolt axis, so that the finite element discretization is very easy. This is suitable for the analysis of the large joint system. However, effective material properties for the bolt thread should be used. On the other hand, Model B is more physical because the same material properties are used for the bolt thread. In order to take into consideration the effect of stress concentration in bolt thread, effective cross section should be defined. The material properties used in these modeling are summarized in Table 2.9. These values are determined by the experimental results described in 2.2.1.

The validity of these modeling is checked by an axisymmetric model of high strength bolts. The finite element discretization of these models and boundary conditions are shown in Fig. 2.15. The boundary condition used in this analysis is same as that of exact modeling used in previous section. In the exact modeling a shape of the bolt thread and transition area are exactly modeled. The comparison of the number of the elements and nodes between proposed simple modeling and exact modeling is shown in Table 2.10. From the fact that the number of elements and nodes of proposed simple modeling is much fewer than that of exact modeling. Therefore, the proposed modeling for the high strength bolts is considered to be very effective.

The load-strain curves by the simple modeling are shown in Fig. 2.16. In these figures, the curves obtained by the tensile loading test are also shown for comparison. It is understood that the curve obtained by the simple modeling is in good agreement with the curve obtained by the experiment. Therefore, the proposed simple modeling should be able to be applied for the analysis of structures with the high strength bolts. Next, in order to assess validity of stress distribution predicted by the simple modeling of the bolt, the stress concentration ratios are compared with that of exact modeling. Maximum stress and its location are shown in Table 2.11. The maximum stress is normalized by the average stress of the bolt at uniform cross section(bolt shank). Compared with the results of exact modeling, Model B is more appropriate than Model A as for the prediction of the location where the maximum stress occurs; however, it is due to the geometrical discontinuity at bolt shank and bolt threads. Moreover, both modeling are not sufficient for estimation of the magnitude of the maximum stress. As a result, it is thought that the estimation of stress distribution using proposed simple modeling is not satisfactory and

further modification such as implementation of modification factor should be made. However it is considered to be good enough to use these proposed modeling in order to obtain the global load-deformation relationship of the bolt for structural analysis.

2.3 Fatigue Strength of High Strength Bolts

2.3.1 General remarks on fatigue strength

In this section, fatigue strength of the high strength bolts is discussed. To investigate the fatigue strength of the high strength bolts is important for the design of tensile joints. Because durability assessment for the traffic load is very important in civil engineering structures due to large live load and long service life. Accordingly, the fatigue strength of the bolt, which is basic component of the joint, is a necessary information to establish a rational design procedure of the tensile joints. However, few research on the fatigue strength of the high strength bolt can be found in civil engineering as well as architectural engineering[5][6]. In addition, especially, little study on the fatigue strength of the bolt considering the bolt pre-stress force can be found. Fatigue strength of the high strength bolt is considered to be significantly affected by the bolt pre-stress force because the bolt pre-stress force make a certain section such as the bolt thread or the incomplete bolt thread and the bolt thread be locally yielded. Therefore, the fatigue test for the high strength bolts is carried out and stress analysis by FEM is also done.

2.3.2 Outline of fatigue test

The fatigue test is carried out varying the bolt pre-stress force in order to investigate the effect of the bolt pre-stress force on fatigue strength. The specimens listed in Table 2.12(a) are prepared for the fatigue test. Same as the monotonic tensile loading test, the specimens with different nominal diameter i.e. M12, M20 and M22 are considered. Dimensions of test specimens are shown in Table 2.12(b). Material properties of bolts specified in JIS are also summarized in this table. Test setup used in this fatigue test is shown in Fig. 2.17, which is the same as that used in the tensile monotonic loading test. Stress ranges applied in this fatigue test are tabulated in Table 2.13. They are determined based on the guideline for fatigue design of steel structures[7]. The S-N curve specified in the guideline is shown in Fig. 2.18. Magnitude of the applied stress range is constant for specimens with different nominal diameter. As mentioned above, in order to investigate the effect of the bolt pre-stress force on fatigue strength, the stress cycles are applied by setting mean stress to the bolt pre-stress force. Here, the bolt pre-stress force are determined to be 61.3 (kN) according to the specification of JIS[1]. In addition, 30.7 (kN) which is 0.5 times of the bolt pre-stress force is also considered. This fatigue test is carried out by load control. Before the fatigue test, the test loading is carried out in order to obtain the maximum frequency in which the load-time curve can be reproduced by the sinusoidal curve, and then, its frequency is determined to be 2.0 (Hz) according to the

loading capacity of the testing machine. However, it is determined to be 0.5 Hz in case of the large stress range. Loading procedure is summarized as follows: At first, the prescribed bolt pre-stress force is given to the high strength bolt; then, the stress cycles applied in the sinusoidal wave form with specified stress range.

2.3.3 Results of fatigue test and discussions

The fatigue life for each stress range obtained from the test is tabulated in Table 2.14 and plotted in Fig. 2.19. The design S-N curve specified in the guideline is also shown for a reference. All the specimens are failed at the bolt thread near the nut as shown in Fig. 2.20. Comparing with the result of monotonic loading test, the location of failure in the fatigue test is much closer to the nut. It is observed that the failure surface is very fine, so that the brittle failure is considered to occur. It is found from this figure that the fatigue life of all the cases are longer than that given by the guideline for fatigue design. Therefore, fatigue life estimated by the guideline is considered to have enough safety margin, namely, fatigue life given in the guideline is considered to be very conservative. Moreover, compared with the bolt which has different nominal diameter, there exist little difference on fatigue life. Therefore, it is concluded that fatigue life is not significantly affected by the difference in geometrical configurations of bolts as long as if the bolt configuration satisfies JIS.

Comparing M12-A with M12-D, M12-B with M12-E, M20-A with M20-D, M20-B with M20-E, it can be seen that the fatigue life of the high strength bolt is moderately affected by the bolt pre-stress force. In case that 50 % of bolt pre-stress force determined by JIS is given, it is found that the fatigue life is 1.2 times longer than that in case that 100 % of bolt pre-stress force is given. It may be thought that the higher bolt pre-stress force makes the fatigue life shorter because the severe stress concentration at the bolt thread and the bolt shank near the bolt head make bolts yielded locally. In addition, it is found from this figure that the slope of design S-N curve is different from that obtained in this fatigue test. This also concludes that the slope of S-N curve is also affected by the level of the pre-tension force. In the future, farther fatigue test is required to set the reliable design S-N curve considering bolt pre-stress force.

2.3.4 Outline of stress concentration analysis

As mentioned in the previous section, the local stress concentration might affect the fatigue strength of bolts. Since the fatigue test cannot provide actual stress distribution or maximum stress, stress analysis is carried out by axisymmetric finite element modeling for bolts in order to investigate the physical aspect of the fatigue strength based on local stress concentration. The finite element model is shown in Fig. 2.21 where the washer is omitted for simplicity. In addition, boundary conditions used in this analytical model and finite element discretization by triangle elements with constant strain are also shown in Fig. 2.21. Three cases taken into consideration for different nominal diameter such as M12, M20, M22 are prepared.

The geometry of the analytical model is the same as that of the specimens use in the fatigue test in previous sections. The shape of the bolt thread in the analytical model is referred to the specification of JIS. As for the discretization, the location considered to have a high stress concentration, such as the bolt thread and bolt shank near the bolt head, is discretized by fine mesh. The number of the elements and degrees of freedom for each cases are summarized in Table 2.15 respectively. Material properties used in this analysis are also given in Table 2.16, which are determined based on the specification of JIS and stress-strain relationship of the material is assumed to be elastic perfectly plastic.

2.3.5 Analytical results and discussions

Maximum stress concentration factor of the bolt and its location obtained from the analysis are shown in Fig. 2.21. Here, stress concentration factor K is defined to be the ratio of the actual stress to the nominal stress as follows;

$$K = \frac{\sigma_{eq}}{\sigma_n} \tag{2.3}$$

in which K, σ_n ,σ_{eq} are the stress concentration factor, the nominal stress and the equivalent stress respectively. The nominal stress σ_n in this consideration is the stress by dividing the applied tensile load by the effective cross sectional area of the bolt specified in JIS.

For all the cases, it is found that the maximum stress concentration is about 3.0, and that it occurs at the transition area between the bolt shank and the bolt thread; namely, incomplete bolt thread. It is understood that higher stress compared with the nominal stress exists, therefore, the bolt pre-stress force may cause a local yielding. Next, the stress concentration factor at the bolt shank near the bolt head, incomplete bolt thread and the bolt thread are compared in Fig. 2.23. In this figure, the order of the stress concentration factor of the each location is also shown in Fig. 2.23. It is found that there is almost no difference on stress concentration at the bolt thread and at the incomplete bolt thread among the bolts which have different nominal diameters. But the difference of stress concentration exists at the bolt shank near the bolt head; namely, stress concentration factor of M22 is 30 % smaller than that of M12 at the bolt shank near the head. As for the stress state of the bolt when the prescribed pre-stress force(61.3 kN) by JIS is given, incomplete bolt thread and the bolt thread is locally yielded for all the cases, but the bolt shank near the head is not yielded for M20, M22, but yielded for M12.

From these analytical results, it is found that the location where the shape of cross section is changed, such as bolt shank near the bolt head, incomplete bolt thread and the bolt thread is yielded. It is concluded that the fatigue strength of the pre-tensioned high strength bolt is considered to be affected by the bolt pre-stress force significantly.

In the future, compared with the fatigue test results, the failure occurred at the bolt thread near the nut. But the stress concentration at the bolt thread obtained from the stress concentration analysis is

not so high due to the lack of nut modeling. Therefore, in order to assess the actual phenomena, the modeling including the nut section in the finite element analysis may be required.

2.4 Conclusions

In this chapter, the mechanical behavior of the high strength bolts under both static and cyclic loading are investigated experimentally and analytically. In addition, the simple modeling of high strength bolts considering the effective local-elongation relation of each section such as the bolt shank and the bolt thread is proposed, and its applicability is investigated. The following conclusions and future research needs are obtained:

1) When the tensile load is applied to the high strength bolts, strain of the bolt thread is larger than that of the bolt shank, and total strain of the bolt is larger than that of the bolt shank and smaller than that of the bolt thread. Namely, it is understood that severe plastic deformation take place in bolt thread and that load-displacement curve of the bolt depends on relative length of the bolt thread.
2) The effective cross sectional area specified in JIS has considerably high safety margin in general use, but in case of the bolt with long bolt thread, the effective cross sectional area specified in JIS may become critical from the view point of the stiffness of the bolts; however the ductility could be improved.
3) The simple finite element modeling of the high strength bolts useful for the joint system analysis is proposed based on the load-deformation behavior of the bolt shank and bolt thread, and it is verified that this modeling is effective for investigation of load-deformation behavior of bolted joints. In the future, for the stress verification, this simple modeling should be modified.
4) Fatigue failure of high strength bolts occurs at the bolt thread near the nut. Fatigue strength of high strength bolts given by the guideline for fatigue design of steel structures is considerably conservative, and it is significantly affected by bolt pre-stress force. When bolt pre-stress force is applied to the bolt, the bolt has already yielded locally at the bolt thread and incomplete bolt thread.

In the future, in order to estimate the fatigue strength quantitatively, further fatigue test and parametric stress analysis varying the shape of the bolt and bolt pre-stress force should be required. Moreover, the analysis including the nut section is expected for accurate consideration of failure mode of the bolts. Especially, based on these results, relationship between stress concentration factor and fatigue strength should be made clear. Furthermore, the results obtained in this chapter are expected to be used as the fundamental information of the joints with high strength bolts.

References

1) Japanese Industrial Standard Committee : Sets of High Strength Hexagon Bolt, Hexagon Nut and Plain Washers for Friction Grip Joints(B1186), 1979.
2) Japanese Society of Steel Construction, Joint Subcommittee, Strength of bolts Working Group : Delayed Fracture of High Strength Bolt, JSSC, Vol. 15, No. 158, Mar. 1979.
3) A.Hashimoto : Mechanical Properties of F10T High strength Bolts Subjected to Direct Tension, Journal of Structural and Construction Engineering, No. 309, Nov. 1981, Architectural Institute of Japan.
4) K.Wakiyama, K.Hirai : A Study on Fatigue of High Strength Bolt, Journal of Structural and Construction Engineering, No. 288, Feb. 1980, Architectural Institute of Japan(in Japanese).
5) Y.Miki, K.Horikawa : Fatigue Behavior on Split Tee Flange Joints, Proc. of the 46th Annual Conference of JSCE, 1, JSCE, Sep. 1991, pp. 606-607(in Japanese).
6) K.Wakiyama, K.Hirai : A Study on Fatigue of High Strength Bolt, Journal of Structural and Construction Engineering, No. 288, Feb. 1980, pp. 21-27, Architectural Institute of Japan(in Japanese).
7) Japanese Society of Steel Construction : Recommendation for Fatigue Design, Apr. 1993(in Japanese).

Table 2.1 Material Properties of High Strength Bolt specified in JIS

Classification	Yield Stress (kgf/mm^2)	Ultimate Stress (kgf/mm^2)	Elongation (%)	Contraction of Area(%)
F8T	more than 64	80-100	16以上	more than 45
F10T	more than 90	100-120	14以上	more than 40
F11T	more than 95	110-130	14以上	more than 40

Table 2.2 Dimensions of Specimens

(a)Design Dimensions

(unit : mm)

Type of Bolt	Diameter of Bolt Shank (d1)	Length of Bolt shank and Bolt Thread (l)	Length of Bolt Thread (s)
M12	12	210	115
M20	20		
M22	22		

(b) Table of Measuring Dimensions of the Specimens

Specimen	B	C	d_{11}	d_{12}	d_{13}	d_{10}	d_1	d_2'	d_2	d_3	d_0	H	l	s
M12-1	26.80	23.40	12.00	11.95	12.00	11.98	12.00	-	12.00	11.95	11.98	10.10	199.80	116.15
M12-2	26.75	23.35	11.95	11.95	12.05	11.98	12.00	-	12.05	12.00	12.02	10.20	199.60	115.65
M12-3	26.75	23.35	11.95	12.00	12.05	12.00	12.00	-	12.00	11.95	11.98	10.25	199.60	115.15
M12-4	26.75	23.35	12.00	11.95	12.00	11.98	12.00	-	12.00	11.95	11.98	10.00	199.95	115.90
M12-5	26.80	23.35	11.90	11.95	12.00	11.95	12.00	-	12.05	11.95	12.00	10.20	199.90	115.00
M20-1	33.90	29.60	19.90	19.85	19.80	19.85	19.90	19.90	19.35	19.90	19.90	13.10	199.70	114.50
M20-2	33.65	29.50	19.90	19.80	19.80	19.83	19.85	19.85	19.15	19.85	19.85	13.40	199.25	115.25
M20-3	34.00	29.55	19.95	19.85	19.80	19.87	19.80	19.85	19.15	19.80	19.82	13.05	199.90	115.60
M20-4	33.75	29.45	19.85	19.80	19.80	19.82	19.85	19.85	19.20	19.85	19.85	13.50	199.55	114.60
M20-5	34.20	29.50	20.00	19.90	19.85	19.92	19.80	19.80	19.15	19.85	19.82	13.25	199.95	115.25
M22-1	35.90	31.35	22.60	22.05	22.00	22.22	22.05	22.00	21.05	21.85	21.97	15.15	199.40	114.15
M22-2	35.80	31.30	22.60	22.20	22.10	22.30	22.10	22.00	21.10	21.80	21.97			
M22-3	35.85	31.35	22.40	21.10	21.95	22.15	21.95	22.10	21.15	21.80	21.95			
M22-4	35.90	31.30	22.40	21.95	21.95	22.10	21.95	22.00	21.15	21.80	21.92			
M22-5	36.10	31.30	22.55	21.95	22.00	21.17	21.95	22.00	21.05	21.80	21.92			

Note : $d_{10}=(d_{11}+d_{12}+d_{13})/3$, $d_0=(d_1+d_2+d_3)/3$

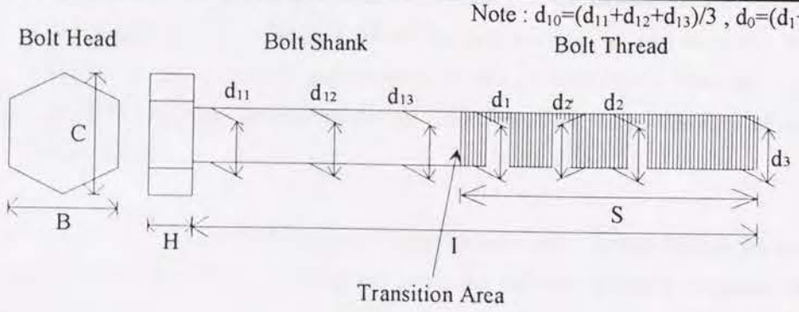

Table 2.3 Slope of Load-Strain Curve at Elastic Area

(a) M20

Specimen	Bolt Shank (tonf)	Bolt Thread (tonf)	Total (tonf)	Young's Modulus (Bolt Shank) (kgf/mm^2)
M20-01	-	-	-	-
M20-02	6200	5014	5799	19730
M20-03	6900	4531	4462	21960
M20-04	6395	4904	5934	20350
M20-05	7013	4710	7783	22320
Mean	6627	4790	5995	21090
Coefficient of Variation	0.05115	0.03859	0.1972	0.05122

(b)M12

Specimen	Bolt Shank (tonf)	Bolt Thread (tonf)	Total (tonf)	Young's Modulus (Bolt Shank) (kgf/mm^2)
M12-01	-	-	-	-
M12-02	-	-	-	-
M12-03	2402	1814	1746	21240
M12-04	2458	1820	1858	21730
M12-05	2534	1600	2226	22400
Mean	2465	1745	1943	21790
Coefficient of Variation	0.02195	0.05864	0.1055	0.02182

Table 2.4 List of Ultimate Strength

Specimen	Ultimate Strength (tonf)	Specimen	Ultimate Strength (tonf)
M12-01	(9.6480)	M20-01	(27.9720)
M12-02	-	M20-02	27.6180
M12-03	9.7560	M20-03	27.7860
M12-04	9.6720	M20-04	27.8640
M12-05	9.6560	M20-05	27.8640
Mean	9.695	Mean	27.783
Coefficient of Variation	0.004524	Coefficient of Variation	0.003615
Minimum Tensile Strength	8.43	Minimum Tensile Strength	24.5

Table 2.5 Numbers of Elements and Nodal Points

Analytical Model	Number of Elements	Number of Nodal Points	Number of Degrees of Freedom
M12	4,418	2,687	5,374
M20	3,867	2,387	4,774
M22	3,867	2,387	4,774

Table 2.6 Material Properties used in The Analysis

Young's Modulus (kgf/mm^2)	Poisson's Ratio	Yielding Stress (kgf/mm^2)
21,000	0.3	95.0

Table 2.7 Comparison of the Stiffness between the Experimental Results and Analytical Results

Bolt Type		Bolt Shank (tonf)	Bolt Thread (tonf)	Total (tonf)	Young's Modulus (kgf/mm^2)
M12	Experiment	2,465	1,745	1,943	2,1790
	Analysis	2,367	1,582	2,043	2,0927
M20	Experiment	6,627	4,790	5,995	2,1090
	Analysis	6,578	4,905	5,599	2,0938

Table 2.8 Comparison of the Total Stiffness(EA_0) between the Experiment and Proposed Model

Bolt Type	Experiment	Proposed Model	Relative Error
M12	5,995	5,561	7.2%
M20	1,943	2,033	4.6%

unit : tonf

Table 2.9 Material Properties for Simple Analytical Model

Bolt Type		a	c	n	Yielding Stress σ_y (kgf/mm^2)	Young's Modulus at Bolt Thread E (kgf/mm^2)	Cross Sectional Area at Bolt Thread A (mm^2)
M12	Method 1	0.00156	100.6	0.0416	76.8	15,422	113.1
	Method 2	0.00115	139.6	0.0383	109.9	21,790	80.2
M20	Method 1	0.00198	106.9	0.0476	79.5	15,245	314.1
	Method 2	0.00116	142.5	0.0392	109.3	21,090	228.1

Table 2.10 Comparison of Numbers of Elements and Nodal Points between the Exact Model and the Simple Model

	M12		M20	
	Number of Nodal Points	Number of Elements	Number of Nodal Points	Number of Elements
Exact Model	2,699	4,418	2,387	3,868
Method 1 Model	253	402	345	582
Method 2 Model	278	427	370	607

Table 2.11 Maximum Stress and its Location

		Exact Model	Method 1	Method 2
Stress Concentration Factor	M12	2.6705	0.8613	1.0829
	M20	2.9246	0.7888	1.2284
Location where Maximum Stress is Arisen		TA	BH	TA

[NOTE]

TA: Transition Area between Bolt Shank and Bolt Thread

BH: Bolt Shank near Bolt Head

Table 2.12 List of Specimens for Fatigue Test

(a) Design dimensions

Bolt Type	Diameter of Bolt d_1 (mm)	Length of Bolt Shank and Bolt Thread l (mm)	Length of Threaded Portion s(mm)	Yielding Stress (kgf/mm^2)	Effective Cross Sectional Area (mm^2)	Minimum Tensile Strength (kgf)	Standard Bolt Pre-stress Force P_1 (kgf)	One Half of P_1 $P_2=0.5P_1$ (kgf)
M12	12	200	115	90.0	84	8,430	6,260	3,130
M20	20				245	24,500	18,200	9,100
M22	22				303	30,300	22,600	11,300

(b)Measuring Dimensions

(unit : mm)

Specimen	B	C	d_{11}	d_{12}	d_{13}	d_{10}	d_1	d_2'	d_2	d_3	d_0	H	l	s
M12-A	26.75	23.35	11.95	11.95	12.00	11.97	12.00	-	12.00	12.00	12.00	10.25	199.70	116.20
M12-B	26.80	23.35	11.95	12.00	12.00	11.98	12.00	-	12.00	12.00	12.00	10.00	200.00	114.95
M12-C	26.75	23.40	12.00	12.00	12.00	12.00	12.05	-	12.00	12.00	12.02	10.25	200.00	115.65
M12-D	26.75	23.35	11.95	12.00	12.05	12.00	12.00	-	12.05	11.95	12.00	10.20	199.70	114.70
M12-E	26.80	23.45	11.95	11.95	12.00	11.97	12.00	-	12.00	11.95	11.98	10.20	200.00	114.10
M20-A	33.90	29.60	19.90	19.80	19.80	19.83	19.80	19.80	19.10	19.80	19.80	12.85	200.00	115.65
M20-B	33.80	29.50	19.90	19.80	19.85	19.85	9.85	19.85	19.20	19.80	19.83	13.00	200.00	118.60
M20-C	34.00	29.60	19.90	19.80	19.80	19.83	19.80	19.80	19.15	19.80	19.82	13.00	199.75	114.65
M20-D	33.90	29.60	19.85	19.80	19.85	19.83	19.85	19.85	19.10	19.80	19.83	13.00	200.10	116.45
M20-E	33.90	29.40	19.90	19.80	19.85	19.85	19.85	19.85	19.10	19.85	19.85	13.00	199.75	116.85
M22-A	35.90	31.30	22.40	22.00	22.00	22.13	22.05	22.00	21.15	21.80	21.95	15.45	200.60	117.95
M22-B	35.90	31.40	22.50	22.10	22.05	22.22	21.95	22.00	21.10	21.85	21.93	14.60	200.50	116.60
M22-C	35.85	31.35	22.40	22.00	22.00	22.13	21.95	21.95	21.20	21.85	21.92			
M22-D	35.90	31.35	22.45	22.05	22.05	22.18	22.05	22.00	21.10	21.90	21.98			
M22-F	36.00	31.35	22.50	22.00	22.00	22.17	22.00	22.00	21.10	21.85	21.95			

Note : $d_{10}=(d_{11}+d_{12}+d_{13})/3$, $d_0=(d_1+d_2+d_3)/3$

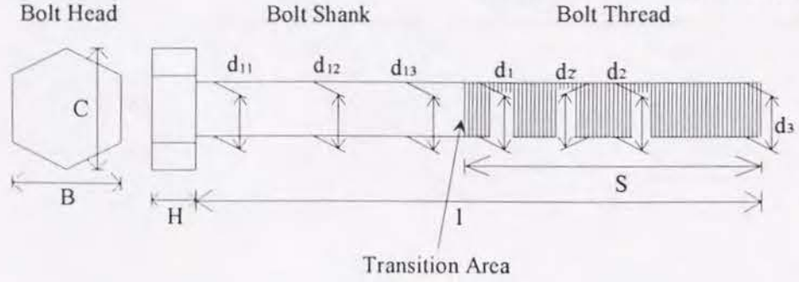

Table 2.13 List of Stress Ranges Applied to the Specimens

Specimen	Bolt Pre-stress Force (kgf)	Load Range (kgf)	Stress Range σ_a (kgf/mm^2)	Bolt Pre-stress σ_P (kgf/mm^2)	σ_a/σ_b	Loading Period (Hz)
M12-A	6,260	2,520	30	74.3	0.41	2
M12-B	6,260	1,680	20	74.3	0.27	2
M12-C	6,260	840	10	74.3	0.14	2
M12-D	3,130	2,520	30	37.1	0.41	2
M12-E	3,130	1,680	20	37.1	0.27	2
M20-A	18,200	7,350	30	74.3	0.41	2
M20-B	18,200	4,900	20	74.3	0.27	2
M20-C	18,200	2,450	10	74.3	0.14	2
M20-D	9,100	7,350	30	37.1	0.41	2
M20-E	9,100	4,900	20	37.1	0.27	2
M22-A	22,600	9,090	30	74.3	0.41	0.5
M22-B	22,600	6,060	20	74.3	0.27	0.5
M22-C	22,600	3,030	10	74.3	0.14	0.5
M22-D	11,300	9,090	30	37.1	0.41	0.5
M22-E	11,300	6,060	20	37.1	0.27	0.5

Table 2.14 Result of Fatigue Test (Number of Cycle to Failure)

Specimen	A	B	C	D	E
M12	23,913	68,688	not failed	35,589	123,580
M20	26,516	89,513	676,074	32,132	122,459
M22	25,975	59,562	-	-	-

[NOTE] - : Experiment was not carried out.

Table 2.15 Number of Elements and Nodal Points of Stress Concentration Analysis

Analytical Model	Number of Elements	Number of Nodal Points	Number of Degrees of Freedom
M12	4,418	2,687	5,374
M20	3,867	2,387	4,774
M22	3,867	2,387	4,774

Table 2.16 Material Properties of Stress Concentration Analysis

Young's Modulus (kgf/mm^2)	Poisson's Ratio	Yielding Stress (kgf/mm^2)
21,000	0.3	95.0

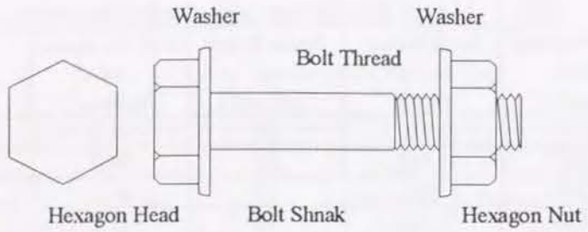

Fig. 2.1 High Strength Bolt and Nut Set

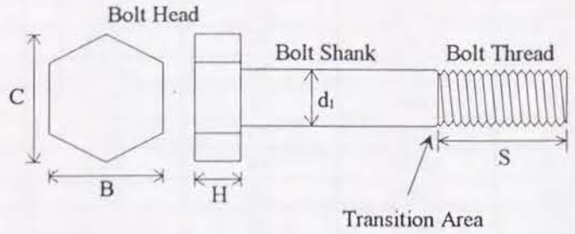

Dimensions of High Strength Bolt Specified by JIS(JIS B 0205)

Bolt Type (d)	d_1 Standard Length	d_1 Tolerance	H Standard Length	H Tolerance	B Standard Length	B Tolerance	C About	s Standard Length	s Tolerance
M12	12	+0.7 -0.2	8	+0.8 -0.8	22	0 -0.8	25.4	25	+5 0
M20	20	+0.8	13	+0.9	32	0	37	35	+6
M22	22	-0.4	14	-0.9	36	-1	41.6	40	0

(unit : mm)

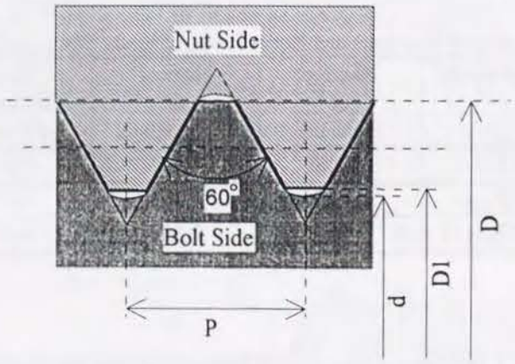

Dimensions of Bolt Thread Specified by JIS (JIS B 0205)

	Pitch (P)	Diameter (D1)	Diamter (D)	Diameter (d)
M12	1.75	10.106	12.000	4.91
M20	2.5	17.294	20.000	8.467
M22	2.5	19.294	22.000	9.467

(unit : mm)

Fig. 2.2 Geometrical Configurations of High Strength Bolt

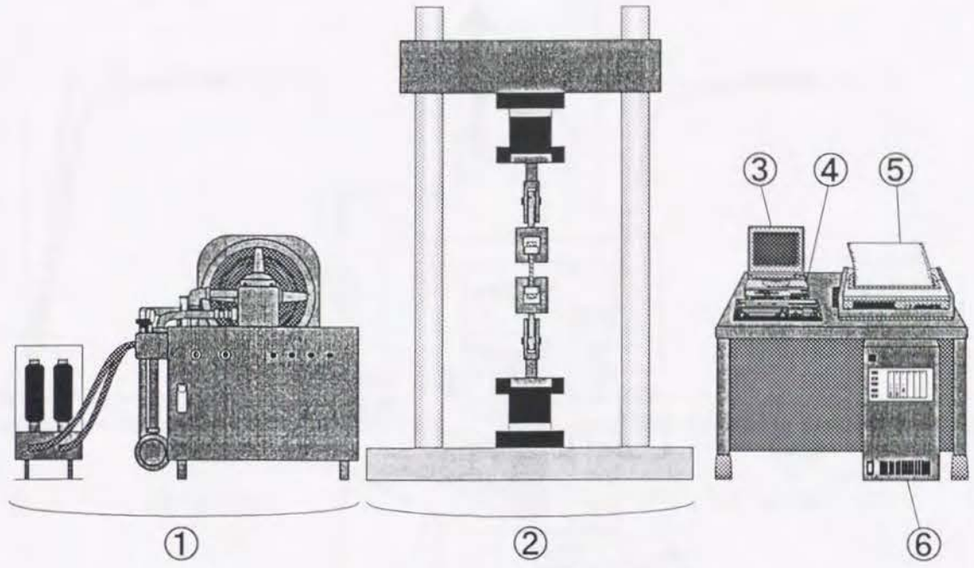

① Hydraulic Pump
② Testing Machine
③ Display
④ Micro Computer
⑤ Printer
⑥ Controler

Fig. 2.3 Loading System

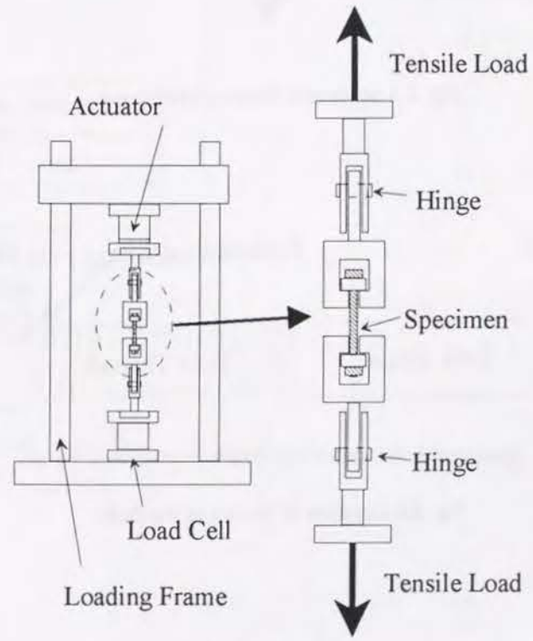

Fig. 2.4 Testing Setup

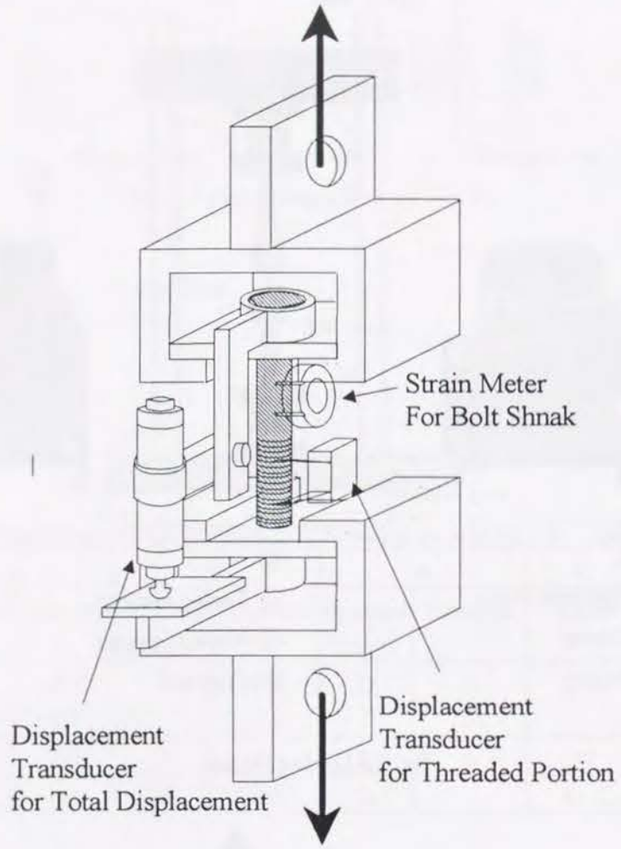

Fig. 2.5 Schematic View of Measuring

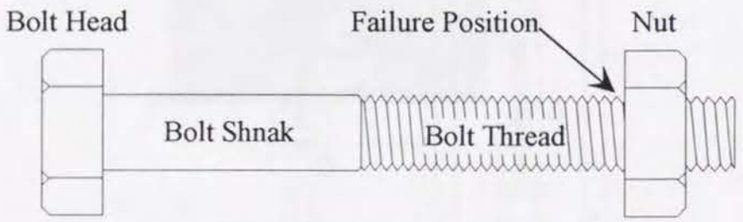

Fig. 2.6 Location of Failure of the Bolt

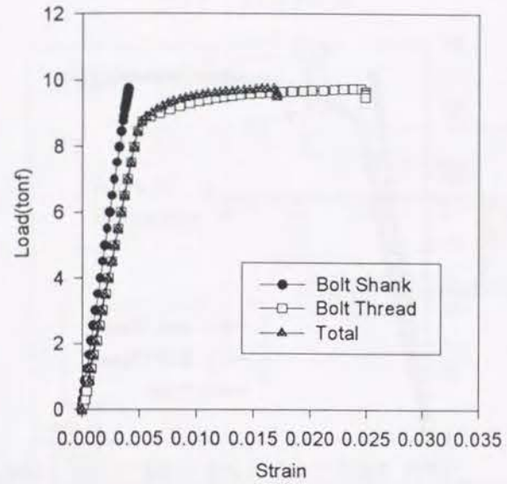

(a) M12-03

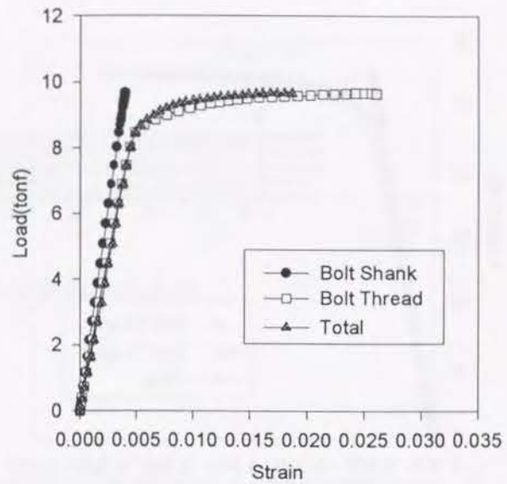

(b) M12-04

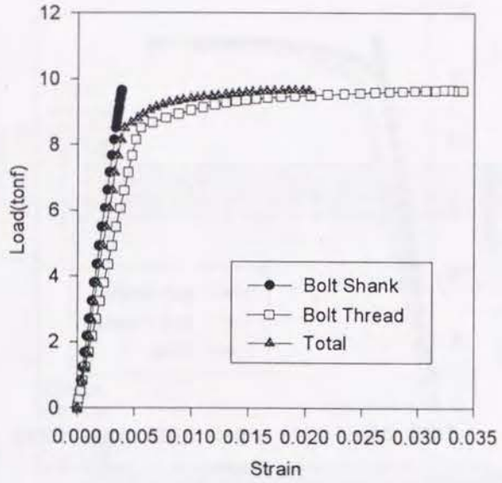

(c) M12-05

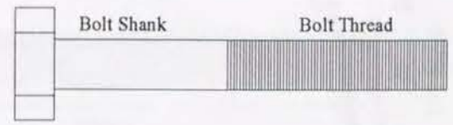

Fig. 2.7 Load-Strain Curves (Experiment) (M12) (continued)

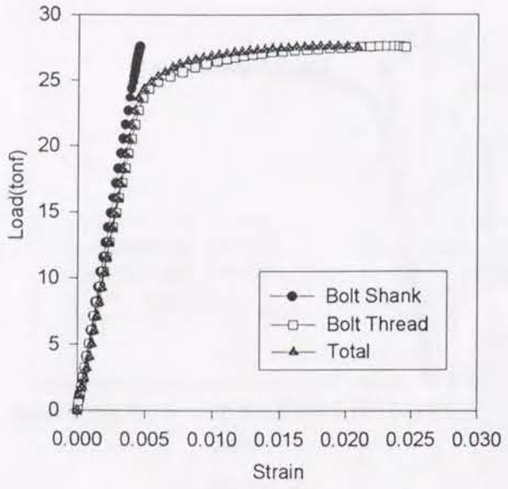

(a) M20-02

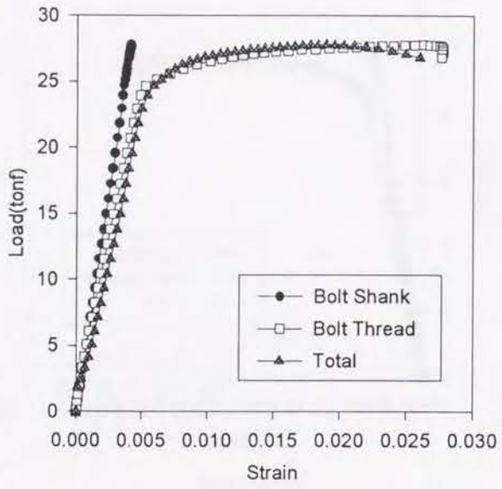

(b) M20-03

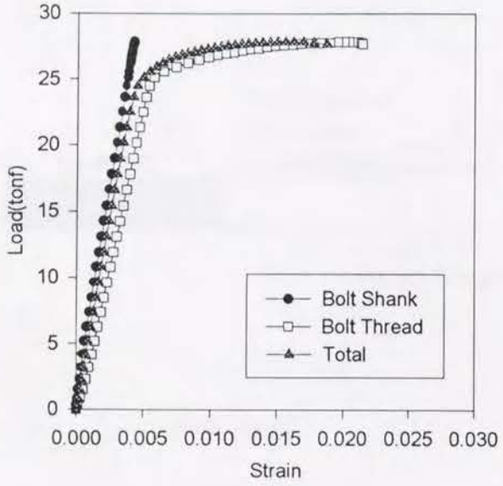

(c) M20-04

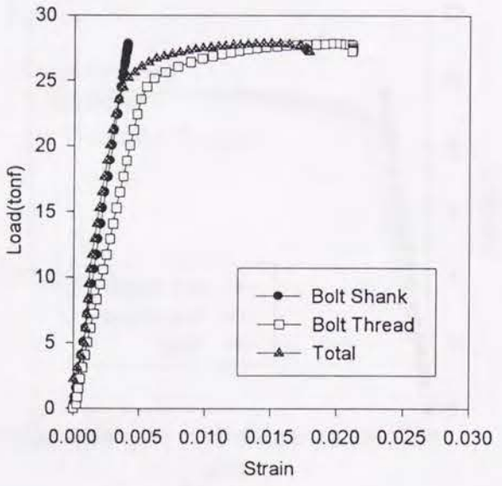

(d) M20-05

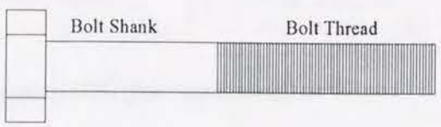

Fig. 2.7 Load-Strain Curves (Experiment) (M20)

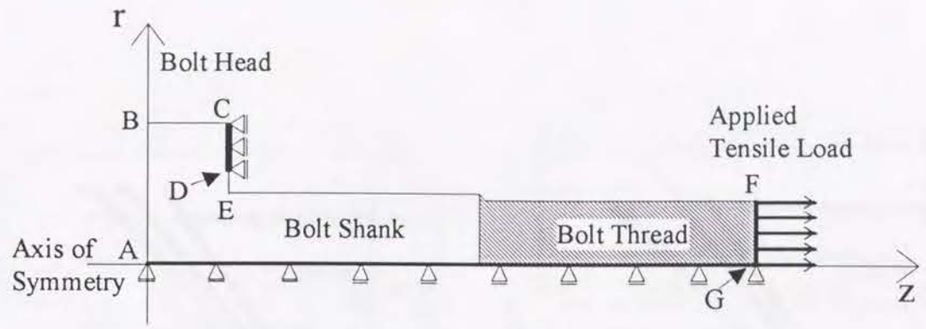

Fig. 2.8 Analytical Model for High Strength Bolts

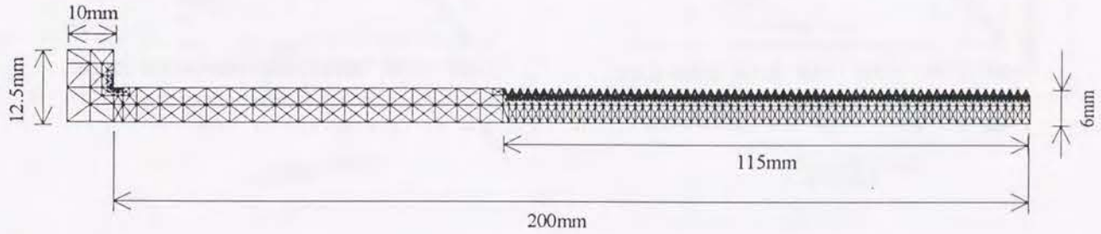

(a) M12

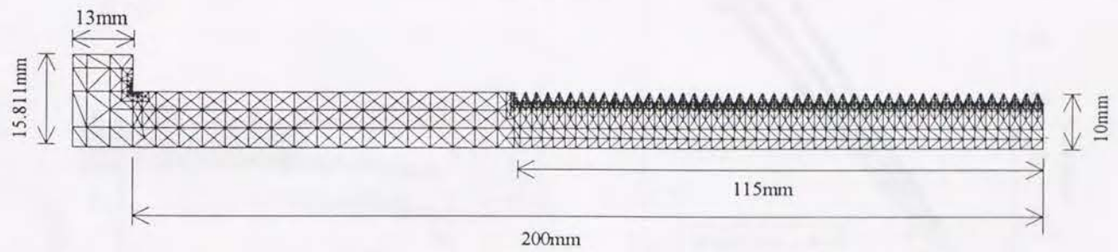

(b) M20

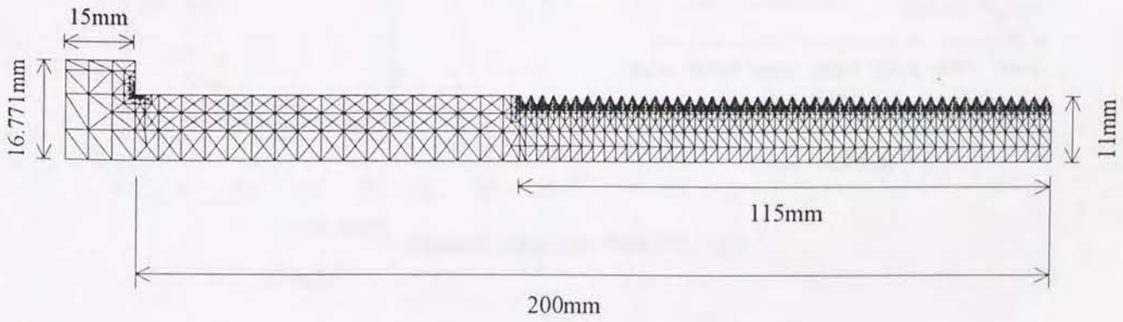

(c) M22

Fig. 2.9 Finite Element Discretization by Triangle Elements

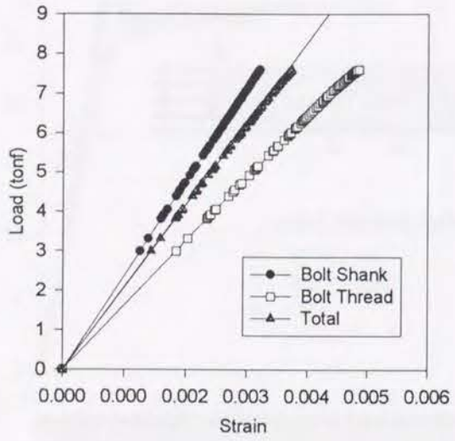

(a) M12

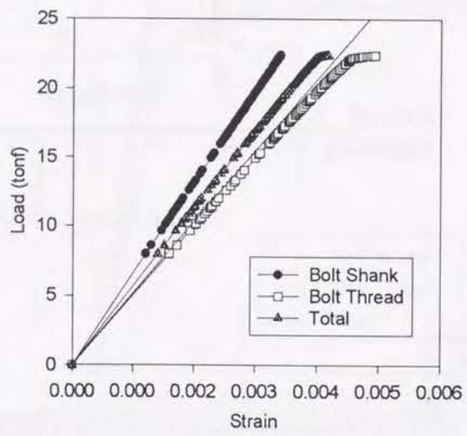

(b) M20

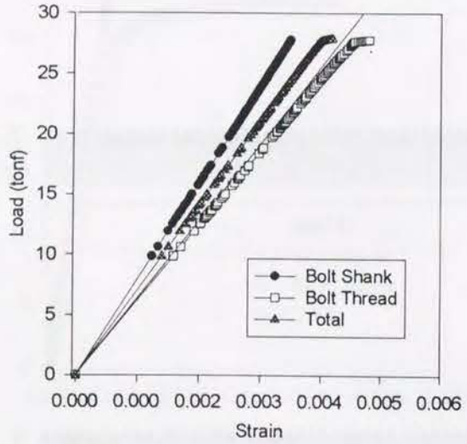

(c) M22

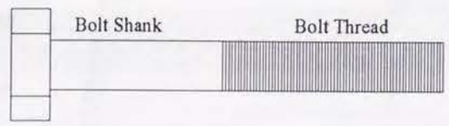

Fig. 2.10 Load-Strain Curves (Analysis)

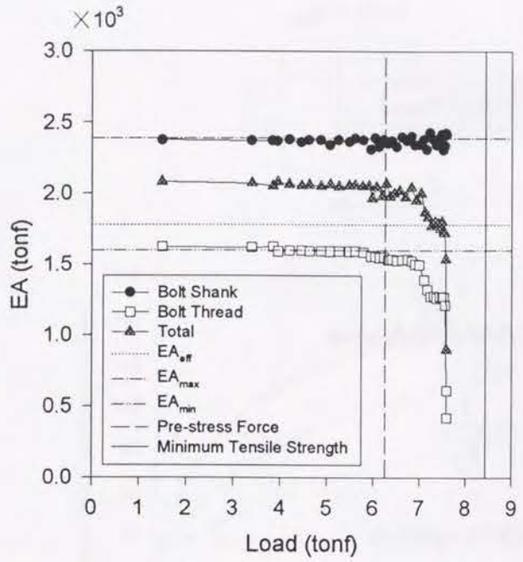

(a) M12

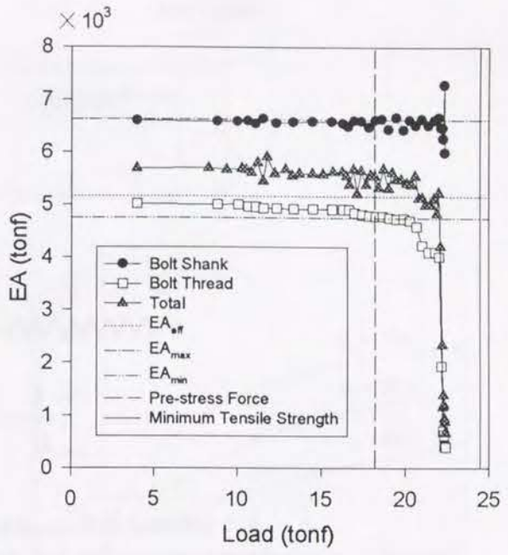

(b) M20

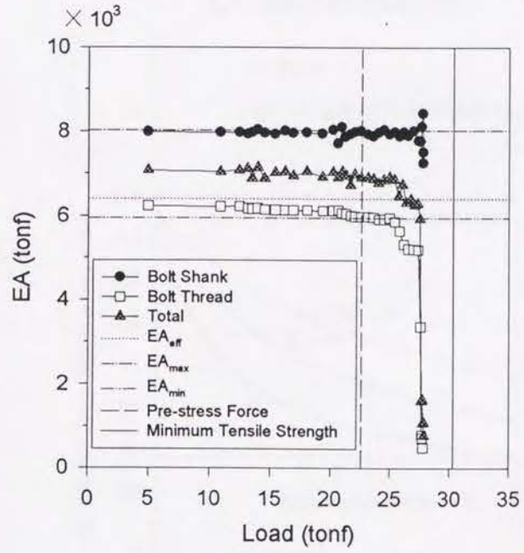

(c) M22

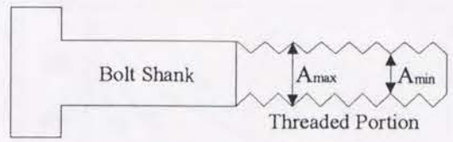

Fig. 2.11 Load-Stiffness Curves (Analysis)

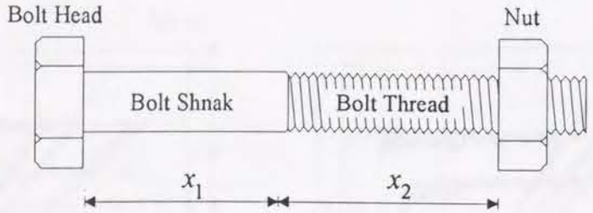

$$\frac{1}{k_0} = \frac{1}{k_1} + \frac{1}{k_2}$$

k_0 : Effective Stiffness of the High Strength Bolt
k_1 : Stiffness of the Bolt Shank
k_2 : Stiffness of the Bolt Thread

Fig. 2.12 Evaluation Model for the Total Stiffness of the Bolt

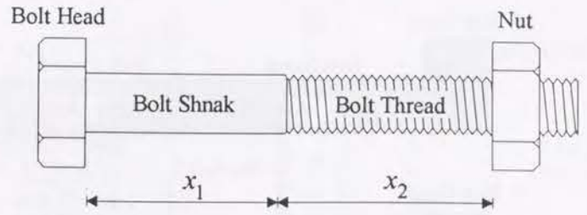

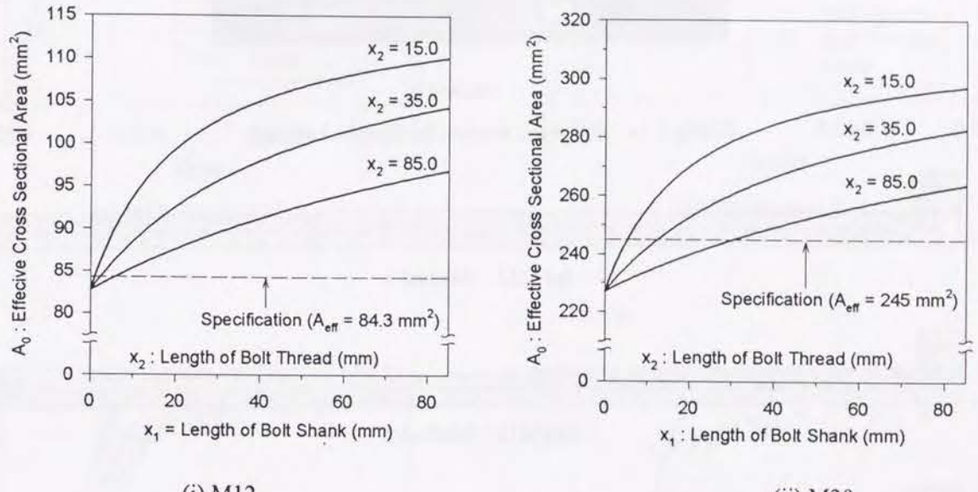

(i) M12 (ii) M20

(a) Length of Bolt Shank vs. Effective Cross Sectional Area

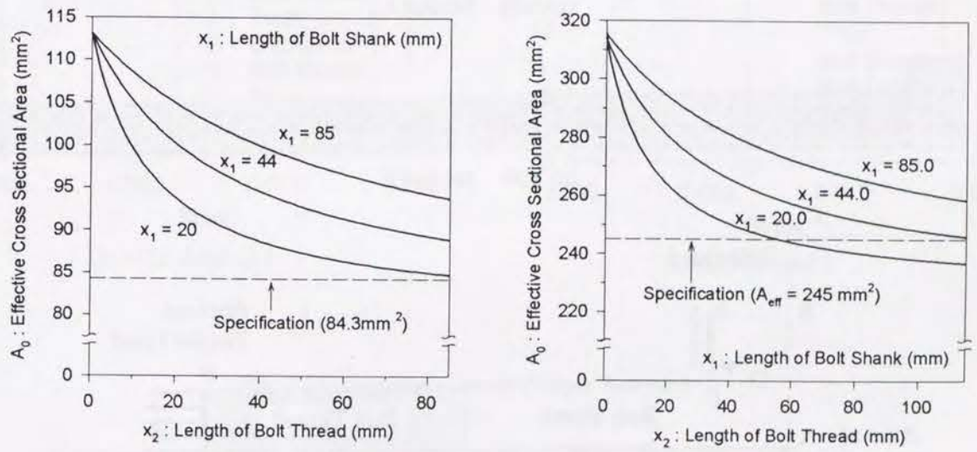

(i) M12 (ii) M20

(b) Length of Bolt Thread vs. Effective Cross Sectional Area

Fig. 2.13 Evaluation Results

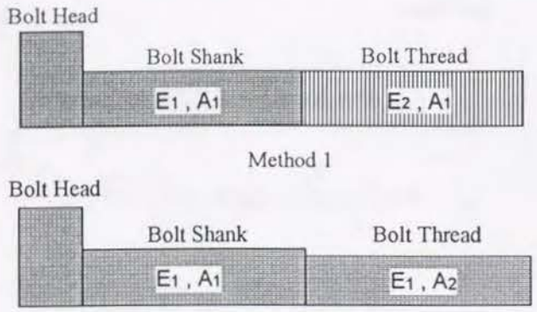

Fig.2.14 Proposed Models for Simple Analysis

(a) M12 Method 1

(b) M12 Method 2

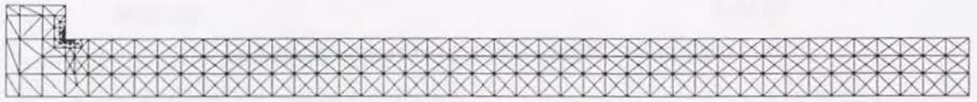

(c) M20 Method 1

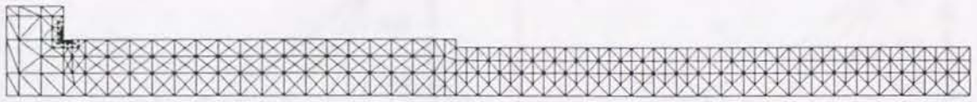

(d) M20 Method 2

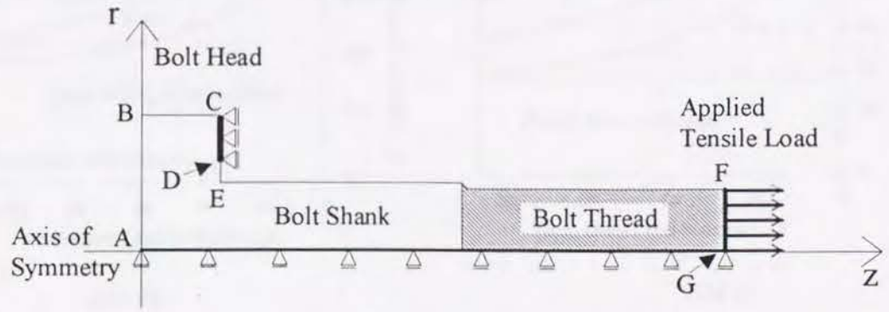

(e) Boundary Condition

Fig. 2.15 Finite Element Discretization and Boundary Conditions of the Simple Models

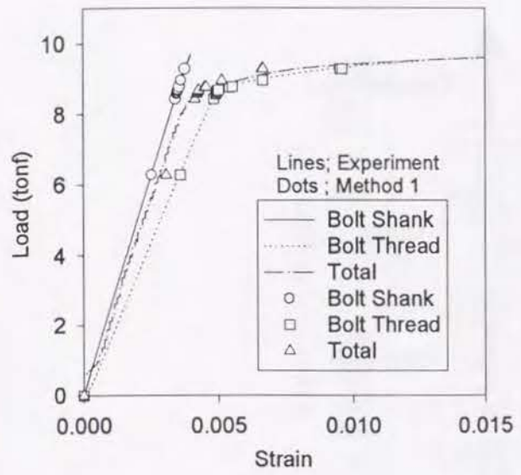

(a) M12 -Method 1

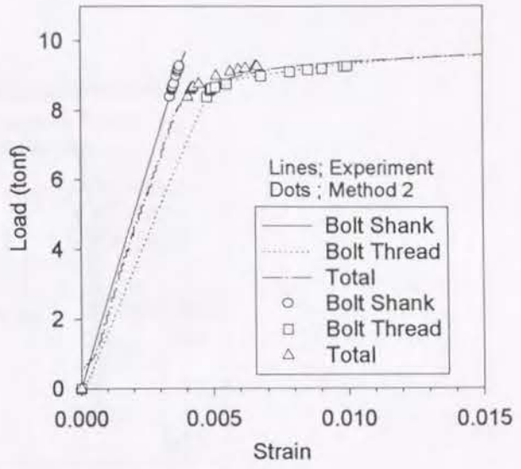

(b)M20-Method 2

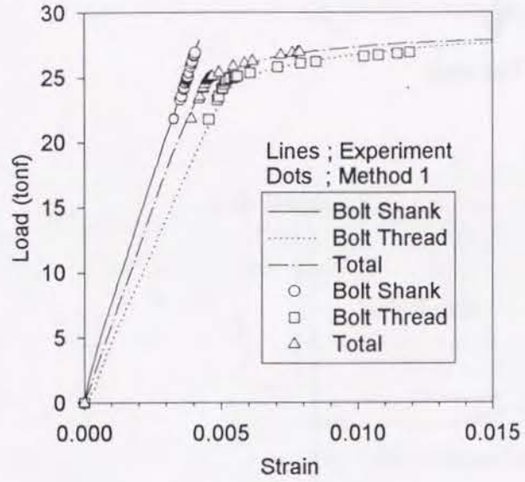

(c) M12 -Method 1

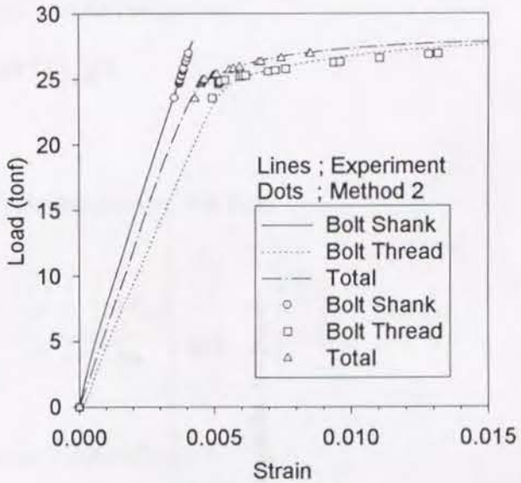

(d)M20-Method 2

Fig. 2.16 Load-Strain Curves (Simple Analysis)

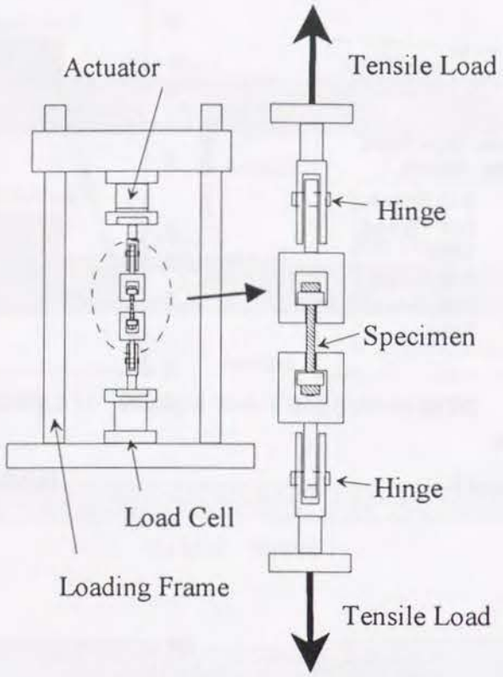

Fig. 2.17 Fatigue Test Setup

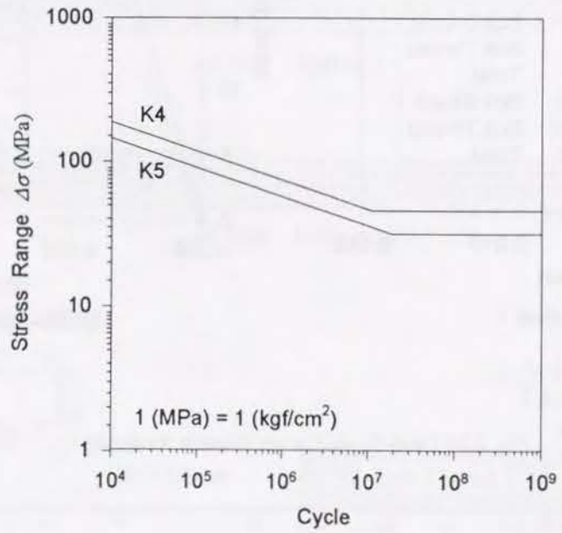

Fig. 2.18 S-N Diagram Specified by Guideline of Fatigue Design

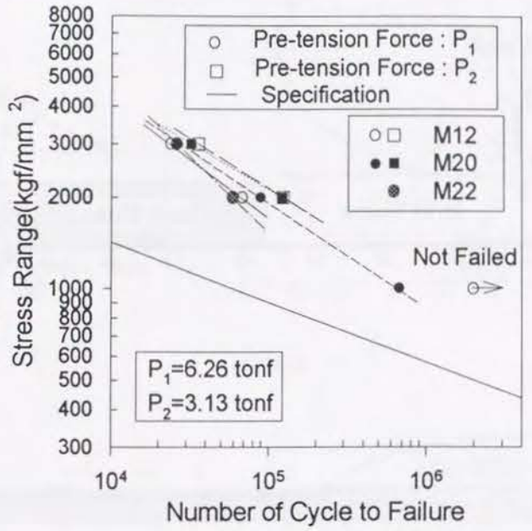

Fig. 2.19 S-N Diagram obtained from the Fatigue Test

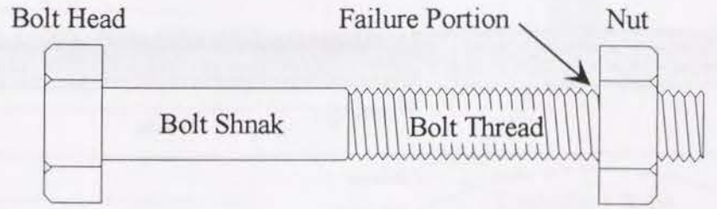

Fig. 2.20 Location of the Fatigue Failure of the Bolt

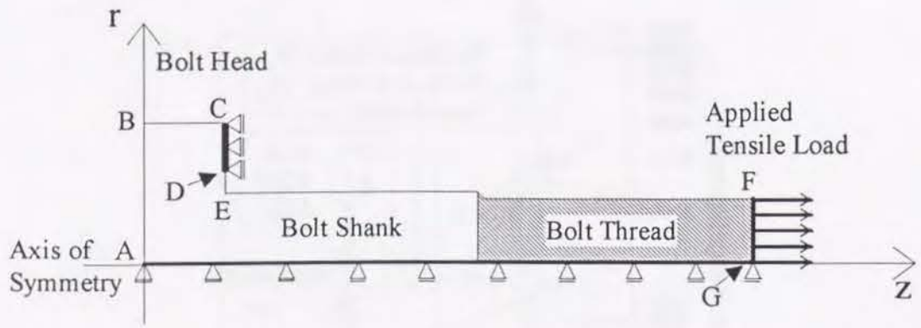

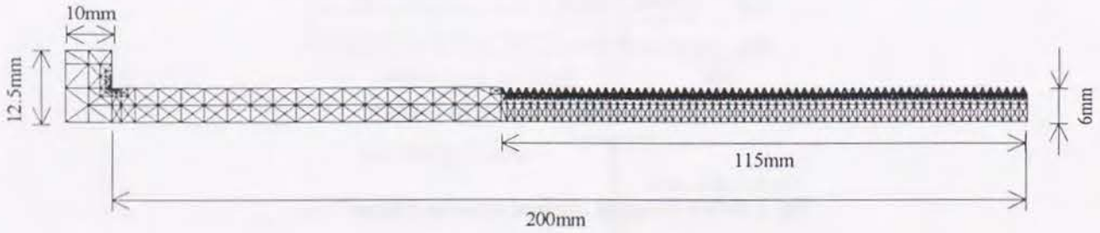

(a) M12

(b) M20

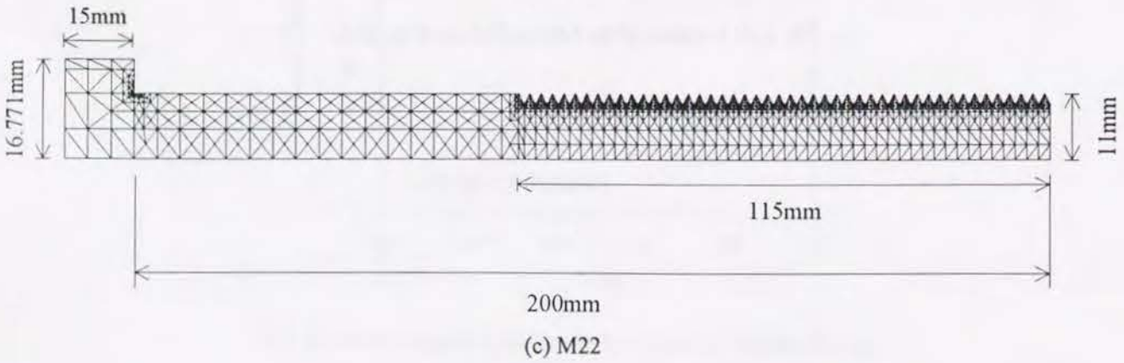

(c) M22

Fig. 2.21 Models of Stress Concentration Analysis

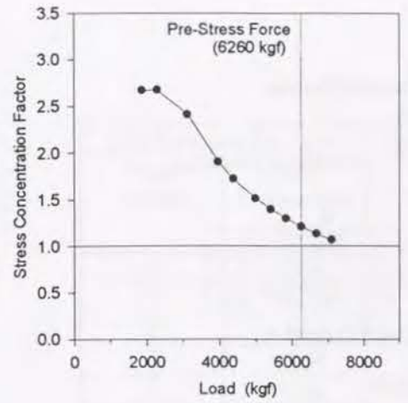

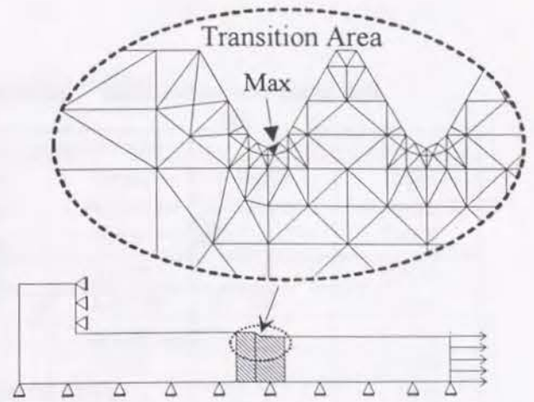

(a) M12

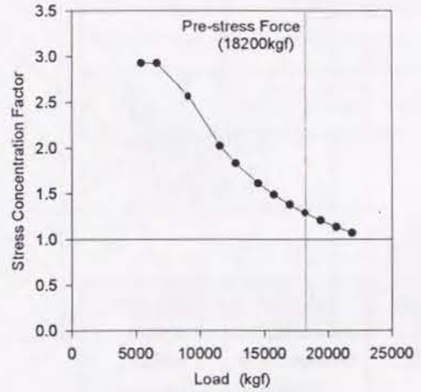

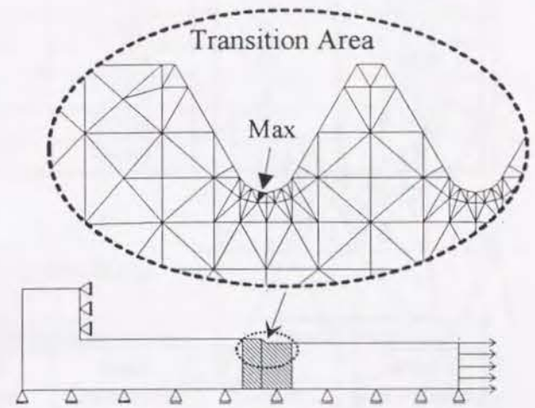

(b) M20

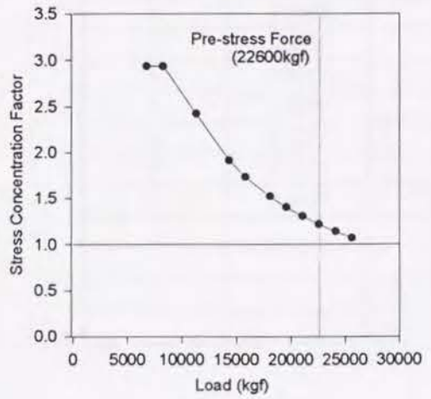

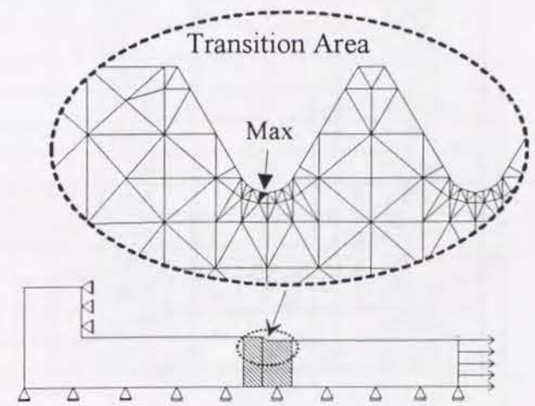

(c) M22

Fig. 2.22 Change of Maximum Stress Concentration Factor

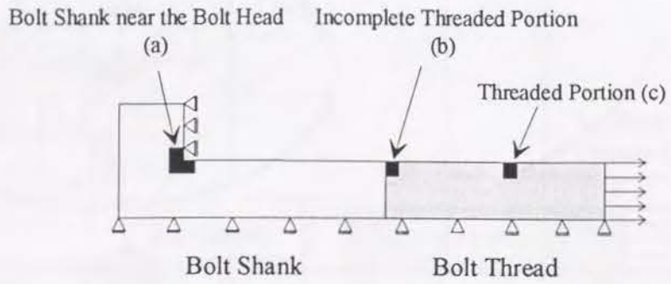

High Strength Bolt

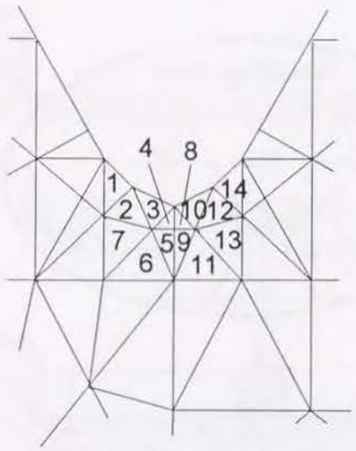

(a) Incomplete Threaded Portion

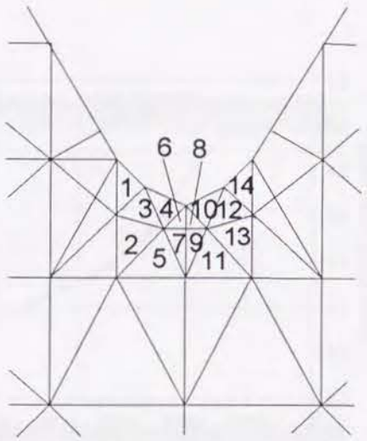

(b)Threaded Portion

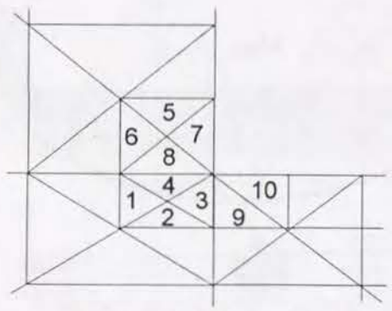

(c) Bolt Shank near the Bolt Head

Fig. 2.23 Stress Concentration Factor of Each Section of the Bolt (M12-1) (continued)

Tensile Load = 5840 kgf

Bolt Shank near Bolt Head		Incomplete Threaded Portion		Threaded Portion	
Nodal Number	Stress Concentration Factor	Nodal Number	Stress Concentration Factor	Nodal Number	Stress Concentration Factor
10	1.5700	3	2.6799	4	2.0641
7	1.2770	10	2.4517	10	2.0641
8	1.1382	1	1.6790	2	1.3216
9	1.0834	13	1.5675	13	1.3216
5	1.0414	2	1.5435	3	1.2137
6	0.8334	4	1.4607	12	1.2133
1	0.8080	7	1.4272	6	1.2060
4	0.7237	5	1.4239	8	1.2060
2	0.6755	8	1.3967	7	1.1666
3	0.6188	12	1.3801	9	1.1666
		9	1.3308	14	1.1419
		14	1.2376	1	1.1415
		11	0.9718	5	0.9317
		6	0.9074	11	0.9317

Tensile Load = 6260 kgf

Bolt Shank near Bolt Head		Incomplete Threaded Portion		Threaded Portion	
Nodal Number	Stress Concentration Factor	Nodal Number	Stress Concentration Factor	Nodal Number	Stress Concentration Factor
10	1.2793	8	1.2828	4	1.2794
7	1.2544	9	1.2827	10	1.2794
9	1.1531	10	1.2827	6	1.2792
8	1.1059	3	1.2824	8	1.2792
5	1.0225	4	1.2820	7	1.2785
6	0.8147	5	1.2809	9	1.2785
1	0.8109	1	1.2800	2	1.2747
4	0.7253	2	1.2799	13	1.2746
2	0.7079	7	1.2796	3	1.2722
3	0.6550	13	1.2796	12	1.2720
		12	1.2794	14	1.0315
		14	1.0854	1	1.0313
		11	1.0416	5	0.9433
		6	1.0372	11	0.9433

Fig. 2.23 Stress Concentration Factor of Each Section of the Bolt (M12-2) (continued)

Tensile Load = 7520 kgf

Bolt Shank near Bolt Head		Incomplete Threaded Portion		Threaded Portion	
Nodal Number	Stress Concentration Factor	Nodal Number	Stress Concentration Factor	Nodal Number	Stress Concentration Factor
10	1.0651	8	1.0685	4	1.0652
7	1.0650	9	1.0685	6	1.0652
9	1.0650	10	1.0679	8	1.0652
8	1.0597	3	1.0675	10	1.0652
5	1.0035	4	1.0674	7	1.0646
1	0.8228	5	1.0665	9	1.0646
6	0.7820	1	1.0656	3	1.0645
2	0.7808	2	1.0655	12	1.0644
4	0.7469	13	1.0655	2	1.0611
3	0.7350	7	1.0653	13	1.0610
		12	1.0653	14	1.0022
		6	1.0627	1	1.0018
		14	1.0571	5	0.9607
		11	1.0560	11	0.9607

Fig. 2.23 Stress Concentration Factor of Each Section of the Bolt (M12-3) (continued)

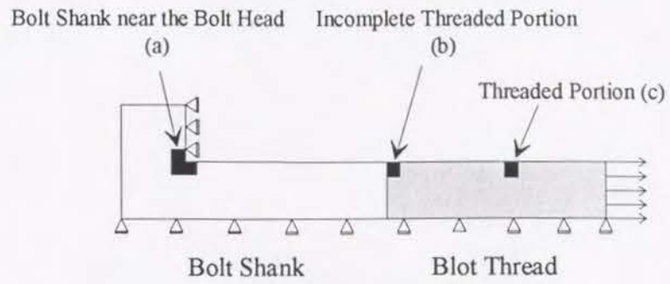

High Strength Bolt

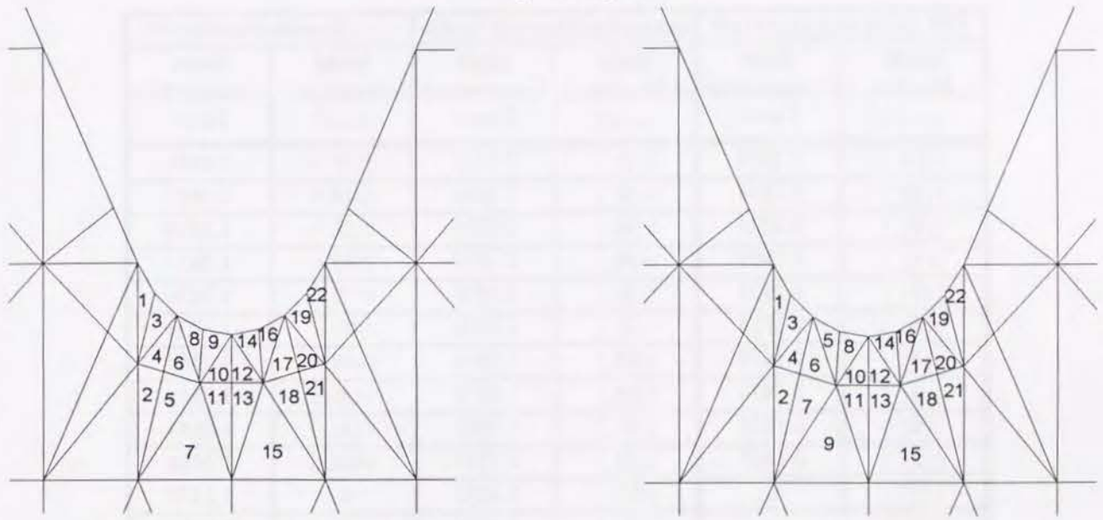

(a) Incomplete Threaded Portion

(b)Threaded Portion

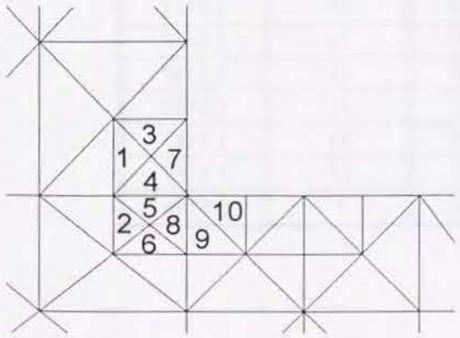

(c) Bolt Shank near the Bolt Head

Fig. 2.23 Stress Concentration Factor of Each Section of the Bolt (M20-1) (continued)

Tensile Load = 16975kgf

Bolt Shank near Bolt Head		Incomplete Threaded Portion		Threaded Portion	
Nodal Number	Stress Concentration Factor	Nodal Number	Stress Concentration Factor	Nodal Number	Stress Concentration Factor
10	0.5906	9	2.9238	7	2.0488
8	0.2844	8	2.9064	18	2.0485
5	0.2026	14	2.7709	5	1.3838
4	0.1999	16	2.4507	21	1.3834
9	0.1978	3	2.0599	9	1.3230
6	0.1735	1	1.7592	20	1.3230
7	0.1670	18	1.6314	19	1.2364
3	0.1474	19	1.5775	8	1.2361
2	0.1420	6	1.5702	4	1.2184
1	0.1263	10	1.5337	22	1.1488
		11	1.5153	6	1.1476
		5	1.5116	2	1.0858
		4	1.4962	3	1.0718
		12	1.4801	11	1.0224
		21	1.4589	17	1.0224
		17	1.4579	10	1.0212
		13	1.4487	16	1.0212
		2	1.3933	12	1.0187
		20	1.3267	13	1.0187
		22	1.1834	14	1.0187
		15	1.0231	15	1.0187
		7	0.9722	1	0.8746

Fig. 2.23 Stress Concentration Factor of Each Section of the Bolt (M20-2) (continued)

Tesile Load = 18200 kgf

Bolt Shank near Bolt Head		Incomplete Threaded Portion		Threaded Portion	
Nodal Number	Stress Concentration Factor	Nodal Number	Stress Concentration Factor	Nodal Number	Stress Concentration Factor
10	0.5910	9	1.2839	19	1.2784
8	0.2845	8	1.2837	8	1.2779
5	0.2027	16	1.2818	20	1.2778
4	0.1999	3	1.2809	9	1.2776
9	0.1979	12	1.2807	7	1.2772
6	0.1735	14	1.2807	18	1.2770
7	0.1669	10	1.2805	4	1.2367
3	0.1474	1	1.2798	22	1.2082
2	0.1421	2	1.2798	6	1.2070
1	0.1264	5	1.2791	5	1.1329
		18	1.2791	21	1.1324
		17	1.2790	2	1.1236
		20	1.2790	11	1.0312
		6	1.2787	17	1.0312
		4	1.2768	10	1.0308
		13	1.2750	16	1.0308
		21	1.2748	12	1.0270
		11	1.2738	13	1.0270
		19	1.1779	14	1.0270
		15	1.1339	15	1.0270
		7	1.1252	3	0.9213
		22	0.9586	1	0.8354

Fig. 2.23 Stress Concentration of Each Section of the Bolt (M20-3) (continued)

Tensile Load = 21875 kgf

Bolt Shank near Bolt Head		Incomplete Threaded Portion		Threaded Portion	
Nodal Number	Stress Concentration Factor	Nodal Number	Stress Concentration Factor	Nodal Number	Stress Concentration Factor
10	0.5910	9	1.0679	4	1.0635
8	0.2844	8	1.0678	19	1.0635
5	0.2028	16	1.0662	22	1.0632
4	0.2000	3	1.0656	8	1.0631
9	0.1979	12	1.0656	20	1.0629
6	0.1735	14	1.0655	9	1.0627
7	0.1670	10	1.0652	7	1.0626
3	0.1475	1	1.0649	18	1.0623
2	0.1421	2	1.0649	6	1.0621
1	0.1263	18	1.0642	2	1.0596
		5	1.0641	5	1.0575
		17	1.0641	21	1.0563
		20	1.0640	10	1.0489
		15	1.0638	16	1.0489
		6	1.0638	11	1.0457
		19	1.0630	17	1.0457
		4	1.0622	13	1.0423
		13	1.0609	14	1.0423
		21	1.0606	15	1.0423
		11	1.0597	12	1.0422
		7	1.0592	3	0.8724
		22	0.9207	1	0.8406

Fig. 2.23 Stress Concentration of Each Section of the Bolt (M20-4) (continued)

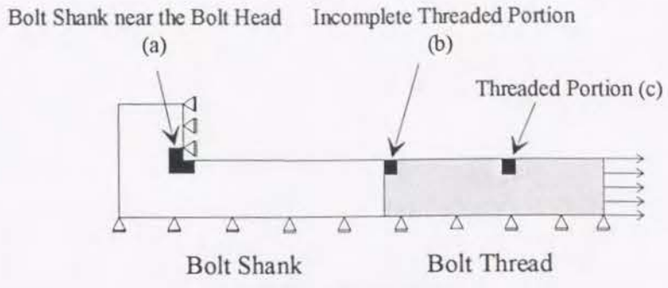

High Strength Bolt

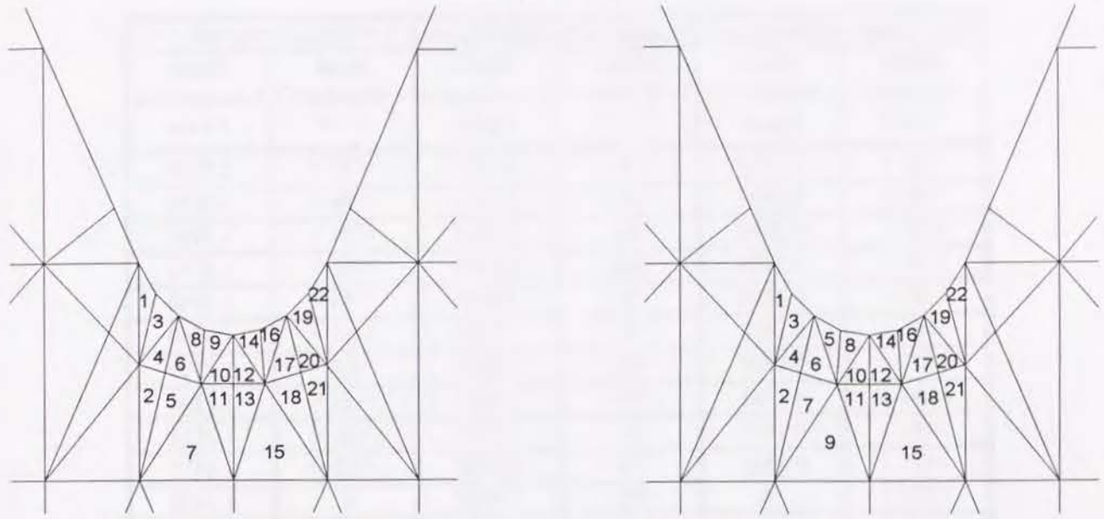

(a) Incomplete Threaded Portion

(b)Threaded Portion

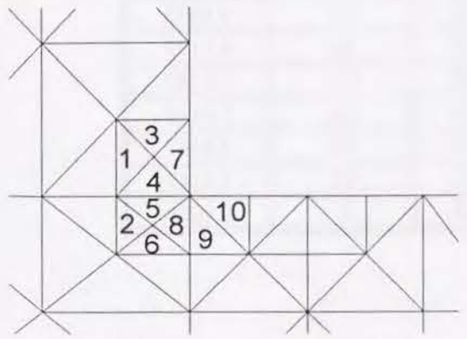

(c) Bolt Shank near the Bolt Head

Fig. 2.23 Stress Concentration of Each Section of the Bolt (M22-1) (continued)

Tensile Load = 18055 kgf

Bolt Shank near Bolt Head		Incomplete Threaded Portion		Threaded Portion	
Nodal Number	Stress Concentration Factor	Nodal Number	Stress Concentration Factor	Nodal Number	Stress Concentration Factor
10	0.5979	9	2.9347	7	2.0358
8	0.3032	8	2.9168	18	2.0355
5	0.2157	14	2.7812	5	1.3763
4	0.2139	16	2.4595	21	1.3759
9	0.2086	3	2.0690	9	1.3160
6	0.1853	1	1.7667	20	1.3160
7	0.1789	18	1.6385	19	1.2299
3	0.1582	19	1.5846	8	1.2296
2	0.1511	6	1.5777	4	1.2124
1	0.1359	10	1.5406	22	1.1418
		11	1.5223	6	1.1406
		5	1.5194	2	1.0808
		4	1.5025	3	1.0658
		12	1.4908	11	1.0184
		21	1.4652	17	1.0184
		17	1.4641	10	1.0172
		13	1.4556	16	1.0172
		2	1.4007	12	1.0147
		20	1.3318	13	1.0147
		22	1.1889	14	1.0147
		15	1.0292	15	1.0147
		7	0.9790	1	0.8696

Fig. 2.23 Stress Concentration of Each Section of the Bolt (M22-2) (continued)

Tesile Load = 22600 kgf

Bolt Shank near Bolt Head		Incomplete Threaded Portion		Threaded Portion	
Nodal Number	Stress Concentration Factor	Nodal Number	Stress Concentration Factor	Nodal Number	Stress Concentration Factor
10	0.5910	9	1.2786	7	1.2753
8	0.2845	8	1.2784	18	1.2747
5	0.2027	16	1.2765	19	1.2728
4	0.1999	3	1.2757	8	1.2726
9	0.1979	12	1.2755	20	1.2712
6	0.1735	13	1.2755	9	1.2700
7	0.1669	14	1.2755	4	1.2297
3	0.1474	10	1.2753	22	1.2002
2	0.1421	1	1.2747	6	1.1990
1	0.1264	2	1.2747	5	1.1284
		11	1.2743	21	1.1279
		18	1.2741	2	1.1166
		5	1.2739	11	1.0262
		17	1.2738	17	1.0262
		20	1.2738	10	1.0258
		21	1.2738	16	1.0258
		6	1.2722	12	1.0220
		4	1.2715	13	1.0220
		19	1.1808	14	1.0220
		15	1.1388	15	1.0220
		7	1.1326	3	0.9173
		22	0.9613	1	0.8314

Fig. 2.23 Stress Concentration of Each Section of the Bolt (M22-3) (continued)

Tensile Load = 24115 kgf

Bolt Shank near Bolt Head		Incomplete Threaded Portion		Threaded Portion	
Nodal Number	Stress Concentration Factor	Nodal Number	Stress Concentration Factor	Nodal Number	Stress Concentration Factor
10	0.5983	9	1.0644	7	1.0616
8	0.3033	8	1.0641	18	1.0612
5	0.2158	16	1.0626	19	1.0600
4	0.2139	13	1.0622	2	1.0599
9	0.2087	3	1.0621	4	1.0598
6	0.1854	12	1.0621	8	1.0596
7	0.1790	14	1.0618	20	1.0577
3	0.1583	10	1.0617	9	1.0575
2	0.1512	1	1.0614	22	1.0572
1	0.1359	2	1.0614	6	1.0561
		11	1.0610	5	1.0532
		18	1.0608	21	1.0521
		5	1.0606	10	1.0419
		17	1.0606	16	1.0419
		21	1.0606	11	1.0389
		20	1.0604	17	1.0389
		6	1.0591	12	1.0354
		4	1.0585	13	1.0354
		7	1.0577	14	1.0354
		15	1.0568	15	1.0354
		19	1.0566	3	0.8684
		22	0.9284	1	0.8350

Fig. 2.23 Stress Concentration of Each Section of the Bolt (M22-4)

Chapter 3

Mechanical Behavior of High Strength Bolts and Its Adjacent Structural Elements

3.1 Introduction

In order to fully understand the mechanical behavior of high strength bolted tensile joints, fundamental characteristics such as load transferring mechanism by bolts and the flange plates should be studied; so that the mechanical behavior of the high strength bolts and its adjacent structural elements as shown in Fig. 3.1 is discussed in this chapter. The mechanical behavior of the bolt and its adjacent structural elements is very basic for understanding of load-bolt force relation and effect of the bolt pre-stress force on mechanical behavior. Moreover, these understandings are considered to be applicable for other connections using high strength bolts. Here, structural elements adjacent to the high strength bolts as shown in Fig. 3.1 is the axisymmetric model for simplicity in order to understand the interaction of bolt elongation and flange plate bending. In this study, this is named BAF model(high strength Bolt and its Adjacent Flange plate). Using this model, mechanical behavior in detail under tensile loading varying thickness of the circular plate diameter of it, and bolt pre-stress force is investigated experimentally and analytically. As shown in Fig. 3.1, this model consists of two circular plates jointed by a high strength bolt at the center of the plates and it is simple enough to identify the contribution of the bolt and the flange plate to joint behavior. It is also very easy to analyze this model using finite element analysis because of structural axisymmetry. In addition, prying force according to the mechanism discussed in the previous studies[1]-[3] does not occur due to the shape of the model, so that it is able to study the effect of the following parameters only: pre-stress force of the bolt, thickness of the circular plate and diameter of circular plate(distance between the center of the bolt and loading point.)

3.2 Experiment on BAF Model

3.2.1 Outline of the experiment

Monotonic tensile loading test for BAF model is carried out in order to study its mechanical behavior. Dimensions of all the specimens are tabulated in Table 3.1. In this experiment, varied are the thickness and the diameter of the circular plate, the bolt pre-stress force as the parameter. SS400 steel is used for the circular plate(flange plate), and either M16(F10T) or M12(F10T) bolt is used for the high strength bolt. The diameter of the circular flange plate is determined by considering the loading capacity of the

testing machine. Material properties obtained from the material test are summarized in Table 3.2.

The characteristics of each specimen are described as follows: BAF-1 and BAF-2 consists of circular flange plates with thickness of 25 (mm) and diameter of 52 (mm) and high strength bolt of M16(F10T), but bolt pre-stress force given to the bolt is different. The objective to test these two models is to investigate the effect of the bolt pre-stress force. In case of BAF-1, the bolt pre-stress force is 11.7 (tonf), which is standard bolt pre-stress force for M16 defined by JIS[4]. On the other hand, in case of BAF-2, pre-stress force of bolt is 5.85 (tonf), which is 1/2 of standard bolt pre-stress force mentioned in the above. The thickness of the circular plate, 25 (mm) is determined as follows: Assuming the simply supported circular plate subjected to the concentrated load at the center of the plate, it is determined such that the maximum bending stress of circular plate reaches to yield stress (30 kgf/mm^2). Among BAF-3, BAF-4 and BAF-5 models, diameter of the circular plate (the loading length between the center of the bolt and the loading point) and the bolt pre-stress force are the same; but only the thickness of the circular plate is different each other. The thickness of the circular plate of BAF-3, BAF-4 and BAF-5 is 1.0 times, 0.5 times and 0.25 times of the standard thickness(BAF-3) respectively, which is determined by the same procedure used for BAF-1 and BAF-2 and this standard thickness of the circular plate is 19 (mm). The high strength bolt of M12(F10T) is used for all the specimens. The objective to compare these models is to investigate the effect of the thickness of the circular plate on contact/separation behavior. It is considered that the failure mode is different by the thickness of the circular flange plate. In case of the thinner circular plate, the bending failure is assumed to occur at the circular plate. On the other hand, in case of the thicker circular plate, the tensile failure of the bolt is assumed to occur. The bolt pre-stress force used into these models is 6.26 (tonf), which is specified in JIS for M12(F10T). Finally, BAF-6 is for investigation of the effect of the distance between the center of the bolt and loading edge by comparing to BAF-4. This distance of BAF-6 is 1.5 times of that of BAF-4, namely, 78 (mm).

In the experiment, attention is paid to the local deformation of the circular plate, the gap developed between two circular flange plates(separation) and the variation of the bolt force in order to study the contact/separate behavior and the stiffness of the joint in detail.

Test setup is shown in Fig. 3.2. The testing machine used in this experiment is SHIMADZU electrically servo-controlled hydraulic actuator whose loading capacity is +/-30 (tonf) statically, +/-20 (tonf) dynamically and maximum stroke is +/-50 (mm). In this system, the loading is controlled by the analog controller operated by micro-computer through GP-IB interface, where the displacement of the actuator is monotonically increased. The tensile load is applied to the test specimen uniformly around the edge of the circular plate. The loading is continued until the maximum load point is obtained. Schematic view of this loading is shown in Fig. 3.3. The bolt pre-stress force is checked by the reading of the strain gages installed in the bolt shank as shown in Fig. 3.4, which is already calibrated to bolt force. In order to avoid the eccentric loading, hinge joints are utilized in the loading apparatus as shown in Fig. 3.2.

In the experiment, tensile applied load, stroke of the actuator, strain on the circular plates,

separation of two circular plates and bolt force are measured. Each measurement is described in the following:

(1) Tensile applied load

Load is measured by the load cell installed in the actuator.

(2) Separation between two circular plates

This is measured by the strain gage type displacement transducer as shown in Fig. 3.5. The location to measure this separation is also shown in Fig 3.6.

(3) Bending deformation of the circular pate

In order to measure the bending deformation of the circular plate, the strain gage for the stress concentration measurement is used. The location to measure bending strain is also shown in Fig 3.6.

(4) Bolt force

Bolt force is obtained by the strain gage installed into the center of the bolt shank as shown in Fig. 3.4. The bolt force is calculated by using data-sheet of the calibration test for each bolt.

3.2.2 Experimental results and discussions

Load vs. separation curves obtained from the experiment are shown in Fig. 3.7. In this figure, the horizontal axis shows the average separation which is given by averaging the reading of 4 displacement transducers in 90 degree pitch around the circular plate. In addition, load vs. bolt force curves and the strain distributions on the circular plate are shown in Fig. 3.8 and Fig. 3.9, respectively. Results and discussions are written in the following for each factor to affect the mechanical behavior.

(a) Effect of the bolt pre-stress force

In order to investigate the effect of the bolt pre-stress force, BAF-1 and BAF-2 are compared. Different bolt pre-stress force is given to BAF-1 and BAF-2; bolt pre-stress force of BAF-2 is half of BAF-1. As shown in Fig 3.7, it is found that two circular plates are not separated in a large scale until the tensile load reaches to the bolt pre-stress force for both cases. Furthermore, it is also shown that the higher the bolt pre-stress force is, the higher the joint stiffness is obtained because of less separation. Here, the stiffness of the joint is defined as the tangential slope of the load-separation curve. In addition, it is found that the stiffness of BAF-1 is same as that of BAF-2 after the tensile load reaches to the bolt pre-stress force. Therefore, it is concluded that the bolt pre-stress force affects only the load level at separation of the two circular plates and initial slope of load-separation curve.

Furthermore, it is understood from Fig. 3.8 that the bolt force is kept constant before the tensile load reached to the bolt pre-stress force, and that after the tensile load reaches to the bolt pre-stress force, bolt force becomes larger as the tensile load increases. At the early stage of loading, the applied load is

considered to be balanced to the release of the compressive force between two circular plates given by the bolt pre-stress force before the tensile load reaches to the bolt pre-stress force, and after that, the applied load is carried only by the bolt. Therefore, it is concluded that prying force does not exist in this model as expected. Moreover, it is shown that circular plate is not deformed significantly even if large separation took place as shown in Fig 3.9. Therefore, it is understood that the bending strength of the circular plate is higher than that of high strength bolt to make only the bolt elongate.

(b) Effect of the thickness of the circular plate

Results of BAF-3, BAF-4 and BAF-5 are compared in order to investigate the effect of the thickness of the circular plate. Among these specimens, only a difference is the thickness of the circular plate and other conditions are the same. The thickness of the circular plate of BAF-3, BAF-4 and BAF-5 are 19 (mm), 10 (mm) and 5 (mm) respectively. From the load-separation curves(Fig. 3.7), it is found that the stiffness of the model becomes higher as the thickness of the circular plate becomes larger. Namely, the stiffness of BAF-3 is the highest among those of these specimens, and that of BAF-5 is the lowest. Furthermore, in the case of the BAF-3, which has the thickest circular plate, after the applied load reached to the maximum load, applied tensile load decreases gradually. On the other hand, in case of the BAF-4 and BAF-5, which has the thinner circular plate than BAF-3, the applied load increases monotonically even if the separation becomes quite large. It is considered that this difference in load-separation curves is caused by the difference of the failure mode. Namely, in case of the thick circular flange plate, the limit state is defined by the failure of the high strength bolt under the tension; on the other hand, in case of the thinner circular flange plate, it is the failure of the circular plate under bending. Therefore, the load-separation curve of BAF-3 significantly depends on load-elongation curve of only the high strength bolt; and in similar way, that of BAF-5 significantly depends on load-bending deflection curve of the simply supported circular plate subjected to point load at the center of the circular plate.

Moreover, from Fig. 3.9 of the load-strain curves at the circular plate, in case of BAF-3, it is found that the strain due to plate deflection is at most 200 (micro). This also concludes that the circular plate is not deformed significantly and that the separation of BAF-3 depends on elongation of the bolt. On the other hand, in case of BAF-5, the circular plate is considered to be bent significantly according to the strain distribution on the circular plate; where the maximum strain is beyond the yield strain. As for BAF-4, which has intermediate thickness of the circular plate, it is understood that the behavior discussed in the above for thin and thick flange plate is somehow combined. As for the load-bolt force relationship, in case of BAF-3, the bolt force is kept constant until the applied load reaches to the bolt pre-stress force, and after that the bolt force increases as the applied load increases where the linear relation exists. On the other hand, in case of BAF-5, the bolt force increases gradually before the applied load reaches to the bolt pre-stress force as compared with BAF-3. Particularly, the bolt force increases even if the applied load is very small. The increase of the bolt force at the early stage of loading is similar to the prying force effect in the previous study[1]-[3]. However bolted circular plate tested in this study cannot have prying force

action. This increase of bolt force is caused by the phenomena that the local deformation of flange plate pull the bolt head; namely, at the edge of the bolt hole, prying force action may occur due to large deflection of the circular plate.

(c) Effect of the loading length

In order to investigate the effect of the loading length between the center of the bolt and the loading edge, results of BAF-4 and BAF-6 are compared. The loading length of BAF-4 and BAF-6 are 52 (mm) and 78 (mm) respectively. From the load-separation curve, the tangential slope of the BAF-4 is higher than that of BAF-6. Moreover, it is understood from the load-bolt force curve that the bolt force of BAF-6 increases at the early stage of loading compared with BAF-4. It is also concluded that the less stiffness of the circular plate with the large loading length(diameter of the circular plate) cause large deflection so that this local deformation cause an additional increase of bolt force.

3.3 Finite Element Analysis on BAF Model

3.3.1 Outline of finite element analysis

In the previous section, the loading test for BAF model is described. The loading test is very useful to understand the mechanical behavior for particular model; however it is not suitable for the problem with many parameters to be considered because of the limitation of the time and cost for the experiment. On the other hand, the numerical analysis only needs the computer which has high computation capacity; in addition, it is very easy to analyze the problem for many combinations of parameters, so that it is considered to be suitable for quantitative evaluation. In this section, finite element analysis for BAF model is carried out by varying the parameter, such as thickness of the circular plate, the diameter of the circular plate, in order to supplement the result of the loading test and further to investigate the mechanical behavior of BAF model quantitatively.

3.3.2 Numerical analysis method

As the tensile load is applied to BAF model, the gap between two circular plates becomes large gradually. That is, a boundary condition on the contact surface should be changed from the state of contact to that of separation during the loading. Therefore, in the analysis, this boundary non-linearity must be taken into consideration. Accordingly, in this study, 2-dimensional axisymmetric finite element analysis is carried out considering both material non-linearity and boundary non-linearity.

The program developed in this study is the finite element analysis program using triangular element with constant strain, whose core utilizes EPIC IV. The detail of EPIC IV can be referred to the reference[5]; here, the function added to EPIC IV is described in the following. As mentioned above, it is required to consider boundary non-linearity for contact/separation behavior on BAF model. In this

program, the change of boundary condition is executed according to a certain condition on the nodal force or nodal displacement along the contact surface(line in 2-D problem). Contact or separation surface is located on x-axis as shown in Fig. 3.10. The nodal points in contact condition is constrained to be zero displacement in y-direction at first, and the nodal point in separation condition is constrained to be zero force in y-direction. If the nodal force becomes negative on the contact surface, the separation occurs and boundary condition is changed from that for contact condition to that of separation condition. On the other hand, if the nodal displacement in the separation condition becomes negative, the contact occurs and boundary condition is changed from that of separation condition to that of contact condition.

3.3.3 Parametric study for BAF model

Here, parametric study is carried out in order to estimate the stiffness of BAF model, where the thickness of the circular plate and the loading length between the center of the bolt and loading edge are considered to be parameters. In this analysis, 11 cases are taken into consideration. All the cases are listed in Table 3.3. In the name of analytical cases considered, the character following "A" denotes the half of the diameter of the circular plate. The characters "S" ,"M" and "L" denotes 52 (mm), 78 (mm) and 104 (mm) respectively. The nominal diameter of the bolt and the bolt pre-stress force for each case are the same as those used for test specimens, namely, M12(F10T) and 6.26 (tonf) respectively.

Finite element model for BAF model and its discretization by triangular elements are shown in Fig. 3.11. The location considered to have high stress concentration is discretized by fine mesh such as the bolt shank near the head and the loading edge. Boundary conditions are also shown in Fig. 3.12. Locating the surface to be judged either in contact or separation condition on x-axis, nodal points on x-axis is fixed in y-direction at the initial state. Furthermore, in this model, it is assumed that the bolt head and the circular plate are kept in contact all the time; that is, both are treated to be a continuous body. Difference between the circular plate and the bolt is just made by changing material properties. Material properties used in this analysis are summarized in Table 3.4. These are determined based on the specification of JIS. The material is assumed to be elastic perfectly plastic. As shown in Table 3.4, the properties of the bolt thread are different from those of the bolt shank in order to consider the shape of the bolt thread. The yielding stress and the stiffness of the bolt thread is 75% of those of the bolt shank. This ratio is defined based on the ratio of cross sectional area of bolt shank to that of the bolt thread. Moreover, in this model, the washer is omitted for simplicity. Because the objective of this analysis is mainly to understand the global mechanical behavior of bolted joints, that is, the separation of the flange plates. Furthermore, the difference between the diameter of the bolt head and that of the washer is a little, i.e., 0.6 mm and the thickness of the washer is much thinner than that of the flange plate.

In case of the thickest and largest circular plate, total number of the nodal points and elements is 390 and 684 respectively. The procedure of this analysis is summarized in the followings(referred to Fig. 3.13):

(Step 1) Bolt pre-stress force is given to the bolt, by applying the tensile load at the end of the bolt as uniformly distributed load.

(Step 2) After bolt pre-stress force prescribed in JIS is given, the bolt end is fixed at the displaced position in vertical direction(y-direction).

(Step 3) Uniformly distributed tensile load is applied along the edge of circular plate; namely, ring load

3.3.4 Results and discussions

(a)Load-deformation curve

Load vs. deformation curves obtained by the analysis are shown in Fig. 3.14. The vertical axis shows the applied tensile load and the horizontal axis shows the displacement of the loading point as shown in Fig. 3.11.

In case of small diameter-to-thickness ratio of circular plate, large displacement begin to occur when the applied tensile load becomes about 8.0 (tonf), so that the curves become bi-linear, which is very similar to that of the bolts. It is considered that mechanical behaviors of these cases depend on only load-elongation curve of the high strength bolt, not the thicker circular plate. In addition, it is found that in the case of small diameter-to-thickness ratio of circular plate, the slope of the load-displacement curve is steeper. On the other hand, in case of large diameter-to-thickness ratio of circular plate, large deformation begin to occur even before the tensile applied load reaches to 8.0 (tonf) which is a minimum yielding load of the bolt specified in JIS. And, it is found that the load-deformation curve is significantly non-linear. This is considered to be caused by the yielding of the circular plate. The magnitude of the load when the large deformation occurs is different and depend on the geometrical configuration of the circular plate. Therefore, the mechanical behavior of these cases is considered to depend on not the high strength bolt but the circular plate.

Next, the process to spread the yielding region are shown in Fig. 3.15. It is understood from these figures that in case of small diameter-to-thickness ratio, the bolt yields. On the other hand, in case of large diameter-to-thickness ratio, the circular plate is found to yield. This characteristics is in good agreement with the results observed in the experiment.

(b)Joint stiffness of the BAF model

Stiffness vs. load curves obtained by the analysis are shown in Fig. 3.16. The vertical axis shows the stiffness, and the horizontal axis shows the applied tensile load. In these figures, the spread of the contact surface to be separated, the stiffness of the high strength bolt under tension and the bending stiffness of the circular plate and the total stiffness of the joint are also shown for reference. The joint stiffness is defined by the slope of load-separation curve. The stiffness of the circular plate is defined by the slope of the load-deflection curve for a simply supported circular plate subjected a concentrated load at the center of the plate[6]. The stiffness of the bolt is the tensile stiffness of the bar which has the same cross

sectional area as the bolt. joint stiffness K, stiffness of the high strength bolt K_B, and bending stiffness of the circular plate K_P is derived by the following equation.

$$K = \frac{\Delta P}{\Delta u} \tag{3.1}$$

$$K_B = \frac{AE_B}{\ell} \tag{3.2}$$

$$K_P = \frac{16\pi D}{R^2}\frac{1+\nu}{3+\nu} \tag{3.3}$$

$$D = \frac{E_P t^3}{12(1-\nu^2)} \tag{3.4}$$

in which ΔP, Δu, E_B, l, R, t, ν, and E_P, is the increment of the tensile load at each loading step, the increment of the separation at each loading, Young's modulus of the bolt, clamped length of the bolt, radius of the circular plate, thickness of the circular plate, the Poisson's ratio of the circular plate and Young's modulus of the circular plate respectively.

On the other hand, the total stiffness of the joint for a simple model assumed that the high strength bolt and the circular plate are connected in series is derived. Total stiffness of the joint K_T is given in the following based on the stiffness of the bolt and the bending stiffness of the circular plate defined by equation (3.2) and (3.3).

$$K_T = \frac{K_B K_P}{K_B + K_P} \tag{3.5}$$

It can be seen from Fig. 3.16 that after the nodal point in contact condition turns to be separated, the stiffness of the joint decreases gradually. It means that the stiffness decreases as the more separation takes place. Furthermore, the sudden decrease of the stiffness as the tensile load increases is considered to be due to a coarse discretization on the contact surface. It can be concluded that the compressive force between flange plates given by the bolt pre-stress force is contributed to the high stiffness of joints. In addition, in case of small diameter-to-thickness ratio, it is found that the circular plates are separated completely without any significant deflection of circular plate; as a result, only the bolt resist against applied tensile load. Finally the stiffness becomes to zero suddenly after the tensile load reaches to the yielding load of the bolt. On the other hand, in case of large diameter-to-thickness ratio, it is shown that two circular plates are not separated completely, and it is considered that the applied tensile load causes the significant deformation on the circular plate and only the flange plates compressed by the bolt head are in contact condition. The failure mode of all the cases can be summarized in the followings: in case of AS-1, AS-2, AM-1, AM-2, AL-1, a decrease of the stiffness is caused by the yielding of the bolt thread, in case of AS-4, AS-5, AM-4, it is caused by the yielding of the circular plate, in case of AS-3, AM-3,

AL-2, it is caused by the yielding of both the bolt and the circular plate.

Based on a result of observations mentioned in the above, stiffness-load curve is classified into three patterns by the thickness of the circular plate and the diameter of the circular plate (the loading length between the center of bolt and loading edge). Schematic view of three patterns for stiffness-load curve is shown in Fig. 3.17. In case of small diameter-to-thickness ratio, initial stiffness is very high. As the applied tensile load increases, the stiffness decreases significantly at the early stage of loading; and then the stiffness is kept almost constant. This constant stiffness is considered to be equivalent to that of the circular plate. After the tensile load reaches to the bolt yielding load, finally the stiffness decreases again and becomes almost zero. On the other hand, in case of large diameter-to-thickness ratio, initial stiffness is not so high as that of small diameter-to-thickness ratio, and the stiffness decreases gradually as the applied tensile load increases and then it becomes almost zero very quickly before the applied tensile load reaches to the bolt yielding load. Finally, in the case of that medium diameter-to-thickness ratio, the decrease of the stiffness is in between the above two cases.

Next, in order to investigate the effect of the bolt pre-stress force on initial stiffness, the stiffness obtained by the analysis is compared with total stiffness K_T of the model. If the total stiffness is higher than that obtained from the analysis, the stiffness of the model increases by the bolt pre-stress force. As already shown in Fig. 3.16, total stiffness calculated by equation (3.5) is compared to that obtained from the analysis. Here, the effect of the bolt pre-stress force is observed for all cases. It is found that in case of small diameter-to-thickness ratio, the stiffness increases by 100 % at the initial state due to the bolt pre-stress force; but less for case of large diameter-to-thickness ratio. Therefore, it is concluded that the thicker the circular plate is and the smaller the diameter is, the higher the stiffness is obtained by the bolt pre-stress force.

3.3.5 Evaluation of the stiffness on BAF model

From the view point of the design of the joint considering the energy absorption or rational economical design, accurate evaluation of the stiffness of the joint is very important. Accordingly, in this section, in order to establish the quantitative evaluation formula for the joint stiffness of the BAF model which should be applicable in general use, multiple regression analysis is carried out based on the results of the finite element analysis for the BAF model.

In this evaluation, used are the following normalized parameters considered to be most influential on the stiffness of the joint. These are t/R, P/P_0, P/P_u. t/R is the ratio of radius to thickness for circular plate. P/P_0, and P/P_u are normalized load, where P_0, P_u is bolt pre-stress force given into the bolt and the ultimate load of joints respectively. This ultimate load is small force of either the bolt yielding force or the plastic collapse load of the circular plate subjected to ring load at the edge of the circular plate. This plastic collapse load of the circular plate is given by the following equation.

$$P = \pi \frac{6R}{3R-2a} \frac{\sigma_y t^2}{4} \tag{3.6}$$

in which R, t, σ_y and a is the radius of the circular plate, the thickness of the circular plate, the yielding stress and the radius of the loading area respectively.

Accordingly, the equation for evaluation of the stiffness on BAF model is proposed by using the above parameters as follows:

$$\frac{K}{K_0} = \left\{ C_1 \left(\frac{t}{R} \right)^{C_2} - 1 \right\} \left(1 - \frac{P}{P_u} \right)^{C_3} + \left\{ 1 - C_4 - C_5 \left(\frac{t}{R} \right)^{C_6} \right\} \left(1 - \frac{P}{P_u} \right)^{C_3} + \left\{ C_4 + C_5 \left(\frac{t}{R} \right)^{C_6} \right\} \exp\left\{ -1.5 \left(\frac{P}{P_0} \right)^8 \right\} \left(1 - \frac{P}{P_u} \right)^{C_7} \tag{3.7}$$

in which K and K_0 are the stiffness of the joint and the stiffness of the circular plate defined by the equation (3.3). Furthermore, C_1-C_7 are coefficients to be determined.

This equation is determined based on 3 patterns of the decrease of the stiffness as increase of the applied tensile load. The first and the second terms are the functions to represent a decrease of the stiffness exponentially, which is concerned with the ratio of the radius to the thickness of the circular plate. The third term is a function to have characteristics shown in Fig. 3.18, and it represents the rapid decrease of the stiffness when the applied tensile load reaches to the ultimate load. All the terms are concerned with the ultimate load of the joint, so that the stiffness becomes almost zero if the applied tensile load reaches to the ultimate load.

If the linear least square method is used in multiple regression analysis, in case of this equation (3.7) proper linearization must be needed. Here, the different weight for each data may be taken if this linearization is carried out; therefore, it is difficult to carry out regression analysis for this type of equation accurately. Accordingly, in this study non-linear least square method is utilized to obtain the coefficients directly[7][8]. The coefficients in this equation obtained by the multiple regression analysis are shown in Table 3.5. The applied tensile load P and the stiffness K at the each loading step obtained by the finite element analysis are used as the input data. But the data that a stiffness is very small is neglected for accurate estimation because of avoiding that the small stiffness is improperly weighted in the analysis. Here, the data that a load is larger than 1.1 times of the yielding load of the bolt are neglected.

The regression curves of the stiffness of BAF model for each analytical case are compared and shown in Fig. 3.19. In these figures, the error in the regression analysis is also shown. This error is normalized such as the relative error divided by the maximum stiffness of each case obtained by the finite

element analysis. From these figures, the evaluation of the stiffness using the equation (3.7) is considered to be applicable and in case of thicker circular plate, it is understood that the evaluation by this equation is very accurate. On the other hand, it is observed that the error tends to be big as the tensile load reaches to the ultimate load, where the stiffness is very small. However, form the view point of the order in the stiffness, the range that the stiffness is almost zero is not so important. In addition, The comparison with the stiffness obtained by the evaluation and that obtained by finite element analysis for all the cases is also shown in Fig. 3.20. It is also understood from this figure that the regression results for all the data using the equation seems quite good except for the data that a stiffness is very large. Therefore, the evaluation for the stiffness of BAF model using this equation could be applicable.

3.4 Conclusions

In this chapter, mechanical behavior of the high strength bolt and its adjacent structural element(BAF model) is investigated experimentally and analytically. In particular, the contact/separation behavior and its stiffness are taken into consideration. The stiffness is an important information for design of the joint considering the energy absorption capacity or earthquake resistance of structures. Therefore, the simple evaluation method for the stiffness such a basic element are proposed. The conclusions and future needs are obtained as follows:

1) The mechanical behavior of BAF model depends on the diameter-to-thickness ratio of circular flange plates and bolt pre-stress force, and failure mode of this model is affected by diameter-to-thickness ratio. In case of smaller diameter-to-thickness ratio, the initial stiffness is higher and the failure is caused by the bolt yielding, which is brittle. On the other hand, in case of larger diameter-to-thickness ratio, the initial stiffness is not so high and the failure is caused by the circular plate yielding. Furthermore, energy absorption capacity is considered to be higher. As for the effect of the bolt pre-stress force, the higher the bolt pre-stress force is, the higher the stiffness is obtained.
2) In general, the bolt force is kept constant until the tensile load reaches to the bolt pre-stress force given to the bolt, the applied load is carried by the release of the compressive force given by the bolt pre-stress force. However, in case of thinner circular plate, that is, the bending strength of the circular plate is low, it is observed that the increase of the bolt force occurs at the early stage of loading. It is considered to be similar to the prying force effect where the bolt is pulled by local deformation of the circular plate.
3) The evaluation method for the stiffness of the BAF model is proposed based on the results of multiple regression analysis using non-linear least square method. It is concluded that the

proposed equation is applicable for the evaluation of the stiffness.

In the future, the equation should be further modified in order to evaluate the stiffness more accurately at the wide range and large intense of stiffness. And the utilization of the results obtained in this chapter is expected to be implemented in the design for the various bolted connections.

References

1) B.Kato, A.Tanaka : High Strength Bolted Tensile Joints -Influence of Bolt Pre-stress Force-, Journal of Structural and Construction Engineering, No. 146, Apr. 1968, pp. 21-27, Architectural Institute of Japan(in Japanese).
2) B.Kato, A.Tanaka : Experimental Study on High Strength Bolted Tensile Joints -Mechanical Behavior under monotonic tensile loading-, Journal of Structural and Construction Engineering, No. 147, May 1968, pp. 33-41, Architectural Institute of Japan(in Japanese).
3) R.T.Douty, W.McGire : High Strength Bolted Moment Connections, Journal of the Structural Division, Proceedings of ASCE, Vol. 91, No. ST2, Apr. 1965, pp. 101-128.
4) Japanese Industrial Standard Committee : Sets of High Strength Hexagon Bolt, Hexagon Nut and Plain Washers for Friction Grip Joints(B1186), 1979(in Japanese).
5) Y.Yamada, Y.Yokouchi : The Programming of Elasto-Plastic Analysis by Finite Element Method - EPIC IV Manual-, Baihukan, 1971.3(in Japanese).
6) S.Timoshenko, S.Woinowsky-Krieger : Theory of Plates and Shells, Second Edition, McGraw-hill, 1970.
7) ASNOP Research Group : The Programming of Non-Linear Optimization, Nikkan Kougyo Shinbunsha, Apr. 1991(in Japanese).
8) T.Watanabe, M.Natori, T.Oguni : Numerical Analysis Software by FORTRAN 77, Maruzen, Dec. 1989(in Japanese).

Table 3.1 Dimensions of the Specimens

Specimen	Thickness of the Circular Plate (t)	Radius of the Circular Plate (R)	Bolt Pre-Stress	High Strength Bolt
NB-1	25	78	11.7	M16(F10T)
NB-2	25	52	5.85	M16(F10T)
NB-3	19	52	6.26	M12(F10T)
NB-4	10	52	6.26	M12(F10T)
NB-5	5	52	6.26	M12(F10T)
NB-6	10	52	6.26	M12(F10T)

unit : mm

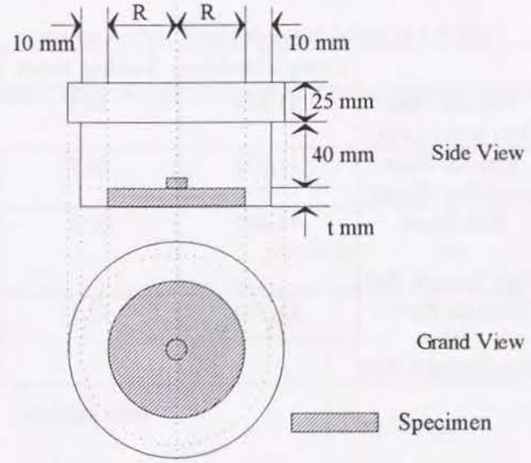

Half Part of Specimen

Table 3.2 Material Properties

Circular Plate	Yung's Modurus	Yielding Stress
(less than 10 mm)	21000	28.5
(more than 10 mm)	21000	26.9

unit kgf/cm2

Table 3.3 List of Analytical Cases

Case	Thickness of the Circular Plate	Radius of the Circular Plate	Radius to Thickness Ratio
AS-1	22	52	2.36
AS-2	19	52	2.74
AS-3	15	52	3.47
AS-4	10	52	5.2
AS-5	5	52	10.4
AM-1	25	78	2.08
AM-2	19	78	4.11
AM-3	15	78	5.2
AM-4	10	78	7.8
AL-1	25	104	4.16
AL-2	19	104	5.47

(unit : mm)

Table 3.4 Material Properties used in the Analysis

	Young's Modulus	Yielding Stress
Circular Plate (less than 10 mm)	21,000	28.5
Circular Plate (more than 10 mm)	21,000	26.9
Bolt Shank of High Strength Bolt	21,000	90.1
Threaded Portion of High Strength Bolt	15,700	67.1

(unit kgf/mm^2)

Table 3.5 Results of Regression

C_1	C_2	C_3	C_4	C_5	C_6	C_7
1.63	0.01	3.65	0.845	1.34	7.30	0.01

$$\frac{K}{K_0} = \left\{C_1\left(\frac{t}{R}\right)^{C_2} - 1\right\}\left(1-\frac{P}{P_u}\right)^{C_3} + \left\{1 - C_4 - C_5\left(\frac{t}{R}\right)^{C_6}\right\}\left(1-\frac{P}{P_u}\right)^{C_3} + \left\{C_4 + C_5\left(\frac{t}{R}\right)^{C_6}\right\}\exp\left\{-1.5\left(\frac{P}{P_0}\right)^{8}\right\}\left(1-\frac{P}{P_u}\right)^{C_7}$$

t : Thickness of the Circular Plate

R : Radius of the Circular Plate

P : Applied Tensile Load

P_0 : Bolt Pre-stress Force

P_u : Ultimate Strength of the Joint

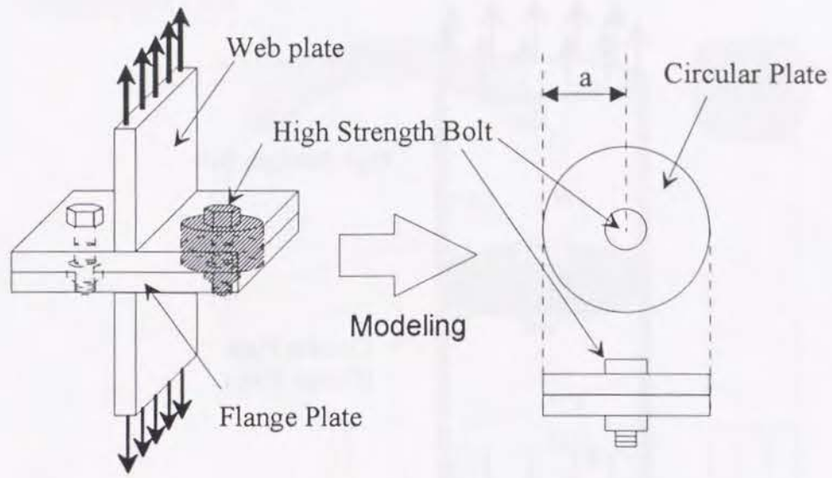

Fig. 3.1 Model of High Strength Bolt and its Adjacent Flange Plate (BAF Model)

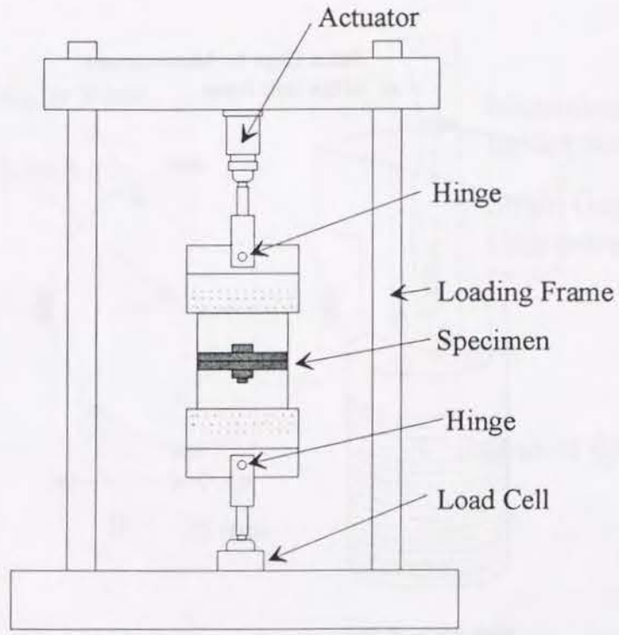

Fig. 3.2 Testing Setup

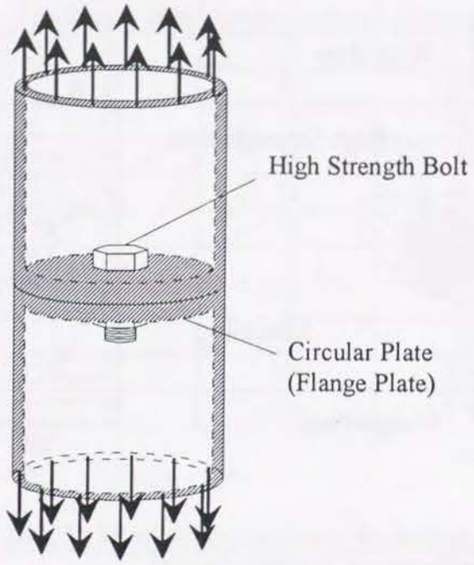

Fig. 3.3 Schematic View of Loading

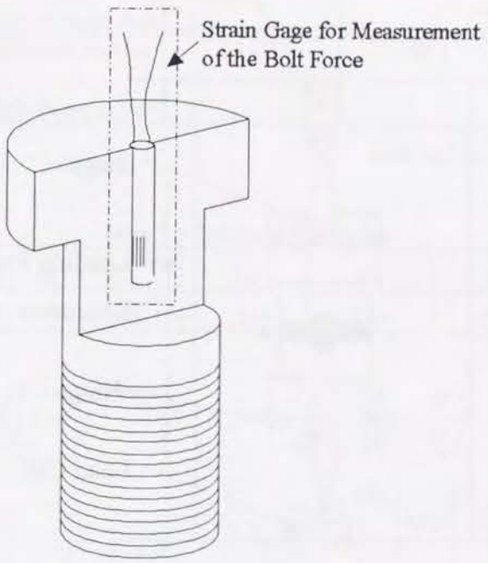

Fig 3.4 Schematic View of the Strain Gage for Measurement of the Bolt Force and its Location

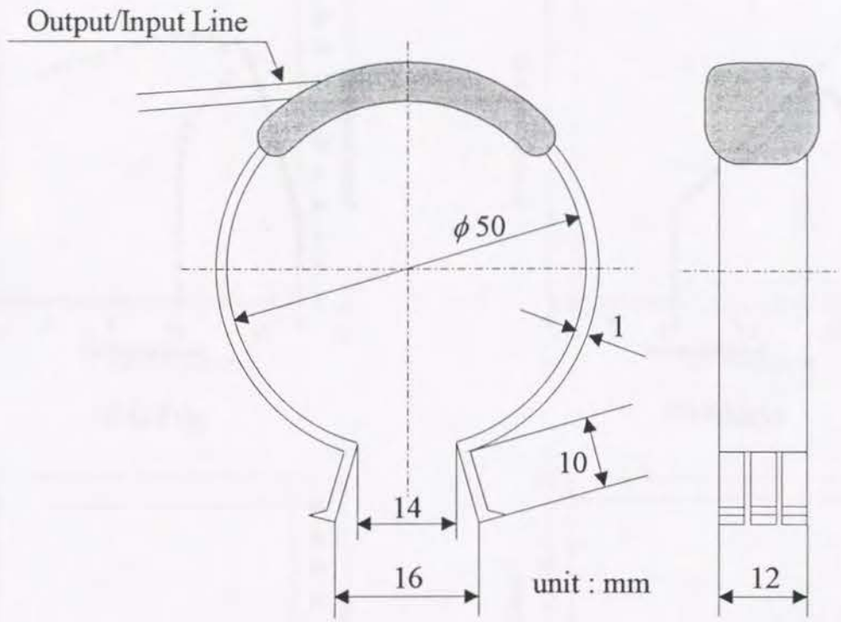

Fig. 3.5 Displacement Transducer for Measuring the Gap

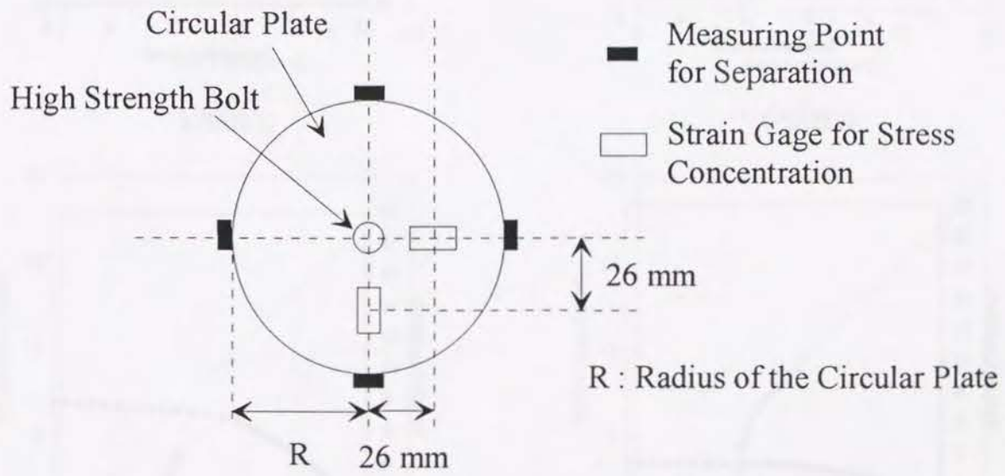

Fig. 3.6 Location of the Strain Gages glued on the Circular Plate and Displacement Transducer

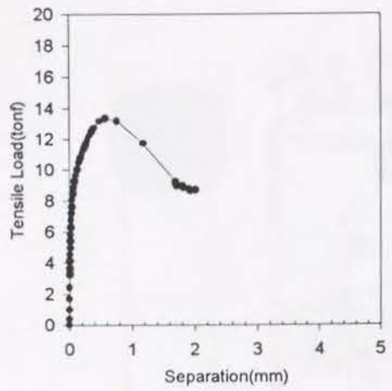

(a)BAF-1

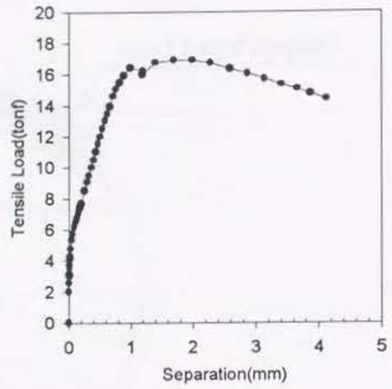

(b) BAF-2

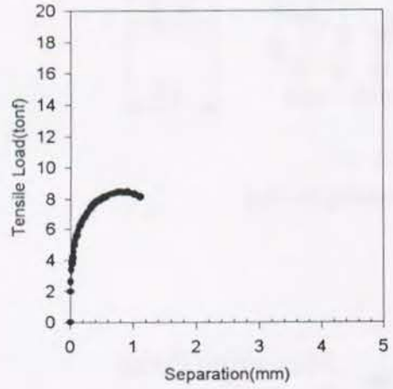

(c)BAF-3

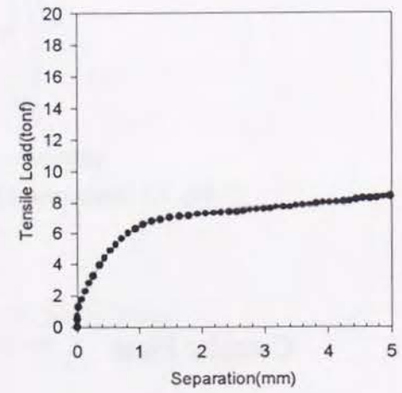

(d)BAF-4

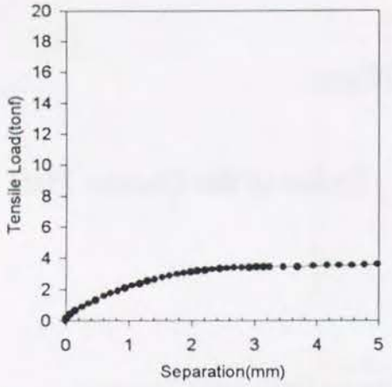

(e)BAF-5

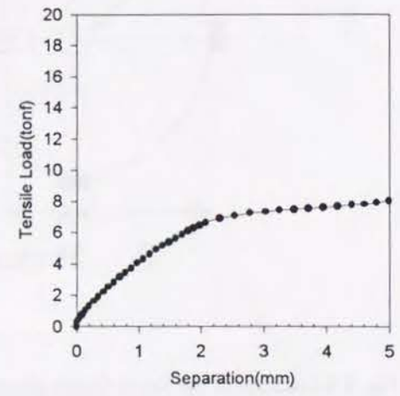

(f)BAF-6

Fig. 3.7 Load-Separation Curves of BAF Model

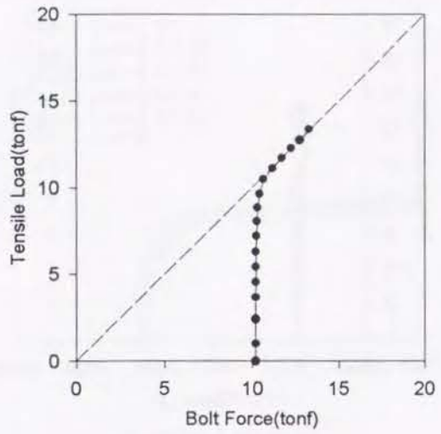

(a) BAF-1

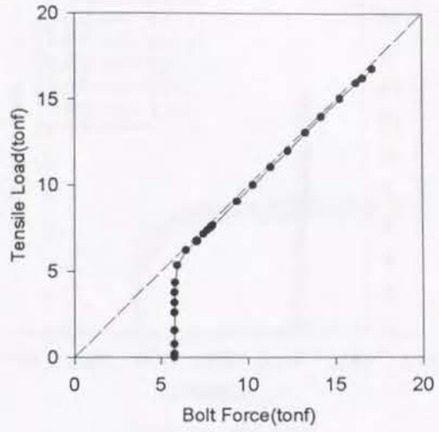

(b) BAF-2

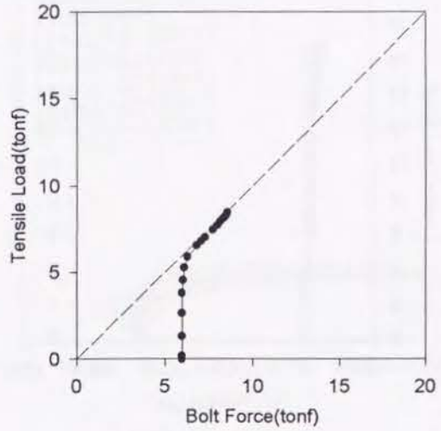

(c) BAF-3

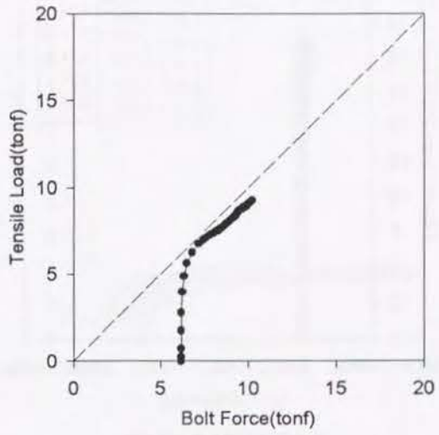

(d) BAF-4

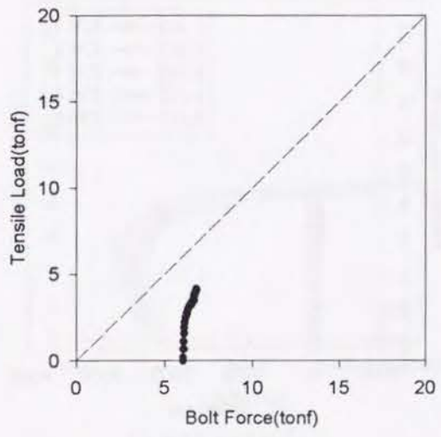

(e) BAF-5

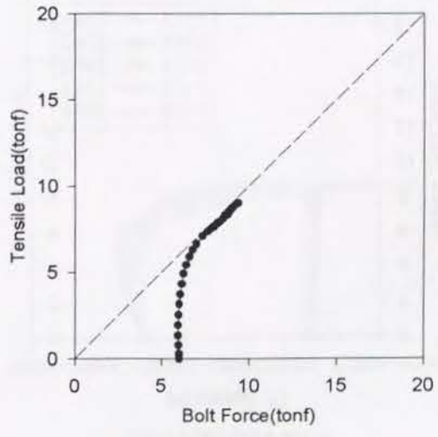

(f) BAF-6

Fig. 3.8 Load-Bolt Force Curves of BAF Model

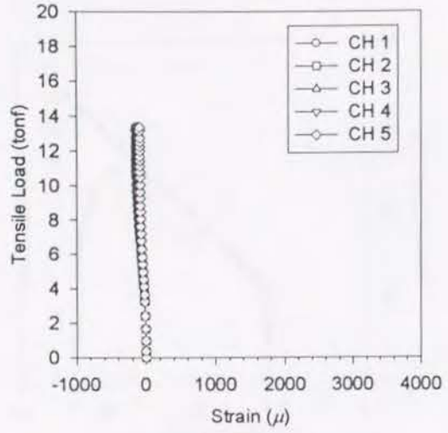

(a) BAF-1 (A side)

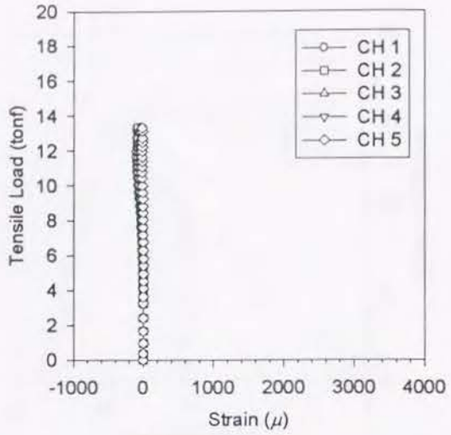

(b) BAF-1 (B side)

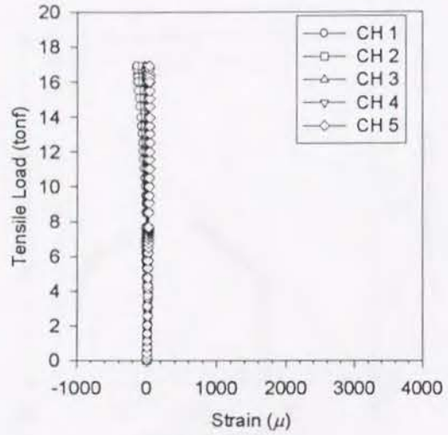

(c) BAF-2 (A side)

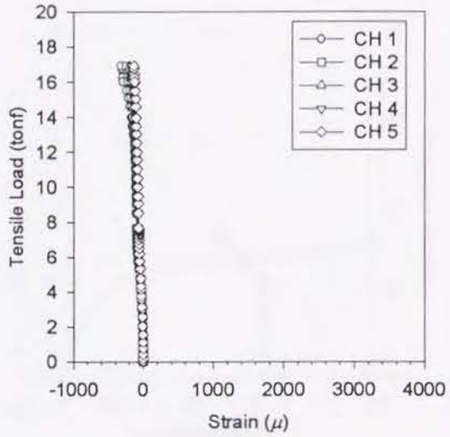

(f) BAF-2 (B side)

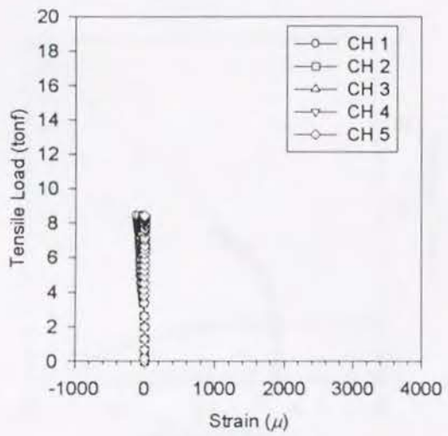

(e) BAF-3 (A side)

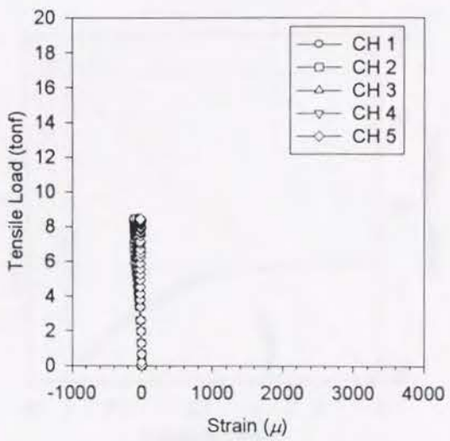

(f) BAF-3 (B-side)

Fig. 3.9 Strain Distribution on the Circular Plate (continued)

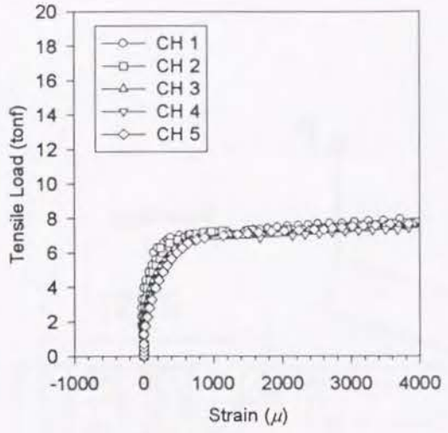

(g) BAF-4 (A side)

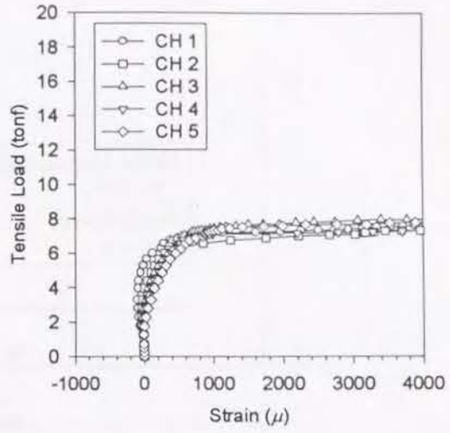

(h) BAF-4 (B side)

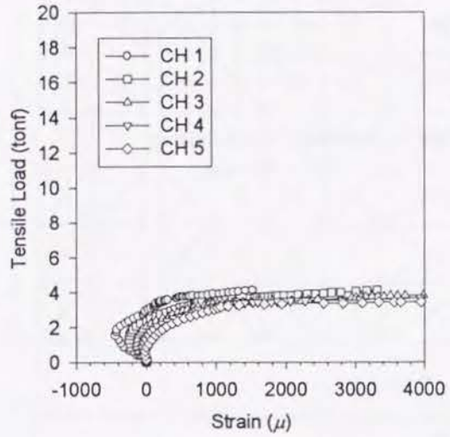

(i) BAF-5 (A side)

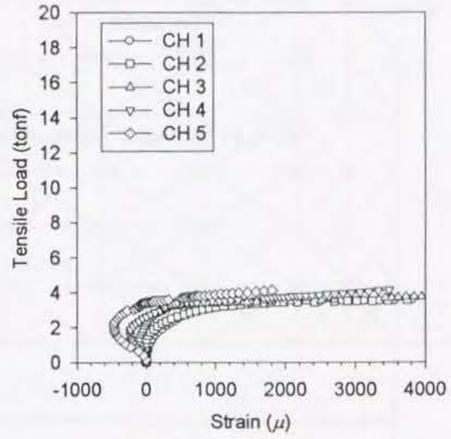

(j) BAF-5 (B side)

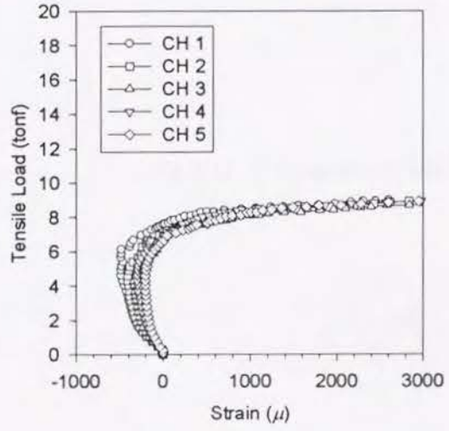

(k) BAF-6 (A side)

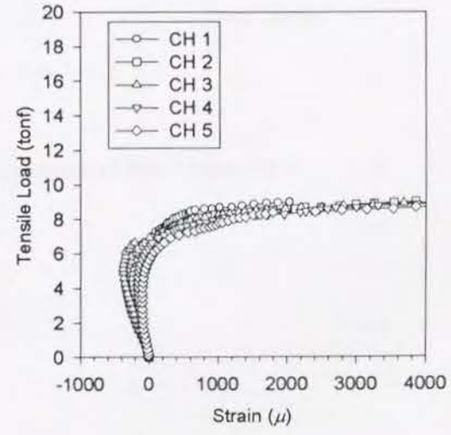

(l) BAF-6 (B side)

Fig. 3.9 Strain Distribution on the Circular Plate

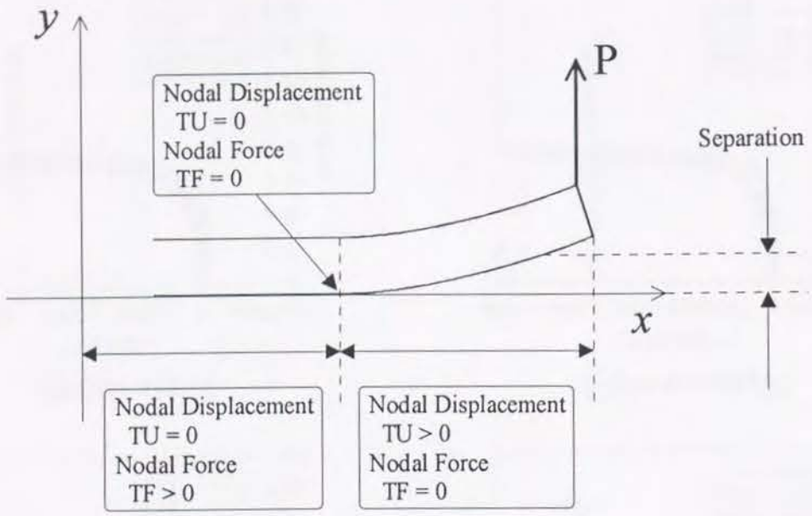

Fig .3.10 Schematic Figure of Procedure considering Boundary Non-Linearity

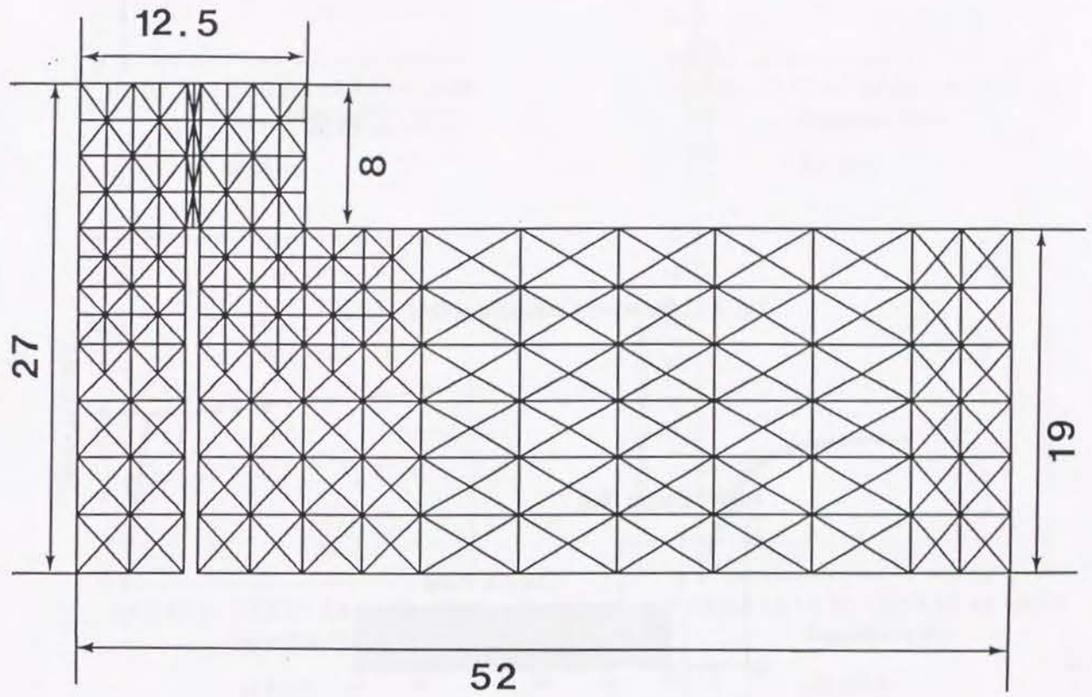

(unit : mm)

Fig. 3.11 Example of Finite Element Discretization of BAF Model(AS-2)

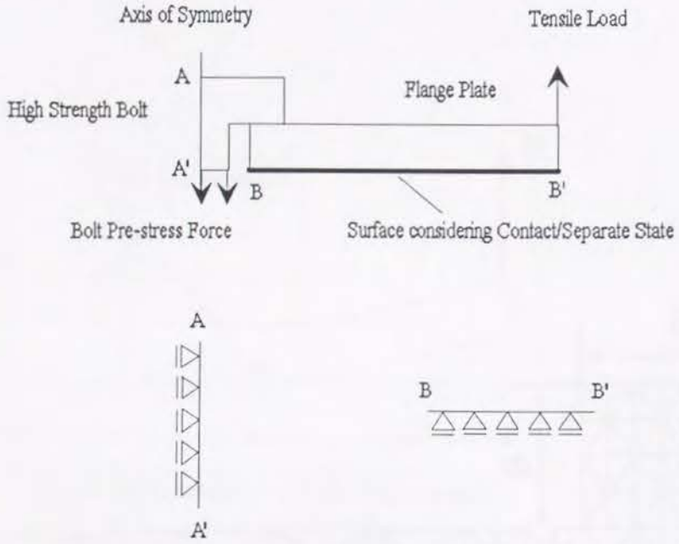

Fig. 3.12 Boundary Conditions of BAF Model

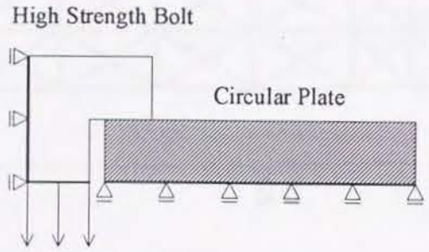

(a) Introducing Bolt Pre-stress Force

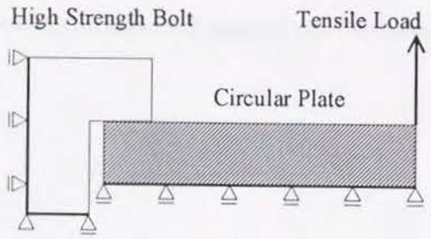

(b) Applying Tensile Load

Fig. 3.13 Loading Procedure of the Analysis

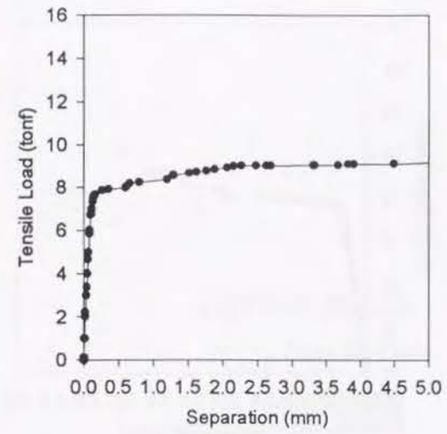

(a) AS-1

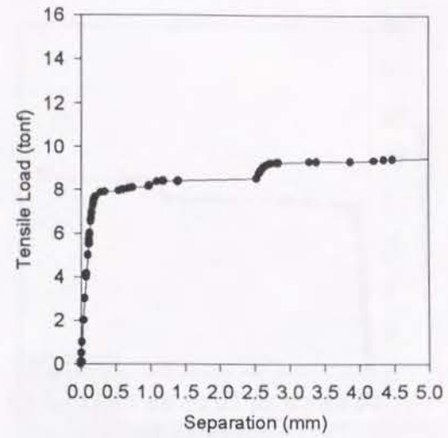

(b) AS-2

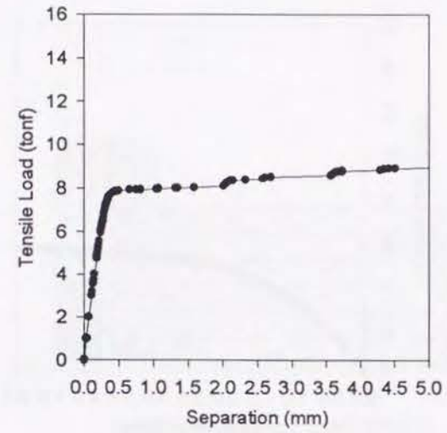

(c) AS-3

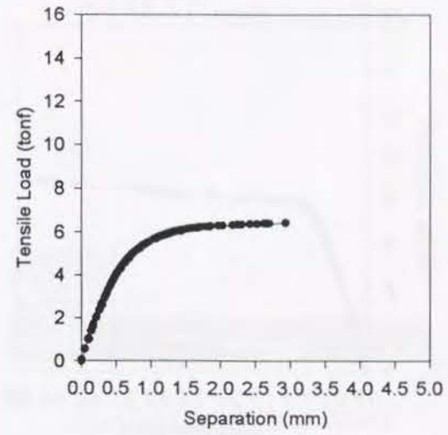

(d) AS-4

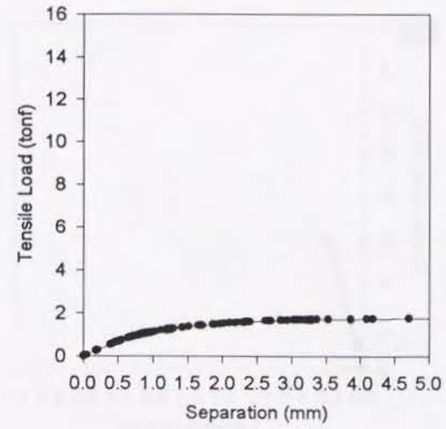

(e) AS-5

Fig. 3.14 Load- Deformation Curves (Analysis) (continued)

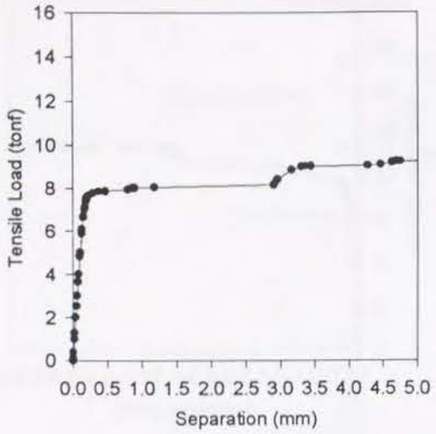

(f) AM-1

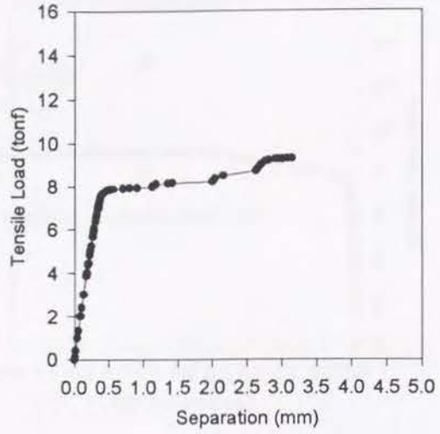

(g) AM-2

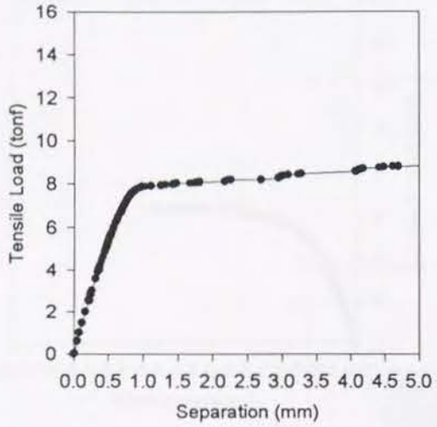

(h) AM-3

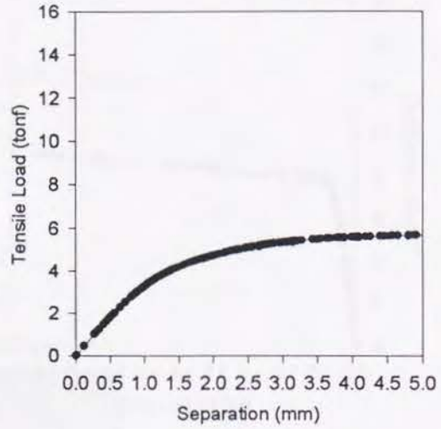

(i) AM-4

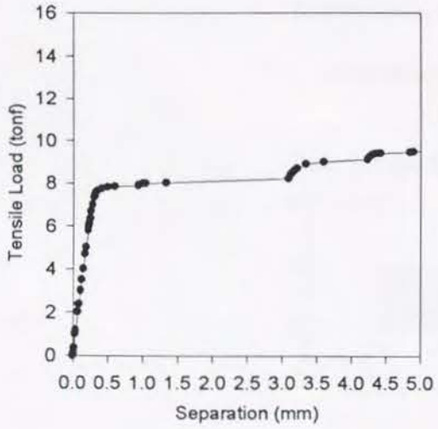

(j) AL-1

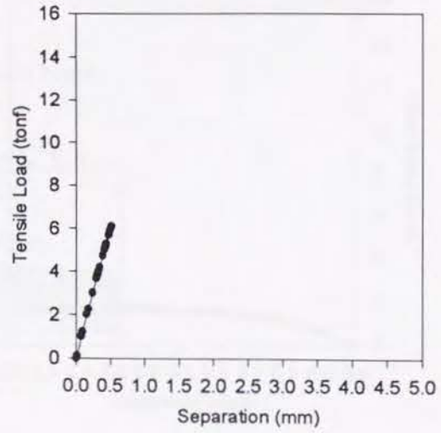

(k) AL-2

Fig. 3.14 Load-Deformation Curves (Analysis)

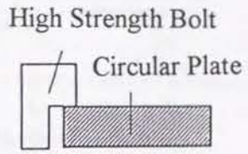

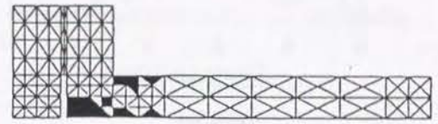

(b) AS-5 (Tensile load 10kN)

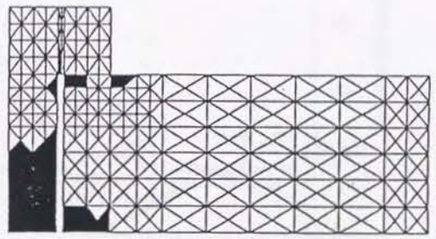

(a) AS-2 (Tensile load 80kN)

(c)AS-5 (Tensile load 20kN)

■ : Yielding Element

Fig. 3.15 Progress of Yielding Area

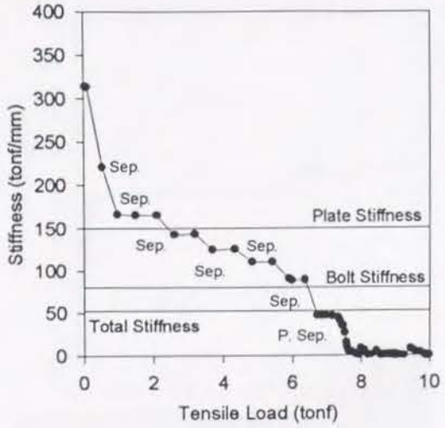

(a) AS-1

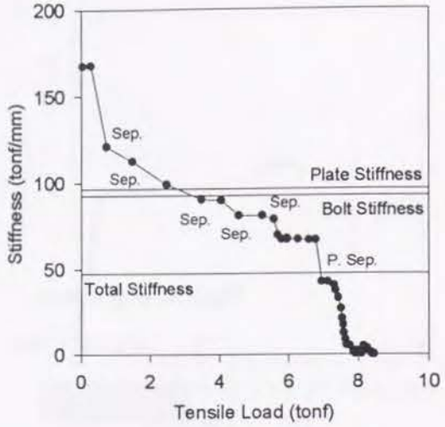

(b) AS-2

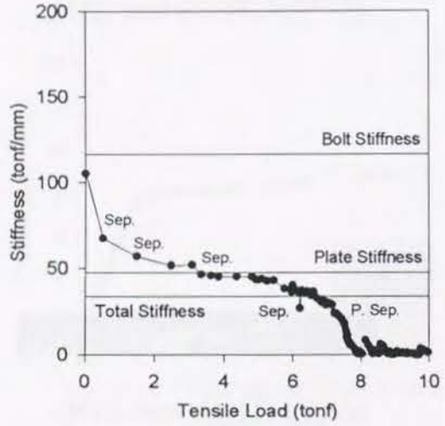

(c) AS-3

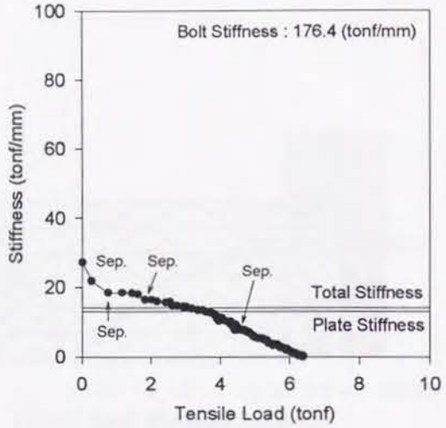

(d) AS-4

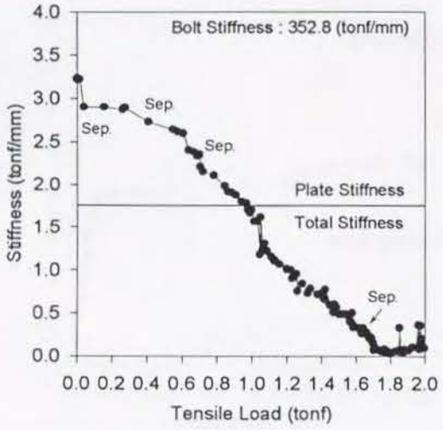

(e) AS-5

Fig. 3.16 Stiffness-Load Curves (Analysis) (continued)

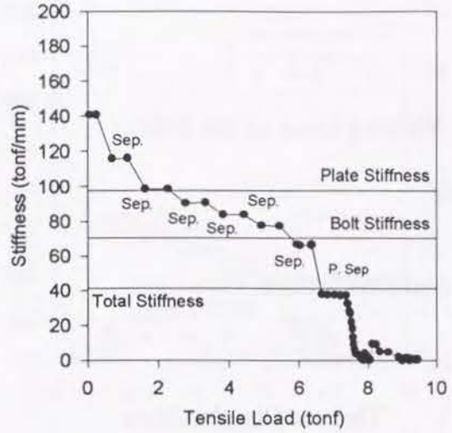

(f) AM-1

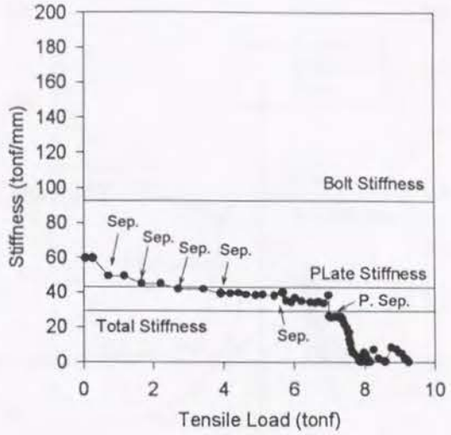

(g) AM-2

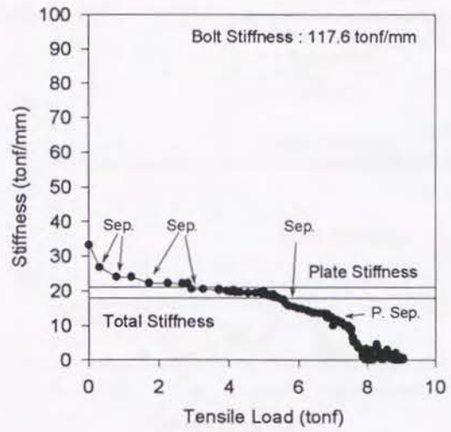

(h) AM-3

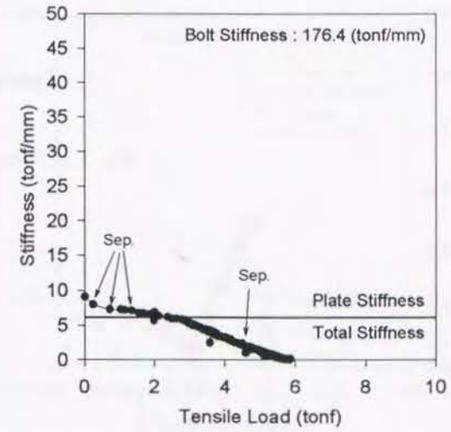

(i) AM-4

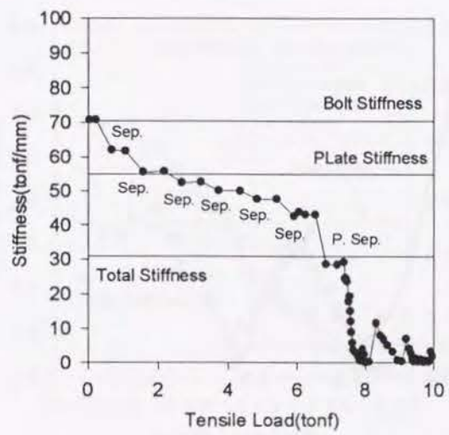

(j) AL-1

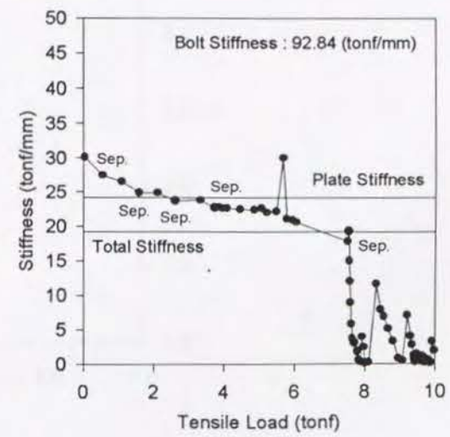

(k) AL-2

Fig. 3.16 Stiffness-Load Curves (Analysis)

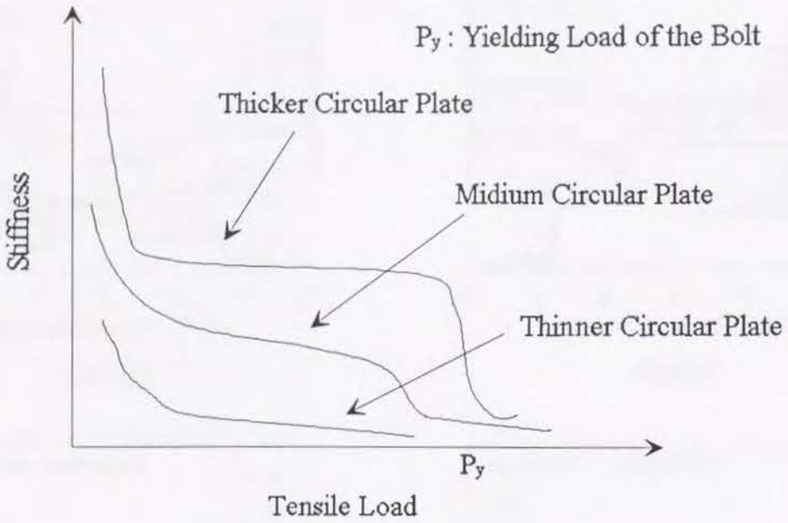

Fig. 3.17 Pattern of Stiffness-Load Curves

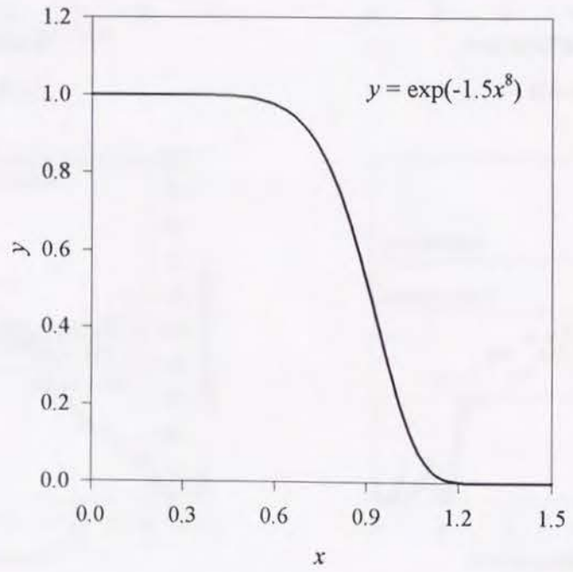

Fig. 3.18 Outline of the Function

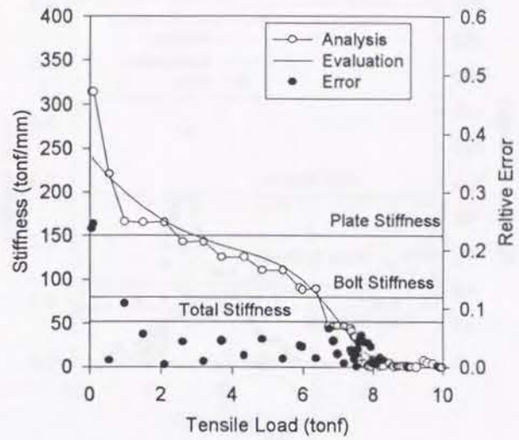

(a) AS-1

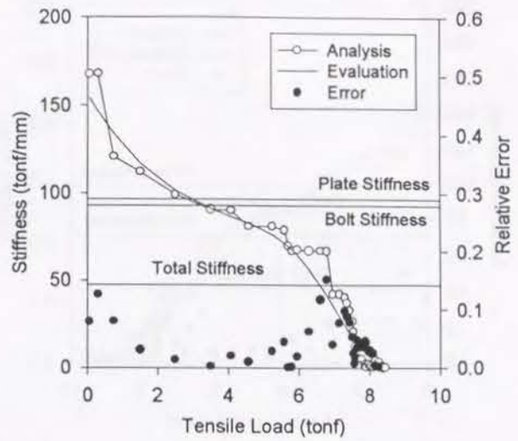

(b) AS-2

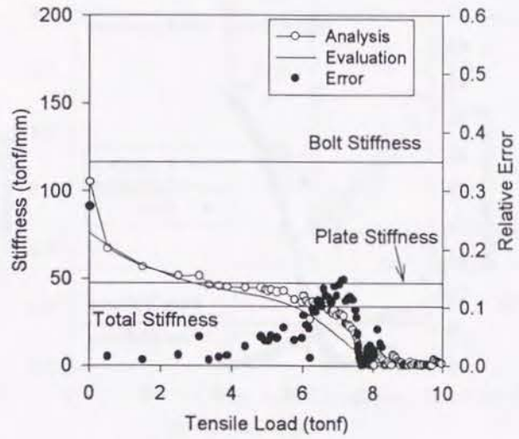

(c) AS-3

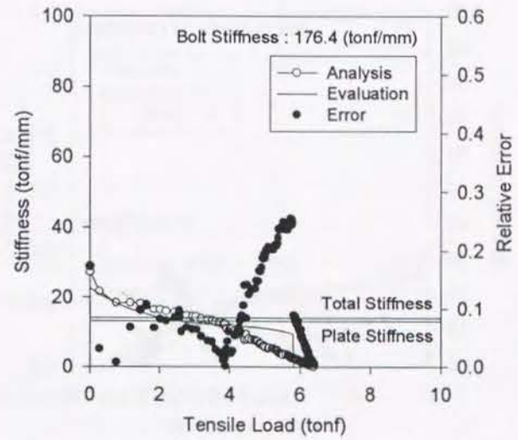

(d) AS-4

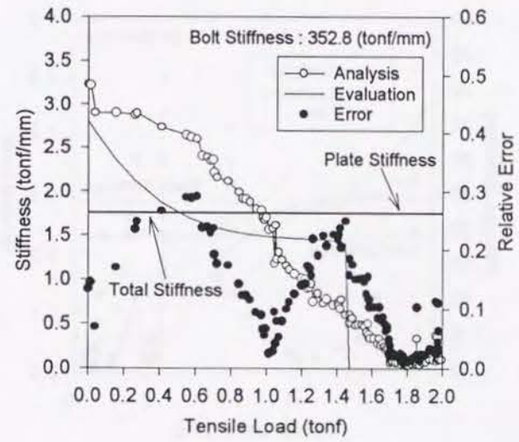

(e) AS-5

Fig. 3.19 Evaluation Results of the Stiffness (continued)

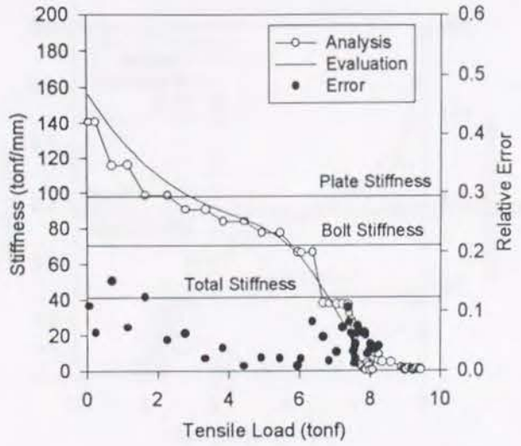

(f) AM-1

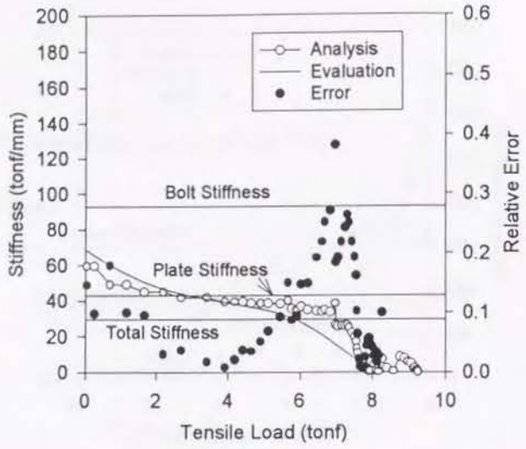

(g) AM-2

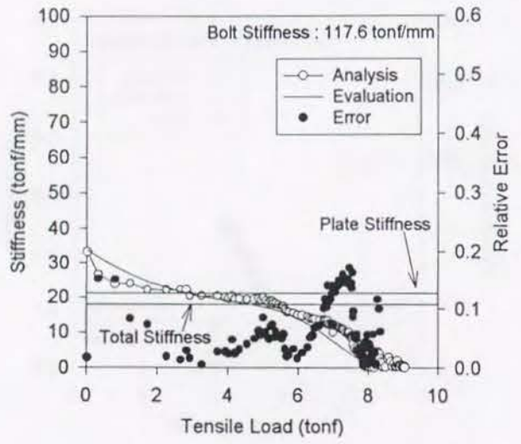

(h) AM-3

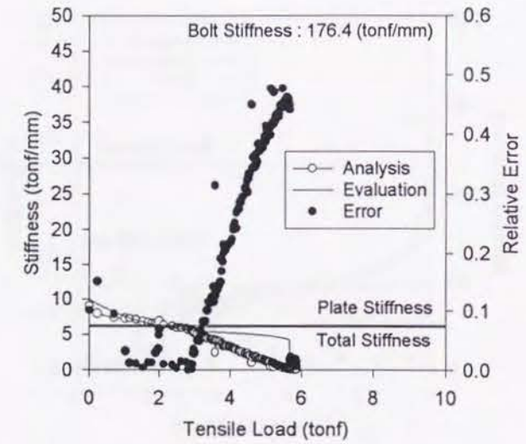

(i) AM-4

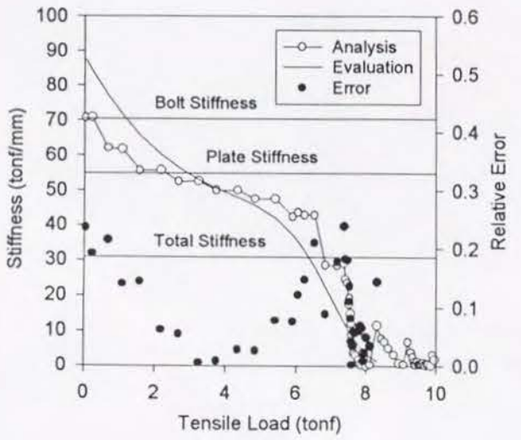

(j) AL-1

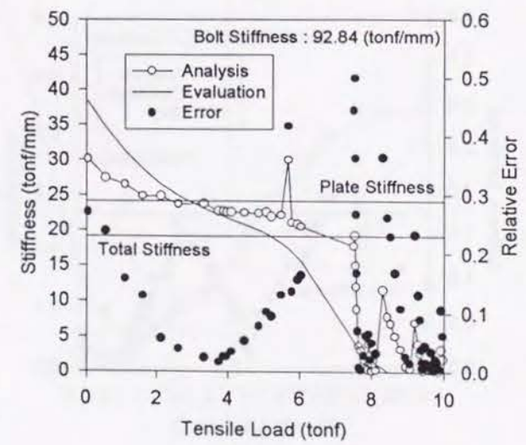

(k) AL-2

Fig. 3.19 Evaluation Results of the Stiffness

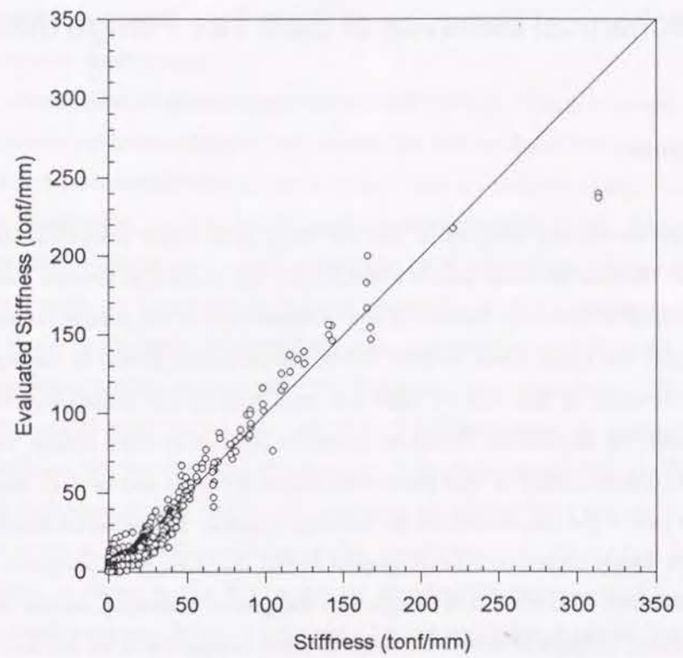

Fig. 3.20 Comparison between the Experimental and Analytical Results

Chapter 4

Mechanical Behavior of Split Tee Flange Joints

4.1 Introduction

In this chapter, the mechanical behavior of split tee flange joints under monotonic loading and cyclic loading is studied. The split tee flange joint is a fundamental type of the high strength bolted tensile flange joints and it is classified into short connection type. Overall view of the joint is shown in Fig. 4.1. As shown in this figure, two flange plates (in other words, end plates) are jointed by the high strength bolts. The mechanical behavior of this type of joints has been investigated extensively during 1970's for architectural engineering applications. Based on the results obtained by these studies, various evaluation methods of the maximum strength of such joints were proposed(refer to section 1.2), and results of these studies became a part of the specification in the building design[1]. But proposed evaluation method for maximum strength mainly depend on the experimental results; therefore, the applicability of it for various joint types are unknown. Therefore, it is thought that the general evaluation method for the maximum strength, which should be applicable for wide range of joints, is expected to be developed. However, the studies in the past on such joints have not been extended to such ranges.

Recently, attention is paid to the advantages of such joints because of its structural simplicity, easiness of erection, and superiority in the aesthetic design; so that the study on such joints is being actively carried out in. On the other hand, the present circumstance that the draft design code of high strength bolted tensile flange joints for bridge structures are proposed by the subcommittee of establishment of design code of JSSC based on the results obtained from the studies for both architectural and civil engineering structures[2]. However, as discussed in that draft code, there are many technical problems on this type of joints to be solved. Therefore, in order to establish the rational design code for this type of joints, further studies should be suggested to be carried out.

The objective of this study is to investigate the mechanical behavior of split tee flange joints in detail by not only the experiment but also finite element analysis, especially for the joint which has various thickness and width of the flange plate. Furthermore, the joint stiffness, separation behavior and cyclic behavior of such joints are also discussed.

4.2 Mechanical Behavior under Static Loading

4.2.1 Experimental approach

(a)Outline of tensile loading test

Extending the investigation on contact/separation behavior of high strength bolts and its adjacent flange plate model to that of fundamental bolted joint, namely, the split tee flange joint, the tensile loading test is carried out. Since the mechanical behavior of this type of joint is considered to significantly depend on the thickness of the flange plate, it is determined to make the thickness of the flange plate be variable, and the effect of flange plate thickness on the mechanical behavior is investigated. The specimens prepared for this experimental study are shown in Fig. 4.2 and dimensions of all the specimens are summarized in Table 4.1. As shown in this table, 3 types of specimens are prepared, and thickness of the flange plate among these specimens is different each other. The thickness of the flange plate of ST1, ST2 and ST3 are 5 (mm), 10 (mm) and 22 (mm) respectively. The width of the flange plate, the loading length between the center of the bolt and the web plate and the diameter of the high strength bolt are the same among the specimens. The high strength bolt used in the specimens are M12 (F10T) and the bolt pre-stress force (6.26 tonf) is given to the bolt according to the specification of JIS[3]. Test setup used in this experimental study is shown in Fig. 4.3, where the electrically servo controlled hydraulic actuator is utilized, whose loading capacity is +/-30 (tonf) under static loading. The detail of testing machine can be referred to section 2.2.1. As shown in this figure, 4 hinge connections used for loading apparatus can eliminate the eccentric loading, so that bending moment will not be subjected to the specimens.

Tensile load, separation between two flange plates and bolt forces are measured during the loading, where applied tensile load is measured by the load cell built in the actuator. The separation between two flange plates are measured by the strain gage type displacement transducer as shown in Fig. 4.4. On the other hand, Bolt force is obtained based on the output of the strain gage installed into the center of the bolt shank as shown in Fig. 4.5. The calibration sheet of the strain of the bolt to the bolt force is made by the proof loading in fabrication process. The separation at the center of the specimen where the tensile load is applied and the separation at the bolt position which is useful information for investigation of the bolt elongation are also measured as shown in Fig. 4.6.

The loading is operated by the micro computer; the loading command is sent to analog-controller of actuator through GP-IB. The control of applied load is made by the displacement of the actuator. In this experiment, the loading is continued until the maximum loading point is obtained. In addition, on line measuring are made by the same computer.

(b) Results and discussions

The load vs. separation curves obtained from the experiment are shown in Fig. 4.7. The horizontal axis shows the separation between two flange plates, and the vertical axis shows the applied tensile load. It is understood that the thicker the flange plate is, the higher the initial slope of the curve is obtained.

particularly, in case of thicker flange plate, it is understood that the separation is relatively small; so that it is considered that the deformation of the flange plate is not significant. In addition, as for the failure mode, the high strength bolt is severely pulled and failure occurs at the bolt thread. On the other hand, in case of thinner flange plate, the deformation of the flange plate is severe and the separation between two flange plates occurred at the early stage of loading; namely, the flange plate is bent between the location of the bolt and the loading point and the failure only occurs at the flange plate; whereas, the high strength bolt is not observed to have severe deformation.

The load vs. bolt force curves obtained by the experiment are shown in Fig. 4.8. The horizontal axis shows the bolt force and the vertical axis shows the load which is one half of the applied tensile load to compare with a change of the bolt pre-stress force. Here, the bolt force is calculated based on the calibration table. It is found that in case of the thinner flange plate, the bolt force increases at the early stage of loading; Particularly, before the load reaches to the bolt pre-stress force. On the other hand, if the split tee flange joint has thick flange plate, the bolt force is considered to not increase until the applied tensile load reaches to the bolt pre-stress force. Therefore, the considerable thick flange plate should be required in order to prevent the increase of the bolt force.

4.2.2 Analytical approach

(a) 3 -dimensional analysis for split tee flange joints

In this section, 3-dimensional analysis for split tee flange joints is discussed. The analysis is carried out in order to investigate the mechanical behavior in detail, especially, the contact/separate behavior, the stiffness of the joints and the deformation of the bolts. Generally speaking, the numerical analysis is expected to be very powerful for investigation of mechanical behavior quantitatively because of its versatility and its advanced technology. From the view point of design for the tensile joints in practice, 2-dimensional analysis is desired due to the simplicity compared with 3-dimensional analysis. Since 2-dimensional analysis for this model may have some difficulties due to non-uniformity of the shape in width direction and the local deformation characteristic is focused in this study, 3-dimensional analysis is carried out.

The analytical model for the split tee flange joint is shown in Fig. 4.9. This model is one eighth of overall joint by considering axisymmetry of structures. Since the gap between two flange plates increases as the tensile load is applied, not only the material non-linearity but also boundary non-linearity must be considered in this analysis. That is, the boundary condition on the contact surface is changed based on the nodal force and displacement at each loading step. The procedure to change the boundary condition is the same as the analysis used for the BAF model(refer to section 3.3.2). This 3-dimensional finite element analysis program is coded by extending the 2-dimensional analysis program described in Chapter 2.

All the cases of the analysis are listed in Table 4.2. The thickness and the width of the flange plate are varied. Because it is considered that the mechanical behavior of split tee flange joints are significantly affected by the geometrical dimensions of the flange plate. The thickness of the flange plate is determined to be 10 (mm), 15 (mm) and 22 (mm), and the width of the flange plate is determined to be 63 (mm), 78.75 (mm) and 94.5 (mm), where the width, 63 (mm) is the same as that of test specimen and standard among analytical cases. Other dimensions of the models for all the cases are determined based on the specimens used in the experiment. Here, attention is paid to the capability to model with various shapes of the flange plates and the finite element discretization is made by the tetrahedral elements shown in Fig. 4.10. As for the discretization by finite element in this study, the analytical model is discretized by the hexahedrons at first; and then, each hexahedron is further discretized into 24 tetrahedrons. In this figure, discretization by the hexahedrons is only shown. The discretization of the bolt and its adjacent structural elements where high stress concentration is predicted to occur is made by the fine mesh. The number of the nodal points and the elements in the case that a specimen has the thickest and the widest flange plate(ST-A8) is 4,531 and 18,540 respectively.

Boundary conditions of this model are also shown in Fig. 4.11. The surface that two flange plates contact each other is the plane to consider the boundary non-linearity, namely, separation or contact state. At this plane considering contact/separation conditions, the friction is assumed to be infinity; therefore, the slip of contact surface is not assumed to occur. On the other hand, on the surface where the bolt and the flange plate contact each other, such a boundary non-linearity is not considered and these are assumed to be continuous. The material constants for the bolt and the flange plate are provided independently as shown in Table 4.3. In addition, the washer is neglected in this model. Because it is considered that there exist only little effect on the overall mechanical behavior of the joint. Moreover, the bolt thread is also not exactly modeled but modeled by uniform cross section same as bolt shank. However, different material properties are used for the bolt thread. Material properties for the bolt shank and the bolt thread used in the analysis are also shown in Table 4.3. Referring the specifications of JIS[3], the material properties of the bolt thread is determined based on that of the bolt shank by taking into account the difference of effective cross sectional area. Furthermore, the stress-strain relation used in this analysis is assumed to be elastic perfectly plastic.

The procedure of this analysis is briefly summarized in the followings: at first, bolt pre-stress force (6.26 tonf specified by JIS) is applied at the end of the bolt as uniform load. Secondary, after this bolt pre-stress force is obtained, the bolt end is fixed in vertical direction(*z*-direction). Finally, uniform tensile load is applied along the edge of the tee web plate. The flow of the procedure of this analysis is shown in Fig. 4.12.

(b) Results and discussions

1) Load-separation relation and yield strength

The load vs. separation curves of all the cases obtained from the analysis are shown in Fig. 4.13. In these

figures, the horizontal axis shows the separation at the center of the flange plates. The vertical axis shows the applied tensile load divided by the width of the flange plate; that is, the applied load per unit width. In addition, the yield strength for each case are summarized in Fig. 4.14(a). Horizontal axis is width of the flange plate normalized by the standard width 63 (mm) and the vertical axis is the yield load divided by the width of the flange plate, namely, yield load per unit width. Here, the yield load is defined by the point "Y" on the load-separation curve obtained from this analysis as indicated in Fig. 4.14(b). This point "Y" is defined as the intersection of the tangential lines in the elastic area and plastic area.

From these figures, in case of the thinnest flange plate that is 10 (mm), it is understood that the shape of curves is almost same in spite of the difference of flange plate width. On the other hand, in case of the thickest flange plate that is 22 (mm), it is found that the post yielding behavior is different, and the yielding strength decreased gradually as the width of the tee web plate becomes large. Moreover, in case of the medium thickness among analytical cases, little difference of the load-separation curve can be found. Therefore, it is concluded that if the tensile yield strength is evaluated by tensile applied load per unit width, the thinner flange plate makes no difference on the strength but thicker flange plate makes significant difference on the strength. This phenomenon is caused by the difference in the failure mode of the split tee flange joint. In case of the thinner flange plate, the flange plate is considered to be bent uniformly in width direction and it failed, so that the tensile yield strength per unit width is almost same. On the other hand, in case of thicker flange plate, the behavior is considered to depend on the failure of the bolt, not the flange plate. Therefore, if the estimation of yield strength is made based on the tensile load per unit width, the yield strength becomes lower as the width of the flange plate becomes larger. As shown in Fig. 4.14(a), whether the behavior is mainly affected by the flange plate or by the bolt can be judged according to the yield strength vs. width relation. In other words, if the yield strength is constant in spite of the different width, the behavior of the joint depends on the flange plate; on the other hand, if the yield strength is not same for the different width, the behavior of the joint depends on the bolt. In addition, the more decrease in yield strength as the width becomes large is obtained, the more significantly the behavior of the joint is affected by the bolt. Furthermore, if the flange plate is assumed to be in elastic or rigid, the curve of yield strength vs. width relation can be given by hyperbolic type.

It is discussed about the applicability of the existing draft specification[2] for the split tee flange joint whose thickness of the flange plate is 22 (mm), comparing with the analytical results. The strength obtained by the specification is also shown in Fig. 4.14(a). From this figure, it is found that the evaluation of the yield strength by the existing specification is in a good agreement with analytical results and it is considered to be applicable to the case of thick flange plate. However, the error of the yield strength evaluation is considered to be larger as the width of the flange plate becomes larger. Therefore this evaluation procedure used in the specification should be modified by taking into consideration the width as a parameter for accurate evaluation. In addition, for the split tee flange joint whose thickness of the flange plate is out of the range by the specification, the yield strength evaluation is proposed and

carried out by the following procedure: The simple model as shown in Fig. 4.15 is considered. This model is the beam with the same cross section as that of the flange plate fixed at the edge of the web plate and the location of the bolt center. Then, the yield load is defined by the reaction force when the maximum stress reaches to the yield stress as the rotationally fixed end of this beam is displaced. The result of the evaluation obtained by this procedure is compared in Fig. 4.14(a). It is found from this figure that the yield strength is estimated to be a little lower than that of the analytical results. Accordingly, it is considered that the proposed yield strength evaluation method gives a safe value and it may be enough applicable.

2)Load-bolt force relation

Tensile load vs. bolt force curves obtained by the analysis are shown in Fig. 4.16. The horizontal axis is bolt force, and the vertical axis is one half of the applied tensile load to the model because of the comparison with the bolt force. In addition, the tensile load vs. bolt force curve in case of the rigid flange plate, is also shown in this figure. If the flange plate is rigid, the bolt force is kept constant until the applied tensile load reaches to the bolt pre-stress force; and then the bolt force increases equally as the applied tensile load increases.

It is understood from this figure that the bolt force increases before the applied tensile load reaches to the bolt pre-stress force for all the cases. Here, the increase of the bolt force in case of the thinner flange plate is larger than that in case of the thicker flange plate. Although it is considered to be caused by the prying force, this increase of the bolt force particularly for the case of thinner flange plate is considered to depend on the deformation of the flange plate not like the conclusion obtained in the past studies(refer to section 1.2). That is, in case of the thicker flange plate, it mainly depends on the prying force, on the other hand, in case of thinner flange plate, it depends on the tension and bending of the bolt caused by only the local deformation of the flange plate. This will be further discussed in the following section on the contact surface.

As for the width of the flange plate, the change of the bolt force for each case with different width of the flange plate is almost the same at the initial loading stage, however, the behavior of the bolt force is different after the difference of the load-separation curve is observed. It is found that the larger the width of the flange plate is, the smaller the bolt force is at the same level of applied tensile load. Since the deformation of the flange plate becomes large as the width of the flange plate is much narrower, the increase of the bolt force is considered to occur.

3) 3-dimensional deformation behavior on the contact surface and the distribution of the nodal force.

Deformations of the contact surface for all the cases when the applied tensile load reaches to the yielding load are shown in Fig. 4.17. In addition, deflection modes along the centerline of the flange plate in the longitudinal direction are also shown in Fig. 4.18. In Fig. 4.18, the deflection is magnified by 20 times of the computed deflection in order to show the state of the deformation clearly.

From these figures, in case of the thinner flange plate, it can be seen that the flange plate is bent at the bolt position and that there is almost no gap between two flange plates at the area from the bolt position to the outer edge of the flange plate. Moreover, it is understood that the deflection along the center line of the flange plate is smaller than that at the side edge of the flange plate. On the other hand, in case of the thicker flange plate, no significant bending deformation of the flange plate is observed, that is, the flange plate is rotated and translated and its rotation center is located on the outer edge of the flange plate. In addition, the significant gap at the bolt position is observed and it is considered that the large plastic deformation of the bolt took place. It is concluded that in case of the thicker flange plate, the bolt thread is elongated severely, on the other hand, in case of the thinner flange plate, the flange plate is deformed.

Distributions of the nodal forces on the contact surface when the applied tensile load reaches to the yielding load are shown in Fig. 4.19. In case of the thinner flange plate, the nodal forces are distributed between the bolt position and the outer edge of the flange plate; on the other hand, in case of the thicker flange plate, nodal forces are distributed only around the outer edge of the flange plate. Therefore, it is understood from the distributions of the nodal forces that in case of the thicker flange plate, the mechanical behavior of the joint is affected by the prying force, on the other hand, in case of the thinner flange plate, the mechanical behavior of the joint has no relation with the prying force. As for the width of the flange plate, in case of the narrower flange plate, the nodal forces tend to be distributed all over the flange plate in width direction. On the other hand, in case of the wider flange plate, the nodal forces do not tend to be distributed in width direction; namely, the nodal force at the side edge of the flange plate is not large. This is caused by the difference of the deflection along the width direction due to the less stiffness of the wider flange plate. Moreover, from these results, the effective width of the flange plate where the applied tensile load would be carried should exist and this effective width of the flange plate is considered to relate to the bolt pre-stress force.

4) The stiffness-load relationship

Stiffness vs. load curves for all the cases obtained from the analysis are shown in Fig. 4.20. The horizontal axis shows normalized applied tensile load divided by 2 times of the yielding load of the bolt. The vertical axis shows the stiffness of the joint per unit width based on the load-separation curve which has already shown in Fig. 4.13. The stiffness in this figure is the tangential slope of the load-separation curve, and it is calculated by dividing the increment of the load by the corresponding increment of the separation.

It is found from this figure that the thicker the thickness of the flange plate is, the higher the stiffness of the flange plate is obtained. In addition, it is considered that the initial stiffness until the normalized applied tensile load is about 0.2, is significantly affected by the thickness of the flange plate. Moreover, it is found that in case of thicker flange plate, initial stiffness is so high, but its decrease is significantly large. As for the width of the flange plate, in case of the thicker flange plate, it is found that

the shape of the curve is almost same for different width of the flange plate; on the other hand, in case of the thinner flange plate, the stiffness becomes different as the applied tensile load becomes larger, and the smaller the width of the flange plate is, the higher the stiffness is kept. Therefore, it is considered that there is almost no difference of the initial stiffness among the analytical cases with various width of the flange plate if the stiffness is estimated by the unit width of the flange plate. In addition, for both the case of thicker flange plate and the case of thinner flange plate, it is understood from this figure that the normalized applied tensile load is smaller than unity when the stiffness becomes almost equal to zero. Therefore, it is considered that the load carrying capacity of the bolt is not utilized effectively. Especially, even in case of the thicker flange plate, the normalized applied tensile load is about 0.8 when the stiffness becomes zero. The additional increase of the bolt force occurs in addition to that of the bolt force caused by the applied tensile load. Accordingly, in order to prevent this additional increase of the bolt force and to make it zero, the considerable thicker flange plate may be required. Moreover, it is also found that the stiffness at the yielding load specified by the draft specification of the high strength bolted tensile joints for bridge structures[2] is almost zero, so that the strength until the stiffness becomes to zero is expected in this specification.

In order to assess the effect of the initial bolt pre-stress force, the stiffness of the high strength bolt, the stiffness of the flange plate and total stiffness of the joint for all the cases are listed in Table 4.4. Here, these values are divided by the width of the flange plate; therefore, these are the stiffness per unit width of the flange plate. The stiffness of the bolt is also determined by using the model that assume the bolt to be the bar. It is defined by the following equation.

$$K_B = \frac{A_B E_B}{\ell_B w_B} \tag{4.1}$$

in which, K_B is the stiffness of the bolt, A_B, the effective cross sectional area of the bolt, E_B, Young's modulus of the bolt, l_B, one half of the clamped length of the bolt, w_B, the diameter of the bolt.

Next, the stiffness of the flange plate is also determined by using the model as shown in Fig. 4.21. This model is the plate which has three fixed edges and one free edge subjected to concentrated load at the center of the free edge. This concentrated load corresponds to the load applied to the bolt. The definition of the stiffness of the flange plate is as follows:

$$K_P = \frac{E_P h^3}{12(1-\nu^2)} \frac{1}{0.168 l_P^2} \frac{1}{w_P} \tag{4.2}$$

in which, K_P is the stiffness of the flange plate, E_P, Young's modulus, h, the thickness of the flange plate, ν, Poisson's ratio, l_P, the length between the edge of the web plate and the center of the bolt, w_P, the width of the flange plate.

In addition, the total stiffness of the joint is determined by using the model in which the flange plate model

and the bolt model is assumed to be connected in series. The equations of the total stiffness is shown as follows:

$$K_T = \frac{K_B K_P}{K_B + K_P} \tag{4.3}$$

in which, K_T is the total stiffness, K_B, the stiffness of the bolt, K_P, the stiffness of the flange plate.
From the results, it is found that the stiffness of the joint obtained by the analysis is higher than the total stiffness for all the cases. The ratio of the stiffness obtained from the analysis to the total stiffness is about 3 in case of thinner flange plate or about 2 in case of thicker flange plate when the load level is about 0.2. Therefore, the increase of the stiffness is also expected for the case that has thinner flange plate.

4.3 Fatigue Behavior of the Split Tee Flange Joints

4.3.1 Outline of fatigue test

High strength bolted tensile joints have promising superiority such as easiness of the erection, good mechanical behavior due to high pre-stress force given to the bolt. Especially, according to the fact that the variation of the bolt force can be kept as small as possible due to the bolt pre-stress force, high strength bolted tensile joints seems to have a good characteristics for fatigue behavior as well. However, in order to apply tensile joints for bridge structures, it is important to investigate fatigue behavior of this type of joints, very little study on fatigue strength or fatigue behavior of tensile joints has been carried out except for only a reference[4] in civil engineering. Considering such a present situation, the necessity of further study based on both analytical and experimental approaches is one of motivations of current study. Therefore, in order to understand the cyclic behavior of split tee flange joints, the cyclic loading test up to fatigue failure is carried out and the fatigue behavior of split tee flange joints is discussed based on the experimental results.

In this fatigue test, the effect of the thickness of the flange plate on the mechanical behavior of the joint under cyclic loading is focused because it is understood from the discussion in the previous section that the thickness of the flange plate is very important parameter to control the mechanical behavior of the joint. Dimensions of all the specimens are shown in Fig. 4.22. Geometrical configurations of each specimen are the same except for the thickness of the flange plate. In addition, the high strength bolts used in these specimens are M12(F10T). In order to compare the behavior under cyclic loading to that under monotonic loading, dimensions of the specimens are determined to be same with those of the specimen used in the previous monotonic tensile loading test.

Stress ranges applied to each specimen are tabulated in Table 4.5 and the yield strength obtained from the monotonic loading test is tabulated in Table 4.6 for reference. Here, the stress ranges

are determined based on the yield strength of the joint, namely, 1/4 of yield strength and 1/2 of yield strength as the basic pattern. However, in case of thinner flange plate, yield strength is very low, so that 3/4 of the yield strength and 1.0 times of the yield strength are determined to be applied to the test specimens.

The specimens are carefully manufactured by paying attention to the welding section where the flange plate and tee web plate are connected because the less fatigue strength due to the stress concentration is expected. As for the welding of the flange plate to the tee web plate, partial group welding is used, and after then, the notch smoothing of the welding surface is made by hand grinding in order to reduce unexpected extremely local stress concentration.

Testing machine by SHIMADZU is used in the experiment. The detail of the testing machine can be referred to section 2.2.1 or 4.2.1(a). The test setup as used for the monotonic loading test is also utilized. An example of time history of the applied tensile load is shown in Fig. 4.23, where a frequency is set to 2.0 (Hz) by considering the loading capacity of the testing machine. The procedure of the applying the load is summarized as follows: at first, the tensile load is applied up to one half of the load range; after then, the sinusoidal tensile load is applied by the function generator. Tensile load and the displacement of the actuator are only measured from the beginning to the end. At the specific number of cycles of loading as shown in Fig. 4.23 for example each 10,000 cycles, the loading is made very slowly with frequency of 0.001 (Hz). During this loading cycle, the bolt force and the deformation of the flange plate in addition to tensile load and displacement of the actuator are measured continuously for assessing the damage accumulated in the specimens.

In this loading test, average bolt force and the deformation of the bolt and the flange plate are focused. The bolt force is measured by four strain gages glued on the surface of the bolt shank. Since the bolt shank remains in the elastic state, the bolt force is calculated based on the average strain of four strain gages. The location of these four strain gages is shown in Fig. 4.24. It is determined in such a way that the bending deformation of the bolt can be investigated. Moreover, the strain gages to evaluate stress concentration are also glued on the flange plate in order to investigate the local bending deformation of the flange plate. The location of these strain gages are determined by considering the possible distribution of strain on the flange plate surface near the bolt head as well as the web plate and shown in Fig. 4.24. Total number of the measuring points including the strains of the bolt and the flange plate is 48.

The complete measurement of strains is carried out for the pre-set number of loading cycle such as each 10,000 cycles. This measurement is carried out through high speed data logger with sampling speed of 1000 points per a second.

When the specimen is assembled by tightening the high strength bolts, the bolt pre-stress force is given up to 6.26 (tonf) according to the specification of JIS[3] by checking the strain reading of the bolt shank

4.3.2 Results of fatigue test

(a) Fatigue failure mode

The number of loading cycles at fatigue failure are tabulated in Table 4.7, where the fatigue failure is defined by either breaking of bolts or large deformation of the flange plate due to cracking at toe of tee web plate less than 2,000,000 cycles. The modes of fatigue failure is classified as follows: In case of thinner flange plate(SPT1B, SPT1C), the specimens are failed by the crack at the toe of welding section of the flange plate to the web plate. On the other hand, in case of thicker flange plate(SPT2A), the specimen failed at the bolt thread near the nut. The location of these failure is shown in Fig. 4.25. It is understood that the failure mode under cyclic loading is similar to that of the deformation mode under monotonic loading. Therefore, the fatigue strength should be determined by either the fatigue strength of the welding section or that of the high strength bolt. Especially, the fatigue strength of the welding section highly depends on the thickness of the flange plate as well. For example, in case of thicker flange plate, the fatigue failure at the welding section does not occur because of the low bending stress on the flange plate surface. On the other hand, in case of the thinner flange plate, the fatigue failure occurs at the welding section due to the high bending stress as well as high stress concentration at the same location.

For the cases that specimens did not fail, namely, fatigue life is more than 2,000,000 cycles, bolts are checked carefully. There exists no remarkable change of bolts such as bending or torsion both at the bolt shank and the bolt thread for both thicker flange plate case (SPT2C) and thinner flange plate case(SPT1A). In these cases, it is considered that the applied load is not large to cause fatigue failure. Particularly, the additional stress increase given to the bolt due to applied tensile load to the joints is not high; therefore, it is thought that the bolt did not fail. In addition, bending stress of the flange plate is also not large enough to cause the fatigue failure at the toe of welding section of the flange plate to the web plate.

For the case that stress range of the bolt is predicted to be the highest, namely SPT2A, the load range of the bolt is up to 20% of the applied load range to the joint. Therefore, it is understood that the applied tensile load range should be limited to very low level by taking into account the high bolt pre-stress force given initially, namely 80% of yield strength.

(b)Change of the bolt force under one cycle

The difference in time history of both the bolt force and applied tensile load during a particular loading cycle are compared in Fig. 4.26. The horizontal axis shows elapsed time for a loading cycle, and the vertical axis shows the bolt force(left) and the applied tensile load(right). The bolt force is calculated based on averaging the readings of 4 strain gages on the bolt shank.

Regardless of the thickness of the flange plate and applied tensile load range, time history of the bolt force is summarized as follows: Since the applied tensile load is given in the form of the sinusoidal wave, the load is applied to the specimen up to 1/2 of the load range at first. After then, the cyclic loading is given and the bolt force is varied with the same frequency of applied tensile load. It is found from these

figures that the higher the tensile load is or the thinner the flange plate is, the larger the increase of the bolt force is. In addition, it can be understood that the decrease of bolt force while the applied load is less than mean value of applied tensile load is relatively small and this relates to the release of the compressive force between two flange plates given by the bolt pre-stress force. This minimum value of the bolt force corresponded to the bolt pre-stress force. Comparing time history of the bolt force at different number of loading cycles, it is found that the time history of the bolt force at the initial cycle is quite different form those at following loading cycles. That is, at the initial cycle, the bolt force after one cycle is completed is lower than that before the loading cycle. On the other hand, at the following loading cycles, the bolt force before at the beginning of loading cycle is almost the same with that at the end. It is concluded that loss of the bolt force is considered to occur at the early stage of cyclic loading.

Number of loading cycles vs. the maximum and minimum bolt force relation for all the cases are shown in Fig. 4.27. The horizontal axis shows the number of loading cycle, the vertical axis shows the bolt force(left) and the amplitude of the bolt force(right). The amplitude of the bolt force means the increase of the bolt force during a loading cycle. As for the case that the fatigue failure did not occur, that is, SPT1A and SPT2C which has different thickness of the flange plate, the amplitude of the bolt force is similar each other in spite of the difference in the thickness of the flange plate. Here, it is also found that some amount of the bolt force loss occurs at the initial loading cycle; after then the bolt force decreases very little cycle by cycle. This tension loss of the bolt force is 3.0 (%) of the bolt pre-stress force given at the beginning and this observation is good agreement with the result obtained in the short term tension loss test[5]. The tension loss at the initial loading cycle is considered to be caused by not the applied tensile load but the plastic deformation of the weak layer on the surface of the flange plate such as paint and rust. In addition, it is found that the amplitude of the bolt force is very small as compared to that of the applied tensile load. For example, in case of the thinner flange plate, the ratio of the amplitude of the bolt force to that of the applied tensile load is 5-7 (%), and in case of thicker flange plate, the ratio is about 3 (%). This results is also in good agreement with those obtained from the monotonic loading test, that is, the bolt force does not increase until the applied tensile load reaches to the bolt pre-stress force. Especially, in case of thicker flange plate, the amplitude of the bolt force remained to be very small, so that the thicker flange plate should be desirable from the view point of the fatigue resistance of the bolt. On the other hand, in case of the thinner flange plate, the reason why this ratio is a little higher than that of the thicker flange plate is considered that the bending force is given to the bolt head and then the bolt force tends to increase. As for the cases that specimens failed by cracking, that is SPT1C and SPT2A, the tension loss of the bolt force is also compared against the case that specimens did not failed at cracking. The ratio of the amplitude of the bolt force to that of the applied tensile load is about 18-20 (%) for both thicker flange plate and thinner flange plate. This ratio is very higher than that of the unfailed cases.

Moreover, it is found that the amplitude of the bolt force becomes very large suddenly at the loading cycle just before the failure for both thinner and thicker flange plate cases, and that the thinner the

thickness of the flange plate is, the higher the increase of the bolt force is. The reason of this phenomena is thought as follows: In case of the thicker flange plate, fatigue failure occurs at the bolt, and the bolt thread is considered to yield. Therefore, it is considered that the minimum bolt force decreases due to plastic elongation of the bolt, and that the applied tensile load is directly transferred through bolts because of less compressive force between flange plates. On the other hand, in case of the thinner flange plate, it also can be seen that the maximum bolt force increases and the minimum bolt force decreases. The increase of the bolt force is caused by the crack at the welding section of the flange plate to the web plate. Namely, the large bending deformation occurs by the crack at the welding section, so that the bolt is considered to be pulled and bent severely. The decrease of the bolt force is considered to be caused by the yield of the flange plate due to the bending deformation as well as the yielding of the bolt. For both thicker flange plate and thinner flange plate, although failure modes are different each other, the increase of the bolt force takes place. Therefore, the prediction of the fatigue life of the split tee flange joint can be made based on the increase of the amplitude of the bolt force.

(c) The deformation of the Bolt

Time-history of the strains of the bolts are shown in Fig. 4.28. The horizontal axis shows elapsed time during a loading cycle and the vertical axis shows the strain. The location of each strain gage can be referred to Fig. 4.24. In this figure, the strain is set to zero when the applied tensile load reaches to the mean value. It is understood from these figures that the difference in strain-time curve for thicker flange plate and thinner flange plate is found. In case of thinner flange plate, the strain of the bolt at the side facing to the tee web plate(R-B2) becomes significantly large tensile strain as the applied tensile load becomes large; on the other hand, the strain at the side to the other edge of the flange plate(R-B4) becomes relatively small compression(the decrease of strain). Therefore, the bolt is considered to be bent significantly. Furthermore, it is also understood that the bolt is not uniformly elongated by tightening the nuts and its in-uniformness is very sensitive in case of thinner flange plate because of less stiffness of the bolt. Whereas, in case of the thicker flange plate, all the strain of the bolt at four locations remain in tension. Therefore, it is considered that the bolt is uniformly pulled, not bent. However, as the strain at the side to the tee web plate is a little larger than that to the outer edge of the flange plate, so that the bolt is slightly bent.

According to the previous study, it is thought that the bolt force may increase by the prying force; however, in accordance with the thickness of the flange plate, the cause to have bolt force increase can be concluded as follows: When the tensile load is applied to the joint, the bolt is bent and tensioned by the flange plate. Therefore, the bolt force is considered to increase by its bending and tensile deformation.

(d) Deformation of the flange plate and maximum stress on the flange plate

The strain distribution of the flange plate at a particular loading cycle obtained from the strain gages for all the cases are shown in Fig. 4.29. The vertical axis shows the strain. The horizontal axis shows the

number of the measuring point whose location can be referred to Fig. 4.24. They are numbered from one side of the flange plate(left) to the other side(right) as shown in Fig. 4.24. Since the strain gages used in the fatigue test is for measuring stress concentration, the local deformation of flange plate can be examined.

In case of the thicker flange plate, it is found that the strain distribution on the flange plate is almost the same as that at the different loading cycle and its magnitude of the strains is very small. For example, the maximum strain of the flange plate for SPT2A, which failed at the bolt, is about 500 (micro); whereas, the yield strain of the flange plate is about 1400 (micro) according to the material test. Accordingly, the flange plate is considered to be still elastic. Moreover, from the results of strain distribution, the flange plate is thought to be deformed as if a concentrated load is applied at the bolt head location. Furthermore, in case of the thinner flange plate which did not fail at the bolt or the toe of welding , that is SPT1A, the maximum strain on the flange plate is about 800 (micro). On the other hand, in case of other thinner flange plate, namely, SPT1B and SPT1C which failed at the welding section of the flange plate to the web plate, the maximum strain is about 1200 (micro). In these cases, the flange plate is considered to yield. The maximum strain of the thinner flange plate is higher than that of the thicker flange plate; therefore, the large deformation of the flange plate takes place. In addition, if it did not fail by fatigue cracking such as the case of SPT1A, the strain distribution was not changed even as the number of loading cycle increases and the flange plate remained in elastic state up to 2,000,000 cycles. On the other hand, if it did fail, such as the case of SPT1B and SPT1C, it is found that the strain distribution is changed as the number of loading cycle increases. In addition, the permanent strain was observed.

The time history of the stress on the flange plate at the location close to the tee web plate are shown in Fig. 4.30. The location to discuss the stress is 10 (mm) far from the edge of the tee web plate. Here, the horizontal axis shows the number of loading cycle, and the vertical axis shows the normalized stress by nominal stress of the tee web plate, namely, applied load divided by cross sectional area of the tee web plate. It can be seen from this figure that the normalized stress of the thicker flange plate and that of the thinner flange plate is 4.0 to 9.0 and 1.0 to 2.0 respectively, and that the normalized stress in case of thinner flange plate is significantly higher than that in case of the thicker flange plate. In addition, as shown in this figure, in case of SPT1C, it is observed that the normalized stress turns to decrease suddenly from 60,000 cycles to 80,000 cycles; therefore, This is due to stress redistribution of the flange plate, so that the cracking at the welding section of the flange plate to the web plate is considered to occur.

Regardless of the thickness of the flange plate, the distribution is not uniform over the flange plate, so that the eccentric loading to the flange plate is more significant to the deformation of the flange plate. Furthermore, it is concluded that it is difficult to assume the pure tension in the bolts. So that, high strength bolts should be assessed against combined loading such as tension, shear force and bending.

(e) Fatigue strength

S-N diagram obtained from the fatigue test is shown in Fig. 4.31. The horizontal axis shows the number of loading cycle to the failure, and the vertical axis shows the applied load range ratio which is a load range normalized by the yield load of the joint obtained from the monotonic loading test. It is calculated using the following equation.

$$P_n = \frac{P}{YL} \tag{4.4}$$

in which, P_n, P, YL is the normalized applied load range, the applied tensile load range and yielding load obtained from the monotonic loading test, respectively. Yielding load is defined by the load level at the intersection point between the tangential line at the initial elastic region of load-separation curve under monotonic loading and the tangential line in the plastic region(referred to Fig. 4.14(b)).

It is found form this figure that the fatigue strength in case of thinner flange plate is higher than that in case of thicker flange plate. Therefore, if the fatigue strength is assessed according to the yield strength based under monotonic loading, the split tee flange joint with the thinner flange plate is considered to be superior form the view point of allowable stress design although the yielding load used in normalization is different each other.

Considering these results, it is concluded that the thickness of the flange plate should be very important parameter to evaluate the fatigue behavior as well. Even though the thicker flange plate is used, the allowable applied load range for the fatigue failure is about 6.5 (tonf) , which is much smaller than total bolt-pre stress force. Therefore, in order to use the high strength bolt efficiently, the additional increase of the bolt force should be prevented from the viewpoint of the fatigue strength, so that considerable thicker flange plate or longer connection type should be required. In addition, if the applied load to the joint is small, the split tee flange joint which has thinner flange plate is desirable from the view point of the allowable stress design because it is very effective for ultimate state, such as initial yielding of the joint. On the other hand, if the applied load is larger, the joint which has thicker flange plate is desirable. Finally, the fatigue strength and failure mode of the split tee flange joint can be easily controlled by varying the thickness of the flange plate,. Furthermore, the design of the split tee flange joint under cyclic loading could be more rational if this procedure to control failure mode and this characteristics should be utilized aggressively.

4.3.3 Simple Estimation of Fatigue Strength

Instead of the normalized load range, S-N diagram is drawn for the absolute applied load range in Fig. 4.32. Fatigue strengths of the bolt and the flange plate are estimated by the following procedure and these are compared in this figure. Here, only the fatigue strength under 2,000,000 cycles is considered: The fatigue strength of the bolt is evaluated based on the guideline for fatigue design of steel structures[6], in

which, the fatigue strength is assumed to be level "K4" for the high strength bolts. As a result, it is determined to be 6.6 (kgf/mm^2) for the bolt. Then, it is converted to the strength in force, 557 (kgf) by multiplying the effective cross sectional area of the bolt prescribed in JIS[3]. The bolt force is further converted to the applied tensile load by using applied tensile load vs. bolt force curve obtained by the experiment under monotonic loading. As a result, the fatigue strength of the joint in case of bolt failure is evaluated. In case of the thinner flange plate, this strength is 4.1 (tonf), and in case of thicker flange plate, this is 6.2 (tonf).

On the other hand, as for the fatigue failure at the welding section of flange plate to tee web plate, fatigue life estimation is made by referring the strength of the joint as shown in Fig. 4.33 in the guideline for fatigue design for steel structures[6], in which fatigue strength of the joint is classified to be level "C" (12.8 kgf/mm^2). This strength is for the joint which has welding smoothened for quality control. Then, the following model for the split tee flange joint as shown in Fig. 4.34 is assumed in order to obtain the working stress of the flange plate. This model is a beam whose both ends are fixed, and uniformly distributed load which corresponds to the applied tensile load at the web plate is given to the center of the fixed beam. The applied tensile load is obtained for the condition that the maximum stress in this model corresponds to the fatigue strength defined in the guideline for fatigue design. As a result, the fatigue strength of the thinner flange plate and that of the thicker flange plate is estimated to be 1.30 (tonf) and (6.25 tonf) respectively. Finally, the fatigue strength of the split tee flange joint is obtained by the smaller value of allowable applied tensile loads defined by two possible fatigue strength. It is found from this result, that the fatigue strength of the thicker flange plate is higher than that of the thinner flange plate as obtained in the fatigue test.

In addition, it is understood that in case of thinner flange plate, the fatigue strength is estimated to be smaller than that of the experiment, which is conservative. Moreover, failure mode is estimated to be by a failure of the flange plate and this is same as the experimental results. Accordingly, it is thought that the estimation of the failure mode by proposed procedure is applicable in the case of thinner flange plate. On the other hand, in case of the thicker flange plate, the split tee flange joint failed at the bolt and fatigue strength of the bolt is well-predicted. However, the poor estimation of the fatigue failure mode is obtained. Although the fatigue strength of the bolt is estimated by a little lower than that of the flange plate which may result in failure of the bolt, the fatigue strength of bolt and that of the flange plate are almost same which cannot conclude that either failure mode should be considered. Therefore, in order to estimate the fatigue failure mode accurately, the proposed model is still further modified.

4.4 Conclusions

In this chapter, the mechanical behavior of the split tee flange joints, which is the most simple high strength bolted tensile joints, under monotonic and cyclic loading is investigated experimentally and analytically. As for the behavior under monotonic loading, the contact/separation behavior and the joint stiffness is assessed in detail by using 3-dimensional analysis. On the other hand, as for the behavior under cyclic loading, the cyclic loading test is carried out considering the local deformation behavior, such as the deformation of the bolts and the flange plate. Based on these results, the fatigue strength is assessed and its estimation procedure is also proposed. The following conclusions and future research needs are obtained as follows:

1) The mechanical behavior of split tee flange joints under monotonic tensile load depends on the mechanical behavior of both of the flange plate and the high strength bolt, in particular it is significantly affected by the thickness of the flange plate. In case of the thinner flange plate, the behavior depends on that of the flange plate and the high deformation capability is observed. On the other hand, in case of thicker flange plate, the behavior depends on that of the high strength bolt and high load carrying capacity is obtained, but the failure is brittle.
2) The stiffness of the joint depends on the geometrical configurations of the flange plate: the thicker and the narrower the flange plate is, the higher the stiffness of the joint is obtained. In addition, the effect of the bolt pre-stress force on the stiffness is made clear, in fact, the stiffness increases by the bolt pre-stress force.
3) In addition to the prying force effect understood in the previous studies, the increase of the bolt force is considered to be caused by pulling up the bolt by the local deformation of the flange plate.
4) The mechanical behavior under cyclic loading depends on the thickness of the flange plate as well. In case of thinner flange plate, the joint failed at the welding section; on the other hand, in case of thicker flange plate, the joint is failed at the bolt thread. The amplitude of the bolt force under cyclic loading is small compared with that of the applied tensile load and the significant effect of the bolt pre-stress force is observed for any thickness of the flange plate.
5) The significant increase of the bolt force is observed before the failure of the joint for both bolt failure and flange plate failure.
6) In case of the evaluation of the fatigue strength of the split tee flange joint based on the yielding load of the joint under monotonic loading, the fatigue strength of the joint with thinner flange plate is higher than that of the joint with thicker flange plate, therefore, the joint with thinner flange plate is effective from the view point of the design based on yield strength. Moreover, the simple estimation method of the fatigue strength is proposed using the guideline of the fatigue design for steel structures and good agreement with the monotonic experimental results are shown.

In the future, in order to make this results reliable, further cyclic loading test is carried out for the joints with various geometrical configurations. Furthermore, considering the practical use for steel bridge structures, the joints with multiple bolts should be considered. In special, the effective area of one bolt and the interaction among the bolt group on the mechanical behavior should be investigated.

References

1) Architectural Institute of Japan : Recommendation for the Design Fabrication of High Strength Bolted Joints, Maruzen, Mar. 1993(in Japanese).
2) Japanese Society of Steel Construction : Recommendation for the design of tensile joints for bridge structures (draft), Feb. 1993(in Japanese).
3) Japanese Industrial Standard Committee : Sets of High Strength Hexagon Bolt, Hexagon Nut and Plain Washers for Friction Grip Joints(B1186), 1979(in Japanese).
4) Y.Miki, K.Horikawa : Fatigue Behavior on Split Tee Flange Joints, Proc. of the 46th Annual Conference of JSCE, 1, JSCE, Sep. 1991, pp. 606-607(in Japanese).
5) A.Ahmad, E.Watanabe, K.Sugiura, K.Hatanaka : Tension Loss in High Strength Bolts, Journal of Structural Engineering, JSCE, Vol. 41A, Mar. 1995, pp. 87-94.
6) Japanese Society of Steel Construction : Recommendation for Fatigue Design, Apr. 1993(in Japanese).

Table 4.1 List of Specimens

Specimen	Thickness of the Flange Plate	Width of the Flange Plate	High Strength Bolt	Bolt Pre-stress Force
ST-1	5	63	M12 (F10T)	6.26 (tonf)
ST-2	10	63	M12 (F10T)	6.26 (tonf)
ST-3	22	63	M12 (F10T)	6.26 (tonf)

(unit : mm)

Table 4.2 List of Analytical Cases

	ST-A1	ST-A2	ST-A3	ST-A4	ST-A5	ST-A6	ST-A7	ST-A8
Thickness of the Flange Plate	10	15	22	10	22	10	15	22
Width of the Flange Plate	63	63	63	78.75	78.75	94.5	94.5	94.5

(unit : mm)

Table 4.3 Material Properties used in the Analysis

	Young's Modulus	Yielding Stress
Flange Plate	21,000	26.9
Bolt Shank of High Strength Bolt	21,000	90.0
Bolt Thread of High Strength Bolt	15,700	67.1

(unit : kgf/cm^2)

Table 4.4 List of Stiffness per a Unit Length at Each Section

Stiffness	ST-A1	ST-A2	ST-A3	ST-A4	ST-A5	ST-A6	ST-A7	ST-A8
Bolt	1.88	1.26	0.856	1.51	0.685	1.26	0.837	0.571
Plate	0.0336	0.113	0.358	0.0269	0.286	0.0224	0.0756	0.238
Total	0.0330	0.104	0.252	0.0264	0.202	0.0220	0.0693	0.168

(unit : tonf/mm/mm)

Table 4.5 List of Loading Pattern

Specimen	Minimum Load (Pmin)	Maximum Load (Pmax)	Amplitude of Load	Stress Ratio (Pmin/Pmax)	Pmax/YL	Loading Period
SPT1A	100	2,500	2,400	0.040	0.49	2.0Hz
SPT1B	100	5,000	4,900	0.020	0.98	2.0Hz
SPT1C	100	3,750	3,650	0.027	0.74	2.0Hz
SPT2A	100	7,500	7,400	0.013	0.54	2.0Hz
SPT2B	100	11,000	10,900	0.0091	0.78	1.0Hz
SPT2C	100	3,750	3,650	0.027	0.27	2.0Hz

(unit : kgf)

YL : Yielding Load of the Specimen under Static Loading

Table 4.6 Results of Monotonic Tensile Loading Test

Thickness of the Flange Plate	Yielding Load
10 mm	5.1 tonf
22 mm	14.0 tonf

Table 4.7 Results of the Fatigue Test

Specimen	Number of Cycle to Failure	Failure Mode	Pmax/YL
SPT1A	–	not failed	0.49
SPT1B	17,848	FL	0.98
SPT1C	82,000	FL	0.74
SPT2A	139,480	BT	0.54
SPT2B	17,113	BT	0.78
SPT2C	–	not failed	0.27

YL : Yielding Load under Monotonic Loading

Pmax : Maximum Load applied to the Specimen

FL : Failure at the Toe of Welding between Flange Plate and Web Plate

BT : Failure at the Bolt Thread

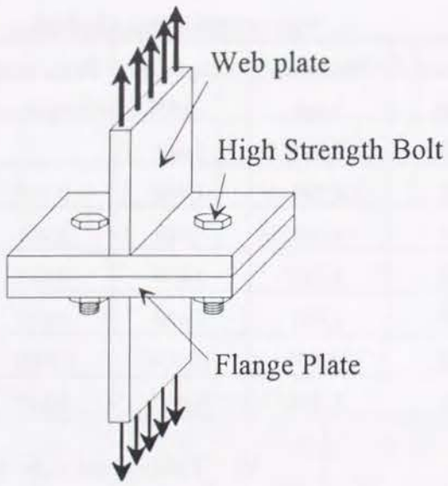

Fig. 4.1 Overview of the Split Tee Flange Joint

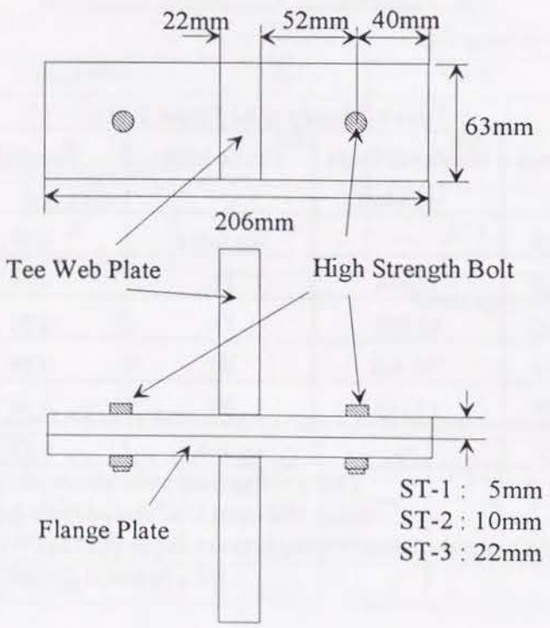

Fig. 4.2 Geometrical Configurations of the Specimens

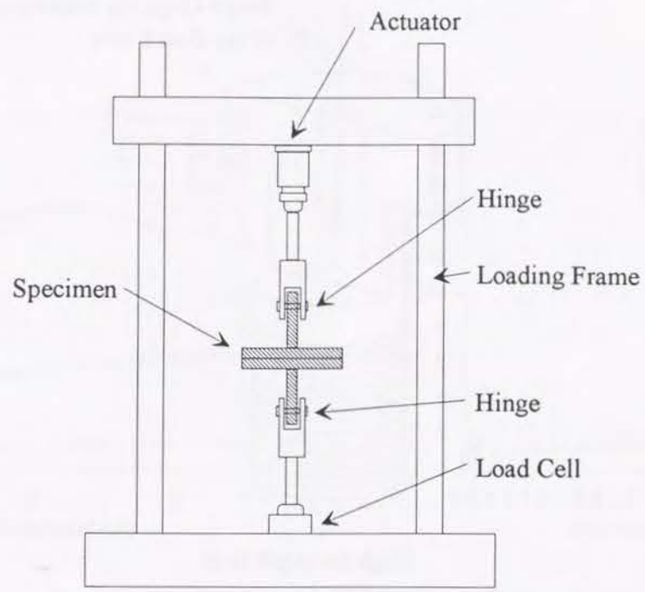

Fig. 4.3 Testing Setup

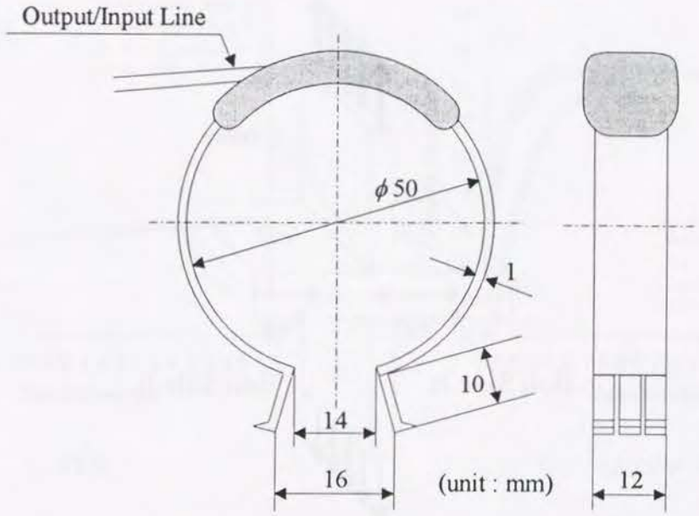

Fig. 4.4 Displacement Transducer for Measuring the Gap

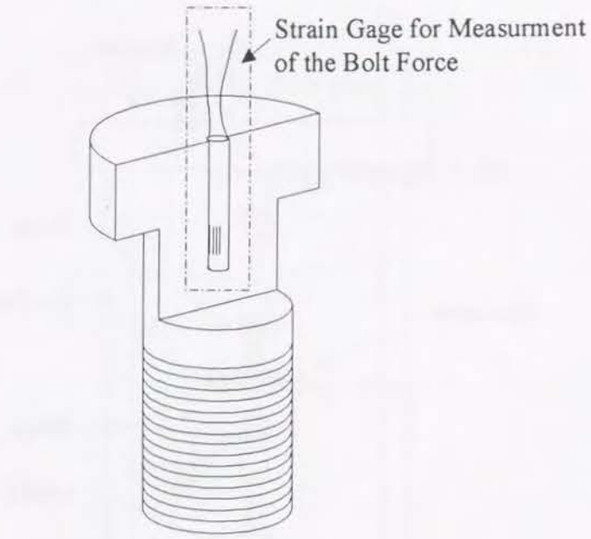

Fig. 4.5 Strain Gage buried into the Bolt

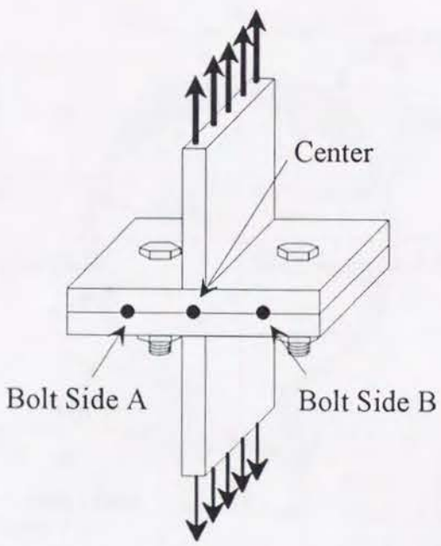

Fig 4.6 Location of Measurement of Gap

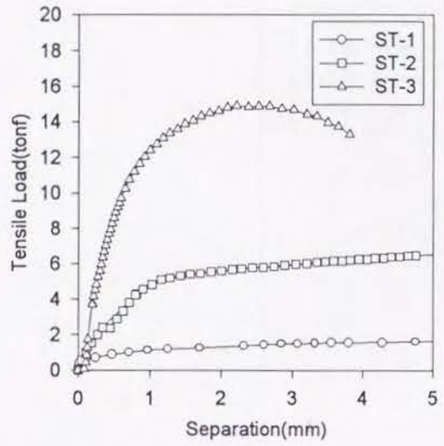

(a) Average Separation

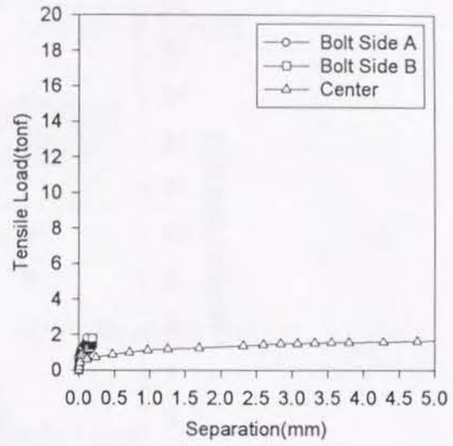

(b) ST-1

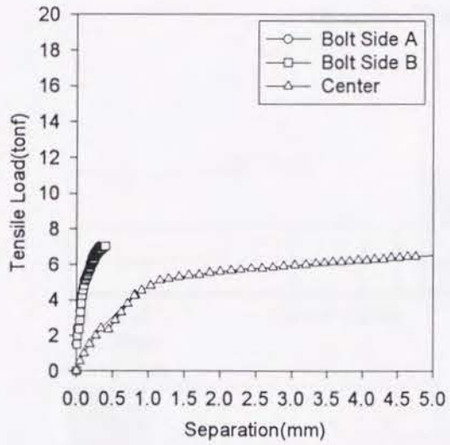

(c) ST-2

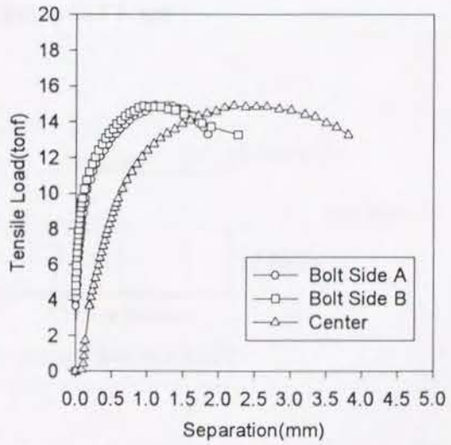

(d) ST-3

Fig. 4.7 Load-Separation Curves (Experiment)

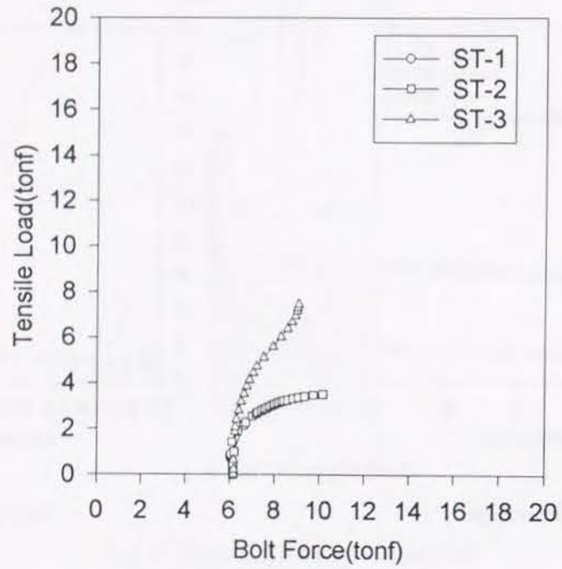

Fig. 4.8 Load-Bolt Force Curves (Experiment)

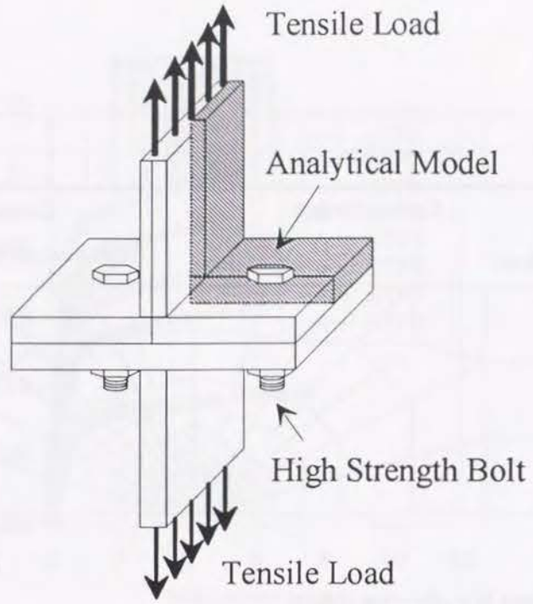

Fig. 4.9 Overview of the Analytical Model

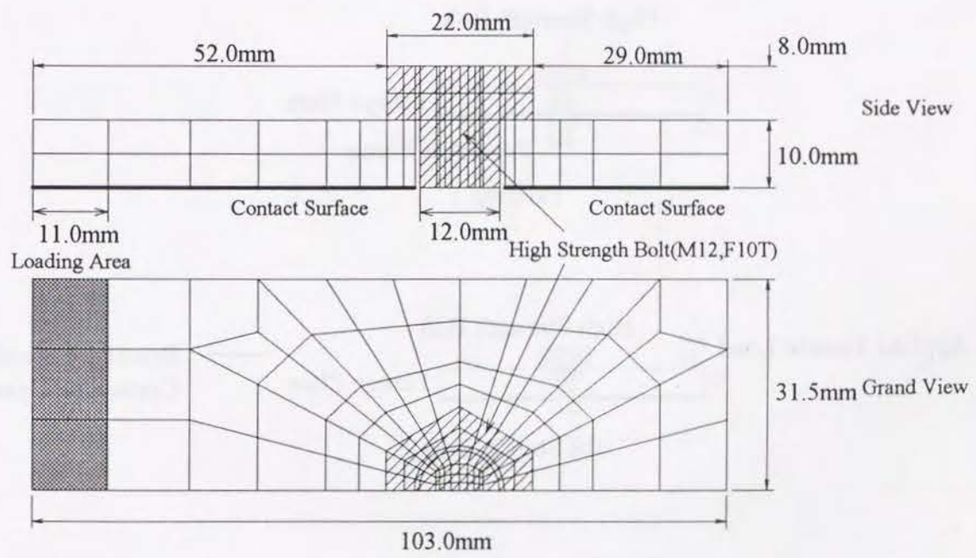

Fig. 4.10 Example of Finite Element Discretization of the Analytical Model(ST-A1)

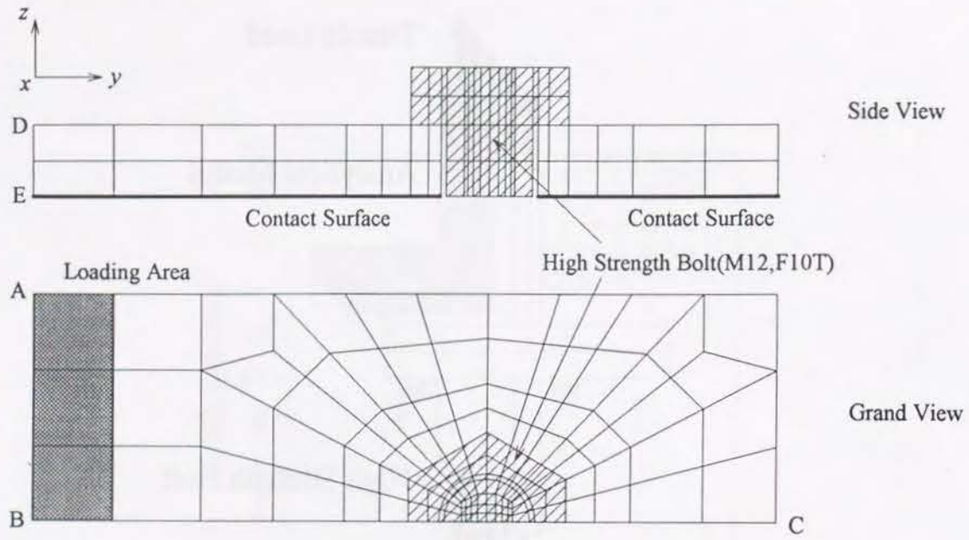

Side View

Grand View

in which

AB : Displacement in y -direction is fixed

BC : Displacement in x -direction is fixed

B : Displacement in both x-direction and y-direction are fixed

DE : Displacement in y -direction is fixed

Fig. 4.11 Boundary Conditions of Analytical Model

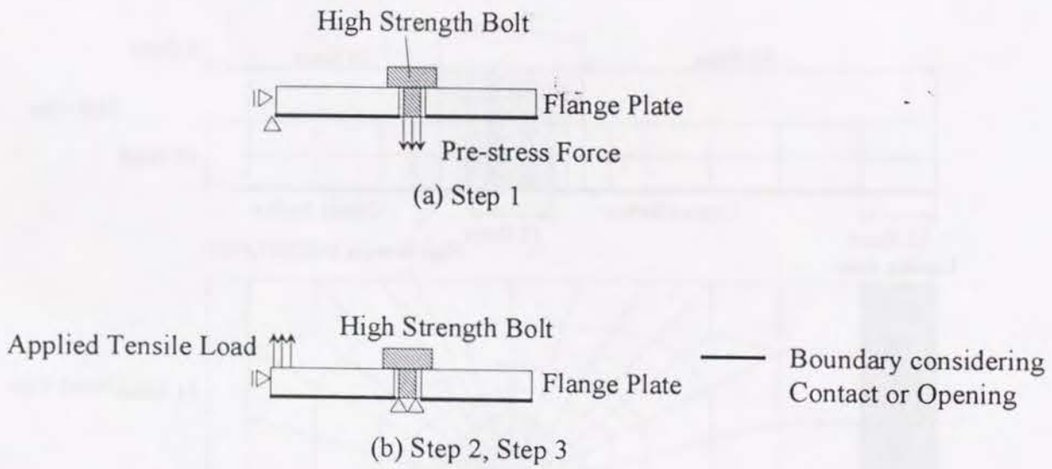

Fig. 4.12 Loading Procedure Analysis

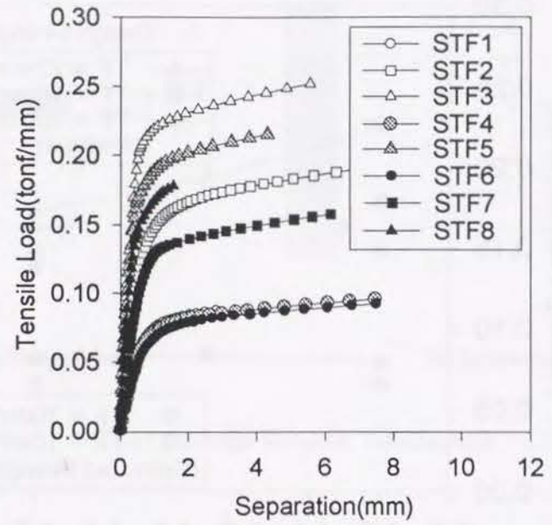

Fig. 4.13 Load-Separation Curves (Analysis)

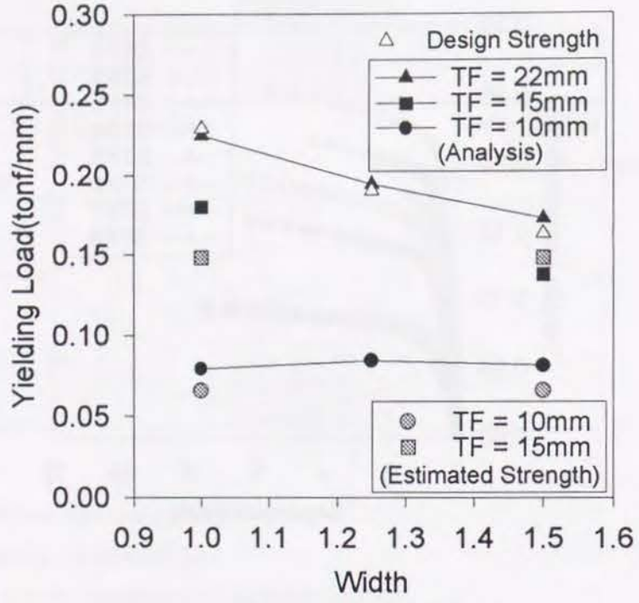

(a) Yield Strength

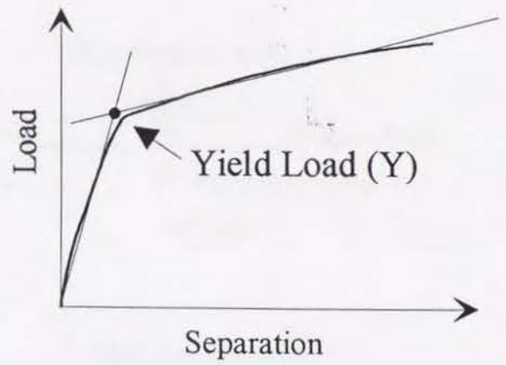

(b) Definition of the Yield Strength

Fig. 4.14 List of Yield Strength of All Cases

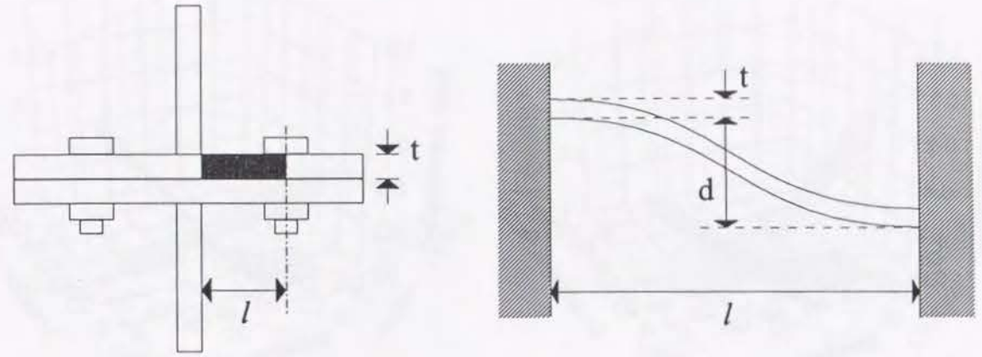

(a) Split Tee Flange Joint

(b) Estimated Model

Fig. 4.15 Estimated Model for Yield Strength

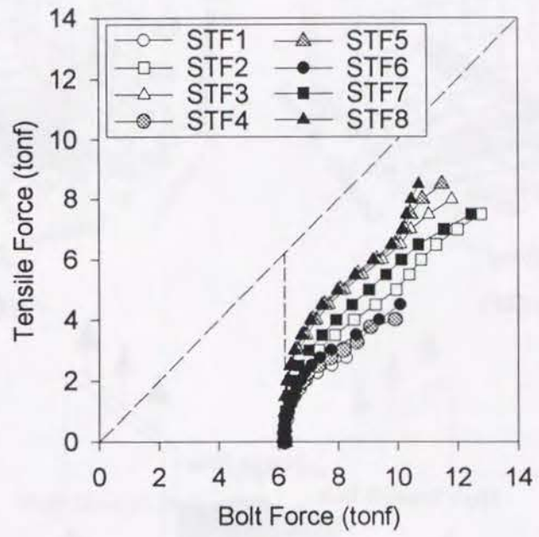

Fig. 4.16 Load-Bot Force Curves (Analysis)

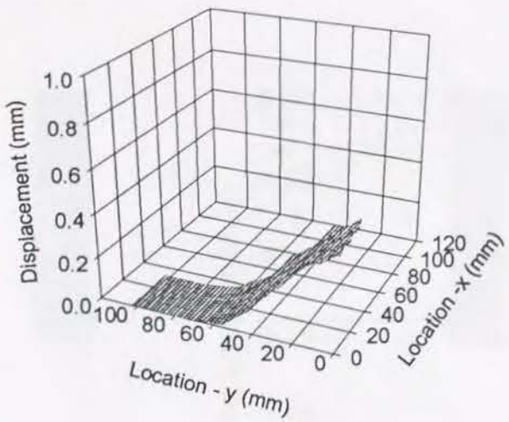

(a) STF1

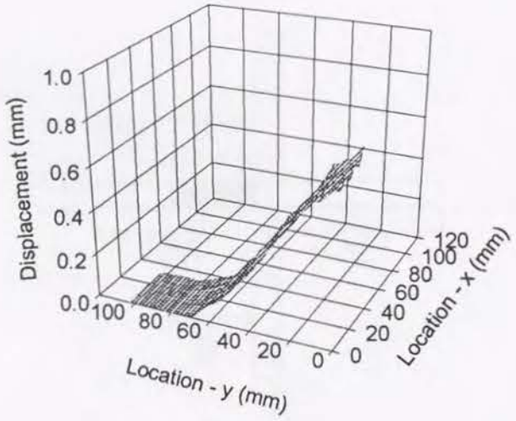

(b) STF2

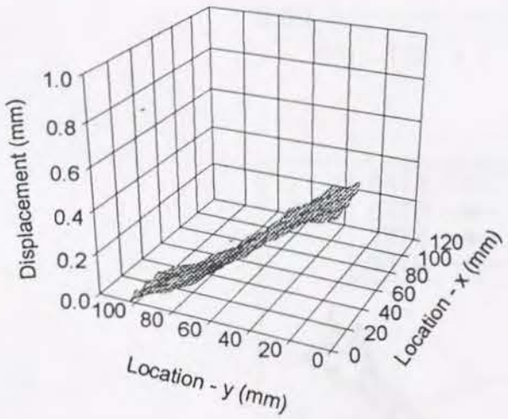

(c) STF3

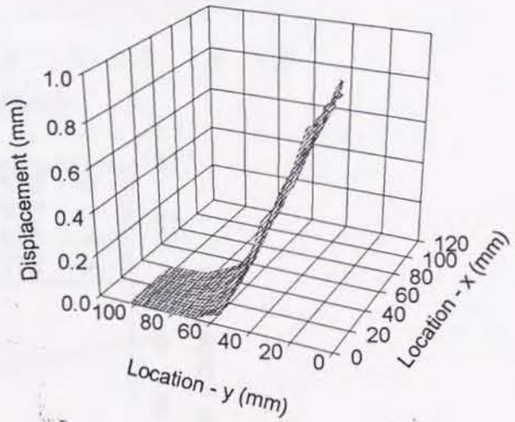

(d) STF4

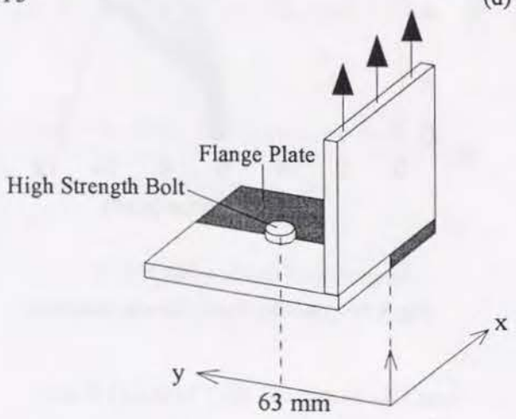

Fig. 4.17 Deformation of the Contact Surface (continued)

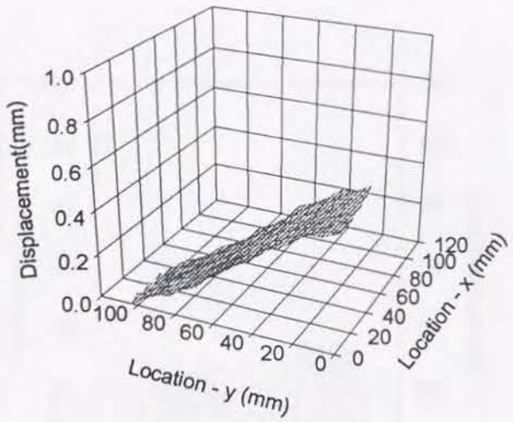

(e) STF5

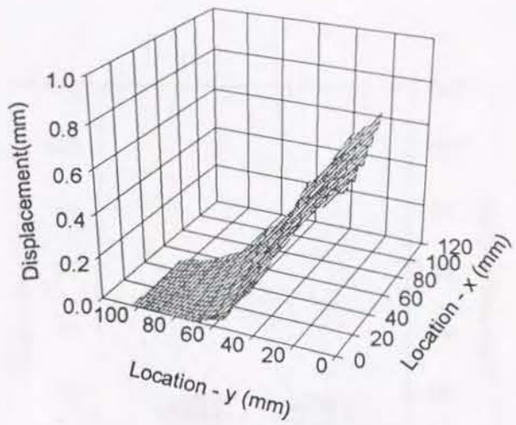

(f) STF6

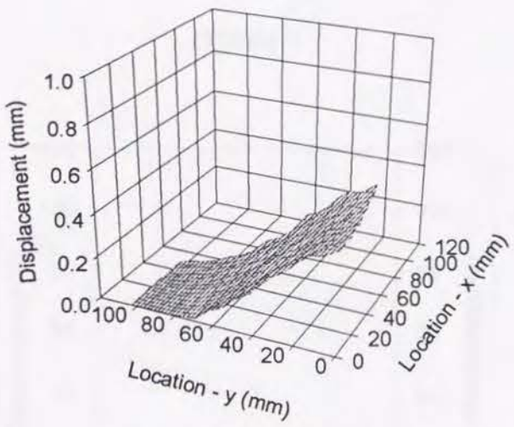

(g) STF7

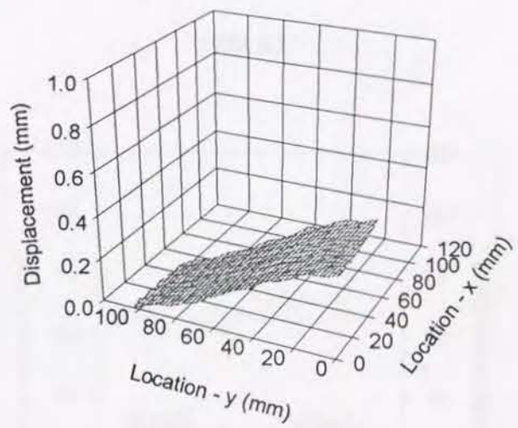

(h) STF8

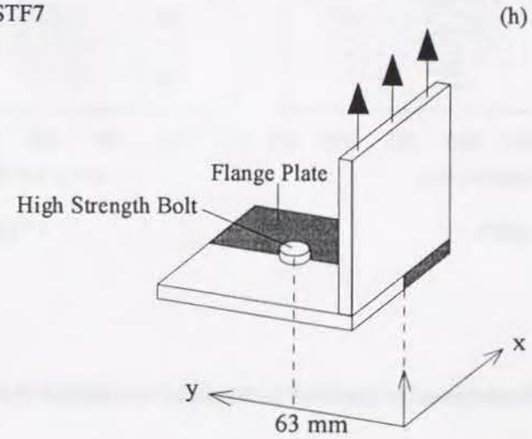

Fig. 4.17 Deformation of the Contact Surface

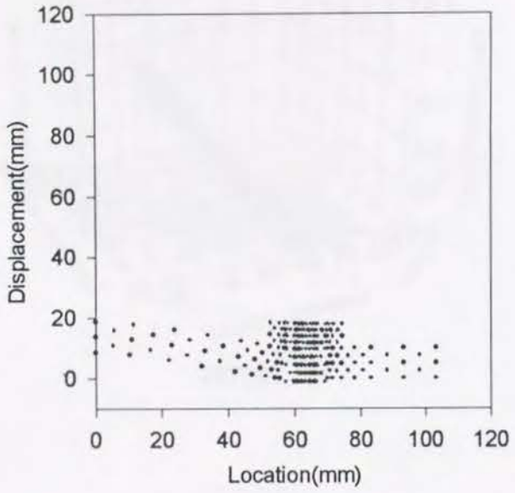

(a) STF1

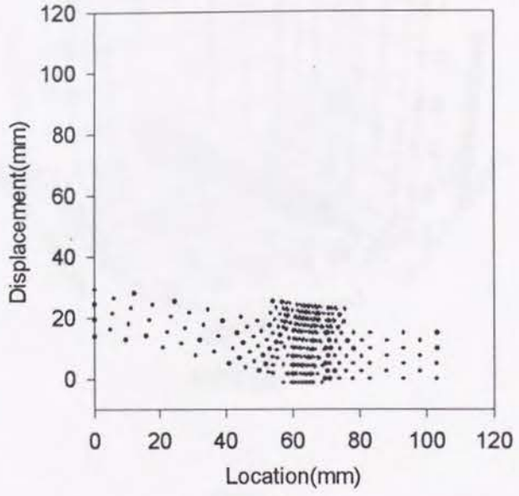

(b) STF2

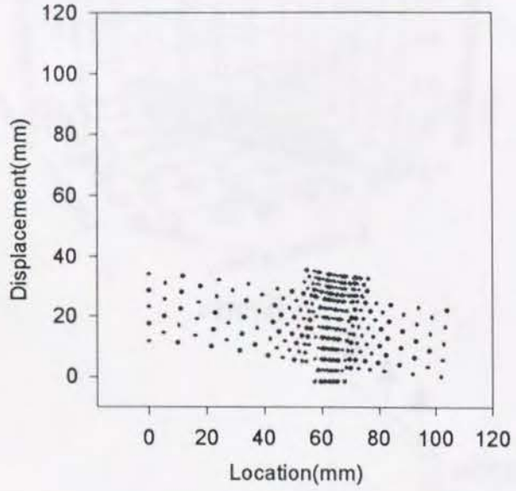

(c) STF3

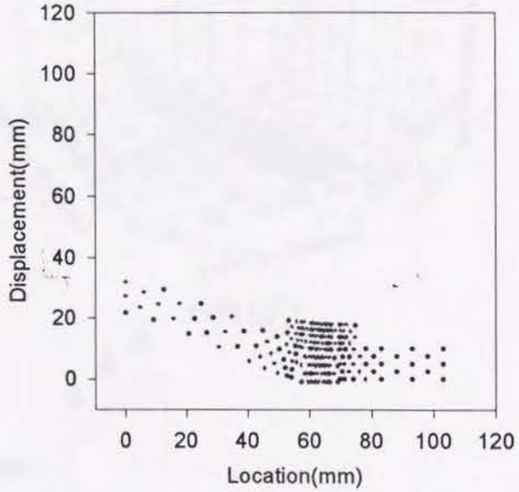

(d) STF4

Fig. 4.18 Deformation at the Center of the Model in Longitudinal Direction (continued)

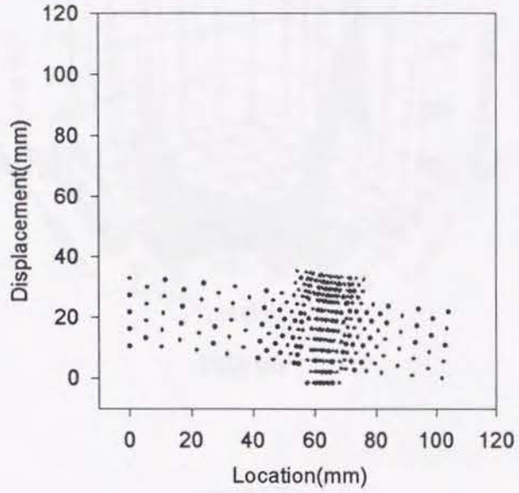

(e) STF5

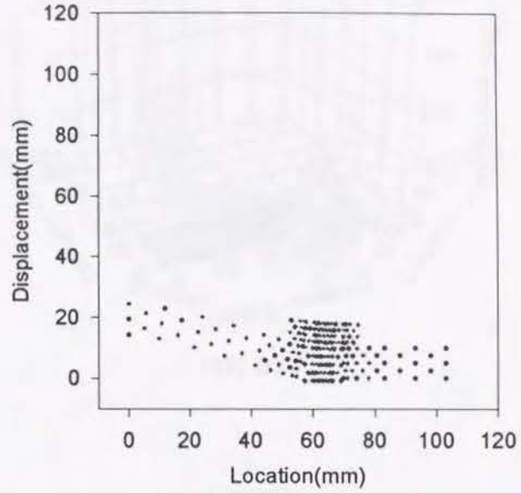

(f) STF6

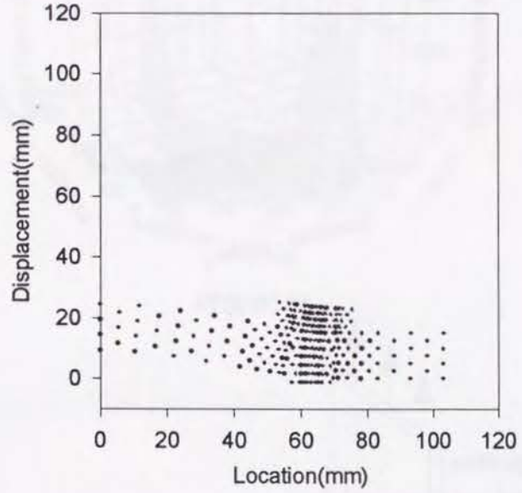

(g) STF7

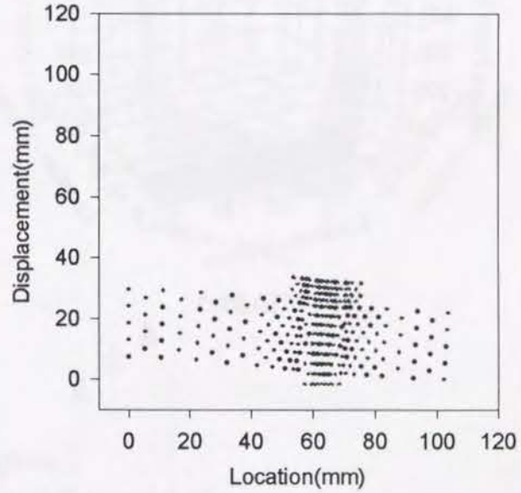

(h) STF8

Fig. 4.18 Deformation at the Center of the Model in Longitudinal Direction

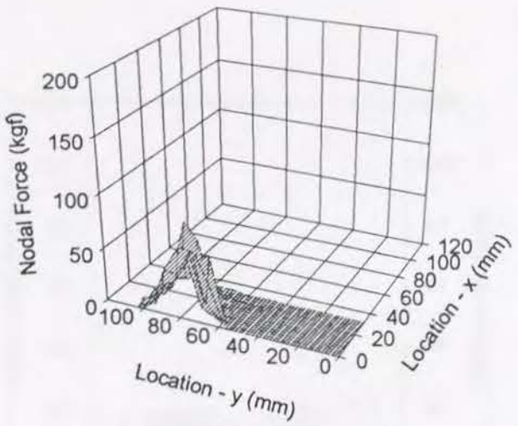

(a) STF1

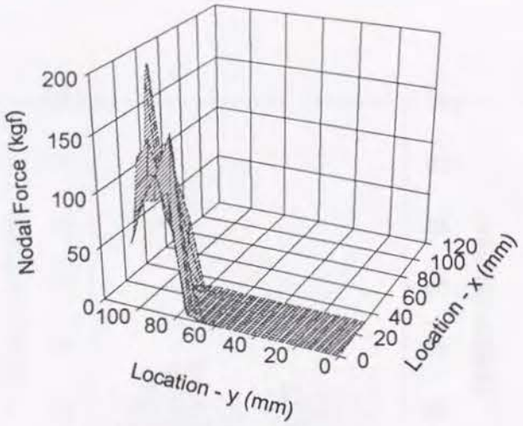

(b) STF2

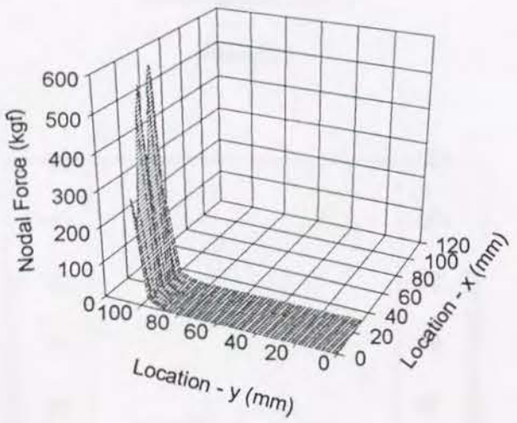

(c) STF3

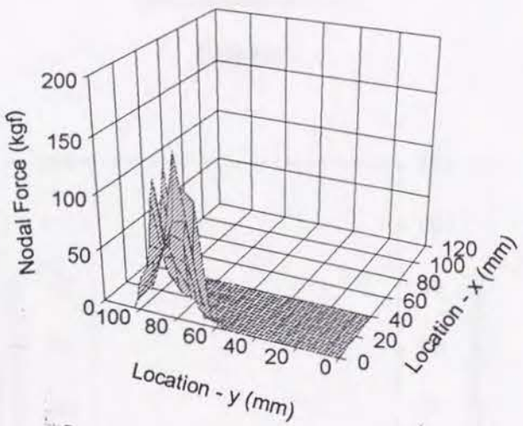

(d) STF4

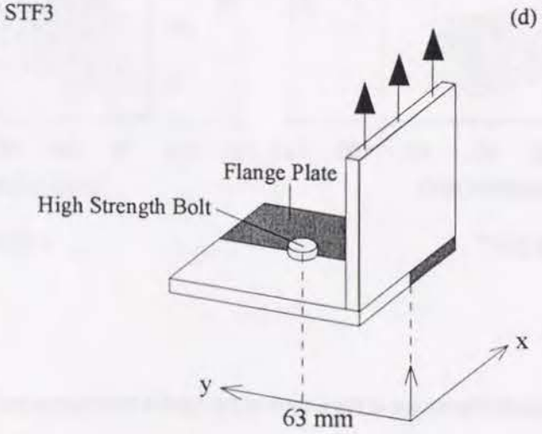

Fig. 4.19 Distribution of Nodal Force on the Contact/Separation Surface (continued)

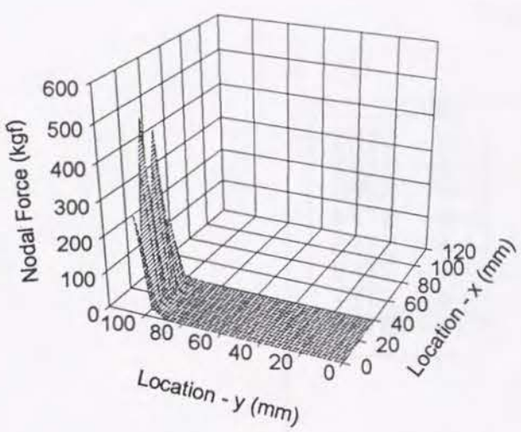

(e) STF5

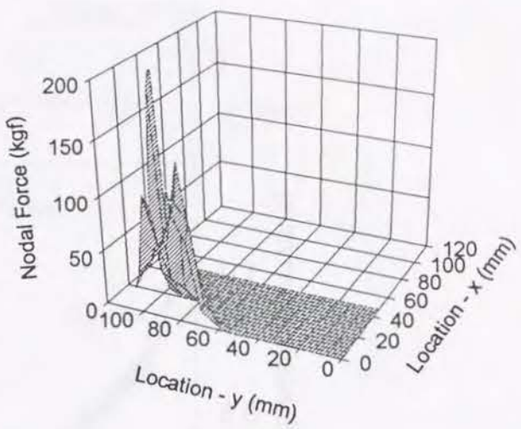

(b) STF6

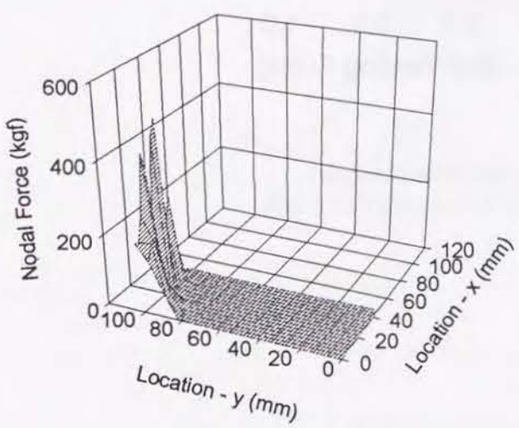

(g) STF7

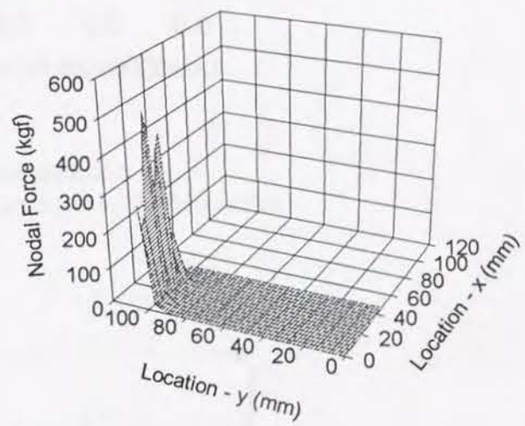

(h) STF8

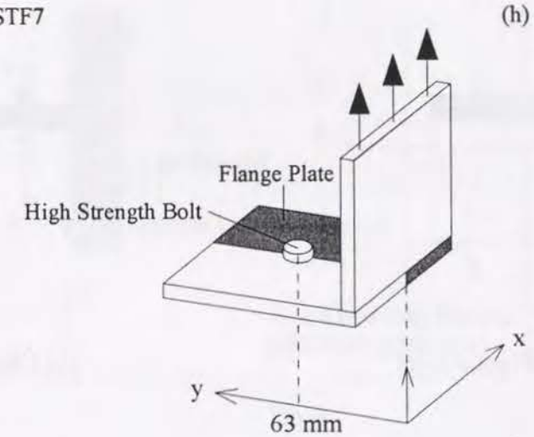

Fig. 4.19 Distribution of Nodal Force on the Contact/Separation Surface

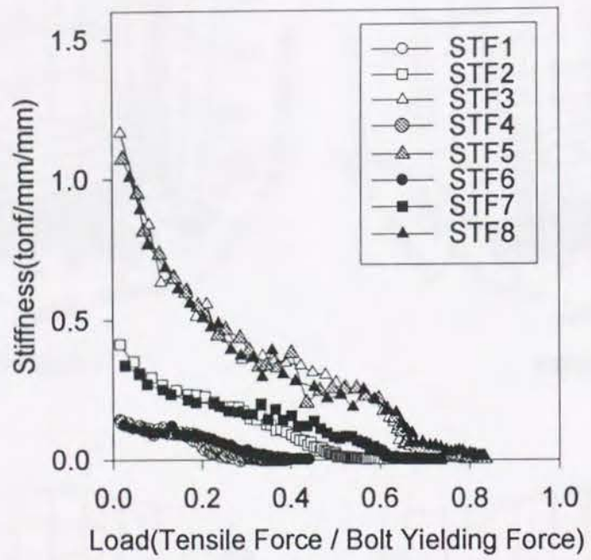

Fig. 4.20 Stiffness-Load Curves (Analysis)

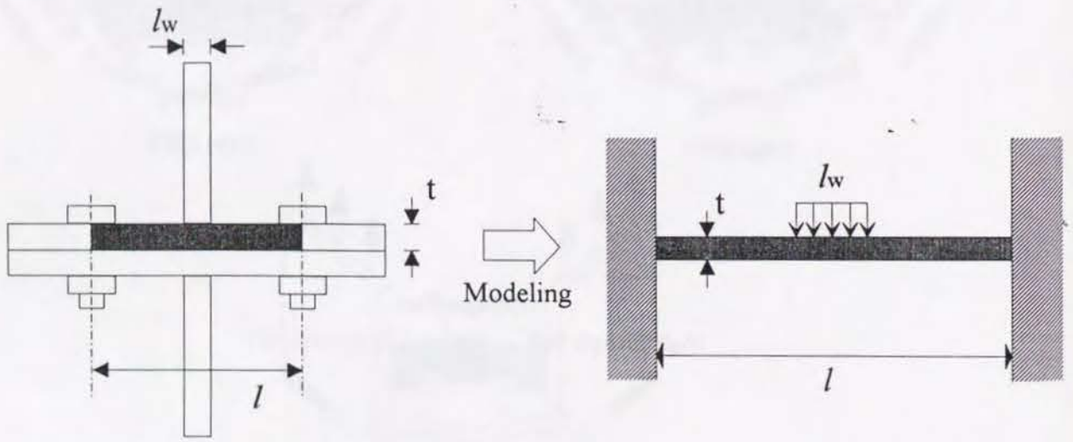

Fig. 4.21 Model for Estimation of the Stiffness of the Flange Plate

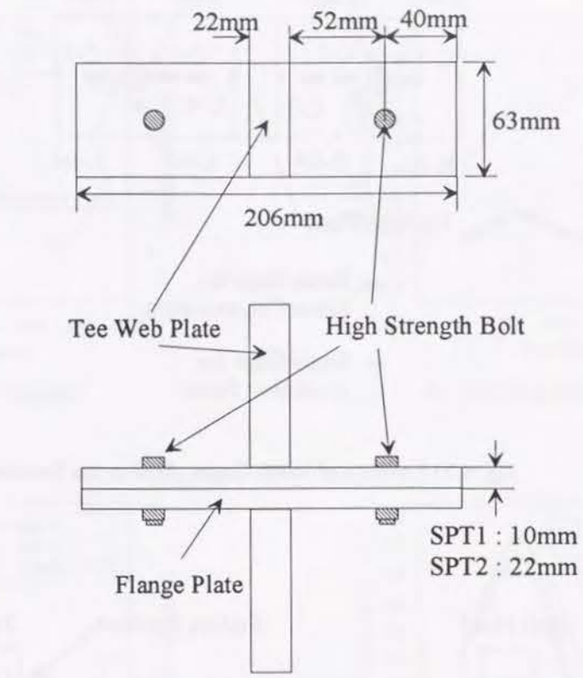

Fig. 4.22 Dimensions of the Specimens for the Fatigue Test

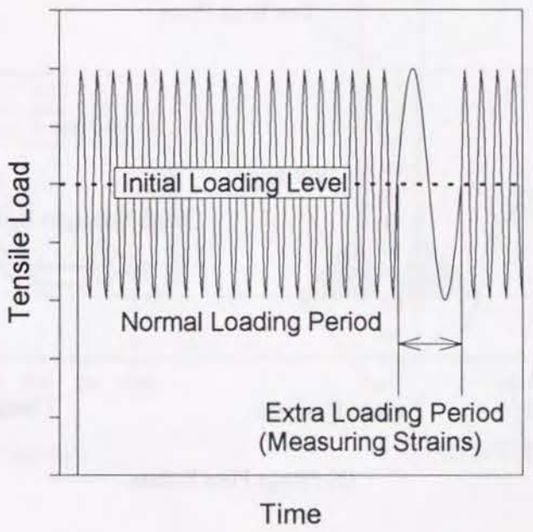

Fig. 4.23 Time History of Applied Tensile Load

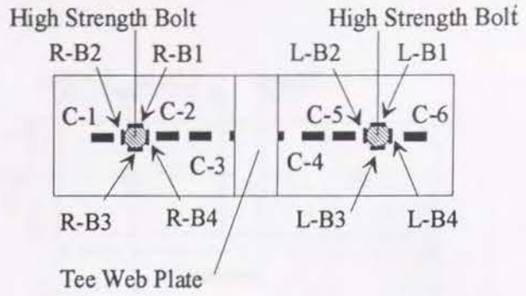

Fig. 4.24 Location of Strain Gages glued on the Specimen

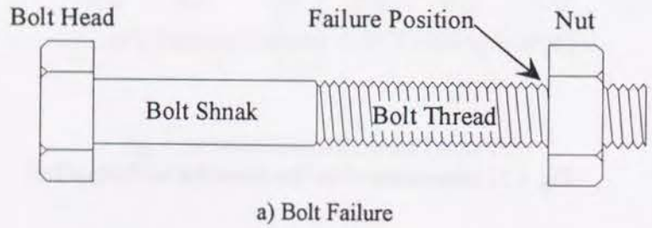

a) Bolt Failure

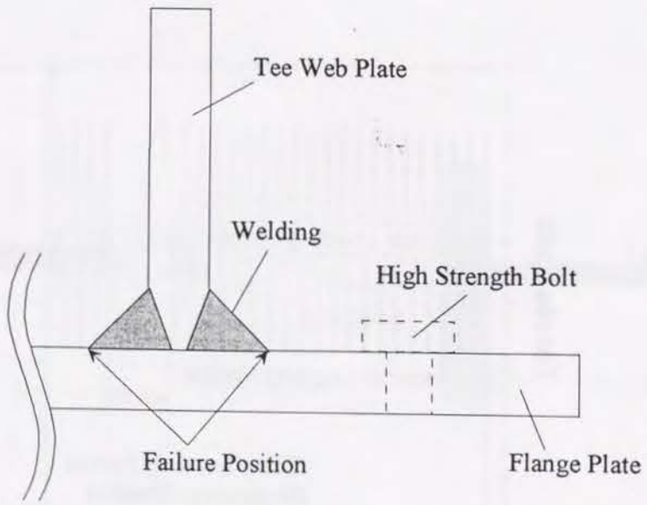

(b) Flange Plate Failure

Fig. 4.25 Location of the Fatigue Failure

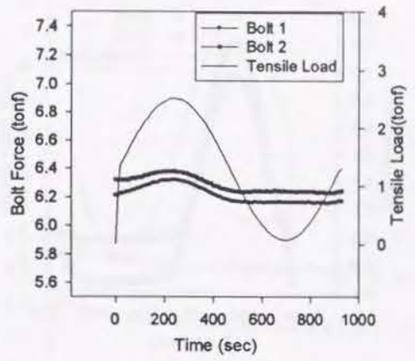

(a) SPT1A (1cycle)

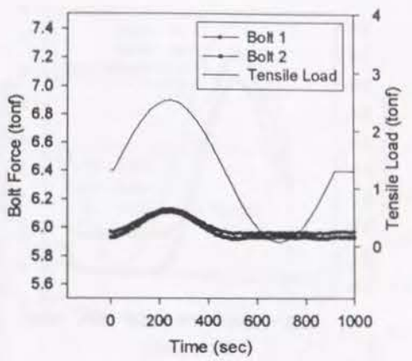

(b) SPT1A (1,000,000cycles)

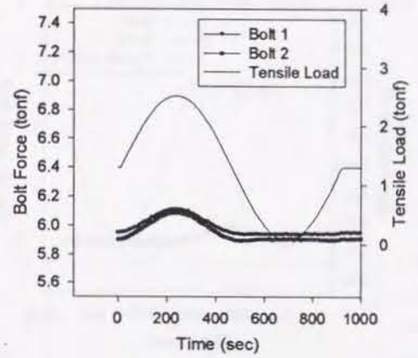

(c) SPTA (2,000,000cycles)

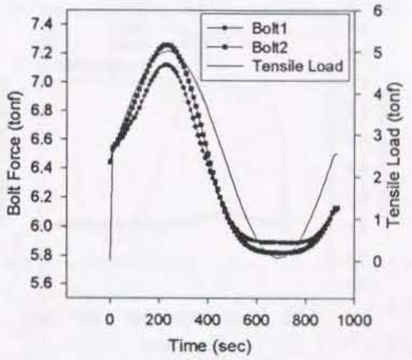

(d) SPT1B (1cycle)

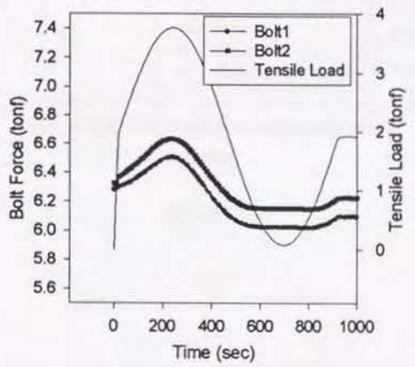

(e) SPT1C (1cycles)

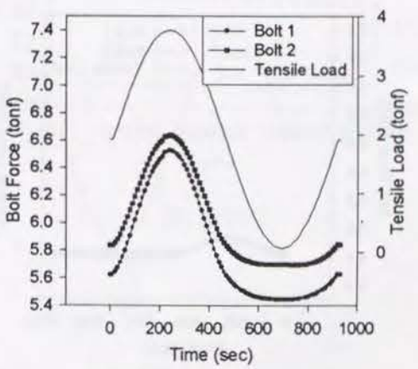

(f) SPT1C (80,000cycles)

Fig. 4.26 Time History of Bolt Force and Applied Tensile Load under One Cycle (continued)

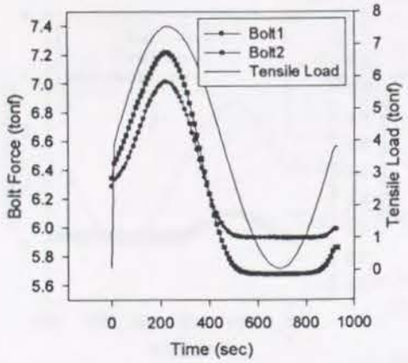

(g) SPT2A (1cycle)

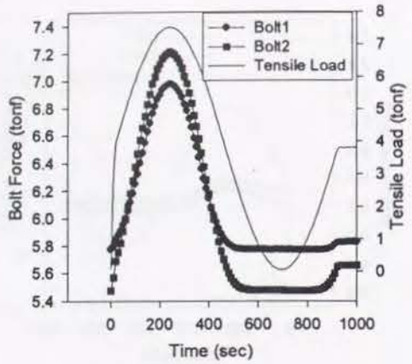

(h) SPT2A (60,000cycles)

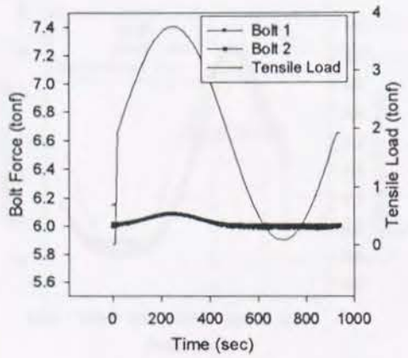

(i) SPT2C (1cycle)

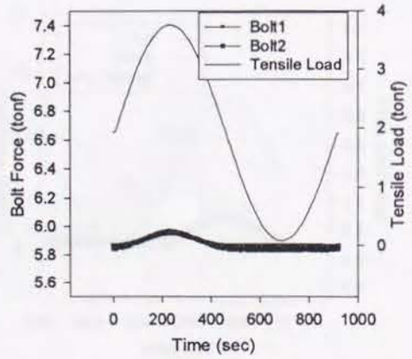

(j) SPT2C (1,000,000cycles)

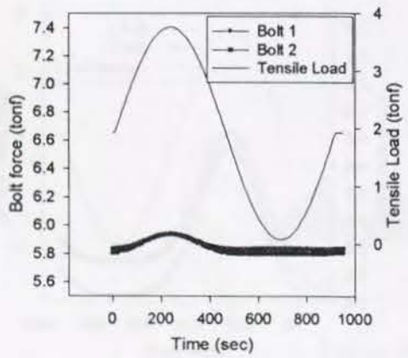

(k) SPT2C (2,000,000cycles)

Fig. 4.26 Time History of Bolt Force and Applied Tensile Load under One Cycle

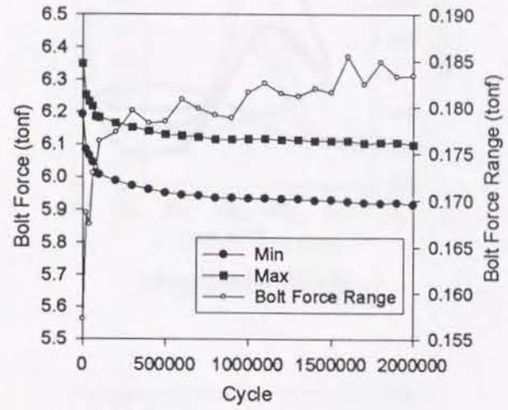

(a) SPT1A

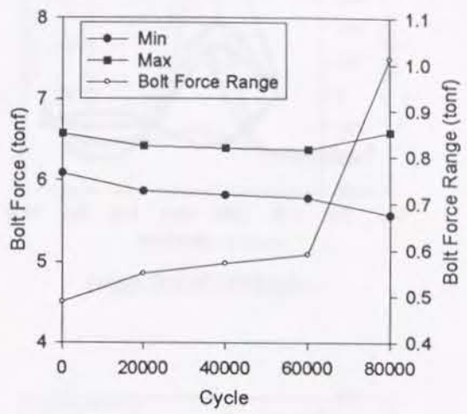

(b) SPT1C

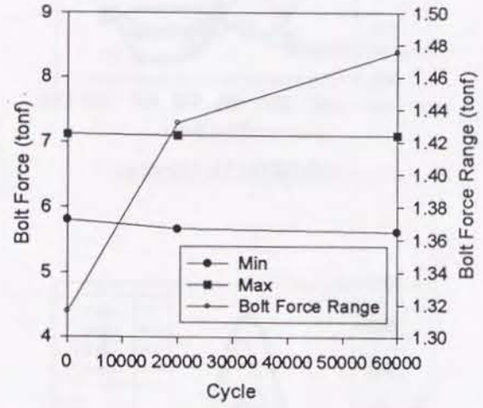

(c) SPT2A

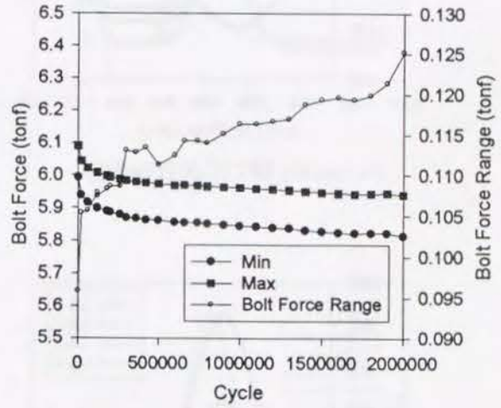

(d) SPT2C

Fig. 4.27 Change of the Maximum and Minimum Bolt Force

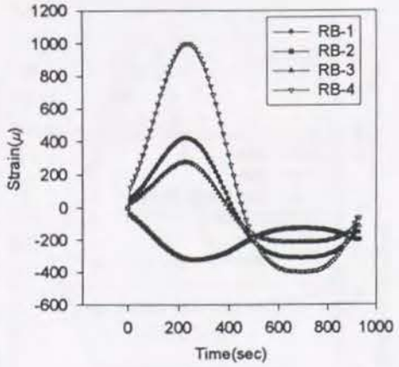

(a) SPT1B-R (1cycle)

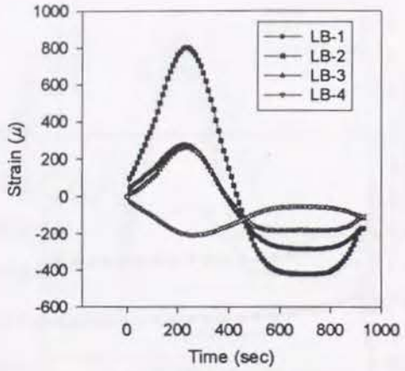

(b) SPT1B-L (1cycle)

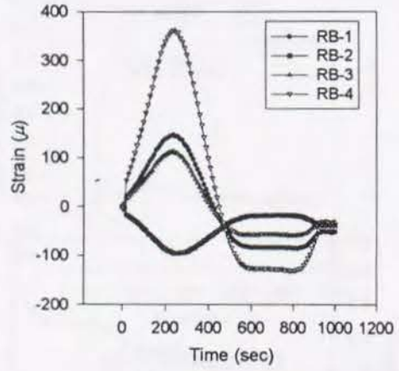

(c) SPT1C-R (1cycle)

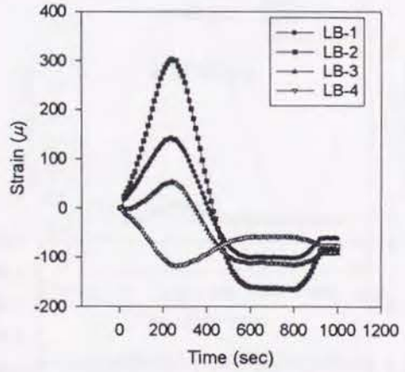

(d) SPT1C-L (1cycle)

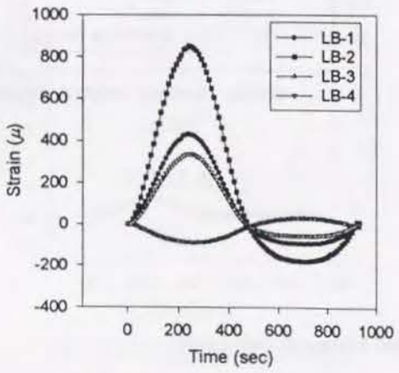

(e) SPT1C-R (80,000cycles)

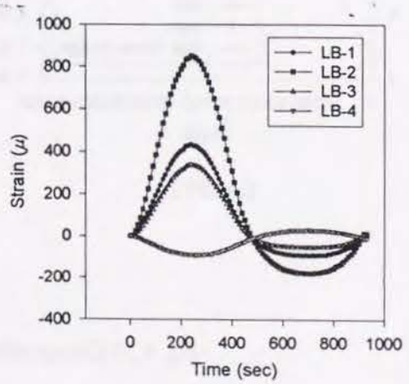

(f) SPT1C-L (80,000cycles)

Fig. 4.28 Time History of the Strain at the Bolt Shank (continued)

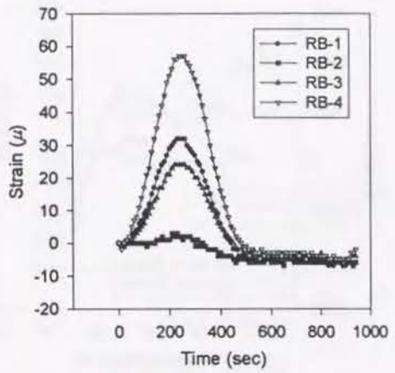

(g) SPT2C-R (1cycle)

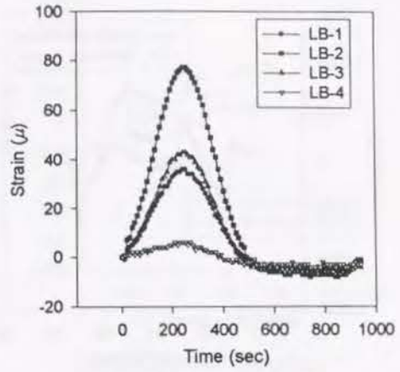

(h) SPT2C-L (1cycle)

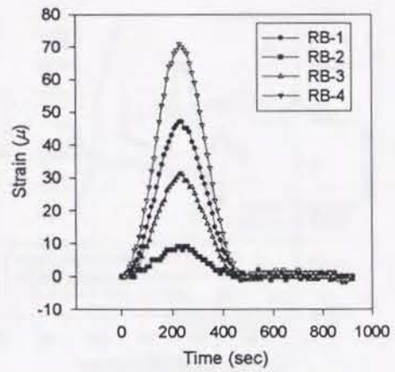

(i) SPT2C-R (1,000,000cycles)

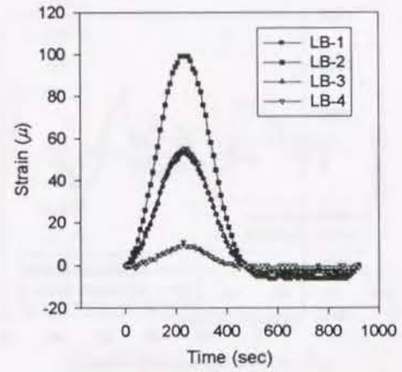

(j) SPT2C-L (1,000,000cycles)

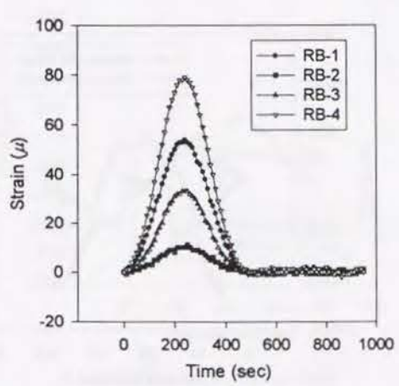

(k) SPT2C-R (2,000,000cycles)

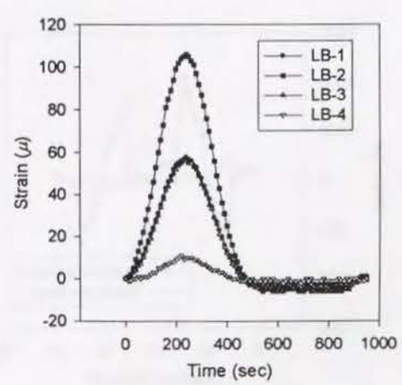

(l) SPT2C-L (2,000,000cycles)

Fig. 4.28 Time History of the Strain at the Bolt Shank

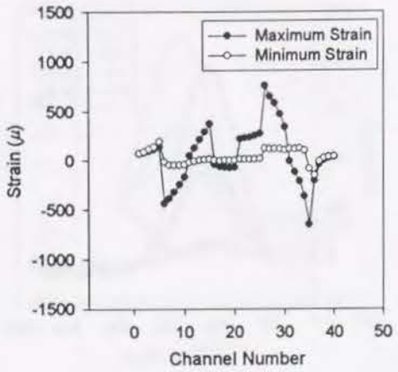

(a) SPT1A (1cycle)

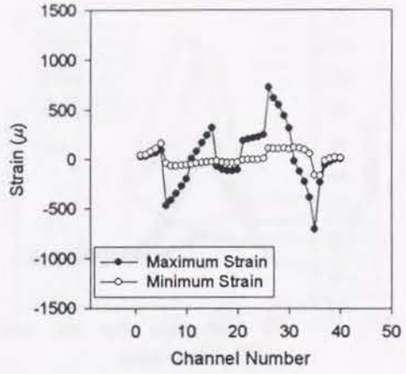

(b) SPT1A (1,000,000cycles)

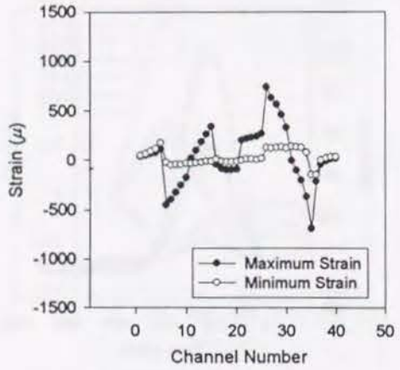

(c) SPT1A (2,000,000)

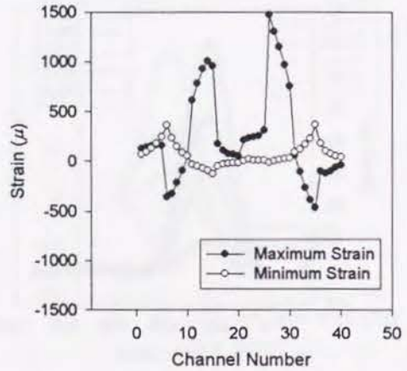

(d) SPT1B (1cycle)

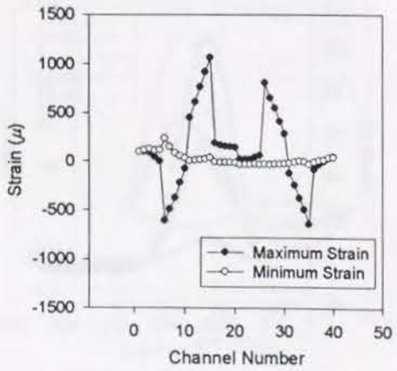

(e) SPT1C (1cycle)

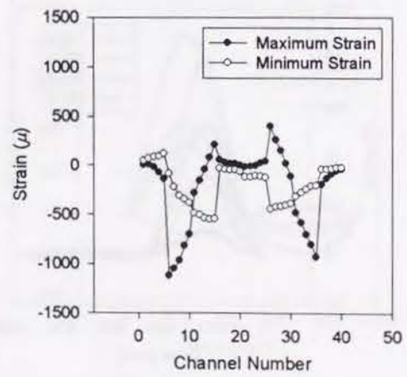

(f) SPT1C (80,000cycles)

Fig. 4.29 Strain Distribution on the Flange Plate (continued)

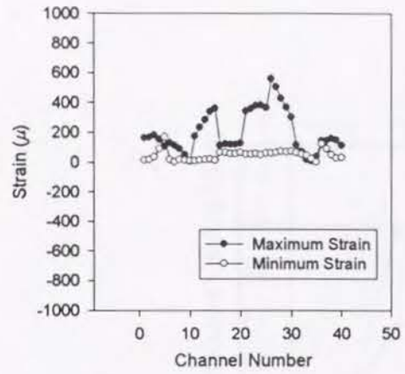

(g) SPT2A (1cycle)

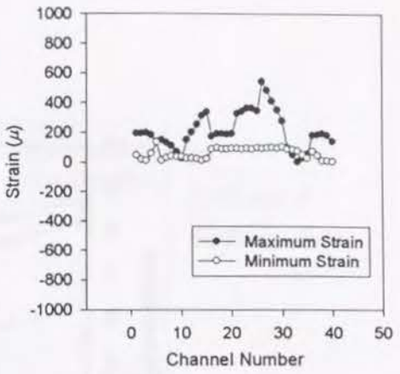

(h) SPT2A (60,000cycles)

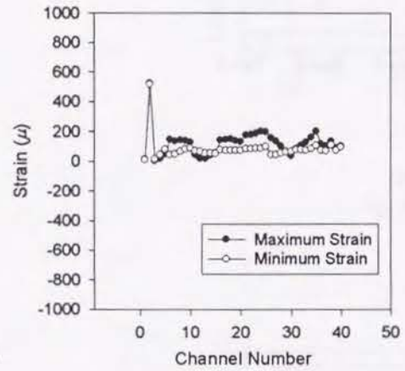

(i) SPT2C (1cycle)

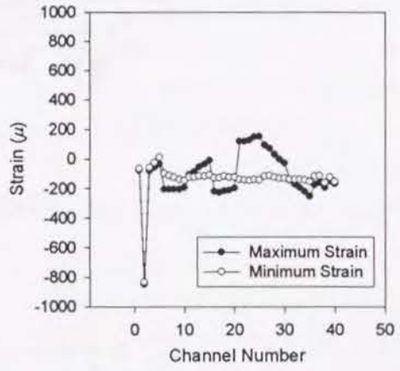

(j) SPT2C (1,000,000cycles)

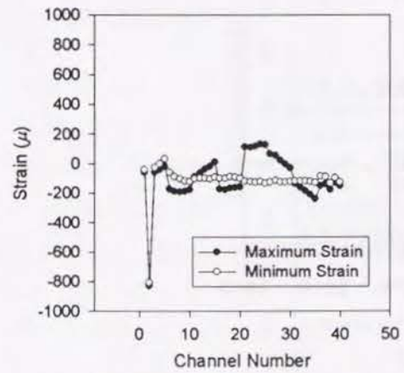

(k) SPT2C (2,000,000cycles)

Fig. 4.29 Strain Distribution on the Flange Plate

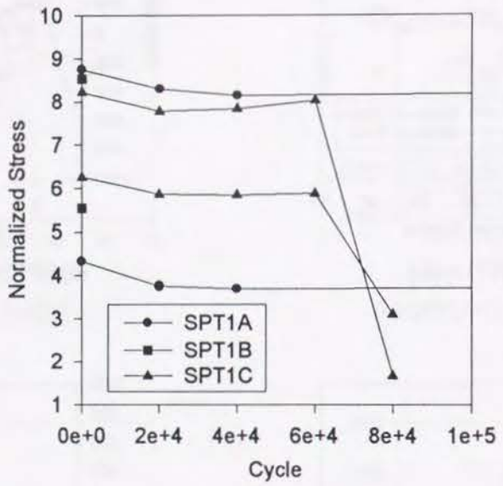

(a) SPT1 Type

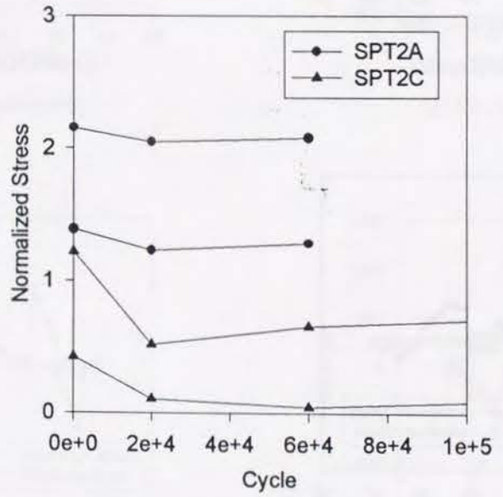

(b) SPT2 Type

Fig. 4.30 Time History of the Stress on the Flange Plate

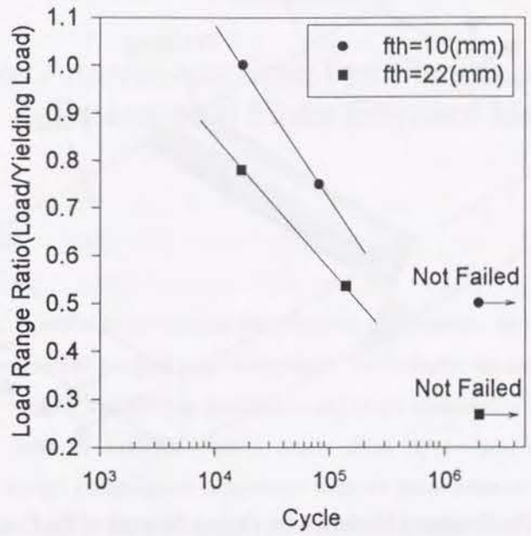

fth : Thickness of the Flnage Plate

Fig. 4.31 S-N Diagram (1)

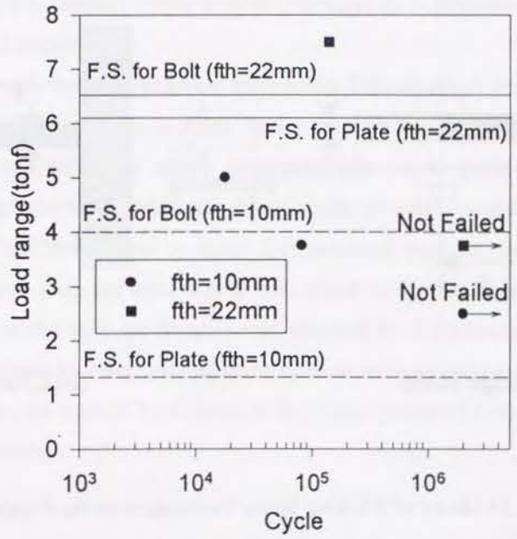

F.S.: Fatigue Strength

Fig. 4.32 S-N Diagram (2)

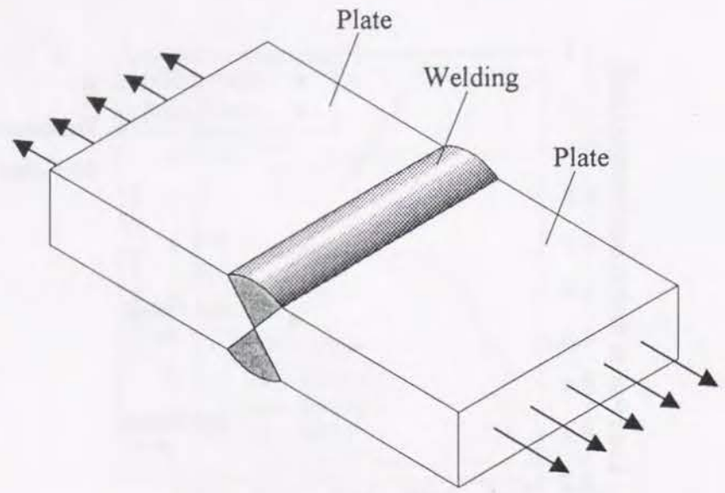

Fig. 4.33 The Estimated Model for the Fatigue Strength of the Flange Plate

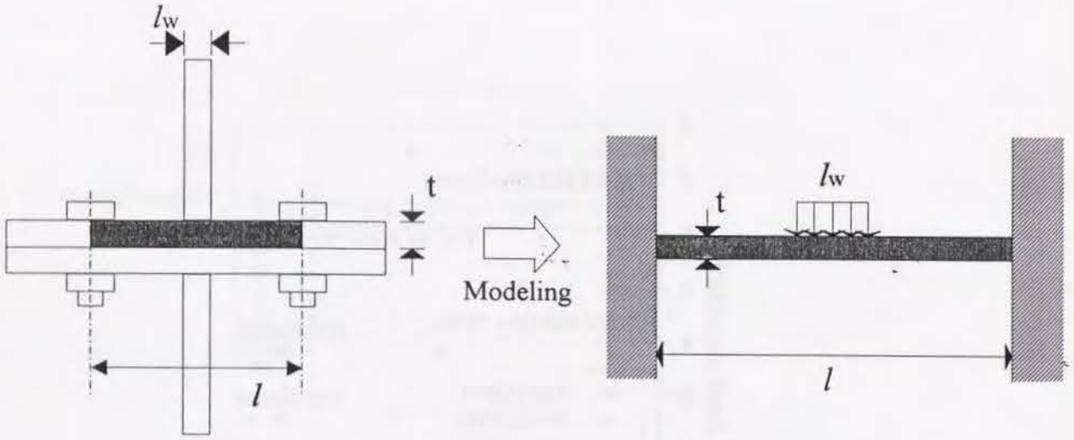

(a) Split Tee Flange Joint (b) Clumped Beam at both Ends

Fig.4.34 Model of Working Stress Verification on the Flange Plate

Chapter 5

Simple Analysis on Split Tee Flange Joints using 2-dimensional Finite Element Method

5.1 Introduction

Generally speaking, in order to investigate the behavior of structures and assess its reliability against external loads, 3-dimensional analysis may be required . Particularly, for complex structural element such as the bolted joints, loading transferring mechanism and stress distribution should be examined by stress analysis. However, such an analysis requires much effort in pre-/post data preparation as well as computation. Even though computation technology such as finite element method has been developed significantly, 3-dimensional stress analysis may face with many difficulties such as computation time and memory. In addition, it is almost impossible for engineers to carry out 3-dimensional analysis to design each structural element of structures. It is better to provide the rational design procedure with parameter limitations based on a data-base or simple analysis method to check the actual 3-dimensional behavior. In particular for the design of joints, the structures have many joints and they are not always same; namely every joint may have its own design condition. Therefore, such a simplification can save a lot of time for tedious joint design. In this chapter, simple analysis procedure by 2-dimensional finite element method for split tee flange joints is discussed.

In order to carry out 2-dimensional analysis for 3-dimensional structures, the assumption such as plane stress or plane strain should be made. As for the split tee flange joints which consists of flange plates and high strength bolts, the above assumption can not be made directly. Accordingly, any modification or proper structural model should be made in order to make it possible to reproduce mechanical behavior and stress state by quasi 2-dimensional analysis. In this study, the concept of effective width for flange plate and bolts is proposed. Based on the data base of complete information on mechanical behavior of the split tee flange joints obtained by 3-dimensional finite element analysis, effective width coefficients in 2-dimensional finite element analysis with assumption of plane strain are discussed. Furthermore, the state of local stress at the flange plate and bolts are assessed for calibrated effective width coefficients.

5.2 Quasi-2 dimensional Analysis on the Split Tee Flange Joints

5.2.1 General procedure for calibration of effective width coefficients

At first, 3-dimensional analysis is carried out in order to make a database of complete information on mechanical behavior of split tee flange joints varying the thickness and the width of the flange plate. Analytical model is shown in Fig. 5.1 and this model is the same as the model considered in the previous Chapter 4. The material properties, boundary conditions and the procedure of the analysis are all the same and can be referred to 4.2.2. In addition, the finite element discretization and its procedure also can be referred. All of the analytical cases are tabulated in Fig. 5.2. As shown in this figure, both the thickness of the flange plate and the width of the flange plate are varied. As for the selection of these analytical cases, attention is paid to the applicable range in the current design procedure for building structures[1] and the design procedure for bridge structures(draft)[2], in which structural dimensions such as the thickness of the flange plate is limited to prevent prying force. In this figure, such limits of the thickness and the width of the flange plate are also shown.

Secondly, 2-dimensional analysis is carried out with a certain effective coefficient of the flange plate and that of the bolt. The effective width coefficients are defined as follows:

$$\begin{aligned} w_f &= k_f \cdot w_{f0} \\ w_b &= k_b \cdot w_{b0} \end{aligned} \tag{5.1}$$

in which, w_f is the effective width of the flange plate, k_f, the effective width coefficient, w_{f0}, the width of the flange plate, w_b, the effective width of the bolt, k_b, the effective width coefficient of the bolt, w_{b0}, the width of the bolt. The effective width coefficients used in the 2-dimensional analysis are determined based on the load-separation relationship for all the cases in order to reproduce the 3-dimensional mechanical behavior of the joint. This 2-dimensional analysis is repeated by varying coefficients until good agreement of results of 2-dimensional analysis with those of 3-dimensional analysis is obtained.

5.2.2 Analytical model

In this analysis, the analytical model of the split tee flange joints is considered to be plane strain problem. As for the element, constant strain triangle element is used considering simplicity of formulation. The analytical model and its finite element discretization are shown in Fig. 5.3. Boundary conditions, such as the condition at the contact surface between two flange plates, the condition at the contact surface between the bolt and the flange plate, material properties are the same as those used in 3-dimensional analysis. These boundary conditions and material properties are also shown in Fig. 5.4 and Table 5.1 respectively. Therefore, the difference between 2-dimensional analysis and 3-dimensional analysis is basically only a dimension. This 2-dimensional model is based on a plane cut of the 3-dimensional model at the center of bolt line. And finite element discretization is the same as that of 3-dimensional analysis on

the out surface. In addition, in this 2-dimensional model, the nodal points of the bolt section, and those of the flange plate section are common in order to reproduce the 3-dimensional structure by uniform cross section in width direction. In this analysis, maximum thickness of the flange plate is 22 (mm) and maximum width of the flange plate is 94.5 (mm), so that the number of the elements and degrees of freedom for the largest analytical case is 576 and 656 respectively. Comparing with 3-dimensional analytical cases, the number of the elements and degrees of freedom is 1/32, 1/21 of 3-dimensional analytical case. Therefore, it is understood that 2-dimensional model is very efficient as compared to 3-dimensional model from the view point of the dimension of the array prepared for the analysis on the micro computer.

5.3 Results and Discussions

5.3.1 Effective width on mechanical behavior

The results of the load-separation curves for several effective width coefficient of the flange plate are shown in Fig. 5.5. The horizontal axis shows the separation between two flange plates at the tee web plate and the vertical axis shows the tensile load applied to the split tee flange joint. In case of the thinner flange plate, it is found from these figures that the behavior of contact/separation is considerably affected by the effective width coefficient of the flange plate and it is understood that the larger the coefficient is, the higher the strength is. On the other hand, in case of the thicker flange plate, the behavior of contact/separation is not affected by the effective width coefficient of the flange plate. This difference is considered to be caused by the difference of the failure mode. Namely, in case of the thinner flange plate, the behavior significantly depends on the flange plate, so that the coefficient of the flange plate is very important. On the other hand, in case of the thicker flange plate, the behavior significantly depends on the bolt not the flange plate, so that the effective width coefficient of the flange plate is not important for the mechanical behavior.

Next, load-separation curves for several effective width coefficients of the bolt obtained from 2-dimensional analysis are shown in Fig. 5.6. The horizontal axis shows the separation between two flange plates at the tee web plate and the vertical axis shows the applied tensile load to the joint in the same way of Fig. 5.5. In case of the thinner flange plate, it is found from theses figures that the shape of the curve is almost the same in spite of varying the effective width coefficient of the bolt. Particularly, this tendency is significant for the joint which has narrow width flange plate. On the other hand, in case of the thicker flange plate, it is understood that the shape of the curve is significantly affected by the effective width coefficient of the bolt, that is, the larger this coefficient is, the higher the strength is. Such a difference of the effect of effective width coefficient on load-separation curves for the different thickness of the flange plate is considered to be caused by the different failure mode as mentioned above. That is, in

case of the thinner flange plate, the mechanical behavior of the joint depends on the behavior of the flange plate, as a result, it is not affected by the effective width coefficient of the bolt, on the other hand, in case of the thicker flange plate, the behavior of the joint depends on the that of the bolt; accordingly, it is affected by the effective width coefficient of the bolt.

5.3.2 Calibration of effective width coefficients for the flange plate and the bolt

Based on all the results obtained from 2-dimensional analysis varying the effective coefficient of both the flange plate and the bolt, these coefficients is calibrated by try and error method. When load-separation curve obtained from 2-dimensional analysis is good agreement with that obtained from 3-dimensional analysis, these coefficients are determined to be effective coefficients. As shown in Fig. 5.5 and Fig. 5.6, if the effective coefficient of the flange plate is 0.90 and the effective coefficient of the bolt is 0.65, it is found that the load-separation curve is well predicted by 2-dimensional analysis.

5.3.3 Deformation and stress verification by 2-dimensional analysis using effective coefficients

Deformations of all the cases using calibrated effective width coefficients, namely 0.90 for the flange plate and 0.65 for the bolt, are shown in Fig. 5.7. In these figures, in order to show the deformation clearly, the displacement is magnified by 20 times of the actual displacement, in which the results of 3-dimensional analysis are also shown for comparison. In case of the thinner flange plate, it is found from these figures that the bolt is not deformed significantly. As for the flange plate, significant deformation occurs at the bolt and it isn't deformed at the outer edge of flange plate and remained original shape. On the other hand, in case of thicker flange plate, it can be seen from these figures that the flange plate is not deformed significantly. In addition, it is observed that flange plate is rotated at the edge of the flange plate as a rigid body and that the significant deformation of the bolt occurs at the bolt thread. Such results of the mechanical behavior of the joints obtained from this 2-dimensional analysis is good agreement with experimental results and 3-dimensional exact analysis. Therefore, it is concluded that this quasi 2-dimensional analysis using effective coefficients of both the flange plate and the bolt can reproduce the deformation mode correctly. However, it is observed that the displacement obtained from 2-dimensional analysis is a little different form that obtained from 3-dimensional analysis. Especially, the difference is observed at the section between the tee web and the bolt. In order to carry out more accurate analysis, this analysis method should be modified.

Secondary, the maximum stress at the flange plate obtained from both 2-dimensional analysis using the calibrated effective width coefficients(0.90 for flange plate and 0.65 for bolt) is tabulated in Table 5.2. In this table, the results obtained from 3-dimensional analysis are listed for comparison. In this table, the location of the maximum stress are also shown. From this Table in case of the thinner flange plate, it is understood that the maximum stress and its location are well predicted by 2-dimensional analysis with effective width coefficients. On the other hand, in case of the thicker flange plate, it is found

that the maximum stress obtained by 2-dimensional analysis is quite different from that obtained by 3-dimensional analysis. Particularly, it is understood that the larger the width of the flange plate is, the larger the difference between 2-dimensional analysis and 3-dimensional analysis are made. However, the location where the maximum stress occurs is in good agreement with the results of 3-dimensional analysis. Accordingly, it is concluded that it is difficult to utilize this analysis directly for stress verification. This difference between 2-dimensional and 3-dimensional analysis is considered to be caused by the fact that the behavior of the joint significantly depends on that of the bolt in case of the thicker flange plate.

Finally, bending stress vs. load curves for all the cases obtained from both 2-dimensional analysis with calibrated effective width coefficients(0.90 for flange plate and 0.65 for the bolt)and 3-dimensional analysis are shown in Fig. 5.8. The horizontal axis shows the tensile load applied to the split tee flange joint and the vertical axis shows the bending stress at the fixed edge of the bolt. The bending stress is calculated based on the bending moment applied to the edge of the bolt which is obtained from the nodal force at the end of the bolt and elastic section modulus of the bolt. It is found from these figures that the bending stress in case of the thinner flange plate is about 2.0 times higher than that in case of the thicker flange plate. Moreover it is observed that there is significant difference between the result of 2-dimensional analysis and that of 3-dimensional analysis for any thickness of the flange plate, and it is found that the result obtained from 2-dimensional analysis is higher than that obtained from 3-dimensional analysis. Therefore, based on these results, it should be concluded that there exist many difficulties to estimate the stress occurred at the bolt, as if the behavior of joint depends on that of the bolt.

Considering the comparisons mentioned above, it is understood that the prediction of stress state by 2-dimensional analysis using the effective width coefficients only is very difficult. In order to reproduce stress state by 2-dimensional analysis, further study should be required.

5.4 Conclusions

In this chapter, quasi-2-dimensional analysis on split tee flange joints for the load-separation behavior is proposed. In this analysis, the effective width coefficients of the bolt and the flange plate is utilized in order to reproduce 3-dimensional behavior. This analysis is very useful for parametric study of the split tee flange joint or the design of this type of joints because of its simplicity compared with 3-dimensional analysis. The following conclusions and future research needs are obtained as follows:

1) 3-dimensional behavior of the split tee flange joint, such as load-deformation curve, deformation characteristics, can be reproduced by quasi-2-dimensional finite element analysis using the effective width of the bolt and the flange plate. In this study, the coefficient of the

flange plate and that of the bolt is determined to be 0.90 and 0.65 respectively by try and error.

2) The stress obtained by this 2-dimensional analysis is very conservative. Furthermore, accurate stress verification is difficult by this 2-dimensional finite element analysis using effective width coefficients. Particularly, in case of thicker flange plate, the difference between 2-dimensional analysis and 3-dimensional analysis tends to be large.

In the future, this 2-dimensional analysis should be applied for the cases with various geometrical configurations, such as various thickness of the flange plate, width of the flange plate, the number of the bolts, and its applicability should be made clear for the application of this analysis for actual joints. Furthermore, in order to estimate the stress state at the flange plate more accurately, this 2-dimensional analysis should be modified.

References

1) Architectural Institute of Japan : Recommendation for the Design Fabrication of High Strength Bolted Joints, Maruzen, Mar. 1993(in Japanese).

2) Japanese Society of Steel Construction : Recommendation for the design of tensile joints for bridge structures (draft), Feb. 1993(in Japanese).

Table 5.1 Material Properties used in 2-dimensional Analysis

	Young's Modulus	Yielding Stress
Flange Plate	21,000	26.9
Bolt Shank of High Strength Bolt	21,000	90.0
Bolt Thread of High Strength Bolt	15,700	67.1

(unit : kgf/mm^2)

Table 5.2 Comparison of Maximum Stress between 2-dimensional and 3-dimensional Analysis

Analytical Case	2-dimensional Analysis		3-dimensional Analysis	
	Maximum Stress	Location	Maximum Stress	Location
STF2	27.4	A	27.7	A
STF4	27.2	A	28.7	A
STF13	21.3	A	27.2	A
STF15	14.6	A	27.2	A

[NOTE]

A : Adjacent of the High Strength Bolt at the Loading Side

STF2,STF4 : Thinner Flange Plate

STF13, STF15 : Thicker Flange Plate

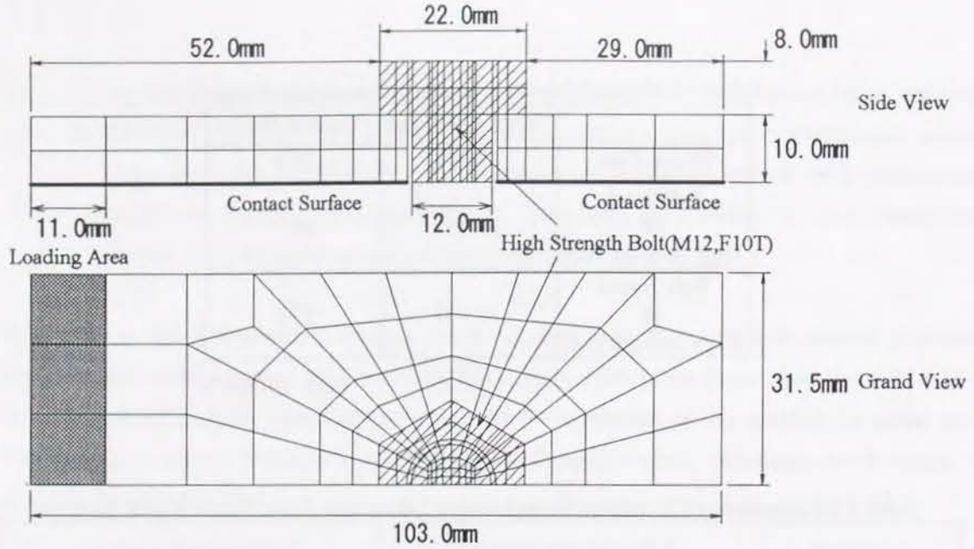

Fig. 5.1 3-dimensuional Analytical Model

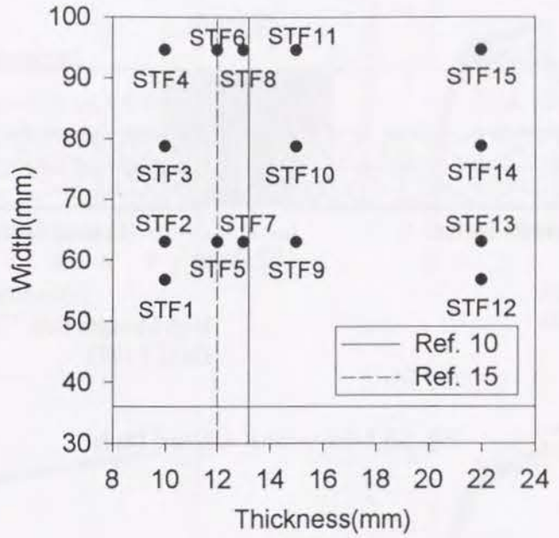

List of All Analytical Cases (unit : mm)

Case	STF1	STF2	STF3	STF4	STF5	STF6	STF7	STF8
Thickness of the Falnge Plate	10	10	10	10	12	12	13	13
Width of the Flange Plate	56.7	63	78.75	94.5	63	94.5	63	94.5

Case	STF9	STF10	STF11	STF12	STF13	STF14	STF15
Thickness of the Flange Plate	15	15	15	22	22	22	22
Width of the Falnge Plate	63	78.75	94.5	56.7	63	78.75	94.5

Fig. 5.2 List of Analytical Cases

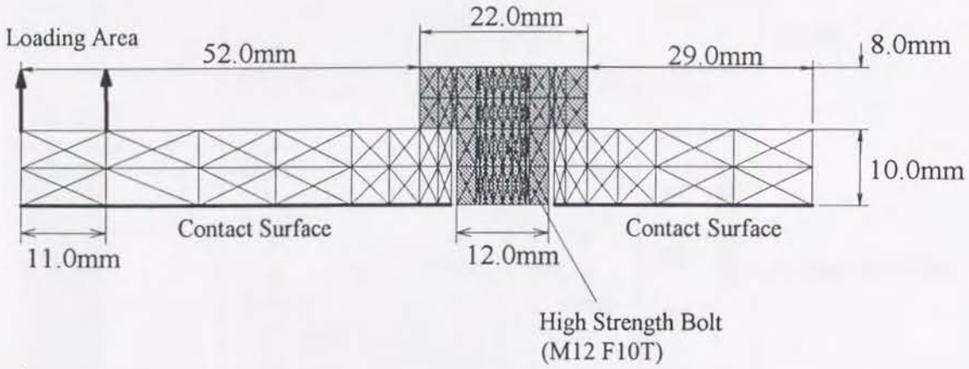

Fig. 5.3 2-dimensional Anlytical Model

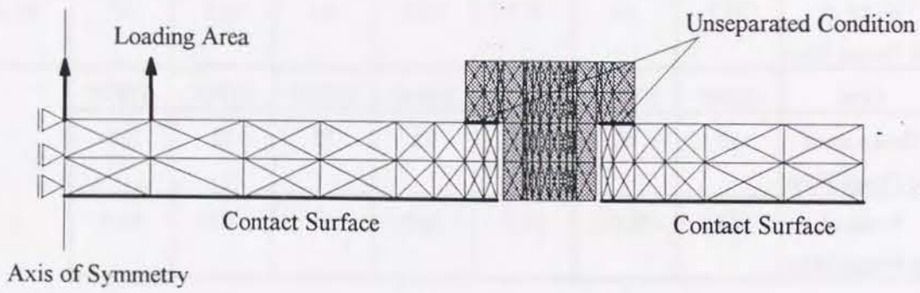

Fig. 5.4 Boundary Conditions of 2-dimensional Analytical Model

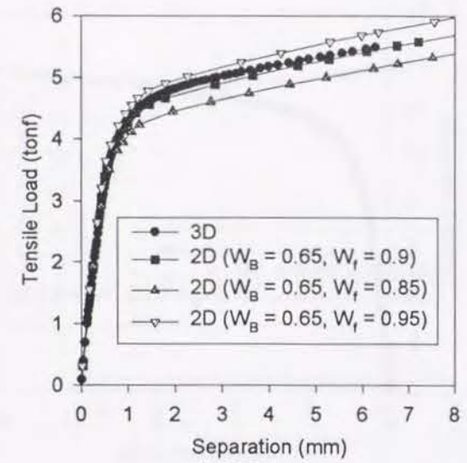

(a) STF1

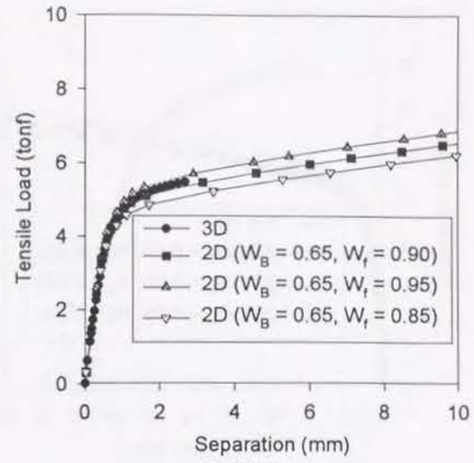

(b) STF2

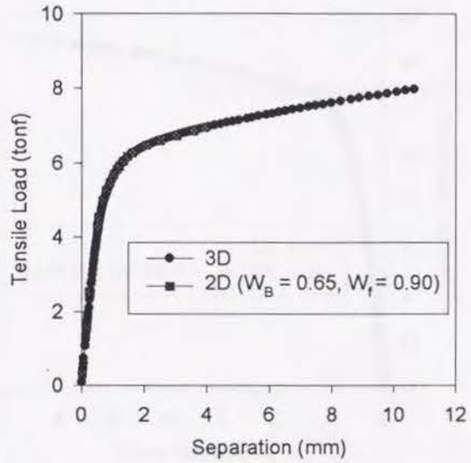

(c) STF3

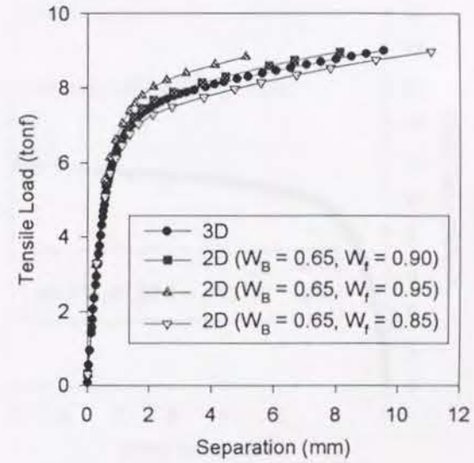

(d) STF4

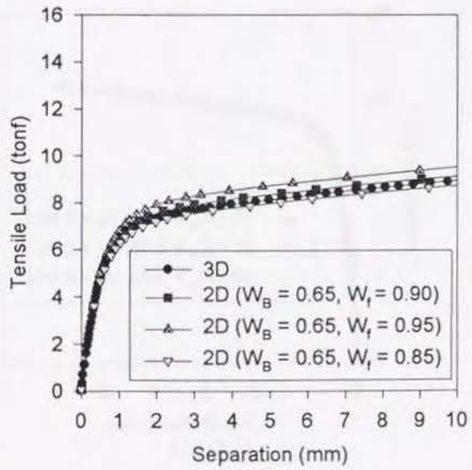

(e) STF5

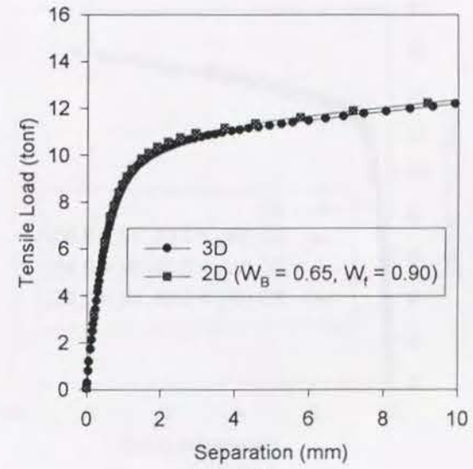

(f) STF6

Fig. 5.5 Load-Separation Curves changing the Coefficient of the Flange Plate (continued)

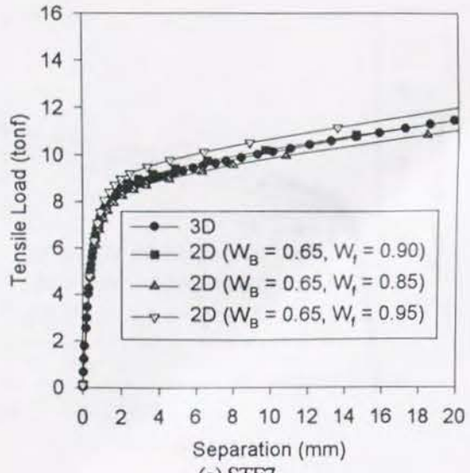

(g) STF7

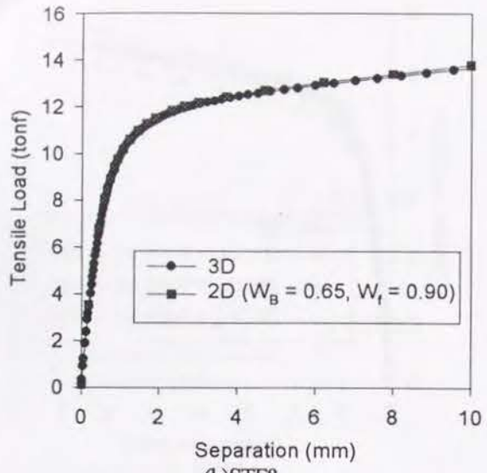

(h)STF8

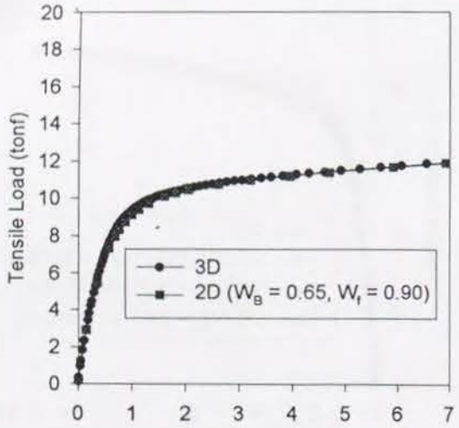

(i) STF9

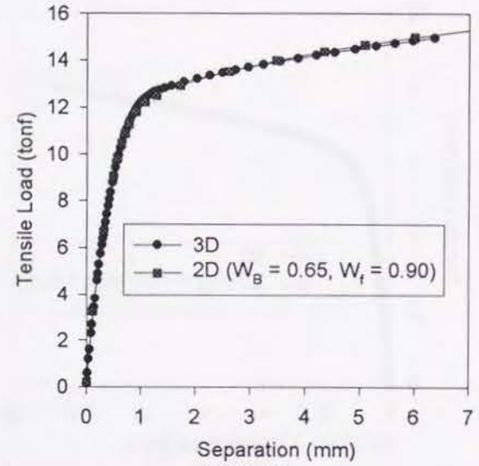

(j) STF11

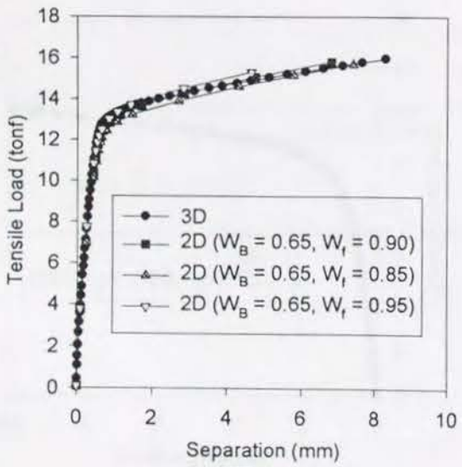

(k) STF12

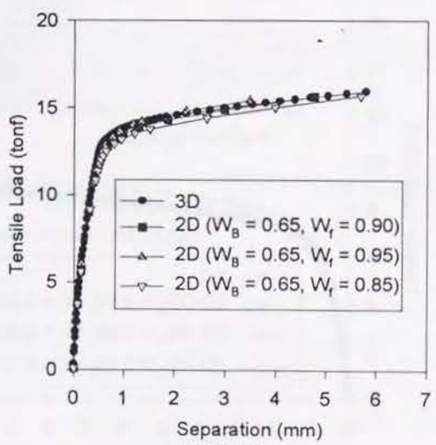

(l) STF13

Fig. 5.5 Load-Separation Curves changing the Coefficient of the Flange Plate (continued)

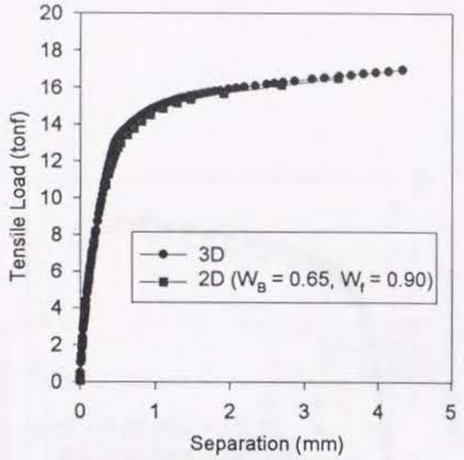

(m) STF14

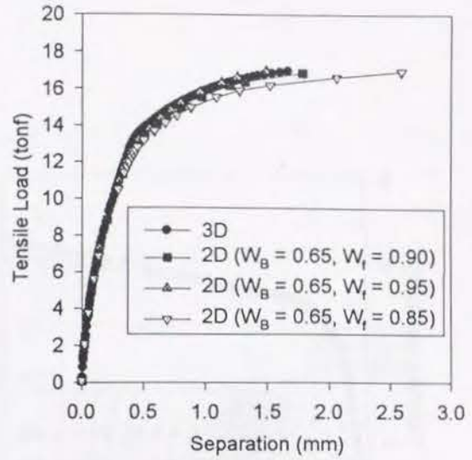

(n) STF15

Fig. 5.5 Load-Separation Curves changing the Coefficient of the Flange Plate

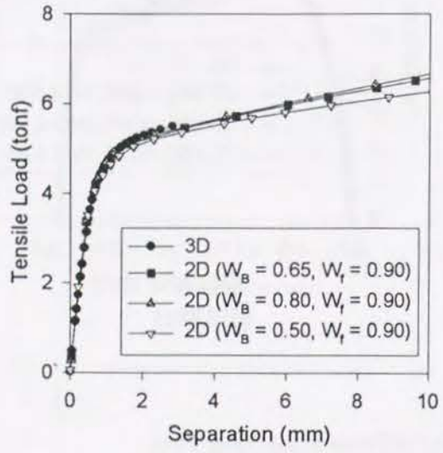

(a) STF2

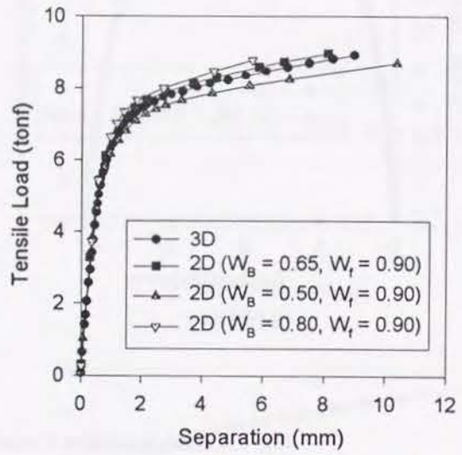

(b) STF4

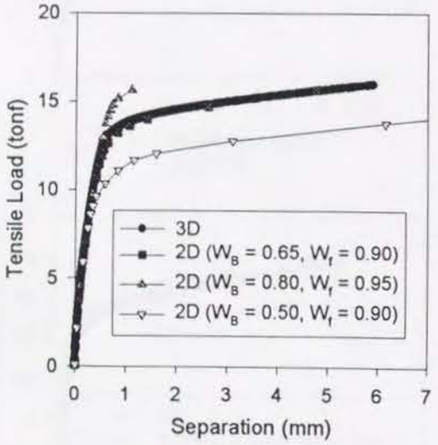

(c) STF13

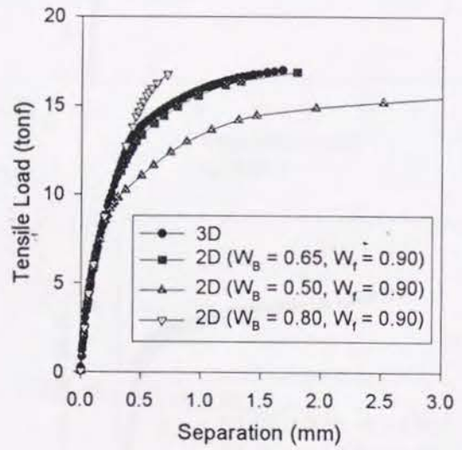

(d) STF15

Fig. 5.6 Load-Separation Curves changing the Coefficient of the Bolt

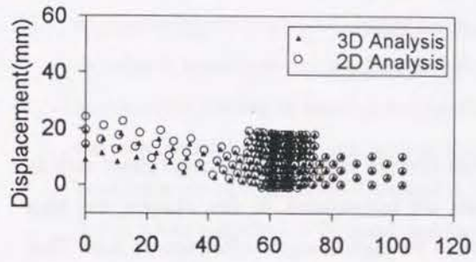

(a)STF2

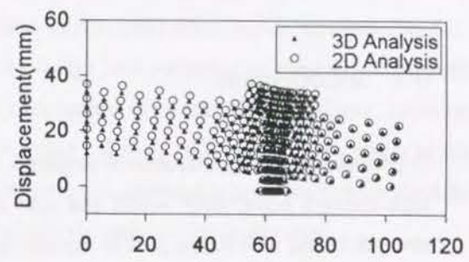

(b)STF13

Fig. 5.7 Deformation of the Bolt and the Flange Plate(Yield Loading Stage)

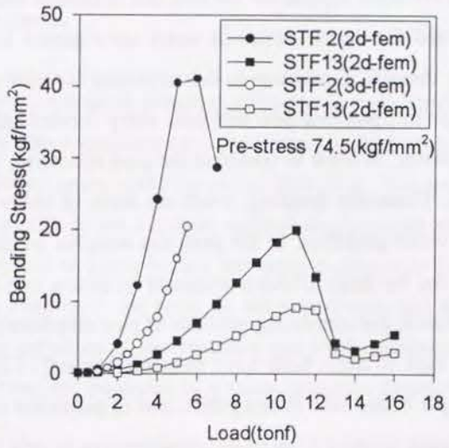

Fig. 5.8 Bending Stress(Bolt)-Load Curves

Chapter 6

Application of the High Strength Bolted Tensile Flange Joint -High Strength Bolted Tube Flange Joint-

6.1 Introduction

In previous chapters, fundamental structural elements of high strength bolted tensile flange joints such as high strength bolts, BAF model and split tee flange joints are investigated. In this chapter, the high strength bolted tube flange joint is focused as an application of the high strength bolted tensile joint. This type of joints is mainly used in the offshore structures, the steel erosion control dam, transmission tower and other temporal facilities. Typical application for the steel erosion control dam and its joint detail are shown in Photo 6.1. This type of joints is classified into 2 types. One type is the joint with rib plates, the other type is the joint without rib plates. Typical examples of these two types of tube joints are schematically shown in Fig. 6.1. As shown in Fig. 6.1, the structural details of the latter is very simple because of no rib plates welded, so that its fabrication can be done easily by the automated machine such as cutting and welding.

The pipe structures are often applied for the offshore structures and the pipe lines for water/gas supply; and particularly utilized for the structures in water environment because of no dependence of loading directions on bending strength. In addition to this structural superiority, the cross section shape of pipe can give better impression to observers than that with sharp corners and it is desired from the view point of aesthetic design. However, in order to construct the pipe structures, the problems such as how to connect members have arisen. Generally speaking, joints are made of either bolt connection or welding. Since welding is superior in water problems, in the past, the complex welding joints have been studied extensively and implemented for the large offshore structures by taking into consideration for the fatigue failure. At present time, as a result, the connecting methods of pipe members such as welding, gusset plate joints and direct splicing by high strength bolts have been established[1][2]. However, there is a little study available on high strength bolted tube flange joints, and in particular no study on the tensile joints subjected to bending can be found because axial tension/compression is only taken into consideration as a result of design assumption that the structures are truss structures. Recently, Watanabe, E. and co-workers carried out the experiment on high strength bolted tube flange joints both with rib plates and without rib plates subjected to bending[3]. It is found that the joint rigidity is as high as that of the tube and not necessary to be assumed pin structures It is also found that both the joints stiffened by the rib plates and the joints not stiffened by the rib plates but with thick flange plate can perform very well under bending and their mechanical behaviors are very similar. It is shown that both structural details are

effective for preventing prying action of the flange plate at tension side of the joints. Therefore, they concluded that the practical use of the high strength bolted tube flange joints with thicker flange plate without any rib plates can be feasible for members under bending.

In this study, the strength and the design of the tube flange joints with thicker flange plate is further studied based on not only the previous experimental works by Watanabe, E. et al. but also experimental and analytical studies for high strength bolted tensile joints described in previous chapters. In order to investigate the mechanical behavior of the tube flange joint subjected to general loading such as combined loading of bending and tension, a series of experiments is carried out. In addition, based on the experimental observations such as the co-relation of global behavior of the tube flange joints to the local behavior of bolt groups discussed in the previous chapters, the rational design procedure for the tube flange joints subjected to the combined loading is proposed and its applicability is assessed.

6.2 The Mechanical Behavior of the Tube Flange Joints

In order to investigate the mechanical behavior on the tube flange joints with thicker flange plate subjected to combined loading, two series of experiments are carried out. The outline of the experiments is described in the following.

6.2.1 Outline of experiments

(a)Pure bending test

In order to investigate the mechanical behavior subjected to pure bending, 4 points bending test on the specimen connected with heavy non-destructive box beam by high strength bolts is carried out using the servo-controlled hydraulic actuators with capacity of 400 (kN). This test setup is shown in Fig. 6.2. The loading is controlled manually to set a certain vertical displacement at the loading point. The uniform bending applied to the specimen given by this test setup is shown in Fig. 6.3. Basically, the loading is continued until the load reaches to the peak. In the experiment, the displacement of the actuator, the applied load, the average curvature of the specimen and local deformation of the joint elements such as the flange plate and the tube, are measured by a micro computer through GP-IB. Each measurement item is summarized as follows:

(1)The applied load and the displacement

These are measured by load cell and displacement transducer built in the actuator. The bending moment M can be given by

$$M = \frac{1}{2} P \cdot L \tag{6.1}$$

in which P and L are applied load and the distance between the loading point and the supporting point respectively.

(2)The average curvature of the specimen

The average curvature of the specimen is measured by the displacement transducers installed on the specimen at the compressive/tensile sides. It is calculated by the following equation.

$$\phi = \frac{u_1 - u_2}{d \cdot L} \tag{6.2}$$

in which, ϕ, u_1, u_2, d and L are the average curvature, the displacement at the compressive side, the displacement at the tensile side, the distance between two displacement transducers and length of the specimen respectively. Schematic view of the setup of those displacement transducers is shown in Fig. 6.4.

(3)Local deformation

The local deformation of the joint elements, such as the deformation of the flange plate, the deformation of the tube and the buckling shape of the tube are measured by the strain gages. The local deformation of the tube is measured by uni-axial strain gages glued on the inner/outer surface of the tube, and the local deformation of the flange plate is measured by rectangular rosette strain gages glued on the surface of the flange plate. The locations of the measuring points are shown in Fig. 6.5.

(b)Combined loading test

In order to investigate the mechanical behavior subjected to combined loading of tension and bending, the test setup shown in Fig. 6.6 is utilized. As shown in Fig. 6.6, two servo-controlled hydraulic actuators with the capacity of 400 (kN) are used in this test. These two actuators are connected to the upper and lower beams by universal joints. The loading control system is shown in Photo 6.2. The test is controlled by the load of the actuators and the operation of loading is made through the micro-computer. The loading procedure is summarized as follows: at STEP 1, the load of each actuator set to zero after finishing the installation of the specimen for starting the loading(because the compressive load about 1 (kN) is already applied to the specimen in order to install the specimen easily); at STEP 2, the tensile load is applied to the specimen by increasing the loads of two actuators equally, namely, bending moment will not be applied to the specimen.; at STEP 3, the bending moment is applied by increasing the load of one actuator and decreasing the load of another actuator by the same rate. This procedure of loading is schematically shown in Fig. 6.7.

In the experiment, the applied load, the average curvature of the specimen, the bolt force, the deformation of the bolt shank, the deformation of the flange plate and deformation of the tube are measured by on-line measurement using the micro computer through GP-IB. Each measurement is

summarized as follows:

(1)The applied load

The applied load is measured by the load cell built in the actuator.

(2)The average curvature

The average curvature of the specimen is calculated by the displacements at the compressive and tensile side. The formula to obtain the average curvature is already described in section 6.2.1(Eq. 6.2).

(3)The bolt force and the strain distribution at the bolt shank

The bolt force and the strain distribution are measured by the strain gages glued on the bolt shank as shown in Fig. 6.8. The average bolt force is obtained by averaging readings of 4 strain gages, and bending deformation of the bolt can be obtained by subtracting a reading of the strain gage from other reading.

(4)The local deformation of the flange plate and the tube

The local deformation is measured by the strain gages glued on the flange plate and the tube. The local deformation of the flange plate is measured by the stress concentration strain gages glued on the flange plate adjacent the tube members. The local deformation of the tube is also measured by the uni-axial strain gages glued on the inner/outer surfaces of the tube. These locations are shown in Fig. 6.9

The number of total measuring points is 100, that is, 40 points for measuring bolt force, 20 points for deformation of the flange plate and 40 points for deformation of the tube.

(c)Test specimens

In these experiments, 12 specimens are made, 6 specimens are used for the pure bending test and the rest are used for the combined loading test. The dimensions of 12 specimens are summarized in Table 6.1. The geometrical configurations of the specimens are shown in Fig. 6.10. As for the specimen name, the first character "BL" or "CL" indicates the experiment type, "BL" indicates the specimen for the pure bending test and "CL" indicates the specimen for the combined loading test. The second character "S" or "L" indicates the diameter of the tube, "S" indicates the specimen with smaller diameter tube and "L" indicates the specimen with larger diameter of the tube, 216.3 (mm) and 267.4 (mm) respectively. The number following the character "TH" denotes the thickness of the flange plate in millimeters. The number following character "P" denotes the axial force ratio to the total bolt pre-stress force.

The materials used to fabricate the specimens are STK400 steel for the tube and SS400 steel for the flange plate. High strength bolts used in the specimens are M20(F10T), whose nominal diameter is 20 (mm). The bolt pre-stress force prescribed in JIS, namely, 178.4 (kN), is given to the bolt[4]. In case of pure bending test, the bolt pre-stress force is given by the torque wrench, on the other hand, in case of

combined loading test, the bolt pre-stress force is given by checking the reading of 4 strain gages glued on the bolt shank.

Since the thickness of the flange plate is concluded from the results of previous study[3] to be a very important parameter which affect on the mechanical behavior, the thickness of the flange plate is varied as the primary parameter. In addition, the diameter of the tube is varied as the secondary parameter in order to investigate the scale effect for application to the actual structures. The thickness of the tubes is determined to keep the radius to thickness ratio constant, so that bending strength of the tubes can be kept constant. Besides, in order to investigate the effect of the axial force, the axial force is varied as the third parameter. The axial force given to the specimens is determined based on the total bolt pre-stress force given to 16 bolts, that is, 2854 (kN). By considering the actual axial force applied to the real structures(steel erosion control dam), the ratio is set to 10 % and 17 %.

Before carrying out these two experiments, the material tests by JIS were carried out for STK400 steel(tube) and SS400 steel (flange plate). The results of the material test are summarized in Table 6.2. It is understood that the material constants are considered to be standard values of steel generally used and prescribed in JIS[5][6].

6.2.2 Experimental results and discussions

(a)Pure bending test

1)Load-deformation characteristics

Specimens were loaded until the ultimate strength was obtained except for BL-S-TH6. The bending moment-curvature curves of all the specimens are shown in Fig. 6.10. The horizontal axis shows the curvature normalized by yield value of the tube and the vertical axis shows the bending moment normalized by yield value of the tube as well. These values are corresponded to the initial yielding of the tube based on the material test results. The initial yielding strength and corresponding the curvature, the position of initial yielding, ultimate strength and the corresponding curvature for each specimen are summarized in Table 6.3. As for the determination of initial yielding, it is based on the local strain of the tube and the flange plate. That is, when any strain gage indicated to reach to yielding strain, the load is determined to be the initial yielding load.

The initial yielding strength under the bending of both S type and L type specimens increases as the flange plate becomes thicker(except for BL-L-TH19 and BL-L-TH25). All the specimens initially yield at the tube except for BL-S-TH6, whose initial yielding occurred at the flange plate. The use of thinner flange plate relative to the wall thickness of the tube causes the premature failure at the flange plate. On the other hand, in case that the flange plate becomes much thicker, it becomes hardly deformed and the failure may take place in the tube such as the buckling of the tube. Furthermore, the ultimate strength and initial stiffness of the joint increase as the thickness of the flange plate becomes larger. However, the ultimate strength becomes almost the same even though the thickness of the flange plate

increases because of the failure at the tube. As a matter of fact, the load-deformation curves of BL-L-TH19 and BL-L-TH25 can be seen to be almost identical; moreover, that of S type can be also identical by using thicker flange plate. It is considered in case of thicker flange plates that the strength depends only on the buckling strength of the tube and that the load-deformation curve can be given by that of the tube.

2)Deformation characteristics and failure mode

The local deformation characteristics of each specimen are summarized in Table 6.4, and the local deformation of the specimens are also shown in Photo 6.3. These photos are taken from the specimen split longitudinally.

From these photos, it is found that the deformation of the flange plate of BL-S-TH6 is very severe; on the other hand such a severe deformation of the flange plate is not observed in BL-S-TH16. The load transferring mechanism of the tube flange joint can be summarized based on these local deformation as follows: When the joint is subjected to bending, the compressive stress of the tube at the joint is transferred to the other side through the flange plate only. On the other hand, the tensile stress at the joint is transferred to the other side through both the flange plate and the high strength bolts. Therefore, the failure mode of the tube flange joint can be classified into the following three modes: 1)local buckling of the tube, 2) local deformation the flange plate and 3) breaking of the bolt. Parameters to affect the above failure modes are considered to be radius-to-thickness ratio of the tube, the thickness of the flange plate, bolt pre-stress force of the bolt and the tensile strength of the bolt and so on.

3)Deformation of the tube

The strain distributions of the tube for BL-S-TH6 and BL-S-TH16 based on the strain gages glued on inner/outer surface of the tube are shown as a typical example in Fig. 6.12. The strain in these figures is normalized by its yield strain obtained from the material test as already shown in Table 6.2. The mean strain is obtained by averaging the strains measured on both inner/outer surface of the tube. The bending strain is also calculated by multiplying one half by the difference between inner and outer strain, which can represent the local out-of plane deformation of the thin wall of the tube. If the bending strain is small, such a deformation by local buckling does not occur, on the other hand, if it is large under the compression, a local buckling may occur because of losing stability under compression.

At the early stage of loading when the local buckling is not observed yet, the strain distributions of BL-S-TH16 both at the section adjacent to the flange plate and far from it are the same and the Bernoulli-Euler's hypothesis is found to be applicable. In addition, the strain at both compressive and tensile sides is distributed uniformly along the axial direction of the tube. On the other hand, that of BL-S-TH6 is distorted significantly and does not correspond to that of the distribution given by Bernoulli-Euler's hypothesis. This is caused by the local deformation of the flange plate. At the same time, the axial strain at the compression side of the tube becomes non-uniform, which implies the local out-of -plane deformation of the tube may occur. Since the thick flange plate can prevent the cross section of the tube

from the distortion as well as the out-of-plane deformation, it is considered that the location where out-of-plane deformation occurs moves away from the flange plate as the thickness of the flange plate increases. Therefore, it is concluded that in case of the joints with a thinner flange plate such as BL-S-TH6 and BL-L-TH12 type, such an distortion of the strain distribution is considered to be significant; and that for the joint with thicker flange plate, the distortion of the strain distribution of the tube is not so significant by further loading even beyond the initial yielding.

4)Deformation of the flange plate

The strain distributions of the flange plate in both the tangential and radial directions of BL-S-TH6 and BL-S-TH16 are shown as a typical example in Fig. 6.13 as well as Fig. 6.12. The dashed line in this figure is drawn by connecting the location of triangular rosettes.

It is understood from this figure that the flange plate is compressed and tensioned in the radial direction at the compressive and tensile sides, respectively. This is caused by the preventing the cross sectional change of the tube, namely, the expansion of the tube at the compressive side and the contraction of the tube at the tensile side In addition, it is found that the strain in the circumferential direction is not as high as that of the radial direction. In general, these strains of the flange plate are not so large at the early stage of loading, except for the thinner flange plate in which the level of the strain of the flange plate becomes more than 10 times of yield strain for BL-S-TH6 when the joint reaches to its ultimate state. However, for *BL-L-TH19 and BL-L-TH25*, it is just as the same as yield strain, namely the failure occurred in the tube; not the flange plate.

The principal strain and its direction of BL-S-TH6 and BL-S-TH16 are shown as a typical example in Fig. 6.14. It is understood that the principal direction coincides with the radial direction at both upper and lower section of a tube. Although the principal direction is not orthogonal to the tube at the middle section, the difference is not so large that the assumption used in the split tee type of the joint can be applied directly for a tube flange joint subjected to bending.

(b) Combined loading test

1)Load-deformation characteristics

The bending moment vs. average curvature curves of all the specimen obtained from the experiment are shown in Fig. 6.15 and the yielding moment and the corresponding curvature determined based on load-deformation curves are listed in Table 6.5. The horizontal axis shows the normalized curvature and the vertical axis shows the normalized bending moment. These are normalized by the yield values of the tube subjected to pure bending based on the material test results. In this figure, yielding moment considering the axial force, M_{py}, M_{py10} and M_{py17} are also shown for reference. M_{py}, M_{py10} and M_{py17} are the yield moment under tension whose magnitude is 0 % , 10 % and 17 % of the total bolt pre-stress force respectively. The yielding moment and corresponding curvature of the tube are shown in this table for reference. The yielding moment of the specimens is defined by the point of intersection of both the

regression lines in the elastic area and plastic area of the moment-curvature curve.

It is found from this figure that the higher the tensile axial force is applied and the thinner the flange plate is, the lower the stiffness and the yield moment are obtained. In particular, it is found that CL-S-TH10-P17, which has the thinnest flange plate and the highest axial tensile load applied, is significantly deformed at the early stage of loading. On the other hand, in case of thicker flange plate, the load-deformation characteristics of CL-S-TH22-P00 is similar to that of CL-S-TH22-P10, therefore, it is concluded that the decrease of yield moment can be small enough to neglect axial force if it is 10 % of the total bolt pre-stress force.

The yield moment of CL-S-TH10-P10 is about 46% of the yield moment of CL-S-TH10-P00 and that of CL-S-TH10-P17 is only 17%, so that the effect of axial force on bending strength is significant if the flange plate is thinner. On the other hand, the yield moment of CL-S-TH22-P10 is almost same as the yield moment of CL-S-TH22-P00, that of CL-S-TH22-P17 is about 78%. It is concluded that the joint with thinner flange plate is more affected by the axial force than the joint with thicker flange plate. In addition, in case of thicker flange plate, it is found that the ratio of yield moment of the specimen to that of the tube considering the tensile axial force is high, so that it is understood that the yield moment of the specimen with thicker flange plate can be expected as high as that of the tube. But, in case of thinner flange plate, this ratio is not so high, it is understood that the yield moment of the specimen is much lower than that of the tube. Therefore, the high strength bolted tube flange joint with thicker flange plate is considered to be comparative to the tube without joint section from the view point of deformation characteristics and the strength.

2) Initial yield state

The location of first yielding and corresponding strain of several sections such as the tube, the flange plate are listed in Table 6.6. In this table, masking cell denotes the section where the first yield occurs.

It is found from this table that the specimen with thinner flange plate firstly yielded at the flange plate; on the other hand, the specimen with thicker flange plate firstly yielded at the tube. For example, the first yield section of CL-S-TH10-A00 is the flange plate at the tensile side, CL-S-TH22-P00 is the tube at the compressive side and CL-S-TH22-P10 and CL-S-TH22-P17 is the tube at the tensile side. Particularly, the specimen with thinner flange plate yielded at the loading stage when the tensile load is being applied, but the bending moment is not applied; therefore, the flange plate is considered to be axi-symmetrically deformed under tension. Moreover, it is found that first yielding of the specimen with thinner flange plate occurs earlier than that with thicker flange plate. Therefore, it is concluded that the mechanical behavior of the joint with thicker flange plate depend on that of the tube; on the other hand, the mechanical behavior of the joint with thinner flange plate depends on that of the flange plate.

3) Deformation of the flange plate

Strain distribution of the flange plate for all the specimens obtained from the reading of the strain gages on the flange plate are shown in Fig. 6.16. The horizontal axis shows the strain normalized by the yield

strain of the flange plate obtained from the material test. The vertical axis shows the location where the strain is measured. The center of the tube is set to zero, positive value indicates compressive side and the negative value also indicates tensile side. In addition, the strains at the compressive and tensile side of the tube obtained from the uni-axial strain gages glued on the tube are shown for reference.

It is found from these figures that in case of the thinner flange plate, the flange plate is significantly deformed but the tube is not deformed. In particular, the strain at the adjacent the tube is much higher than the yield strain of the flange plate. On the other hand, it is found that in case of thicker flange plate, the tube is significantly deformed, and the flange plate is not deformed. In general, it is observed that the tensile strain at the tensile side further increases and little compressive strain at the compressive side occurs as the applied moment becomes larger. It is considered to be caused by the tube deformation such as that the tube contracts at the tension side and expands at the compressive side under bending. As a result, it is considered that the flange plate is compressed in radical direction at the compressive side and it is tensioned at the tensile side as shown in Fig. 6.17. This phenomenon is also observed in the pure bending test and discussed in the previous section. In addition, it is understood that the strain is relative small in case of thicker flange plate.

4)Average axial strain distribution of the tube and the bolt force distribution

Average axial strain distribution of the tube and the bolt force distribution of all the specimens are shown in Fig. 6.18. In these figures, the vertical axis shows the location where the strain gages are glued on the surface of the tube. The center of the tube is also set to zero and the positive value indicates compressive side and negative value indicates tensile side. The upper horizontal axis shows the increase of the bolt force and the lower horizontal axis shows the average axial strain of the tube.

At the loading stage when the tensile load is being applied, the strain distribution of the tube is uniform except for CL-S-TH10-P17; therefore, it is considered that the tensile load is applied uniformly even though two actuators were controlled independently. But in case of CL-S-TH10-P17, the strain distribution of the tube is not uniform due to the large deformation of the flange plate. At this loading stage, in case of thicker flange plate, the bolt force is not changed; whereas, in case of thinner flange plate, the bolt force decreased significantly. Particularly, in case of CL-TH10-P10, the decrease of the bolt force is about 10% of bolt pre-stress force, and in case of CL-TH10-P17, the decrease of the bolt force is about 20% of the bolt pre-stress force. The fact that the bolt force is not changed in case of thicker flange plate is good agreement with the previous study on split tee flange joints, namely, the applied load is carried by the release of the compressive force between two circular plates given by the bolt pre-stress force. On the other hand, the phenomena that the bolt force decreased in case of thinner flange plate can be explained by the decrease of the thickness of the flange plate due to by yielding.

At the loading stage where the bending moment is applied to the specimen, in case of thicker flange plate, the strain distribution of the tube is linear and it is considered that Bernoulli Euler's hypothesis is applicable. In addition, it is found that change of the bolt force is almost zero. It is caused by

the exist of the bolt pre-stress force as already mentioned above. As for the neutral axis, it is found that the position of the neutral axis subjected to pure bending is the center of the tube and the position of this axis moves to the compressive side as the applied tensile force increased. Particularly, in case of CL-TH22-P17, the position of neutral axis is considered to be out of the cross section of the tube. However, at the loading stage when M/M_y is about 1.0, the strain distribution of the tube becomes non-linear, it is considered to be caused by the out-of-plane deformation of the tube. The strain distribution of the tube is distorted significantly after the moment reaches to M_y because of yielding of the tube.

In case of thinner flange plate, the strain distribution of the bolt is not linear even at the earlier loading stage. Particularly, in case of CL-TH10-P17, the strain distribution of the tube is not uniform and bending deformation of the bolt took place. Therefore, Bernoulli Euler's hypothesis is not considered to be applicable in case of thinner flange plates. It is considered to be caused by the significantly deformation of the flange plate. As for the neutral axis, even in case of CL-S-TH10-P00 under pure bending, the position of the neutral axis is not located at the center of the tube. It is caused by the significantly deformation of the flange plate. In addition, it is also found that the bolt force is kept constant while the bending moment is being applied, therefore, it is understood that the decrease of the bolt force is considered to occur only when the axial tensile load is applied to the specimen.

5) Load-bolt force relation

Load vs. average strain of the bolt curves of all the specimens are shown in Fig. 6.19. In these figures, the horizontal axis shows the average strain of the bolt given by averaging readings of 4 strain gages glued on the bolt shank as shown in Fig. 6.8, and the vertical axis shows the load normalized by the yielding moment of the tube. This average strain can be converted the bolt force by multiplying cross sectional area of the bolt shank and elastic modulus.

In case of thinner flange plate, it is found that the bolt force is not changed while the axial force is being applied up to about 100 (kN), after then the bolt force decreases as the axial force is applied. In addition, in case of CL-S-TH10-P17, it is observed that each bolt force is different even though the axial force is applied as compared with the case of CL-S-TH10-P10. Such a decrease of the bolt force is caused by the decrease of the thickness of the flange plate due to the yield of the flange plate. Furthermore, at the loading stage when the bending moment is being applied, the bolt force decreases significantly at the tension side as the bending moment becomes large, at the compressive side, the bolt force almost does not decrease. Therefore it is considered that the compressive load is transferred through only the tube.

On the other hand, in case of thicker flange plate, even at the loading stage when the tensile load is being applied, the bolt force didn't change. It is due to the thick flange plate, and this result is good agreement with that of the split tee flange joints. In addition, at the loading stage when the bending moment is being applied, at the compressive side, the bolt force decreases a little; on the other hand, at the tension side, the bolt force increases. It is understood that the change of the bolt force in case of thicker flange plate is smaller than that in case of the thinner flange plate. This result is also good agreement with

that of the split tee flange joints.

6) Deformation of the bolt

Load vs. bending strain of the bolt curves of all the specimens are shown in Fig. 6.20. In these figures, the horizontal axis shows the bending strain at the inner/outer side as shown in Fig. 6.8, and the vertical axis shows the applied load. If this strain is positive, the bolt is bent in the radial direction to the outer side of the tube, and if this strain is almost zero, the bolt is not bent.

In case of thicker flange plate, at the loading stage when the tensile load is being applied, the bolt is not bent. Therefore, the thickness of the flange plate is considered to be thick enough not to cause the local deformation of the flange plate and it is understood that the bolts are uniformly elongated. In addition, at the loading stage when the bending moment began to be applied, it is found that the bolt at the tension side is significantly bent. Moreover, in case of CL-S-TH22-P17, it is observed that the strain at the compressive side decreases. It is caused by the change of the thickness of the flange plate. Therefore, even in case of thicker flange plate, the bending deformation of the bolt at the tension side is observed.

On the other hand, in case of the thinner flange plate, at the loading stage when the tensile load is being applied, it is found that the bending strain decreases. This phenomenon is considered to be caused by not the deformation of the bolt but the deformation of the flange plate. In addition, at the loading stage when the bending moment is applied, the bending strain at the tension side increases, so that the bolt is considered to be bent to outer side similar to the case with thicker flange plate. Therefore, in case of thinner flange plate, the change of the bolt shank strain is affected significantly by the deformation of the flange plate.

6.3 Simple Design Procedure for the Tube Flange Joints

6.3.1 Current design procedure

In order to design the high strength bolted tube flange joints, the verification of the working stress to yield stress is necessary. Since the shape of the cross section of the tube is circular and at the joints the cross section changes along the member direction, the rational verification of the working stress is very difficult without any assumptions. Therefore, simple modeling of the joint should be made based on the mechanical behavior.

The current design procedure for the high strength bolted tube flange joints is analogous to that of the reinforced concrete members, where the cross section of the flange plate above the neutral axis (compressive side) is assumed to behave as concrete and the high strength bolts below the neutral axis (tensile side) as steel reinforcement as shown in Fig. 6.21. The working stress of the joint has been traditionally computed based on these simple assumptions. However, there exist many ambiguities such that the flange plate in the compressive side can be effective and that the resistance at the tensile side can

be provided only by the bolts just like the reinforcing bars in the RC section without considering the effect of the bolt pre-stress force. Watanebe, E. et al. modified this assumption by assuming that the cross section of the tube in the compressive side can be effective and that the discrete bolt cross section can be replaced by that of continuous circular ring for simplification; then, the working stress of the flange plate is computed based on the model as shown in Fig. 6.22[7]. This model is cantilever circular ring plate fixed along the inner edge and subjected to concentrated load corresponding to the bolt force at the bolt location. The bending stress at the fixed inner edge is computed by solving the differential equation of the circular plate with Fourier series[8]. It was found that the proposed assumptions can provide the rational and conservative evaluation of the working stress. It is also suggested that the effective cross sectional area both at the compressive side and the tensile side must be assessed in order to evaluate the accurate working stress. Particularly, the increase of the effective cross sectional area at the tensile side due to the bolt pre-stress force is suggested to be studied.

6.3.2 Simple design procedure

In this section, based on the effective cross sectional area evaluated in the previous chapters, further modification of current design procedure was made in order to establish the rational design procedure. The flow of current simple design procedure is in the following.

STEP 1: Determination of the neutral axis position and calculation of the working stress at the joint plane;
STEP 2: Calculation of the working stress at the tube; and,
STEP 3: Calculation of the working stress at the flange plate.

At STEP 1, the assumption on effective cross sectional area at the joint plane carrying the external applied load, is the most important and it is assessed that the cross sectional area at both compressive and tensile side as shown in Fig. 6.23(a) are effective. At the compressive side, the effective cross sectional area, A_{eff} may be larger than the cross sectional area of the tube, A_p. Therefore, the ratio of A_{eff}/A_p is determined by using axisymmetric finite element analysis for the model as shown in Fig. 6.23(b). Based on analytical results for the case that the thickness of the flange plate is 10 (mm) and 22 (mm), A_{eff}/A_p is obtained to be 2.24 and 3.55 respectively. According to this ratio, the fictitious tube thickness as shown in Fig. 6.23(a) is considered as the effective cross sectional area at the compressive side. On the other hand, the effective cross sectional area at the tensile side is determined by using BAF model as discussed in Chapter 3, where the proposed formula (Eq. 3.7) for the evaluation of the stiffness of BAF model is used and the stiffness is converted into the cross sectional area. The effective cross sectional area at the tensile side is determined to be 1/2 of the effective cross sectional area of BAF model considering the difference of loading condition between the tensile tube joint and BAF model. As discussed in Chapter 3, the initial

high stiffness decreases and tends to be constant until the sudden decrease occur due to the yielding of bolts as external applied load increases. Although it is relatively small compared to the initial high stiffness of BAF model, this constant value is considered for conservative evaluation. Therefore, the effective cross sectional area at the tensile side is assumed to be 2.45 (cm^2) for the flange plate thickness of 10 (mm) and 2.57 (cm^2) for 22 (mm). Based on the effective cross sectional area at both compressive and tensile sides, the stress at the joint plane is calculated by assuming Bernoulli-Euler's hypothesis in the same way as the current design procedure. This hypothesis is considered to be applicable according to the results obtained from the experiments (referred to section 6.2) if the applied external load is below the yield strength. At STEP 2, the simple model as shown in Fig. 6.23(c) is assumed. This model is a strip with unit width cut in depth direction. Using this model, the working stress at the tube is computed from the working stress at the joint plane considering equilibrium of forces from the joint and the tube. Compressive force P_1 and tensile force P_2 at the tube are obtained by following equations.

$$P_1 = C_1 - \frac{\alpha}{L} C_2 \tag{6.3}$$

$$P_2 = \frac{L+\alpha}{L} C_2 \tag{6.4}$$

in which, C_1, C_2, P_1, P_2, L and α is compressive force at the joint plane, tensile force at the joint plane, compressive force at the tube, tensile force at the tube, distance between the center of the tube wall and distance between the center of the bolt and the center of the tube wall respectively.

At STEP 3, in order to compute the working stress at the flange plate, a strip is considered as the clamped beam shown in Fig. 6.23(d). The length of this beam corresponds to the distance to the position of the high strength bolt at the tensile side from the neutral axis. The boundary condition at both ends of the strip is also considered to be applicable from the results of split tee flange joints in Chapter 4. Maximum stress σ_{max} is obtained by the following equation.

$$\sigma_{max} = \frac{1}{I} \cdot \frac{t}{2} P \frac{a^2 \cdot b}{(a+b)^2} \tag{6.5}$$

in which, σ_{max}, t, a and b, I, P is maximum stress, thickness of the flange plate, distance between the fixed end and loading point, and applied load respectively.

6.3.3 Results and discussions

The working stress is computed using proposed design procedure for the test specimens subjected to tension and bending as described in the previous section 6.2. The working stress obtained from the proposed simple design procedure are shown in Table 6.7. Applied external load at the first yielding obtained from the combined loading test is given as design load. In this table, the working stress obtained

from the current design procedure and experimental results are also shown for comparison. In addition, in case of CL-S-TH10-P10 and CL-S-TH10-P17, the first yielding occurred at the flange plate when the axial force is applied, so that the strip with the boundary conditions as shown in Fig. 6.24 is used to compute the working stress of the flange plate in case of only an axial force applying. Two cases such as the simple supported beam and the clamped beam at both ends are considered.

As for the loading stage in which the axial force is applied, it is found that by the simple supported beam the working stresses are in good agreement with the experimental results in case of thinner flange plate; on the other hand, in case of thicker flange plate, by the clamped beam analytical results agree well with the experimental results. Therefore, it is considered that the boundary condition at the ends of the strip depends on the thickness of the flange plate, and should be considered as hinge for thinner flange plate and the fixed end for thicker flange plate. In general, the evaluation of the working stress of the flange plate can be conservative by the simple supported beam for any thickness of the flange plate. Furthermore, the more rational evaluation can be made by adding elastic constraint at the ends of the strip according to the thickness of the flange plate.

As for the working stress of the tube and the flange plate under bending, it is found from Table 6.7 that the working stress obtained from the proposed design procedure is considerably accurate than that obtained from the current design procedure. In particular, it is found that the location of the initial yielding is well predicted by using the proposed design procedure except for CL-S-TH-22-P00. Since the working stress can be evaluated with enough accuracy by the proposed design procedure, it is considered that the proposed design procedure can be applied to design the tube flange joints. However, in order to evaluate the working stress for the wide range of structural dimensions, further study on the effect of the bolt group and the boundary conditions in modeling may be required.

6.4 Conclusions and Future Needs

In this chapter, the behavior of high strength bolted steel tube flange joints subjected to tension and bending is studied experimentally as an application of high strength bolted tensile joints. Not only the global mechanical behavior such as load transferring mechanism and failure mechanism but also local mechanical behavior of the flange plate, the bolt and the tube are discussed based on the experimental observations. In addition, the simple design procedure for the high strength bolted tube flange joints by means of the results of previous chapters are proposed and its applicability is assessed. The following conclusions are obtained:

1) In case of thinner flange plate, the mechanical behavior of the joint depends on that of the flange plate and the bolts are forced to be bent significantly due to the local deformation of the

flange plate; on the other hand, in case of thicker flange plate, the mechanical behavior can be identical to that of the tube.

2) When the thicker flange plate is used, the interaction between the flange plate and the tube is prevented, and Bernoulli-Euler's hypothesis is considered to be applicable at the joint section. In addition, the initial stiffness, the yield strength and the ultimate strength can be made larger. However, the further increase of the ultimate strength by much thicker flange plate cannot be expected by the buckling of the tube.
3) In case of thinner flange plate, the decrease of the bolt force is observed. The bolt force is found to be very sensitive to the change of the flange plate thickness, even if it is induced by in-plane deformation of the flange plate.
4) By proposed simple design procedure considering the effective cross sectional area, the working stress can be evaluated more accurately than the current design procedure. In particular, the initial yielding and working stress of the tube are in good agreement with experimental results.

In the future, the fatigue strength of the tube flange joints should be studied. Moreover, the proposed design procedure should be further improved in order to be applied for the various ultimate states of the joints.

References

1) Japan Road Association : Specifications of Highway Bridges(JSHB), Maruzen, 1991(in Japanese).
2) Architectural Institute of Japan : Recommendation for the Design and Fabrication of Tubular Structures in Steel, Maruzen, Jan. 1990(in Japanese).
3) T.Yamaguch, E.Watanabe, K.Sugiura, S.Kasai : Experimental Study on High Strength Bolted Tube Flange Joints, Proc. of Annual Conference of Civil Engineers, JSCE Kansai Chapter, Jun. 1991(in Japanese).
4) Japanese Industrial Standard Committee : Sets of High Strength Hexagon Bolt, Hexagon Nut and Plain Washers for Friction Grip Joints(B1186), 1979 (in Japanese).
5) Japanese Industrial Standard Committee : Rolled Steel for General Structure(G3101), 1987 (in Japanese).
6) Japanese Industrial Standard Committee : Carbon Steel Tubes for General Structural Purposes(G3444), 1994 (in Japanese).
7) E.Watanabe, K.Sugiura, T. Yamaguchi, S.Kasai : Design Method of High Strength Bolted Tube Flange Joints, Journal of structural Engineering, JSCE, Vol. 38A, Mar. 1992, pp. 1-12(in Japanese).
8) S.Timoshenko, S.Woinowsky-krieger : Theory of Plates and Shells, Second edition, McGraw-Hill, 1968.

Table 6.1 Geometrical Configurations of the Specimens

(unit : mm)

Specimen	Diameter of Tube	Wall Thickness of Tube	Thickness of Flange Plate	Diameter of Flange Plate	Length of Test Section	Radius to Thickness Ratio
BL-L-TH12	267.4	6.0	12	450	212	44.6
BL-L-TH19			19		219	
BL-L-TH25			25		225	
BL-S-TH6	216.3	4.5	6	400	206	48.1
BL-S-TH10			10		210	
BL-S-TH16			16		216	
CL-S-TH10			10		210	
CL-S-TH22			22		222	

[Note] Tube : STK400 Flange Plate : SS400 High Strength Bolt : M20(F10T)
Bolt Pre-stress Force : 178(kN)

Table 6.2 Results of Material Tests

(a) BL-test

	L type	S type
SS400	0.323	0.323
STK400	0.372	0.377

(unit : kN/mm^2)

(b) CL-test

	TH10-P00	TH10-P10	TH10-P17	TH22-P00	TH22-P10	TH22-P17
SS400	0.2576	0.2576	0.2592	0.253	0.253	0.2489
STK400	0.419	0.419	0.417	0.419	0.419	0.417

[Note] (unit : kN/mm^2)
Tube : STK400 Flange Plate : SS400

Table 6.3 Pure Bending Test Results

Specimen	Thickness of Flange Plate (mm)	Radius -to- Thickness Ratio	Initial Yielding Strength		Ultimate Strength	
			(M / M_y)	(ϕ / ϕ_y)	(M / M_y)	(ϕ / ϕ_y)
BL-L-TH12	12	44.6	0.310	0.871	1.12	18.0
BL-L-TH19	19	44.6	0.365	0.477	1.40	8.39
BL-L-TH25	25	44.6	0.321	0.372	1.39	8.21
BL-S-TH6	6	48.1	0.340	3.51	0.776	24.1
BL-S-TH10	10	48.1	0.390	0.856	1.13	12.5
BL-S-TH16	16	48.1	0.400	0.579	1.29	6.16

Table 6.4 Deformation Characteristics

	BL-S-TH6	BL-S-TH10	BL-S-TH16	BL-L-TH12	BL-L-TH19	BL-L-TH25
Flange Plate	TF	TF	TF(*)	TF	TF(*)	TF(*)
Tube	CT	CT	CT	CT	CT	CT

[Note]

TF : Local deformation of the flange plate at the tension side is observed.

CT : Local deformation of the tube at the compression side is observed.

* : Bernoulli-Euler's hypothesis may be applied at the joint section.

Table 6.5 Combined Loading Test Results

	CL-TH10-P00	CL-TH10-P10	CL-TH10-P17	CL-TH22-P00	CL-TH22-P10	CL-TH22-P17
M_y (kNmm)	$4.334*10^4$	$1.999*10^4$	$0.7235*10^4$	$6.964*10^4$	$7.126*10^4$	$5.379*10^4$
ϕ_y (1/mm)	$2.589*10^{-5}$	$1.681*10^{-5}$	$1.746*10^{-5}$	$1.364*10^{-5}$	$1.618*10^{-5}$	$1.749*10^{-5}$
M_{py} (kNmm)	$6.508*10^4$	$6.508*10^4$	$6.477*10^4$	$6.508*10^4$	$6.508*10^4$	$6.477*10^4$
ϕ_{py} (1/mm)	$1.679*10^{-5}$	$1.679*10^{-5}$	$1.695*10^{-5}$	$1.679*10^{-5}$	$1.679*10^{-5}$	$1.695*10^{-5}$
M_y/M_{py}	0.6659	(0.3072)	(0.1117)	1.070	(1.0950)	(0.8305)
$(M_y/\phi_y)/(M_{py}/\phi_{py})$	0.4319	0.3068	0.1084	1.317	1.136	0.8048
M_y/M_{py10}	—	0.3976	—	—	1.4174	—
M_y/M_{py17}	—	—	0.1827	—	—	1.3582

[Note]

M_{py10} = 0.7725 (kNmm) , M_{py17} = 0.6114 (kNmm)

Table 6.6 List of Strain at the Initial Yielding

			$\varepsilon / \varepsilon_y$	M / M_y	Location
CL-S-TH10-P00	Tube	Side1	-0.6275	0.4078	1
		Side2	-0.6233	0.4078	1
ε_{py}=1816 (μ)	Flange Plate	Side1	0.9999	0.4078	F6
ε_{fy}=1248 (μ)		Side2	1.0481	0.4078	F6
CL-S-TH10-P10	Tube	Side1	0.2316	0(0.2184)	3
		Side2	0.2181	0(0.2184)	2
ε_{py}=1816 (μ)	Flange Plate	Side1	1.0320	0	F5
ε_{fy}=1248 (μ)		Side2	1.0200	0	F5
CL-S-TH10-P17	Tube	Side1	0.3923	0(0.3464)	4
		Side2	0.3817	0(0.3464)	4
ε_{py}=1834 (μ)	Flange Plate	Side1	0.7879	0	F5
ε_{fy}=1287 (μ)		Side2	1.3590	0	F5
CL-S-TH22-P00	Tube	Side1	-0.7295	0.8078	1
		Side2	-1.0105	0.8078	2
ε_{py}=1816 (μ)	Flange Plate	Side1	0.3545	0.8078	F6
ε_{fy}=1227 (μ)		Side2	0.3765	0.8078	F6
CL-S-TH22-P10	Tube	Side1	0.8577	0.7283	9
		Side2	1.0022	0.7283	9
ε_{py}=1816 (μ)	Flange Plate	Side1	0.6170	0.7283	F6
ε_{fy}=1227 (μ)		Side2	0.5949	0.7283	F6
CL-S-TH22-P17	Tube	Side1	0.9209	0.6006	7
		Side2	1.0134	0.6006	8
ε_{py}=1834 (μ)	Flange Plate	Side1	0.7142	0.6006	F6
ε_{fy}=1298 (μ)		Side2	0.7080	0.6006	F6

ε_{py} : Yield Strain of the Tube

ε_{fy} : Yiled Strain of the Flange Plate

[NOTE] Strain Gage Location

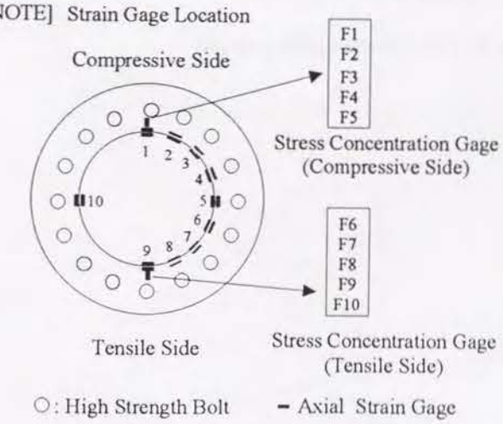

○ : High Strength Bolt — Axial Strain Gage

Table 6.7 Results of Proposed Simple Design Procedure

(a)Working Stress of the Flange Plate(Axial Force applying)

Specimen	Experimental Results (Flange Plate)	Working Stress (Clumped Beam)	Working Stress (Clumped Beam)
CL-S-TH10-P10	yield	0.0512(0.198)	0.303(1.17)
CL-S-TH10-P17	yield	0.138(0.534)	0.818(3.17)
CL-S-TH22-P10	not yield	0.0486(0.187)	0.288(1.11)
CL-S-TH22-P10	not yield	0.0819(0.316)	0.488(1.88)

[NOTE]
unit : kN/mm^2
Applied axial load for the case of thinner flange plate is initial yielding load and in case of thicker flange plate is prescribed axial force.
The value in( ) is the stress normalized by the yield stress of each material.

(b)Working Stress (Bending Moment applying)(Proposed Design Procedure)

Specimen	Experiment (Yielding Position)	Stress at the Tube (Compressive Side)	Stress at the Tube (Tensile Side)	Stress at the Flange Plate	Prediction (Yielding Position)
CL-S-TH10-P00	FL	0.0649(0.155)	0.130(0.312)	0.175(0.678)	FL
CL-S-TH22-P00	CT	0.239(0.572)	0.397(0.95)	0.120(0.461)	TT
CL-S-TH22-P10	TT	0.337(0.806)	0.458(1.09)	0.107(0.414)	TT
CL-S-TH22-P17	TT	0.319(0.762)	0.394(0.943)	0.0922(0.356)	TT

(c)Working Stress (Bending Moment applying)(Current Design Procedure)

Specimen	Experiment (Yielding Position)	Stress at the Tube (Compressive Side)	Stress at the Tube (Tensile Side)	Stress at the Flange Plate	Prediction (Yielding Position)
CL-S-TH10-P00	FL	0.0787(0.188)	0.0459(0.110)	1.14(4.43)	FL
CL-S-TH22-P00	CT	0.250(0.599)	0.146(0.350)	0.752(2.90)	FL
CL-S-TH22-P10	TT	0.311(0.743)	0.212(0.507)	0.883(3.41)	FL
CL-S-TH22-P17	TT	0.279(0.337)	0.217(0.520)	0.801(3.09)	FL

[NOTE]
unit : kN/mm^2
FL, CT and TT denotes the flange plate, the tube at the compressive side and the tube at the tensile side respectively.
The value in( ) is the stress normalized by the yield stress of each material

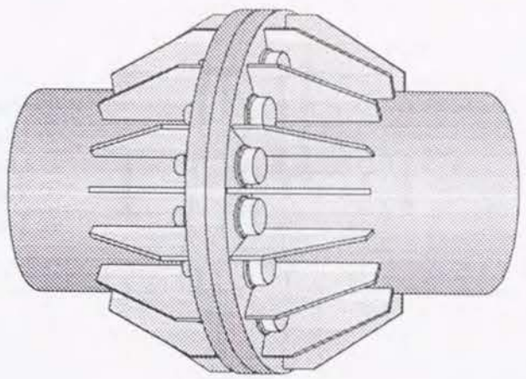

(a) With Rib Plates

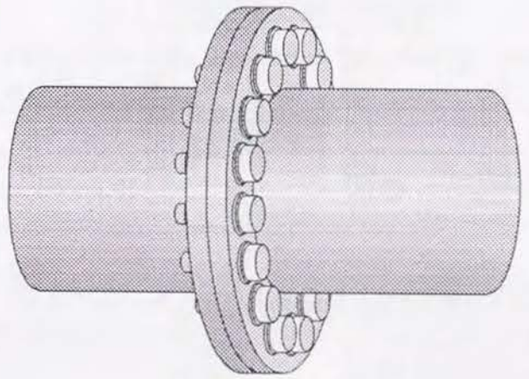

(b) Without Rib Plates

Fig. 6.1 Typical Types of High Strength Bolted Tube Flange Joints

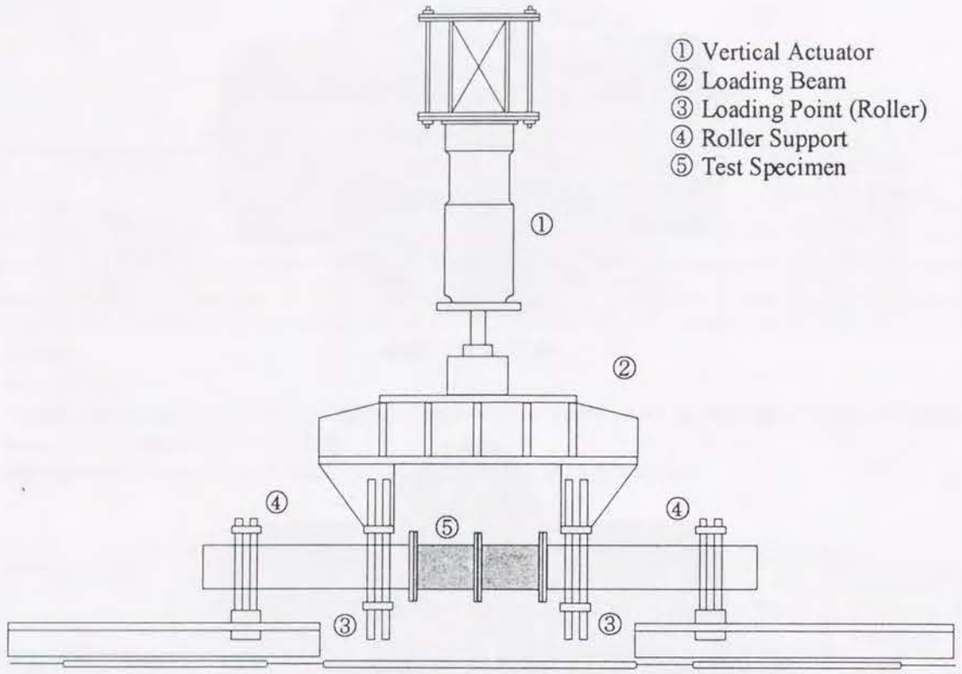

Fig. 6.2 Test Setup for the Pure Bending Test

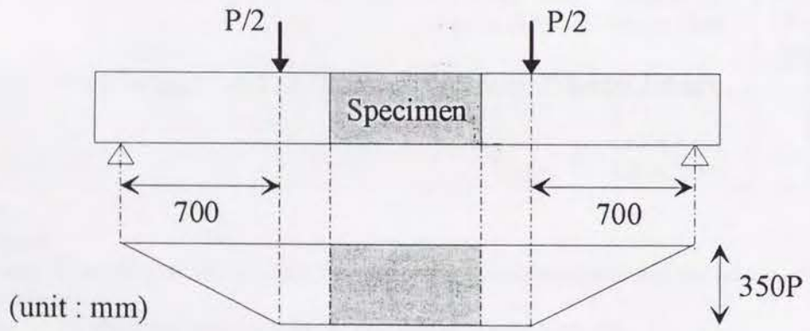

Fig. 6.3 Applied Moment Distribution Diagram

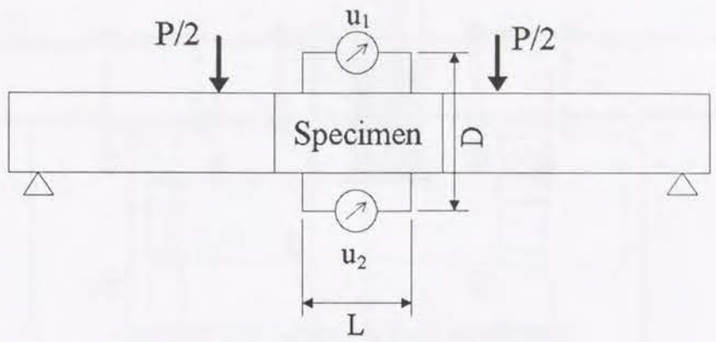

Fig. 6.4 Setup of the Displacement Transducer (BL Test)

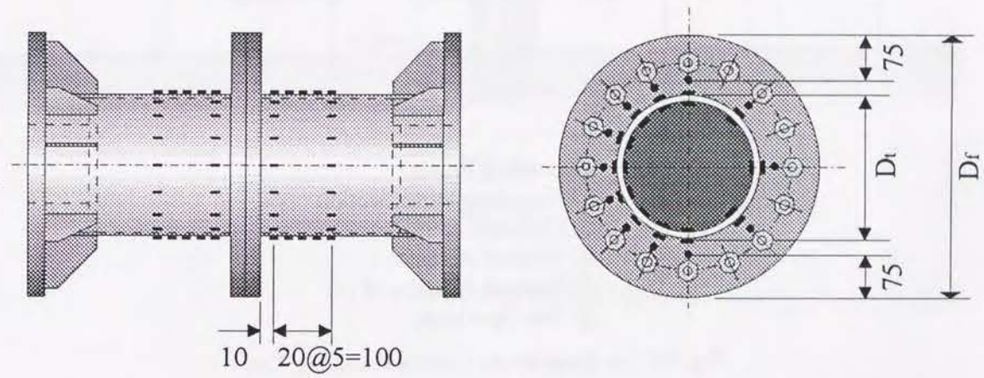

Fig. 6.5 Measuring Points of Local Strain (BL Test)

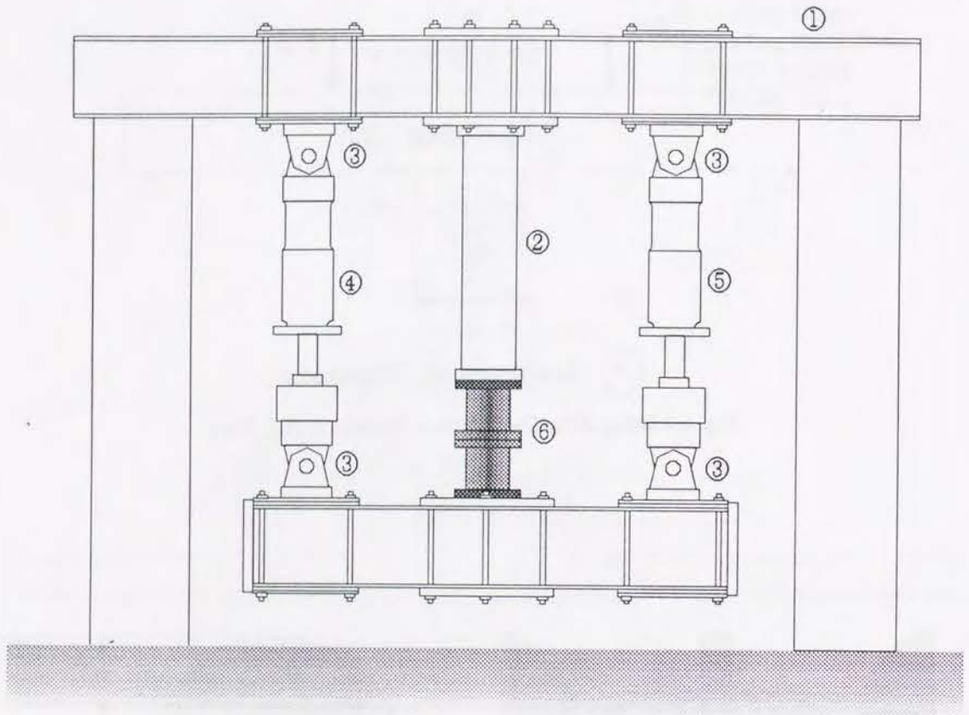

① Loading Frame
② Non-destructive Section
③ Universal Joint
④ Vertical Actuator I
⑤ Vertical Actuator II
⑥ Test Specimen

Fig. 6.6 Test Setup for the Combined Loading Test

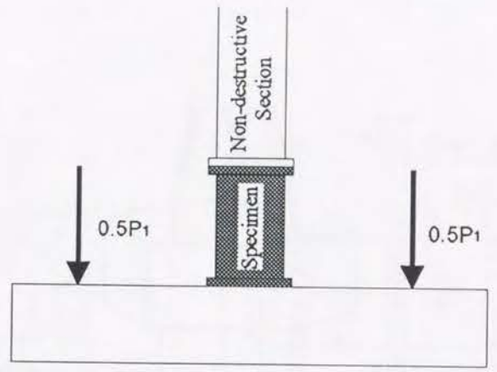

(a) Step 1 (Applying Axial Tensile Force)

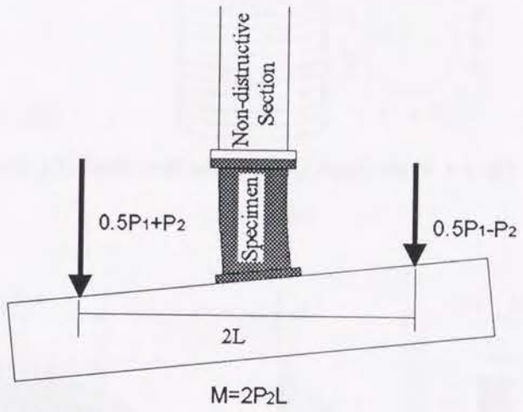

(b) Step 2 (Applying Bending Moment)

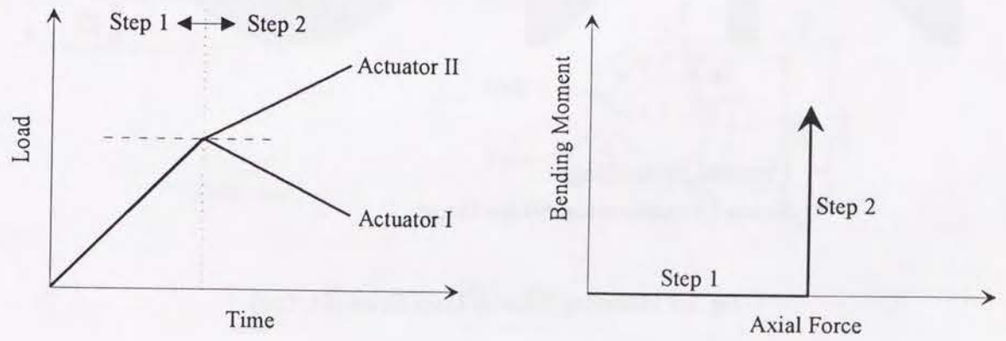

Fig. 6.7 Loading Procedure (CL Test)

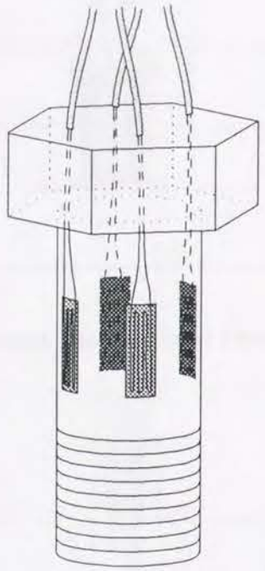

Fig. 6.8 Strain Gages Glued on the Bolt Shank (CL Test)

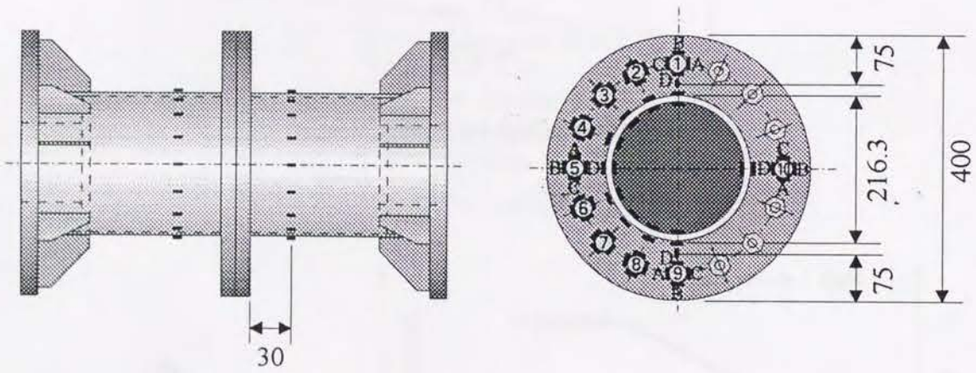

- Uniaxial Strain Gage
- Stress Concentration Strain Gage

Fig. 6.9 Measuring Points of Local Strain (CL Test)

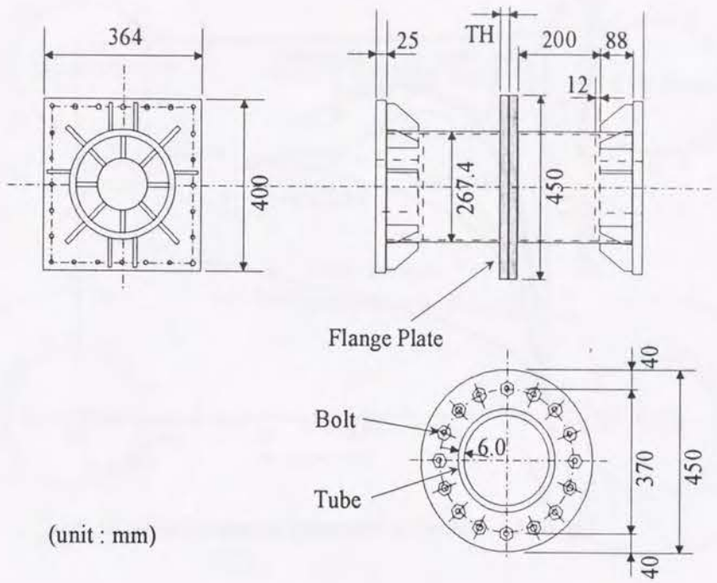

(a) L Type

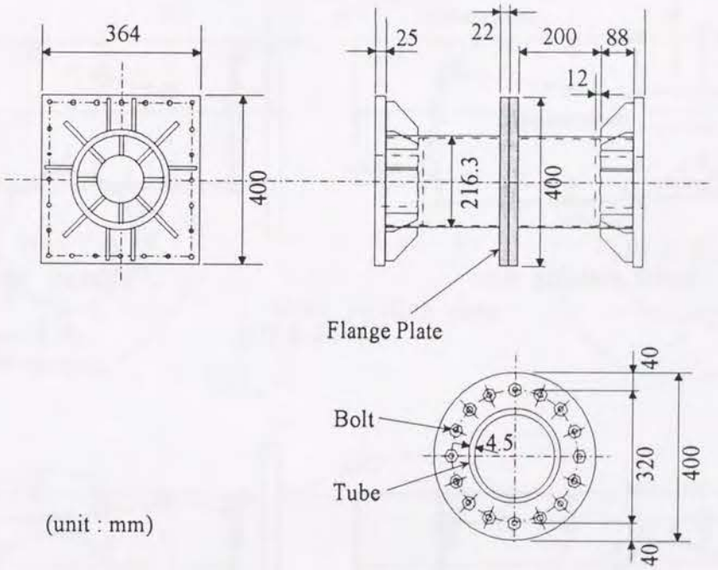

(b) S Type

Fig. 6.10 Dimensions of the Specimens

My : bending moment of the tube corresponding to the 1st yielding

ϕy : curvature of the tube corresponding to the 1st yielding

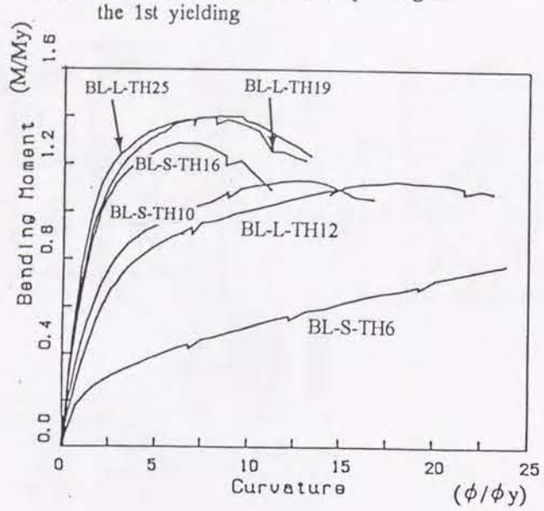

Fig. 6.11 Bending Moment-Curvature Curves(BL Test)

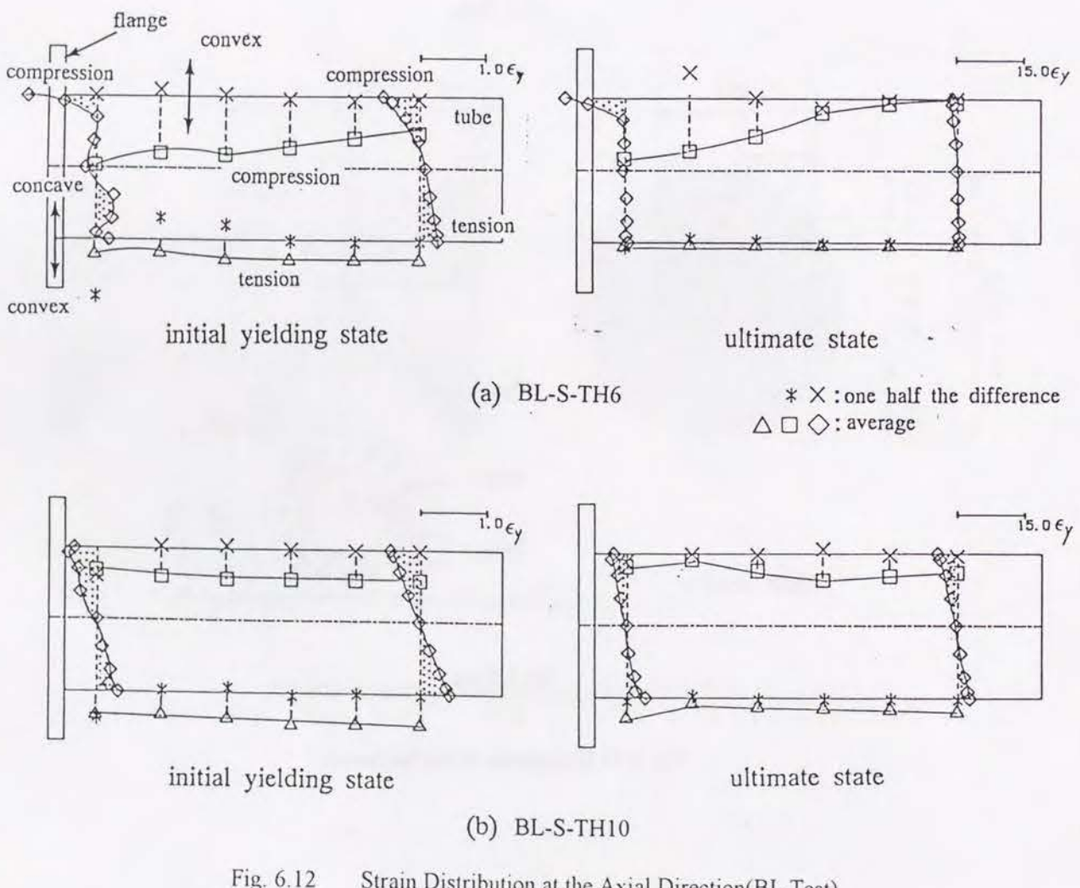

Fig. 6.12 Strain Distribution at the Axial Direction(BL Test)

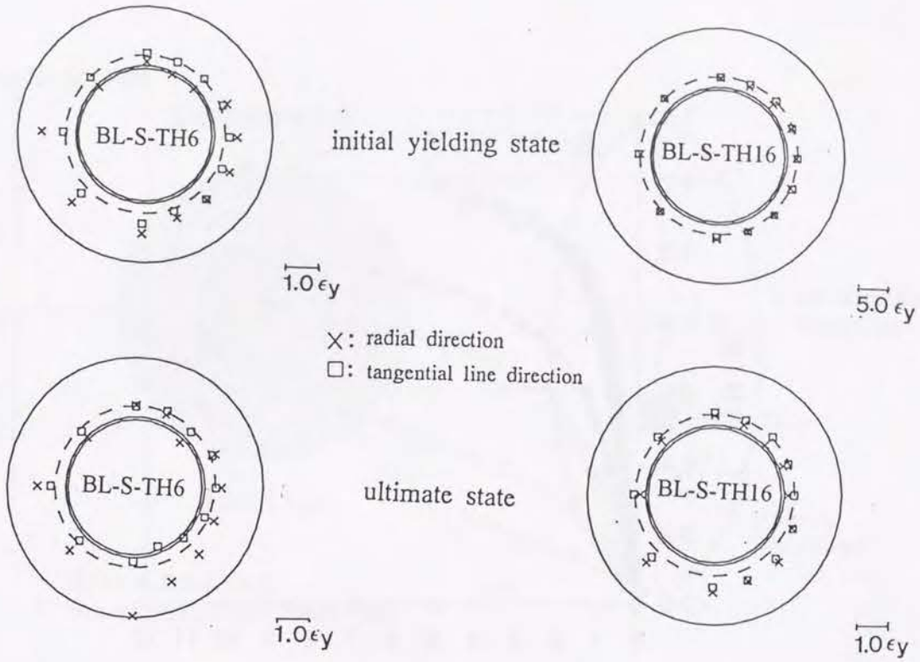

Fig. 6.13 Strains at the Radial Direction and at the Tangential Line Direction at the Flange Plate(BL Test)

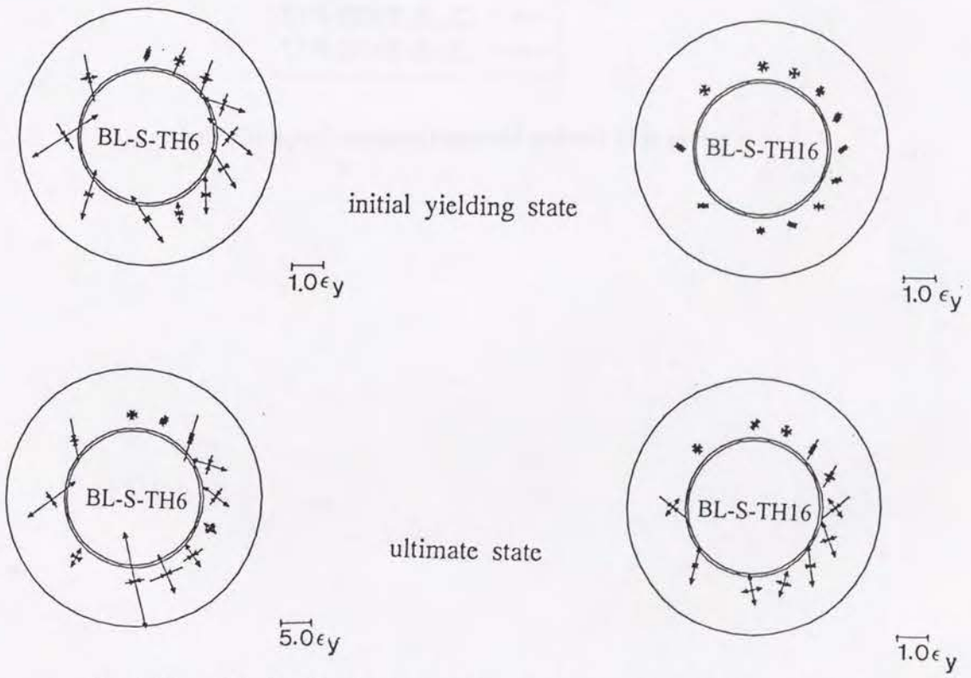

Fig. 6.14 Principal Strains and their Directions at the Flange Plate(BL Test)

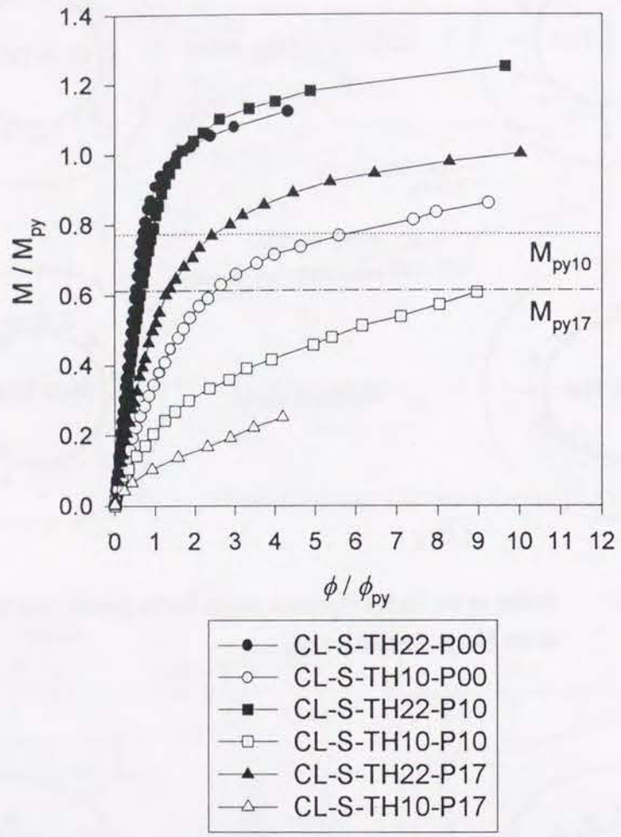

Fig. 6.15 Bending Moment-Curvature Curves (CL Test)

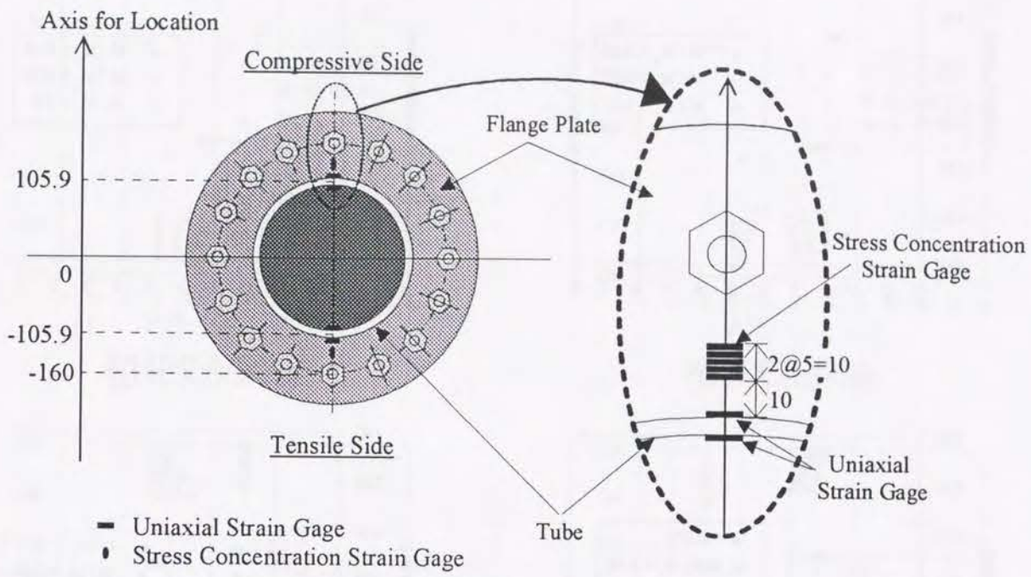

Fig. 6.16 Strain Distribution of the Flange Plate (CL Test) (continued)

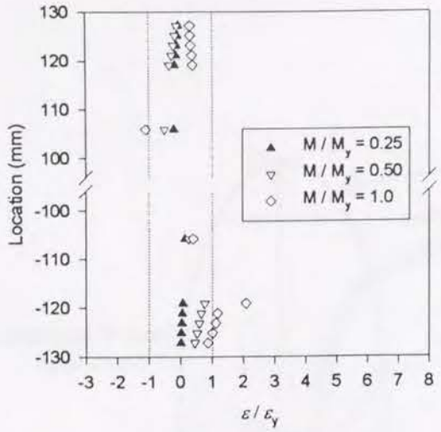

(a) CL-S-TH10-P00

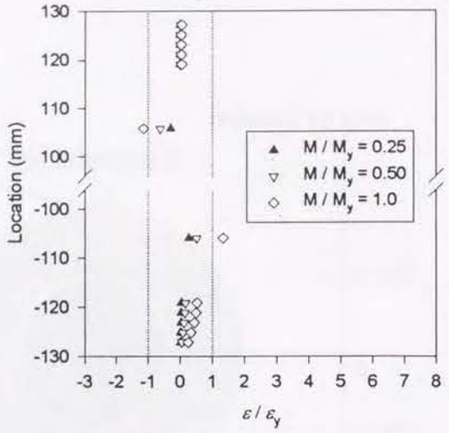

(b) CL-S-TH22-P00

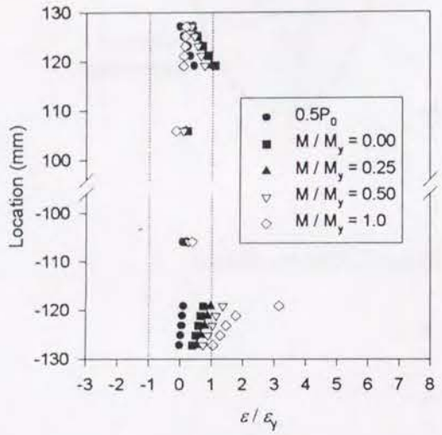

(c) CL-S-TH10-P10

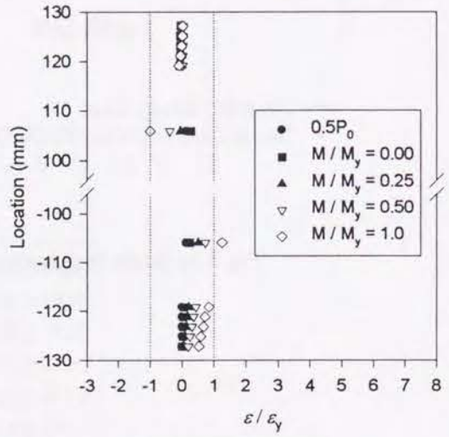

(d) CL-S-TH22-P10

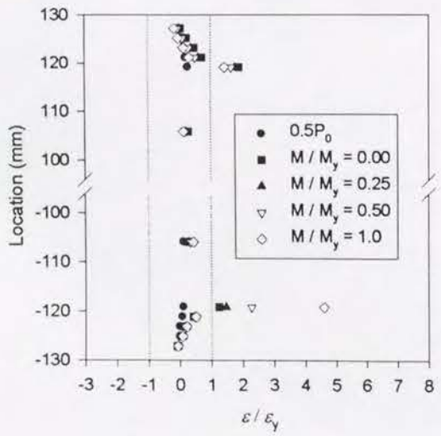

(e) CL-S-TH10-P17

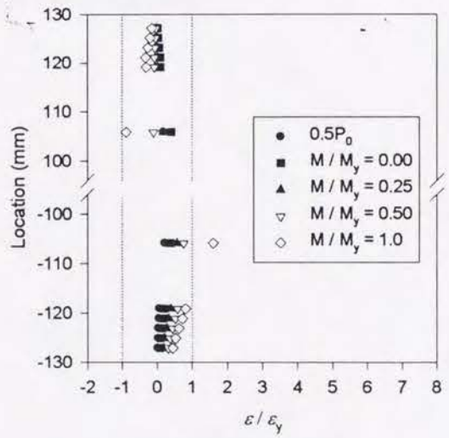

(f) CL-S-TH22-P17

Fig. 6.16 Strain Distribution of the Flange Plate (Side1) (CL Test) (continued)

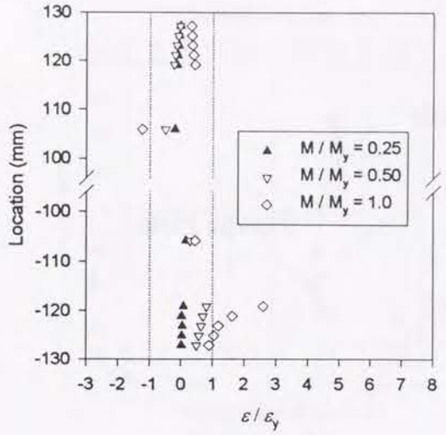

(g) CL-S-TH10-P00

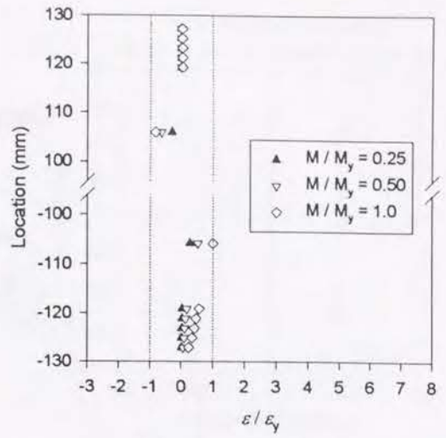

(h) CL-S-TH22-P00

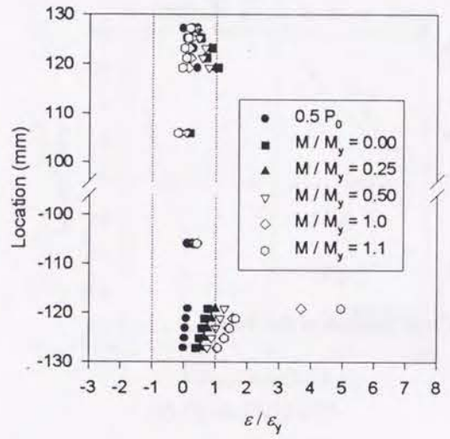

(i) CL-S-TH10-P10

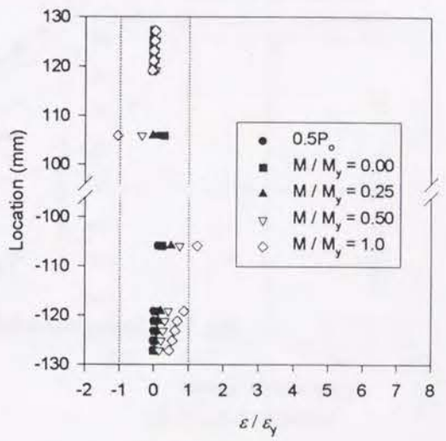

(j) CL-S-TH22-P10

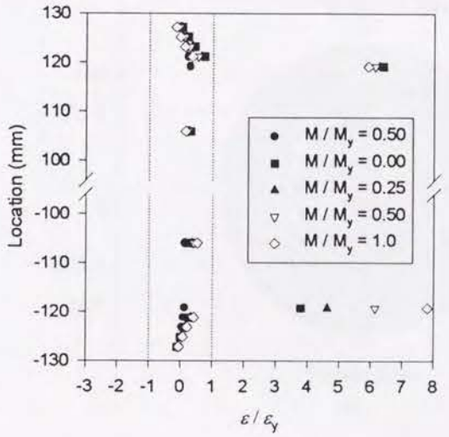

(k) CL-S-TH10-P17

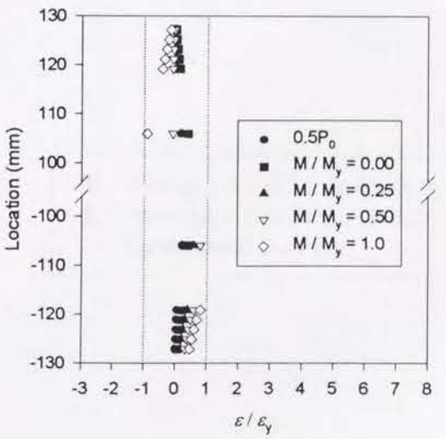

(l) CL-S-TH22-P17

Fig. 6.16 Strain Distribution of the Flange Plate (Side2) (CL-test)

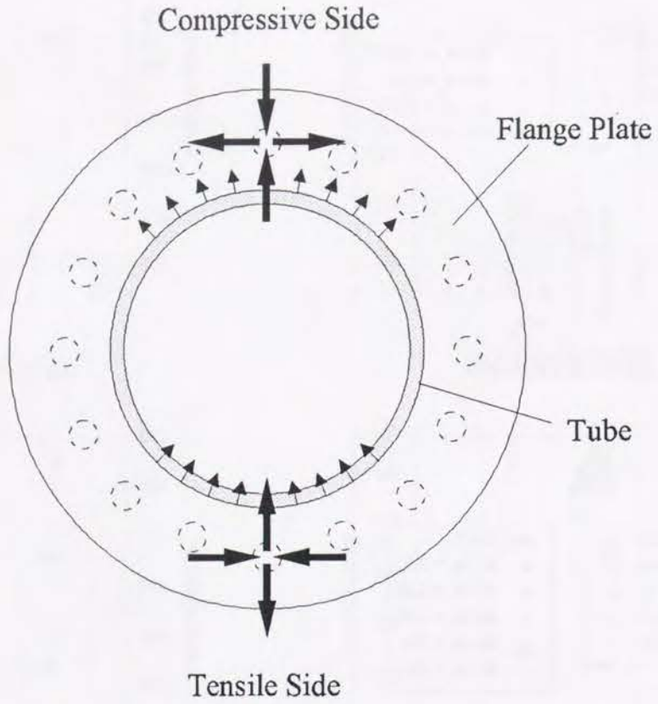

Fig. 6.17 Stress induced by Change of Cross Section of the Tube

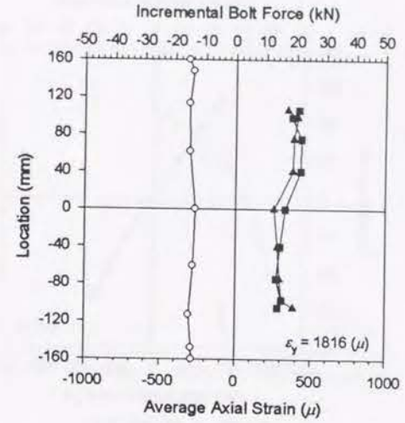

(a) CL-S-TH10-P10

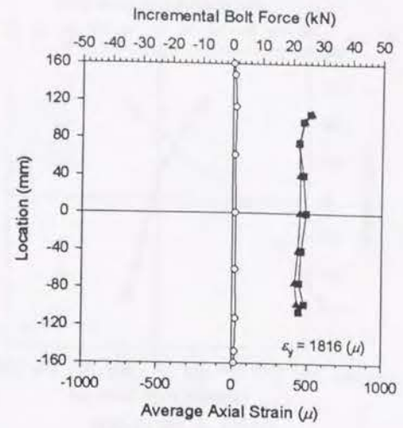

(b) CL-S-TH22-P10

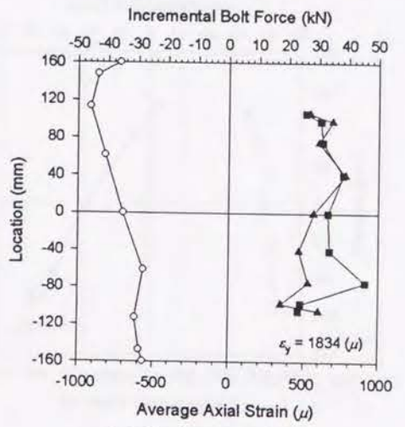

(c) CL-S-TH10-P17

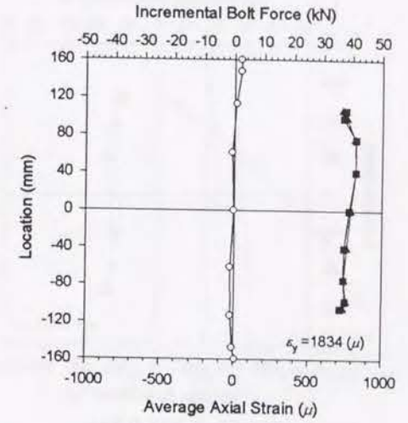

(d) CL-S-TH22-P17

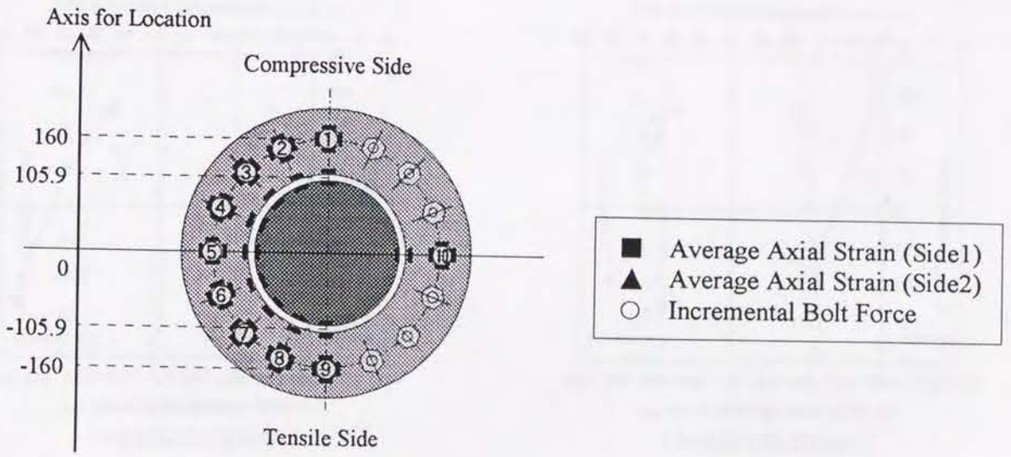

Fig. 6.18 Axial Strain Distribution of the Tube and Strain Distribution of the Bolts (P_0) (CL Test) (continued)

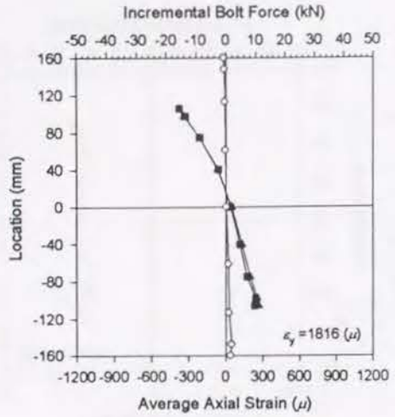

(a) CL-S-TH10-P00

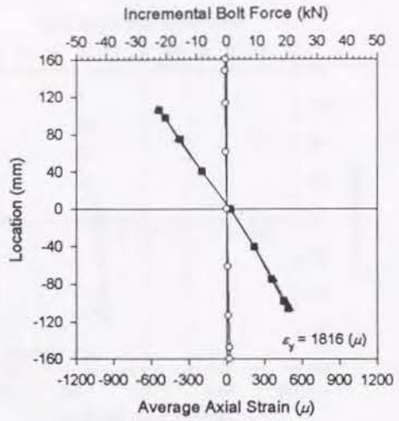

(b) CL-S-TH22-P00

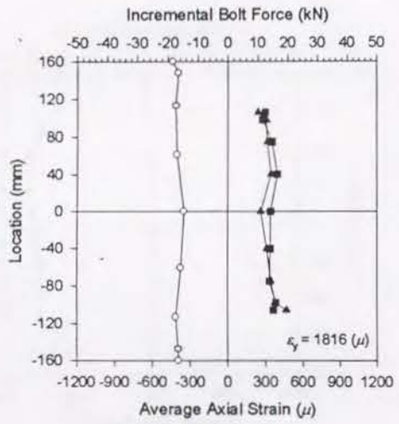

(c) CL-S-TH10-P10

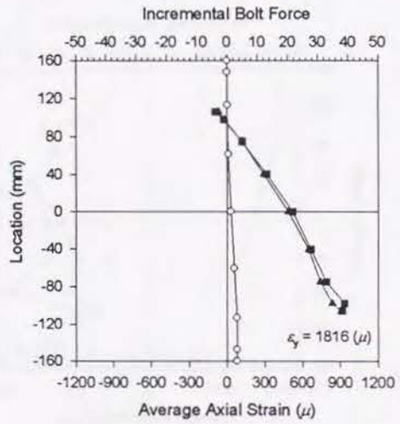

(d) CL-S-TH22-P10

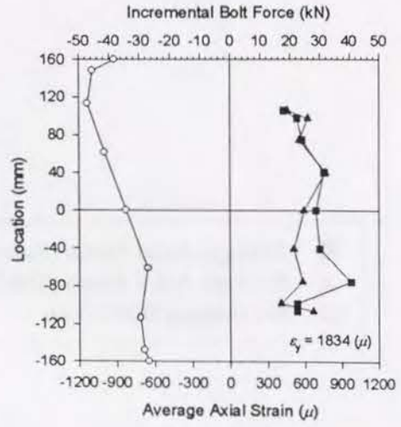

(e) CL-S-TH10-P17

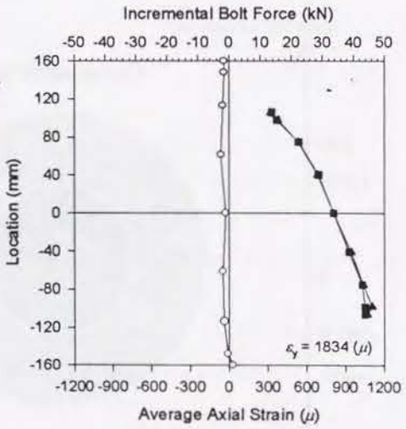

(f) CL-S-TH22-P17

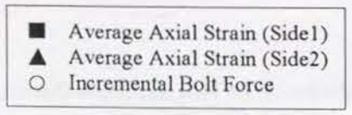

Fig. 6.18 Axial Strain Distribution of the Tube and Strain Distribution of the Bolts ($0.25M_y$) (CL Test) (continued)

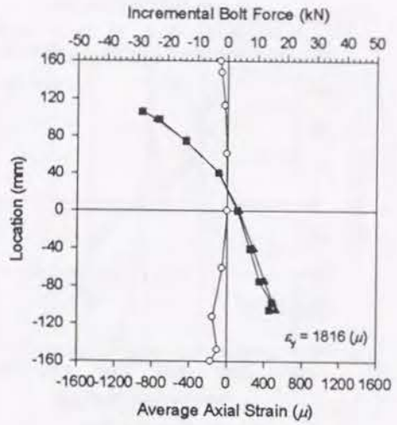

(a) CL-S-TH10-P00

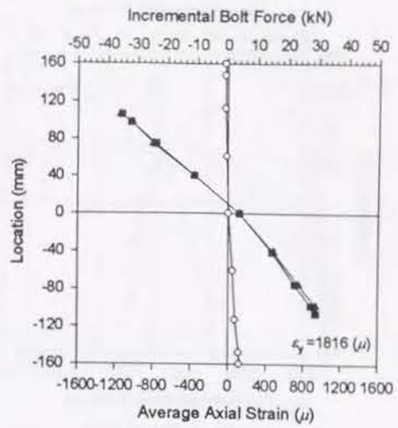

(b) CL-S-TH22-P00

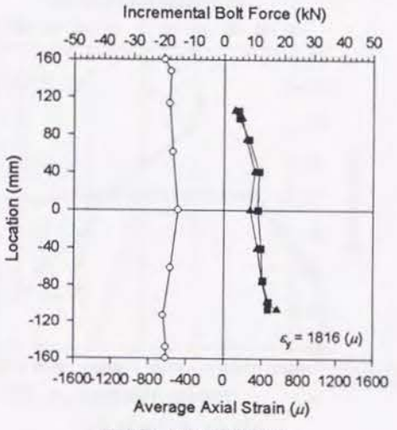

(c) CL-S-TH10-P10

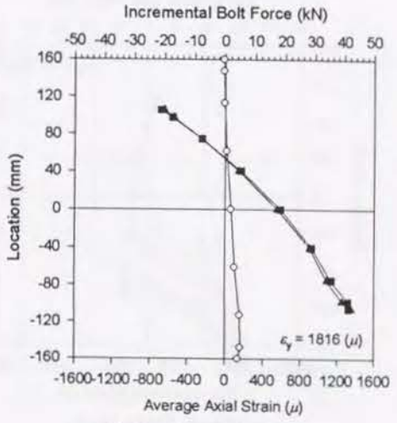

(d) CL-S-TH22-P10

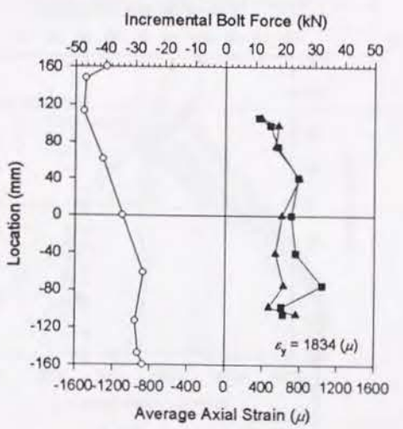

(e) CL-S-TH10-P17

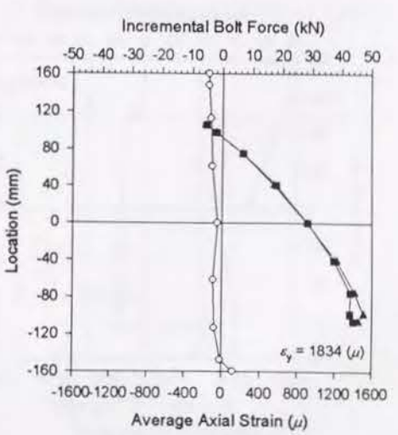

(f) CL-S-TH22-P17

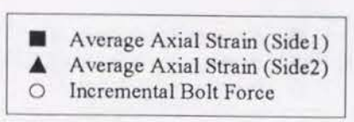

Fig. 6.18 Axial Strain Distribution of the Tube and Strain Distribution of the Bolts ($0.50M_y$) (CL Test) (continued)

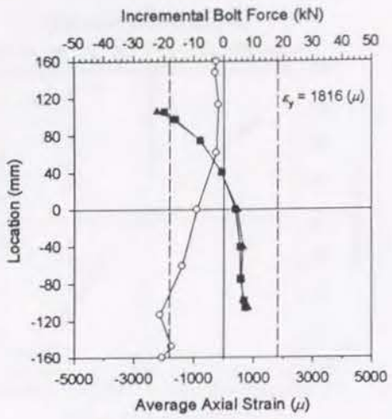

(a) CL-S-TH10-P00

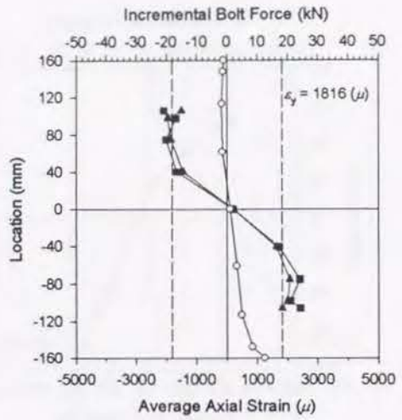

(b) CL-S-TH22-P00

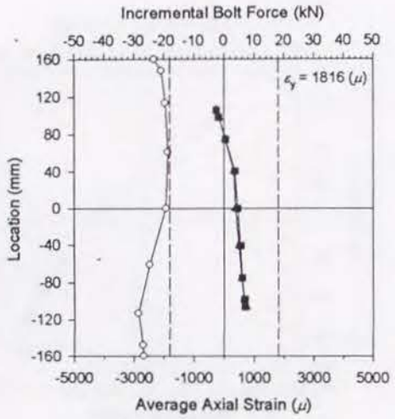

(c) CL-S-TH10-P10

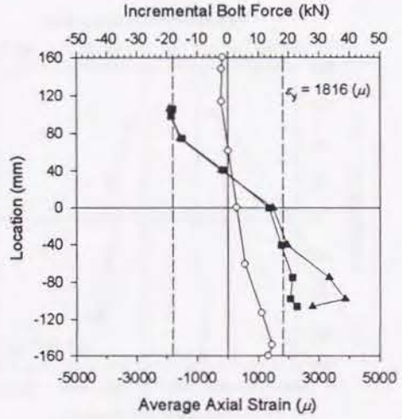

(d) CL-S-TH22-P10

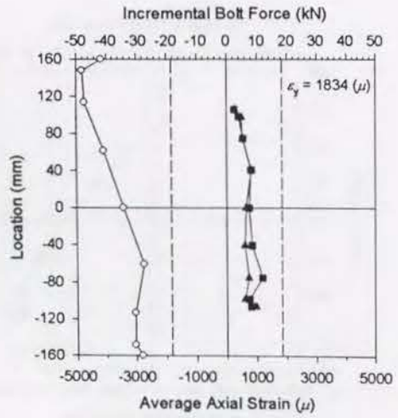

(e) CL-S-TH10-P17

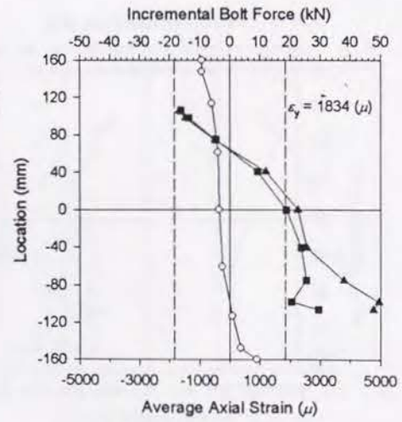

(f) CL-S-TH22-P17

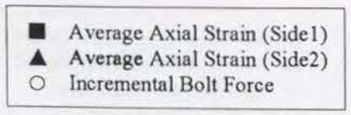

Fig. 6.18 Axial Strain Distribution of the Tube and Strain Distribution of the Bolts (Yielding Stage) (CL Test)

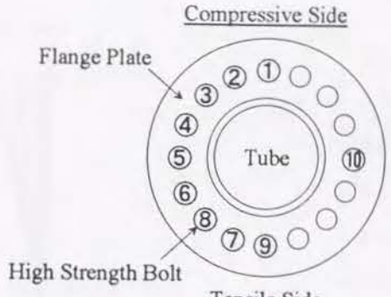

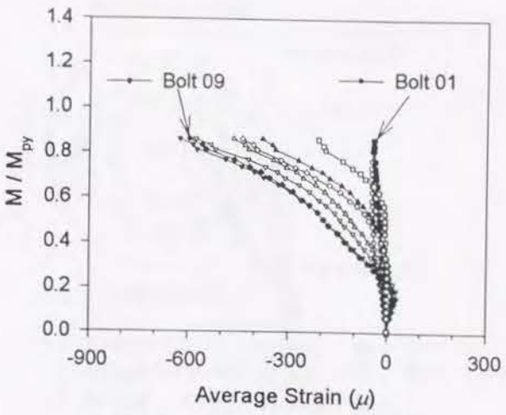

Bending Moment-Bolt Strain Curves

(a) CL-S-TH10-P00

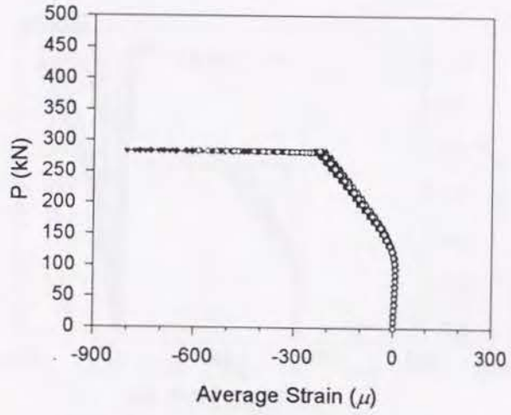

(i) Axial Tensile Load-Bolt Strain Curves

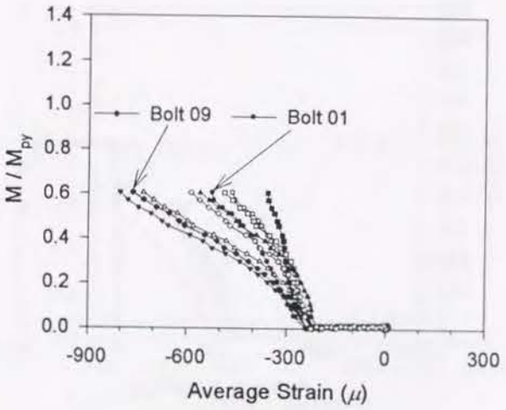

(ii) Bending Moment-Bolt Strain Curves

(b) CL-S-TH10-P10

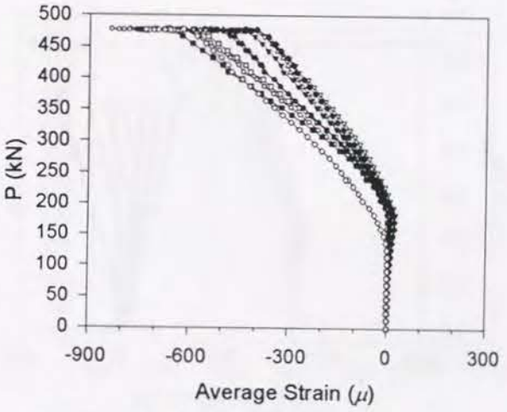

(i) Axial Tension Load-Bolt Strain Curves

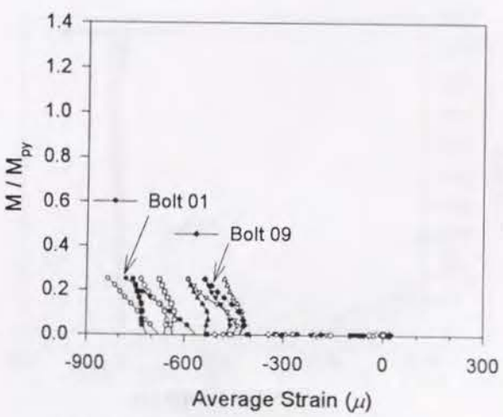

(ii) Bending Moment-Bolt Strain Curves

(c) CL-S-TH10-P17

Fig. 6.19 Load-Bolt Strain Curves (CL Test) (continued)

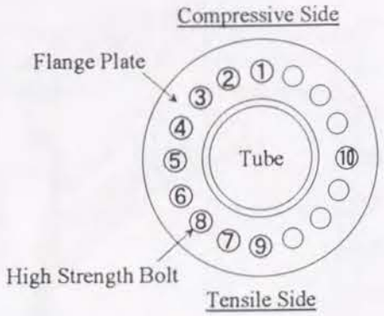

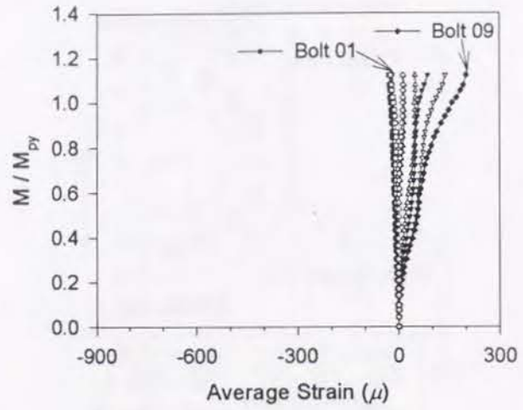

Bending Moment-Bolt Strain Curves

(d) CL-S-TH22-P00

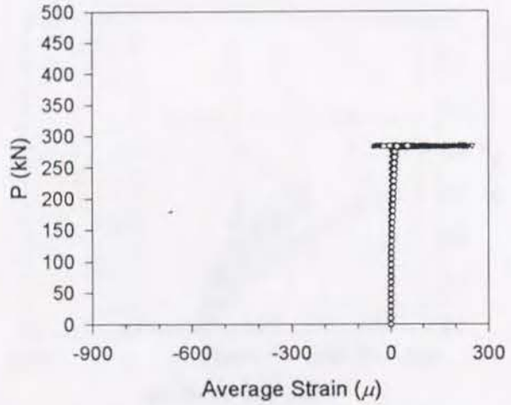

(i) Axial Tensile Load-Bolt Strain Curves

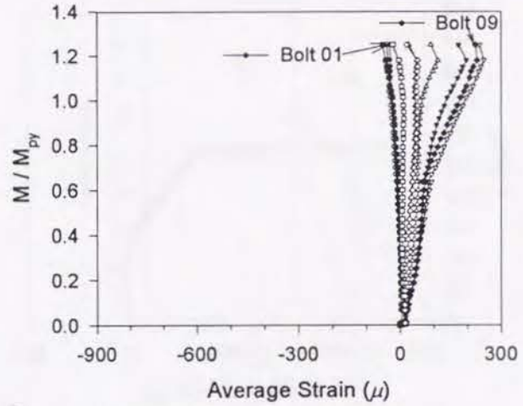

(ii) Bending Moment-Bolt Strain Curves

(e) CL-S-TH22-P10

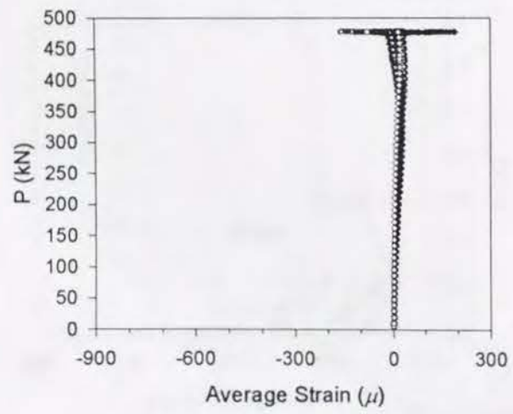

(i) Axial Tensile Load-Bolt Strain Curves

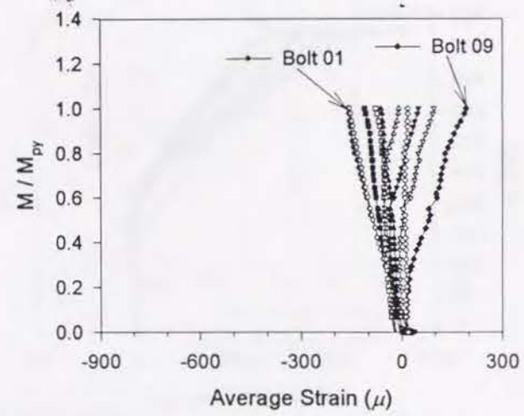

(ii) Bending Moment-Bolt Strain Curves

(f) CL-S-TH22-P17

Fig. 6.19 Load-Bolt Strain Curves (CL Test)

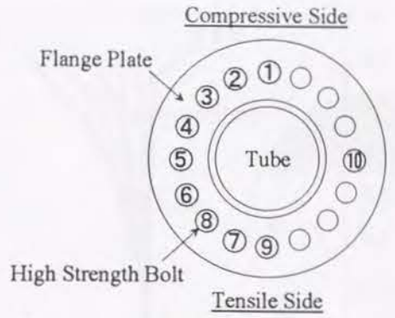

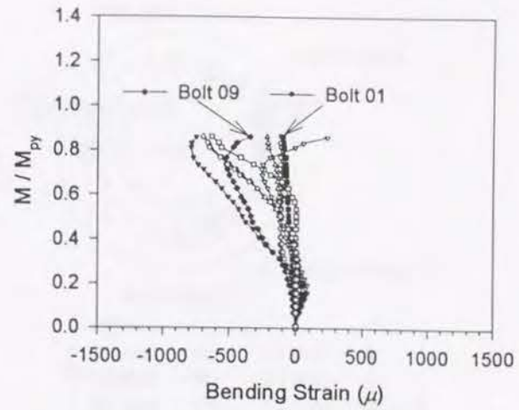

Bending Moment-Bending Strain Curves

(a) CL-S-TH10-P00

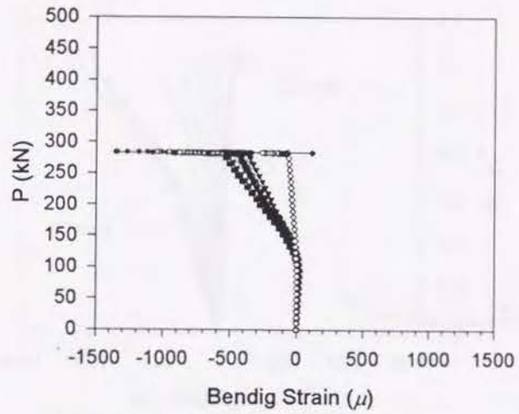

(i) Axial Tensile Load-Bending Strain Curves

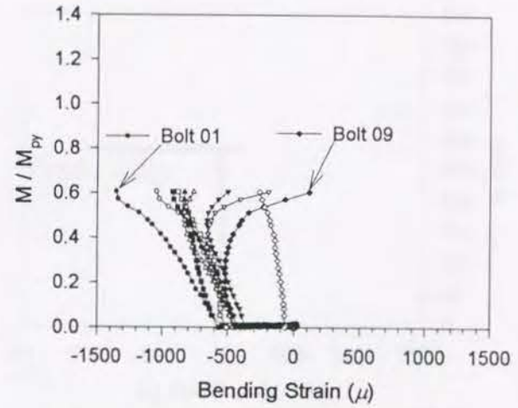

(ii) Bending Moment-Bending Strain Curves

(b) CL-S-TH10-P10

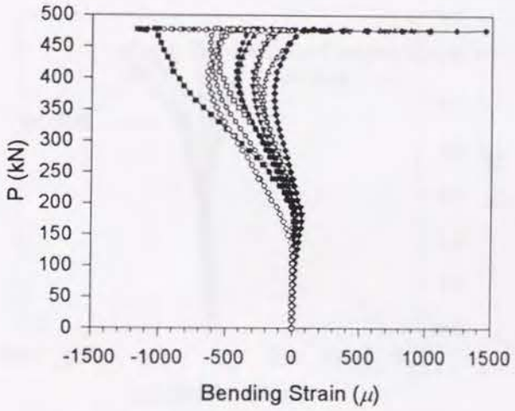

(i) Axial Tensile Load-Bending Strain Curves

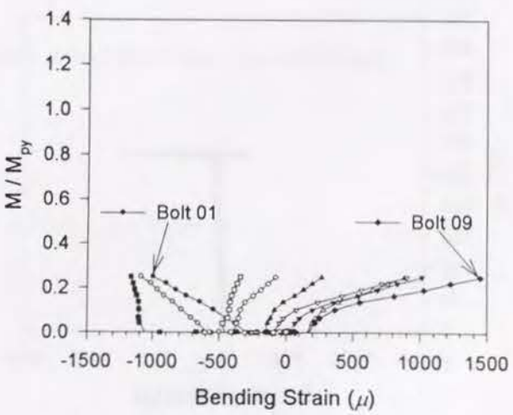

(ii) Bending Moment-Bending Strain Curves

(c) CL-S-TH10-P17

Fig. 6.20 Load-Bending Strain of the Bolt Curves (CL Test) (continued)

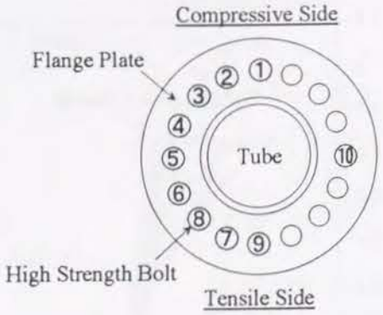

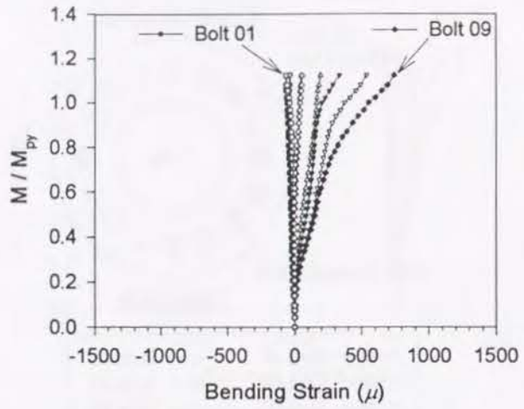

Bending Moment-Bending Strain Curves

(d) CL-S-TH22-P00

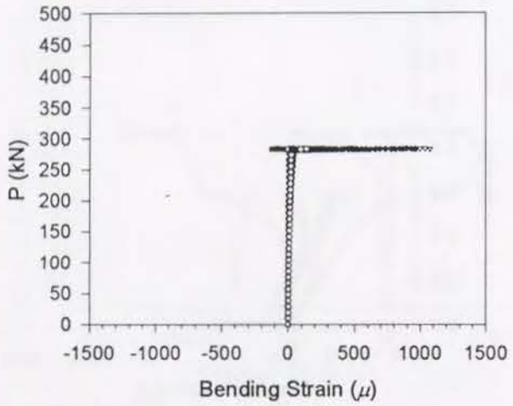

(i) Axial Tensile Load-Bending Strain Curves

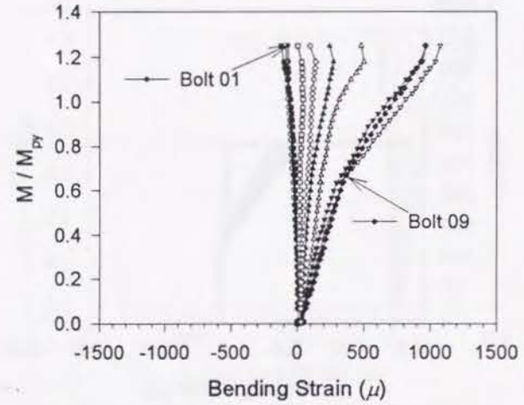

(ii) Bending Moment-Bending Strain Curves

(e) CL-S-TH22-P00

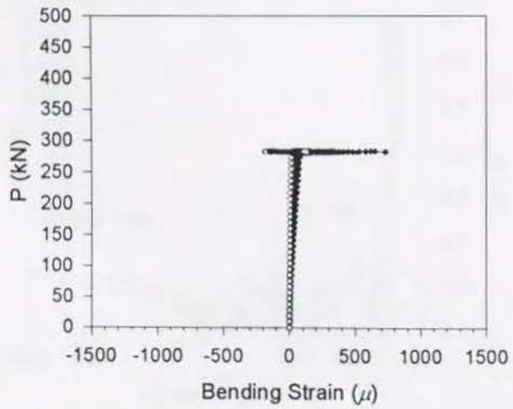

(i) Axial Tensile Load-Bending Strain Curves

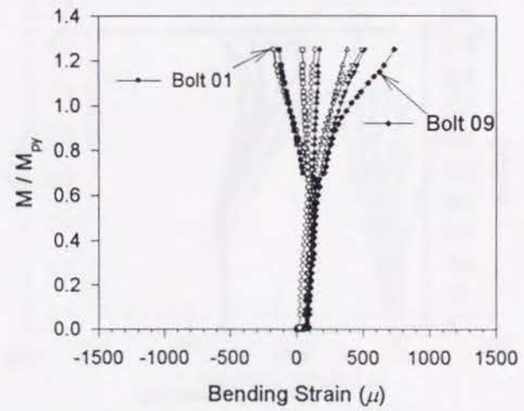

(ii) Bending Moment-Bending Strain Curves

(f) CL-S-TH22-P17

Fig. 6.20 Load-Bending Strain of the Bolt Curves (CL Test)

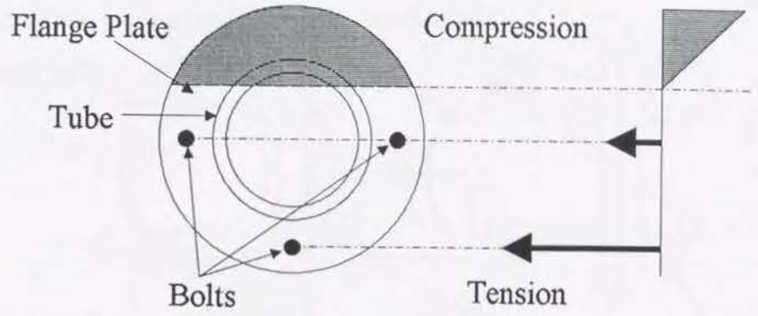

Fig. 6.21 Hypothesis used in the Current Design

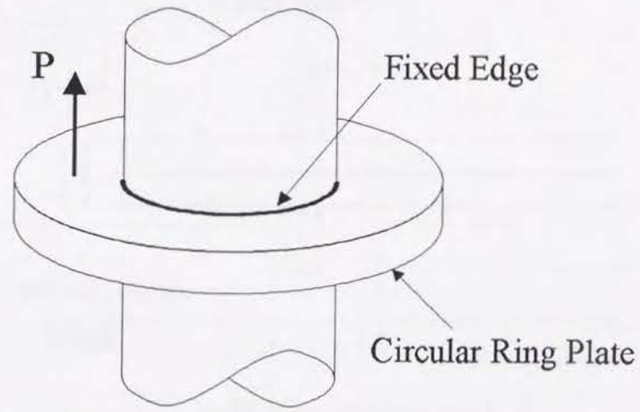

Fig. 6.22 Model for Computation of Working Stress at the Flange Plate (Current Design)

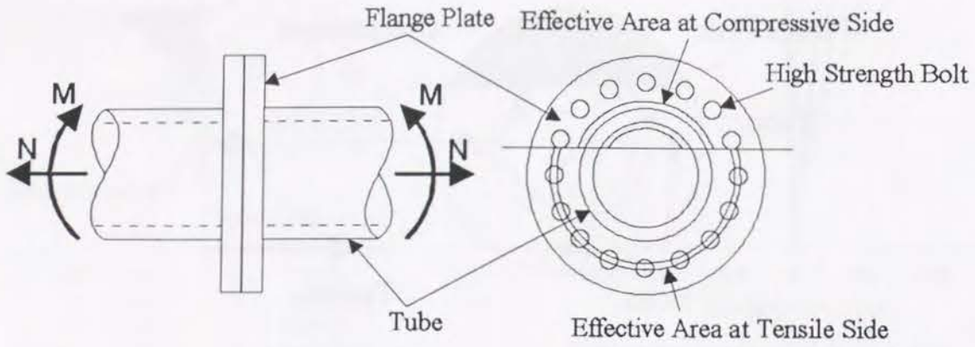

(a) Step 1 (Effective Cross Sectional Area)

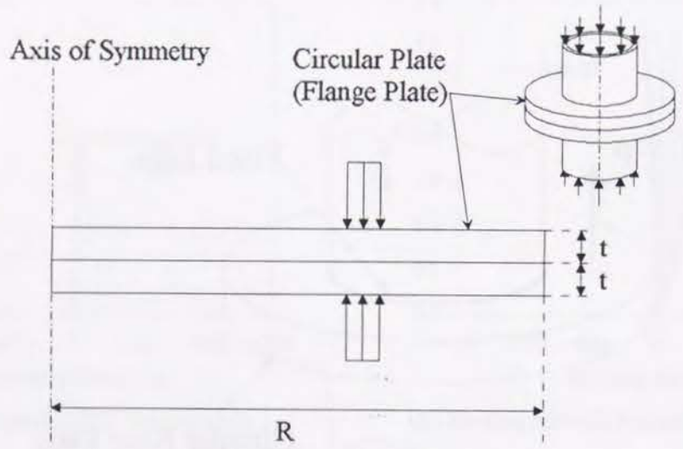

R : Diameter of Circular Plate
t : Thickness of Circular Plate

(b) Step 1 (Evaluation Model of Effective Compressive Cross Sectional Area)

Fig. 6.23 Assumption of Proposed Design Procedure (Continued)

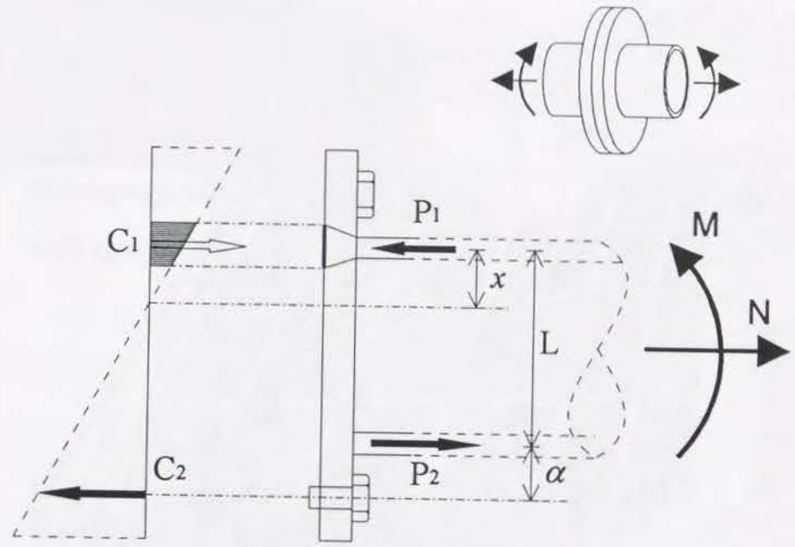

(c) Step 2

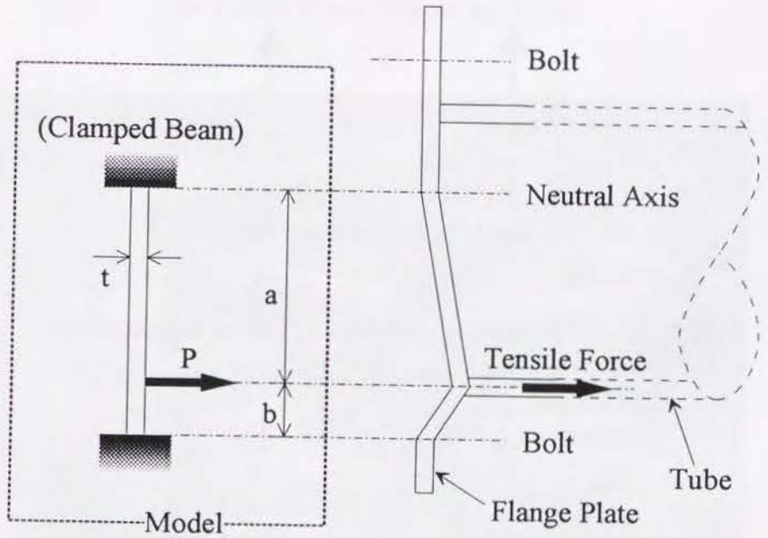

(d) Step 3

Fig. 6.23 Assumption of Proposed Design Procedure

(a)Loading Controller

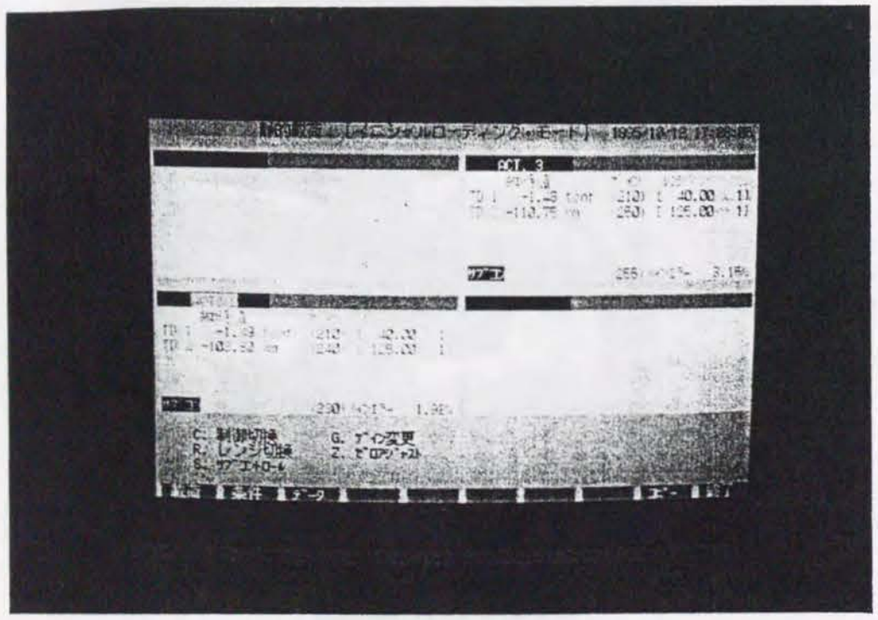

(b)Display

Photo 6.2 Loading Contrler System

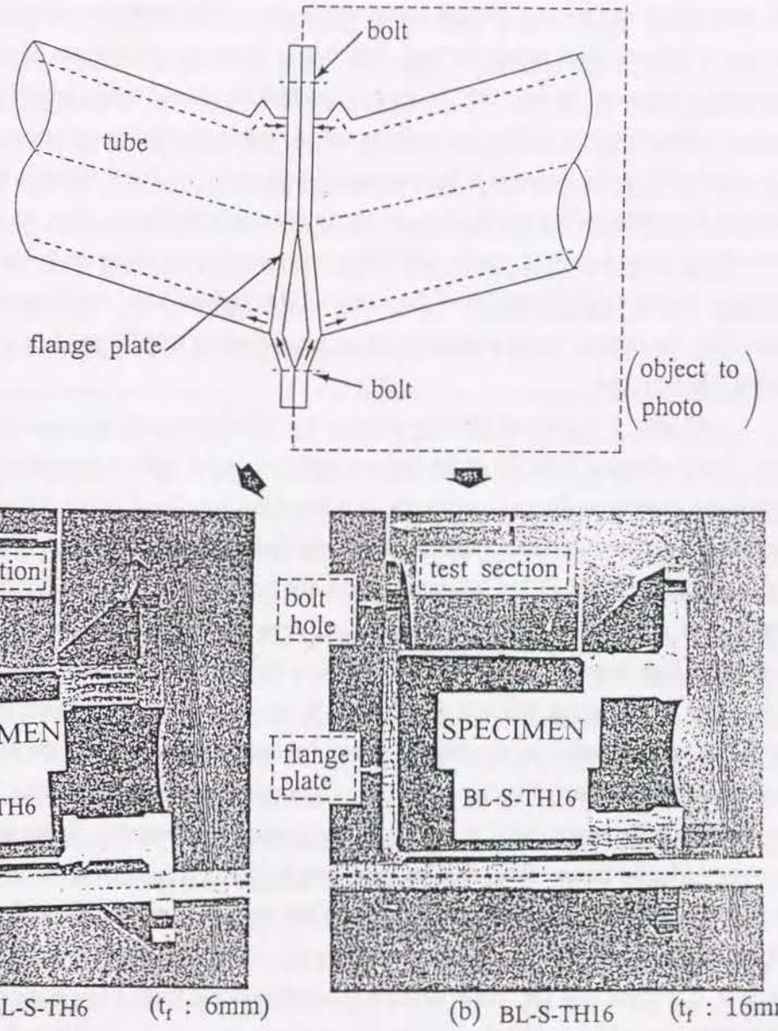

(a) BL-S-TH6 (t_f : 6mm) (b) BL-S-TH16 (t_f : 16mm)

Photo 6.3 Local Deformation after Loading

Chapter 7

Conclusions

This study deals with the high strength bolted tensile joints which have been considered to be superior in mechanical behavior such as high stiffness, high fatigue resistance and easiness of construction compared with other connections. In this study, in order to establish the rational design procedure of such joints, the local and global behavior of the joints under monotonic and cyclic loading are investigated experimentally and analytically paying attention to the mechanical behavior of structural elements such as high strength bolts, the high strength bolt and its adjacent flange plate, split tee flange joints. As an application of the tensile flange joints to pipe structures, tube flange joints are studied, where the assessment of global joints behaviors related to local behavior of the joint elements such as bolts, the flange plate and the tube is made. Then, the rational design procedure of high strength bolted tube flange joints subjected to combined loading was proposed.

Chapter 2 focuses on the high strength bolt which is a basic structural element of the bolted joints. The mechanical behavior of the high strength bolts under both monotonic and cyclic loading are investigated experimentally and analytically. It is found that significant plastic deformation takes place in bolt thread and that load-displacement curve of bolts depends on relative length of the bolt thread to the total bolt length. Therefore, the utilization of the bolt with long bolt thread should be prohibited from viewpoint of strength, but should be recommended from viewpoint of ductility. In addition, the simple modeling of high strength bolts is proposed based on the effective load-elongation relation of each bolt section such as bolt shank and bolt thread; then, its applicability is investigated. Proposed modeling is verified to be very useful to analyze the global 3-dimensional behavior of the joint system by finite element analysis because of saving the effort on data preparation and computation time. However, it is also found that the stress check in the design for yielding by using this simple modeling may not be accurate. As for the fatigue strength of the high strength bolts, it is found from the results of cyclic loading test and finite element stress concentration analysis that the fatigue strength is significantly affected by the bolt pre-stress force. The local yielding is observed at the bolt thread and incomplete bolt thread. However, it is found that the fatigue strength obtained from the loading test is considerable higher than that specified in guideline of fatigue design for steel structures, so it is understood that the guideline is very conservative.

Chapter 3 takes into consideration the high strength bolt and its adjacent flange plate element(BAF model) for the investigation of the contact/separation behavior of flange plates near the bolt. Here, the mechanical behavior of BAF model is investigated experimentally and analytically. In particular, the tensile stiffness of BAF model is assessed against the external applied load. It is understood that the mechanical behavior of BAF model depends on the diameter-to-thickness ratio of circular flange plates

and bolt pre-stress force. In case of small diameter-to-thickness ratio, the initial stiffness is very high and the failure is caused by the bolt yielding. On the other hand, in case of large diameter-to-thickness ratio, the initial stiffness is not high and the failure is caused by the flange plate yielding and its energy absorption capacity may be found to be higher. As for the effect of the bolt pre-stress force, it is found that as the bolt pre-stress force given to the bolt increases, the stiffness becomes large. Moreover, it is observed that the increase of the bolt force occurs at the early stage of loading in case of thinner circular plate. This increase is considered to be caused by the local deformation of the circular plate beneath the bolt head, which is not so called prying action. In addition, the simple evaluation formula for the stiffness to the external applied load are proposed and coefficients in this formula are determined by the multiple regression analysis using non-linear least square method. It is concluded that the proposed equation for the evaluation of the stiffness is applicable for the wide range of structural parameters of BAF model.

Chapter 4 studies the split tee flange joints which is the simplest and typical high strength bolted tensile joints. Its mechanical behavior under monotonic and cyclic loading is investigated both by experimental and analytical approach. Especially, attention is paid to the contact/separation behavior, the joint stiffness and local behavior of the bolts and the flange plate. Under the monotonic loading, the mechanical behavior is dominated by that of either the flange plate or the high strength bolt in accordance with the thickness of the flange plate. In case of the thinner flange plate, the behavior of flange plate is dominant and the high deformabilty is obtained. On the other hand, in case of thicker flange plate, the behavior of the high strength bolt is dominant and the high load carrying capacity is obtained, but the failure becomes very brittle. From the view point of the energy absorption capacity, the use of thinner flange plate is considered to be desirable. Moreover, it is also found that the joint stiffness becomes large if the thicker and the narrower the flange plate is used and that the effect of the bolt pre-stress force on the stiffness is observed to be significant. Furthermore, the significant increase of the bolt force is observed as the externally applied load increases and it is considered to be caused by the local pull-up of the bolt by the local deformation of the flange plate, which is not like a prying force effect. Under the cyclic loading, it is found that the mechanical behavior also depends on the thickness of the flange plate. In case of thinner flange plate, the joint may fail by cracking at the welding section; on the other hand, in case of thicker flange plate, the joint may fail by breaking at the bolt thread. The amplitude of the bolt force under cyclic loading is small compared with that of external applied load. It is also found that the fatigue strength relative to the yield strength of the joint is high in case of thinner flange plate. Therefore, the ultimate state may be defined by the strength under the static loading. However, the joint with thicker flange plate may be required to be checked against fatigue in the design. Moreover, the simple evaluation method of the fatigue strength is proposed in conjunction with the guideline of the fatigue design for steel structures and the experimental results under monotonic loading, and its applicability is proven.

Chapter 5 discusses the development of the quasi-2-dimensional analysis on split tee flange joints considering the load-separation behavior. Proposed is the effective width coefficients of the bolt and

the flange plate utilized for 2-dimensional analysis in order to reproduce 3-dimensional behavior. This analysis is very useful for parametric study of the split tee flange joint or its design because of its simplicity compared with 3-dimensional analysis. It is found that 3-dimensional behavior of the split tee flange joint such as load-deformation curve and characteristics of local deformation can be reproduced by quasi-2-dimensional finite element analysis using the effective width of the bolt and the flange plate. However, the stress obtained by this quasi-2-dimensional analysis is found to be very conservative, so that accurate stress check may be difficult by the proposed 2-dimensional finite element analysis using effective width coefficients.

Chapter 6 makes an assessment of the tube flange joint as an application of high strength bolted tensile flange joints. The mechanical behavior of high strength bolted tube flange joints is studied experimentally in order to develop the practical design procedure. The fundamental characteristics such as the load transferring mechanics in both compressive and tensile sides, failure mechanism under the combined loading are discussed. It is found from the experimental results that the initial stiffness, the yield strength and the ultimate strength can increase significantly by preventing the interaction of the flange plate with the steel tube as the flange plates become thicker. However, the further increase of the ultimate strength may be limited by the buckling of the tube. In addition, the simple analytical model for the stress check based on the load transferring mechanism both in the compressive and tensile sides are proposed. It is understood that the initial yielding of the flange plate under bending is well-predicted by this proposed procedure considering the effective cross sectional area. Therefore, the rational design of tube flange joints can be carried out by using the proposed procedure.

As mentioned above, the high strength bolted tensile flange joints can be utilized for primary members of bridge structures. However, in order to make the proposed design procedure more rational and reliable, further study to solve the following technical problems should be carried out.

1) The significant increase of the bolt force is observed in case of thinner flange plate. This mechanism is quite different from the mechanism considered in the past study. Therefore, the structural detail to reduce this increase of the bolt force should be developed.
2) Generally speaking, the joints are made of numerous bolts. In order to design the economical joints, the contribution of a bolt among the bolt group on the mechanical behavior should be investigated.
3) It is concluded from the experimental results that the tensile joints with thinner flange plate have high energy absorption capacity. Further study should be carried out in order to use the tensile joints as energy absorption device from the view point of earthquake resistance.
4) The cyclic loading tests for high strength bolts and split tee flange joints were carried out for the limited number of test specimens. In order to develop the reliable S-N curve for the fatigue strength evaluation, further cyclic loading tests should be required, particularly for the tube flange joints.

Research Activities

1) T.Yamaguchi, E.Watanabe, K.Sugiura, S.Kasai : Experimental Study on High Strength Bolted Tube Flange Joints, Proc. of Annual Conference of Civil Engineers, JSCE Kansai Chapter, Jun. 1991(in Japanese).
2) T.Yamaguchi, E.Watanabe, K.Sugiura, S.Kasai : Design Method of High Strength Bolted Tube Flange Joints, Proc. of the 46th Annual conference of JSCE, Sep. 1991(in Japanese).
3) E.Watanabe, K.Sugiura, T.Yamaguchi, S. Kasai : Design Method of High Strength Bolted Steel Tube Flange Joints, Journal of Structural Engineering, JSCE, Vol. 38A, Mar. 1992, pp. 1-12(in Japanese).
4) T.Yamaguchi, E.Watanabe, K.Sugiura, S.Kasai, T.Mitamura : Experimental Study on High Strength Bolted Tube Flange Joints subjected to Bending, Proc. of the 47th Annual conference of JSCE, Sep. 1992(in Japanese).
5) E.Watanabe, K.Sugiura, T.Yamaguchi, S.Kasai : Behavior of High Strength Bolted Tube Flange Joints subjected to Bending, Proc. of the 3rd Pacific Structural Steel Conference, Oct. 1992, pp. 391-398.
6 E.Watanabe, K.Sugiura, T.Yamaguchi, S.Kasai : Rigidity of High Strength Bolted Steel Flange Joints, Journal of Construction Steel, Vol. 1, JSSC, July 1993, pp. 31-38(in Japanese).
7) E.Watanabe, K.Sugiura, T.Utsunomiya, T.Yamaguchi, S.Kasai : Simple Analysis of High Strength Bolted Tube Flange Joints, Proc. of the 4th East Asia-Pacific Conference on Structural Engineering and Construction, Sep. 1993, pp. 861-866.
8) T.Yamaguchi, E.Watanabe, K.Sugiura, S.Kasai : Joint Rigidity of High Strength Bolted Tube Flange Joints, Proc. of the 48th Annual conference of JSCE, Sep. 1993(in Japanese).
9) Opening Characteristics of High Strength Bolted Flange Joints and its Tensile Rigidity, Journal of Structural Engineering, JSCE, Vol. 40A, Mar. 1994, pp. 153-162(in Japanese).
10) T.Yamaguchi, E.Watanabe, K.Sugiura, S.Kasai, T.Mitamura : 3D FEM Analysis on Contact/Operation Behavior of Split Tee Flange Joints, Proc. of the 49th Annual conference of JSCE, Sep. 1994(in Japanese).
11) E.Watanabe, K.Sugiura, T.Yamaguchi, S.Kasai : Contact/Opening Behavior of Split Tee Flange Joints and its tensile rigidity, Journal of Construction Steel, Vol. 2, JSSC, Nov. 1994, pp. 93-100(in Japanese).
12) The Assessment of 2-dimensional Analysis on Split Tee Flange Joints, Journal of Structural Engineering, JSCE, Vol. 41A, Mar. 1995, pp. 95-102(in Japanese).
13) E.Watanabe, K.Sugiura, T. Utsunomiya, T.Yamaguchi, S.Kasai et al. : Fatigue Strength of High Strength Bolted Tensile Joints, Proc. of the 5th East Asia-Pacific Conference on Structural

Engineering and Construction, July 1995, pp.

14) T.Yamaguchi, E.Watanabe, K.Sugiura, S.Kasai, et al. : Fatigue Strength on Split Tee Flange Tensile Joints, Proc. of the 50th Annual conference of JSCE, Sep. 1995(in Japanese).

15) K.Fujitani, E.Watanabe, K.Sugiura, T.Yamaguchi, S.Kasai : Effective stress-strain relation of high strength bolts considering threads, Journal of Construction Steel, Vol. 3, JSSC, Nov. 1995, pp. 281-288(in Japanese).